

# **Molecular interrogation of *Campylobacter* infection**

**Submitted by**

**Sok Kiang Lau**

**to the University of Exeter as a thesis for the degree of  
Doctor of Philosophy in Biological Sciences in May 2014**

This thesis is available for Library use on the understanding that it is  
copyright material and that no quotation from the thesis may be  
published without proper acknowledgement.

I certify that all material in this thesis which is not my own work has  
been identified and that no material has previously been submitted  
and approved for the award of a degree by this or any other University.

Signature: .....

## **Declaration**

Unless otherwise stated, the results and data presented in this thesis were solely the work of Sok Kiang Lau.

The BWH algorithm was developed with the help from Dr Ron Yang. All SRS images were taken with the help of Dr Julian Moger. Zebrafish used were maintained by ARC at University of Exeter (UoE). Protein mass spectrometry analysis was performed by the Mass Spectrometry Facility at UoE. Genome sequencing was performed by the Sequencing Facility at UoE. Electron microscopy was performed by Dr Massimo Micaroni from Bio-imaging Centre at UoE. The piglets challenge was performed by Dr Paul Everest from the Institute of Infection, Immunity and Inflammation at University of Glasgow. The prediction of suitable peptides, the making of the selected peptide and generation of antibodies against the peptide were performed by Perbio.

## Abstract

Campylobacteriosis is common in both developing and developed countries. Although there had been numerous studies performed to gain a better understanding of the disease, much still remains to be unravel. In this project, the interactions between the bacteria and host cells or organisms were interrogated. Raman based imaging was initially investigated using an established *Salmonella* Typhimurium and cell infection model. The results obtained showed the potential for real-time imaging. However, due to the instability of the laser system of the microscope, reproducible results could not be obtained. Therefore, this technique was not applied to *Campylobacter jejuni*. Zebrafish embryo was established as a new infection model suitable for *C. jejuni* studies. *C. jejuni* strains and mutants were screened using this model to determine their virulence. This model was used to screen two type six secretion system mutants constructed in this study. The results obtained showed that one of the mutants, Cj1Δ*tssM*(syn)::kan<sup>R</sup>\_cas, was attenuated in the ZFE model. Subsequent competitive index challenges performed in piglets with *C. jejuni* wild-type and the two T6SS mutants, also showed that Cj1Δ*tssM*(syn)::kan<sup>R</sup>\_cas was attenuated. Both T6SS mutants had shown increased adherence to macrophages and Cj1Δ*tssM*(syn)::kan<sup>R</sup>\_cas also showed increased cell invasion. Together, these findings suggested that the T6SS is involved in establishment of infection in ZFE and piglet and as well as in adhesion and invasion of macrophages.

## **Acknowledgements**

This thesis could not have completed without the help and support of others. Firstly, I would like to express my greatest gratitude to my supervisors, Professor Rick Titball, Dr Olivia Champion, Professor Peter Winlove and Dr Julian Moger, who have provided me with great guidance in all aspects. I would like to thank Rachael for her guidance on working with zebrafish embryos, Monika for her guidance on tissue culture, Matt for his help with Southern Blot, Ellen for her help with Raman spectroscopy, Peter for his help on Confocal, and Gwen and Gemma for their efforts in ensuring sufficient laboratory supplies and smooth operations of laboratory equipments at all times. A huge thank you to Nicola for helping to proof read this thesis.

I would like to thank Mom, Dad, Edgar, Meng, Quilan and Edwin for all the love and support they have given me; and my lovely niece, Jiaxin, for bringing me lots of joy especially with her sweet smiles. Big hugs to all my friends who have always been there for me whenever needed, especially Hwee Teng, Hwee Huang, Selina, Rebecca and Harriet. I would also like to specially thank Wayne for his love, support and encouragements especially throughout the writing of this thesis; and also for taking his time to read through and improve the writing of this thesis.

Finally, I would like to thank DSO National Laboratories for funding my PhD and special thanks to Lionel and Boon Huan for believing in me and supporting my scholarship application.

# Table of Contents

<b>Molecular interrogation of <i>Campylobacter</i> infection.....</b>	<b>i</b>
<b>Declaration .....</b>	<b>ii</b>
<b>Abstract .....</b>	<b>iii</b>
<b>Acknowledgements .....</b>	<b>iv</b>
<b>List of figures .....</b>	<b>xi</b>
<b>List of tables .....</b>	<b>xvi</b>
<b>List of abbreviations .....</b>	<b>xviii</b>
<b>Chapter 1: Introduction to <i>Campylobacter</i> and Imaging of infection .....</b>	<b>1</b>
1.1 <i>Campylobacter</i> .....	2
1.1.1 Microbiology of <i>C. jejuni</i> .....	3
1.1.2 Epidemiology and public health.....	5
1.1.3 Detection of <i>C. jejuni</i> .....	8
1.1.4 <i>Campylobacter jejuni</i> genomic information .....	10
1.1.5 Pathogenesis of <i>C. jejuni</i> .....	12
1.1.5.1 Adhesion and invasion.....	13
1.1.5.2 Intracellular survival.....	14
1.1.6 Factors involved in virulence of <i>C. jejuni</i> .....	17
1.1.6.1 Flagellum.....	17
1.1.6.2 LOS and capsule.....	17
1.1.6.3 Toxins.....	18
1.1.6.4 Protein secretion systems.....	19
1.1.6.4.1 Type six secretion system (T6SS).....	23
1.1.7 Animal models .....	32
1.1.7.1 Bovine.....	34
1.1.7.2 Canine and feline.....	34
1.1.7.3 Avian.....	35
1.1.7.4 Murine.....	35
1.1.7.5 Swine.....	36
1.1.7.6 Ferret, rabbit and NHP.....	37

1.1.7.7	<i>Invertebrates</i> .....	37
1.1.7.8	<i>Zebrafish embryo as a possible infection model for Campylobacteriosis study</i> .....	38
1.2	Imaging of infection .....	42
1.2.1	Brief history of microscopy techniques .....	43
1.2.2	Fluorescence microscopy .....	47
1.2.3	Vibrational spectroscopy.....	49
1.2.4	Raman spectroscopy.....	51
1.2.5	Coherent Raman scattering (CRS) microscopy .....	53
1.3	Project aims .....	55
<b>Chapter 2: Materials and methods</b> .....		<b>56</b>
2.1	Bacterial strains, plasmids and primers .....	57
2.2	Bacterial cell culture.....	62
2.2.1	<i>Escherichia coli</i> .....	62
2.2.2	<i>Salmonella</i> Typhimurium.....	62
2.2.3	<i>Campylobacter jejuni</i> .....	63
2.3	Eukaryotic cell culture.....	64
2.3.1	Mouse macrophage-like cells J774A.1 and Raw267.4 .....	64
2.3.2	Zebrafish <i>WIK</i> wild-type and <i>AB fms:nfsB.mCherry</i> transgenic line.....	64
2.4	Nucleic acid extraction .....	65
2.4.1	Genomic DNA (gDNA) .....	65
2.4.2	Plasmid DNA .....	65
2.4.3	RNA .....	66
2.5	Mutant construction.....	67
2.5.1	Transforming plasmids into <i>E. coli</i> Top10 cells .....	67
2.5.2	<i>C. jejuni</i> fluorescence reporters.....	67
2.5.2.1	<i>Making electro-competent C. jejuni cells</i> .....	67
2.5.2.2	<i>Transformation of competent C. jejuni cells</i> .....	68
2.5.3	<i>C. jejuni</i> Cj1 T6SS mutants.....	69
2.5.3.1	<i>Digestion of pGEM_tssD(syn), pGEM_tssM(syn) and pJMK30</i> .....	69
2.5.3.2	<i>Ligation of kanR_cas to pGEM_tssD(syn) and pGEM_tssM(syn) and transformation into E. coli Top10 cells</i> .....	70

2.5.3.3	<i>Transformation of competent C. jejuni cells</i> .....	71
2.6	PCR.....	72
2.6.1	PCR for products less than 1000 base-pairs (bp).....	72
2.6.2	PCR for products more than 1000 bp.....	72
2.6.3	Reverse-transcription (RT) PCR.....	73
2.7	Southern Blot.....	74
2.7.1	Digestion of gDNA.....	74
2.7.2	Depurination and denaturation DNA in gel.....	74
2.7.3	Blotting to membrane.....	75
2.7.4	Construction of a probe for the Southern blot.....	77
2.7.5	Hybridisation of DIG-labelled probe to blotted membrane.....	77
2.7.6	Detection of Southern_Probe hybridised to blotted membrane.....	78
2.8	SDS-Polyacrylamide gel electrophoresis (PAGE).....	80
2.8.1	Precipitation of proteins in culture supernatant.....	80
2.8.2	Extraction of protein in cell pellet.....	81
2.8.2	Separation of proteins in gel.....	81
2.9	Mass spectrometry.....	83
2.9.1	Protein samples from culture supernatant.....	83
2.9.2	Protein samples from cell pellet.....	84
2.10	Whole genome sequencing.....	85
2.11	Growth curve.....	86
2.11.1	<i>S. Typhimurium</i> SL1344 wild-type.....	86
2.11.2	<i>C. jejuni</i> Cj1 wild-type, Cj1Δ <i>tssD</i> (syn)::kan <sup>R</sup> _cas and Cj1Δ <i>tssD</i> (syn)::kan <sup>R</sup> _cas.....	86
2.12	Bacterial-host interaction assays.....	88
2.12.1	<i>S. Typhimurium</i> - macrophages infection assays.....	88
2.12.1.1	<i>Preparation of J774A.1 cells for infection</i> .....	88
2.12.1.2	<i>Preparation of S. Typhimurium for infection</i> .....	88
2.12.1.3	<i>Infection of J774A.1 cells with S. Typhimurium</i> .....	89
2.12.1.4	<i>Fixing of infected J774A.1 cells</i> .....	89
2.12.2	<i>C. jejuni</i> - macrophages infection assays.....	90
2.12.2.1	<i>Preparation of RAW264.7 cells for infection</i> .....	90

2.12.2.2	<i>Preparation of Cj1 cells for infection</i> .....	90
2.12.2.3	<i>Infection of RAW264.7 cells with Cj1 wild-type and T6SS mutants</i> .....	91
2.12.3	<i>C. jejuni - ZFE challenging assays</i> .....	93
2.12.3.1	<i>Preparation of ZFE for bacterial challenge</i> .....	93
2.12.3.2	<i>Preparation of C. jejuni cells for challenging ZFE</i> .....	93
2.12.3.3	<i>Microinjection of ZFE with C. jejuni cells</i> .....	93
2.12.4	<i>C. jejuni - piglet challenging assays</i> .....	97
2.13	Raman spectroscopy .....	98
2.13.1	Raman analysis of SL1344 wild-type grown in LB, LB with 70% D <sub>2</sub> O and MM.....	98
2.13.2	Raman analysis of J774A.1 .....	98
2.14	SRS and Confocal imaging .....	100
2.15	Imaging of ZFE .....	101
2.15.1	Staining of <i>C. jejuni</i> Cj11168H with 5-(6)-carboxyfluorescein-succinylester (FITC).....	101
2.15.2	Imaging of <i>AB fms:nfsB.mCherry</i> transgenic embryos inoculated with fluorescing Cj11168H .....	101
2.16	Electron microscopy (EM) for visualisation of <i>C. jejuni</i> capsule .....	102
<b>Chapter 3: Raman microscopy of <i>S. Typhimurium</i> SL1344 within mouse macrophage-like cells J774A.1 .....</b>		<b>103</b>
3.1	Introduction .....	104
3.1.1	Raman microspectroscopy .....	104
3.1.2	Aim of study.....	104
3.2	Results .....	105
3.2.1	Methodologies developed for Raman spectra collection and processing .....	105
3.2.2	Raman spectra of <i>S. Typhimurium</i> at different stages of growth.....	111
3.2.3	Analysis of normalised spectra and identification of wavenumbers to be used for Raman based imaging.....	114
3.2.4	Coherent Raman based imaging.....	126
3.2.5	SRS imaging of deuterated bacteria .....	131
3.3	Discussion.....	139
<b>Chapter 4: Development of ZFE as an optically transparent infection model for <i>Campylobacter jejuni</i>.....</b>		<b>145</b>
4.1	Introduction .....	146

4.1.1	Animal models for <i>Campylobacter</i> .....	146
4.1.2	ZFE as infection model .....	147
4.1.3	Aim of study .....	147
4.2	Results .....	148
4.2.1	Determining the site of inoculation in ZFE for <i>Campylobacter</i> infection model .....	148
4.2.2	Determining the developmental stage of ZFE for <i>Campylobacter</i> infection model .....	151
4.2.3	Effects of culture conditions on infection of ZFE by <i>C. jejuni</i> .....	153
4.2.4	Effects of inoculation dose on infection of ZFE by <i>C. jejuni</i> .....	156
4.2.5	Testing of <i>Campylobacter</i> strains and mutants using the ZFE infection model .....	159
4.2.6	Imaging of ZFE challenged with <i>C. jejuni</i> .....	163
4.2.6.1	<i>Bright-field imaging</i> .....	163
4.2.6.2	<i>Fluorescence images</i> .....	166
4.2.6.2.1	<u>Reporter <i>C. jejuni</i> Cj11168H cells</u> .....	166
4.2.6.2.2	<u>FITC labelled <i>C. jejuni</i> Cj11168H cells</u> .....	173
4.3	Discussion .....	175
<b>Chapter 5: Identification of T6SS and construction of T6SS mutants in <i>Campylobacter jejuni</i></b> .....		<b>184</b>
5.1	Introduction .....	185
5.1.1	Identification of T6SS .....	185
5.1.2	Mutagenesis in <i>Campylobacter</i> .....	186
5.1.3	Aim of study .....	187
5.2	Results .....	188
5.2.1:	Identification of T6SS in <i>Campylobacter jejuni</i> strain Cj1 .....	188
5.2.2	Gene organisation of T6SS in <i>Campylobacter jejuni</i> strain Cj1 .....	194
5.2.3	Functionality of T6SS in <i>Campylobacter jejuni</i> strain Cj1 .....	196
5.2.4	T6SS mutants in <i>Campylobacter jejuni</i> strain Cj1 .....	201
5.2.4.1	<i>Construction of tssD and tssM mutants in Cj1</i> .....	201
5.2.4.2	<i>PCR screening of tssD and tssM mutants in Cj1</i> .....	208
5.2.4.3	<i>Checking of tssD and tssM mutants in Cj1 by Southern Blot</i> .....	220
5.2.4.4	<i>Checking of tssD and tssM mutants in Cj1 by sequencing</i> .....	224

5.2.4.5	<i>Mass spectrometry of Cj1ΔtssD(syn)::kan<sup>R</sup>_cas and Cj1ΔtssM(syn)::kan<sup>R</sup>_cas culture supernatants.....</i>	226
5.2.4.6	<i>Checking the expression of other T6SS components by reverse transcription PCR (RT-PCR) in Cj1ΔtssM(syn)::kan<sup>R</sup>_cas.....</i>	229
5.3	Discussion.....	233
<b>Chapter 6: Role of T6SS in <i>C. jejuni</i> strain Cj1 .....</b>		<b>240</b>
6.1	Introduction .....	241
6.1.1	Role of T6SS .....	241
6.1.2	Aim of study.....	242
6.2	Results .....	243
6.2.1	Growth rate of <i>C. jejuni</i> strain Cj1 wild-type and its T6SS mutants.....	243
6.2.2	The adhesion and invasion of macrophages by <i>C. jejuni</i> strain Cj1 wild-type and T6SS mutants.....	245
6.2.3	Infection of 28 hpf ZFE with Cj1 wild-type and T6SS mutants .....	247
6.2.4	Infection of newborn piglets with Cj1 wild-type and T6SS mutants.....	249
6.2.5	Detection of capsule in Cj1 wild-type under two growth conditions.....	251
6.3	Discussion.....	253
<b>Concluding remarks.....</b>		<b>259</b>
<b>References .....</b>		<b>266</b>

## List of figures

Figure 1. 1:	Schematic representation of type I to VIII secretion systems in Gram negative bacteria. Extracted from Desvaux <i>et al</i> , 2009.....	22
Figure 1.2:	Assembly of T6SS. Left: T6SS secreting "true" effectors proteins into target cells. ....	25
Figure 2.1:	Set-up for transferring DNA from gel onto Hybond N+ membrane. ....	76
Figure 2.2:	Site of inoculation in 28 hpf ZFE. Bacterial cells were delivered into yolk sac (A) or yolk sac circulation valley (B) via microinjection.....	96
Figure 3.1:	Raw and smoothed Raman spectrum collected from (A) <i>S. Typhimurium</i> SL1344 wild-type and (B) mouse macrophage-like cells J774A.1.....	107
Figure 3.2:	Smoothed and baseline subtracted Raman spectrum collected from (A) <i>S. Typhimurium</i> SL1344 wild-type and (B) mouse macrophage-like cells J774A.1.....	108
Figure 3.3:	Raman spectra of <i>S. Typhimurium</i> SL1344 collected at different focal point, (A) before and (B) after normalisation.....	110
Figure 3.4:	Growth curve of <i>S. Typhimurium</i> SL1344 wild-type in LB broth.....	112
Figure 3.5:	Raman spectra of <i>S. Typhimurium</i> SL1344 wild-type at various growth phases. ....	113
Figure 3.6:	Comparison of normalised Raman spectrum collected from <i>S. Typhimurium</i> SL1344 wild-type grown in LB broth at lag phase with mouse macrophage-like cells J774A.1.....	115
Figure 3.7:	Comparison of normalised Raman spectrum collected from <i>S. Typhimurium</i> SL1344 wild-type grown in LB broth at early log phase with mouse macrophage-like cells J774A.1.....	116
Figure 3.8:	Comparison of normalised Raman spectrum collected from <i>S. Typhimurium</i> SL1344 wild-type grown in LB broth at mid log phase with mouse macrophage-like cells J774A.1.....	117
Figure 3.9:	Comparison of normalised Raman spectrum collected from <i>S. Typhimurium</i> SL1344 wild-type grown in LB broth at stationary phase with mouse macrophage-like cells J774A.1.....	118
Figure 3.10:	Comparison of normalised Raman spectrum collected from <i>S. Typhimurium</i> SL1344 wild-type grown in minimal media pH 5.8 broth for 120 min with mouse macrophage-like cells J774A.1.....	119

Figure 3.11:	Comparison of Raman spectra from <i>S. Typhimurium</i> SL1344 wild-type grown for 120 min in LB and MM broth with mouse macrophage-like cells J774A.1.....	121
Figure 3.12:	Overlay Raman spectra of mouse macrophage-like cells J774A.1 and <i>S. Typhimurium</i> SL1344 wild-type at early-log growth phase in LB broth. ....	125
Figure 3.13:	SRS images of <i>S. Typhimurium</i> SL1344 wild-type at various wavenumbers. ....	127
Figure 3.14:	Confocal images of mouse macrophage-like cells J774A.1 infected with <i>S. Typhimurium</i> SL1344 <i>fliC::gfp</i> mutant at MOI of 100. ....	128
Figure 3.15:	SRS images of mouse macrophage-like cells J774A.1 infected with <i>S. Typhimurium</i> SL1344 wild-type at MOI of 100. ....	130
Figure 3.16:	Comparison of Raman spectra from <i>S. Typhimurium</i> SL1344 wild-type grown in media with and without deuterium oxide with mouse macrophage-like cells J774A.1. ....	132
Figure 3.17:	SRS images at various wavenumbers of <i>S. Typhimurium</i> SL1344 wild-type grown in LB broth made up with 70% Deuterium oxide and 30% water. ....	133
Figure 3.18:	Mouse macrophage-like cells J774A.1 infected with <i>S. Typhimurium</i> SL1344 wild-type and <i>fliC::gfp</i> mutant grown in LB broth made up with 70% Deuterium oxide and 30% water. ....	135
Figure 3.19:	SRS images of mouse macrophage-like cells J774A.1 infected with <i>S. Typhimurium</i> SL1344 wild-type grown in LB broth made up with 70% Deuterium oxide and 30% water, at MOI of 100. ....	137
Figure 4.1:	Mortality chart of ZFE challenged with <i>C. jejuni</i> strain Cj11168H wild-type at 24 hpi. ....	158
Figure 4.2:	Survival chart of ZFE challenged with <i>C. jejuni</i> strain Cj11168H wild-type and four mutants at 24 hpi. ....	162
Figure 4.3:	ZFE at 28 hpf with (insert) and without chorion. ....	164
Figure 4.4:	Uninfected ZFE at 52 hpf. ....	164
Figure 4.5:	Images showing various ZFE infected with <i>C. jejuni</i> , at 24 hpi. ....	165
Figure 4.6:	<i>C. jejuni</i> Cj11168H wild-type, CFP reporter, GFP reporter and YFP reporter cells. ....	167
Figure 4.7:	<i>E. coli</i> strains expressing CFP, GFP and YFP.....	168

Figure 4.8:	Images of Cj11168H GFP reporter cells and yolk sac of infected mCherry-macrophage ZFE. ....	171
Figure 4.9:	Images of yolk sac regions taken at 22 hpi of mCherry-macrophage ZFE infected with <i>C. jejuni</i> Cj11168H GFP reporter cells at OD <sub>600</sub> 1.....	172
Figure 4.10:	Broth grown Cj11168H wild-type cells (OD <sub>600</sub> ~10) were stained with 0.4 µg/ml 5-(6)-carboxyfluorescein-succinylester for 15 min, with constant mixing at room temperature. ....	174
Figure 4.11:	mCherry-macrophage ZFE infected with Cj111668H wild-type cells stained with FITC. ....	174
Figure 5.1:	Alignment of <i>C. jejuni</i> strain Cj1 contig scf_30956_10_contig_1 with contig scf_30956_20_contig_1 in Clone Manager version 7.....	191
Figure 5.2:	PCR confirmation of the fusion of contig scf_30956_10_contig_1 with contig scf_30956_20_contig_1 as predicted <i>in silico</i> .....	193
Figure 5.3:	Gene organisation of putative T6SS locus in <i>C. jejuni</i> strain Cj1.....	195
Figure 5.4:	Report from Antigen Profiler provided by Perbio.....	197
Figure 5.5:	Analysis of <i>C. jejuni</i> strain Cj1 culture supernatant by SDS-PAGE. ....	199
Figure 5.6:	Construction of Cj1 <i>tssD</i> and <i>tssM</i> mutants.. ....	203
Figure 5.7:	Illustration on regions primed by each primer sets in <i>C. jejuni</i> strain Cj1 (A) wild-type and two possible constructs of <i>tssD</i> mutant: (B) kan <sup>R</sup> _cas inserted in the same orientation as <i>tssD</i> and (C) kan <sup>R</sup> _cas inserted in the opposite orientation as <i>tssD</i> . ....	209
Figure 5.8:	PCR screening of <i>C. jejuni</i> strain Cj1 <i>tssD</i> replacement mutant, Cj1Δ <i>tssD</i> (syn)::kan <sup>R</sup> _cas with <i>tssD</i> _Flank forward and reverse primer...	210
Figure 5.9:	PCR screening of <i>C. jejuni</i> strain Cj1 <i>tssD</i> replacement mutant, Cj1Δ <i>tssD</i> (syn)::kan <sup>R</sup> _cas with <i>tssD</i> _In forward and reverse primer. ....	211
Figure 5.10:	PCR screening of <i>C. jejuni</i> strain Cj1 <i>tssD</i> replacement mutant, Cj1Δ <i>tssD</i> (syn)::kan <sup>R</sup> _cas with <i>tssD</i> _Flank forward and Kan_Out forward to determine orientation of kanamycin resistance cassette inserted. ....	211
Figure 5.11:	PCR screening of <i>C. jejuni</i> strain Cj1 <i>tssD</i> replacement mutant, Cj1Δ <i>tssD</i> (syn)::kan <sup>R</sup> _cas with <i>tssD</i> _Flank forward and Kan_Out reverse to determine orientation of kanamycin resistance cassette inserted. ....	212
Figure 5.12:	Illustration on regions primed by each primer sets in <i>C. jejuni</i> strain Cj1 (A) wild-type and two possible constructs of <i>tssM</i> mutant: (B) kan <sup>R</sup> _cas inserted in the same orientation as <i>tssM</i> and (C) kan <sup>R</sup> _cas inserted in the opposite orientation as <i>tssM</i> . ....	214

Figure 5.13:	PCR screening of <i>C. jejuni</i> strain Cj1 <i>tssM</i> replacement mutant, Cj1Δ <i>tssM</i> (syn)::kan <sup>R</sup> _cas with <i>tssM</i> _Flank forward and reverse primer. .....	215
Figure 5.14:	PCR screening of <i>C. jejuni</i> strain Cj1 <i>tssM</i> replacement mutant, Cj1Δ <i>tssM</i> (syn)::kan <sup>R</sup> _cas with <i>tssM</i> _In forward and reverse primer.....	215
Figure 5.15:	PCR screening of <i>C. jejuni</i> strain Cj1 <i>tssM</i> replacement mutant, Cj1Δ <i>tssM</i> (syn)::kan <sup>R</sup> _cas with <i>tssM</i> forward and Kan_Out forward to determine orientation of kanamycin resistance cassette inserted. ....	216
Figure 5.16:	PCR screening of <i>C. jejuni</i> strain Cj1 <i>tssM</i> replacement mutant, Cj1Δ <i>tssM</i> (syn)::kan <sup>R</sup> _cas with <i>tssM</i> forward and Kan_Out reverse to determine orientation of kanamycin resistance cassette inserted. ....	217
Figure 5.17:	Illustration on cutting sites for BspCNI and SpeI along <i>C. jejuni</i> strain Cj1 T6SS locus.....	221
Figure 5.18:	Digested of genomic DNA of <i>C. jejuni</i> strain Cj1 wild-type and T6SS mutants separated on 0.8% agarose gel and stained with SYBR <sup>®</sup> Safe stain post-electrophoresis. ....	222
Figure 5.19:	Illustration on location of Southern blot probe along <i>C. jejuni</i> strain Cj1 T6SS locus (green box). ....	222
Figure 5.20:	Southern blot of <i>BspCNI</i> digested genomic DNA of <i>C. jejuni</i> strain Cj1 wild-type, Cj1Δ <i>tssD</i> (syn)::kan <sup>R</sup> _cas and Cj1Δ <i>tssM</i> (syn)::kan <sup>R</sup> _cas.....	223
Figure 5.21:	Comparison of Sequence data of <i>C. jejuni</i> strain Cj1 wild-type, Cj1Δ <i>tssD</i> (syn)::kan <sup>R</sup> _cas and Cj1Δ <i>tssM</i> (syn)::kan <sup>R</sup> _cas. ....	225
Figure 5.22:	Analysis of <i>C. jejuni</i> strain Cj1Δ <i>tssD</i> (syn)::kan <sup>R</sup> _cas and Cj1Δ <i>tssM</i> (syn)::kan <sup>R</sup> _cas culture supernatant by SDS-PAGE.....	227
Figure 5.23:	SDS-PAGE of <i>C. jejuni</i> strain Cj1Δ <i>tssD</i> (syn)::kan <sup>R</sup> _cas and Cj1Δ <i>tssM</i> (syn)::kan <sup>R</sup> _cas cell pellet lysates.....	227
Figure 5.24:	Expression of unidentified gene FIG00469624 in opposite transcriptional orientation to <i>tssM</i> by RT-PCR. ....	230
Figure 5.25:	Expression of <i>fha</i> in same transcriptional orientation as <i>tssM</i> by RT-PCR. .....	230
Figure 5.26:	Expression of <i>tssM</i> by RT-PCR. ....	231
Figure 5.27:	Expression of <i>tssD</i> in opposite transcriptional orientation to <i>tssM</i> by RT-PCR.....	231
Figure 5.28:	Expression of <i>tssL</i> in same transcriptional orientation as <i>tssM</i> by RT-PCR. .....	232

Figure 5.29:	Expression of <i>tssI</i> in opposite transcriptional orientation to <i>tssM</i> by RT-PCR.....	232
Figure 6.1:	Growth curve of <i>C. jejuni</i> strain Cj1 wild-type, Cj1Δ <i>tssD</i> (syn)::kanR_cas and Cj1Δ <i>tssM</i> (syn)::kanR_cas. ....	244
Figure 6.2:	Percentage of <i>C. jejuni</i> strain Cj1 wild-type, Cj1Δ <i>tssD</i> (syn)::kanR_cas and Cj1Δ <i>tssM</i> (syn)::kanR_cas adhered to or invaded mouse macrophage cells RAW264.7.....	246
Figure 6.3:	Survival chart of ZFE infected with <i>C. jejuni</i> strain Cj1 wild-type, Cj1Δ <i>tssD</i> (syn)::kan <sup>R</sup> _cas and Cj1Δ <i>tssM</i> (syn)::kan <sup>R</sup> _cas at 24 hpi. ....	248
Figure 6.4:	Competitive index challenge performed on 2 groups of newborn piglets, 9 animals in each group.....	250
Figure 6.5:	Electron micrograph of <i>C. jejuni</i> cell stained with Alcian Blue for capsule detection. ....	252

## List of tables

Table 1.1:	Summary on the pros and cons of various animal models. ....	33
Table 1.2:	Summary on the characteristics of microscopy techniques.....	46
Table 2.1:	List of plasmids .....	58
Table 2.2:	List of bacterial strains .....	59
Table 2.3:	List of eukaryotic strains .....	60
Table 2.4:	List of the primers .....	61
Table 3.1:	List of wavenumbers ranges at which Raman signals between J774A.1 cells and SL1344 cells from different growth phases were determined to be significantly different. ....	122
Table 3.2:	List of wavenumbers selected for Raman based imaging. ....	124
Table 4.1:	ZFE were challenged with <i>C. jejuni</i> Cj11168H wild-type cells that were inoculated into CV of 30 or 52 hour post-fertilisation (hpf) embryos.....	150
Table 4.2:	ZFE were challenged with <i>C. jejuni</i> Cj11168H wild-type cells that were inoculated into YS of 28 or 52 hour post-fertilisation embryos.....	150
Table 4.3:	ZFE were challenged with <i>C. jejuni</i> Cj11168H or Cj81-176_CP wild-type cells that were inoculated into YS of 28 or 52 hour post-fertilisation embryos. ....	152
Table 4.4:	ZFE were challenged with <i>C. jejuni</i> Cj81-176_CP wild-type cells that were inoculated into YS of 28 or 52 hour post-fertilisation embryos.....	155
Table 4.5:	ZFE were challenged with <i>C. jejuni</i> Cj11168H wild-type cells that were inoculated into YS of 28 hour post-fertilisation embryos. ....	155
Table 4.6:	List of the number of ZFE tested for each infection dose. ZFE were challenged with <i>C. jejuni</i> Cj11168H wild-type cells that were inoculated into YS of 28-32 hour post-fertilisation embryos.....	158
Table 4.7:	ZFE were challenged with <i>C. jejuni</i> Cj1 or Cj11168H wild-type cells that were inoculated into YS of 28-32 hour post-fertilisation embryos. ....	161
Table 4.8:	ZFE were challenged with <i>C. jejuni</i> Cj11168H wild-type and mutants cells that were inoculated into YS of 28-32 hour post-fertilisation embryos. ...	161

Table 5.1:	Summary of <i>C. jejuni</i> strain Cj1 contig scf_30956_10_contig_1 and contig scf_30956_20_contig_1 annotation from MG-RAST.....	189
Table 5.2:	Assignment of T6SS components in <i>C. jejuni</i> strain Cj1 as annotated by MG-RAST to standardised T6SS nomenclature. ....	191
Table 5.3:	Mass spectrometry data on the analysis of <i>C. jejuni</i> strain Cj1 culture supernatant TCA protein precipitate.....	200
Table 5.4:	List of cloning fragments used in this study.....	204
Table 5.5:	List of plasmids used in this study. ....	205
Table 5.6:	List of strains used in this study. ....	207
Table 5.7:	List of fragments generated from <i>C. jejuni</i> strain Cj1 wild-type T6SS locus after digestion by restriction enzymes, BspCNI and SpeI, repectively. ....	221
Table 5.8:	An extract of mass spectrometry data on the analysis of <i>C. jejuni</i> strain Cj1 $\Delta$ tssM cell pellet lysate. ....	228

## List of abbreviations

PTU	1-phenyl 2-thiourea
FITC	5-(6)-carboxyfluorescein-succinylester
ACD	Actin cross-linking domain
ANOVA	Analysis of variance
APEC	Avian pathogenic <i>Escherchia coli</i>
ARC	Aquarium Research Centre
bp	Base-pairs
BWH	Bayesian Whittaker–Henderson
BSA	Bovine serum albumin
Cia	<i>Campylobacter</i> invasion antigens
CM	<i>Campylobacter</i> motility
CO <sub>2</sub>	carbon dioxide
C-D	Carbon-deuterium bond
C-H	Carbon-Hydrogen bond
CBA+	CBA and <i>Campylobacter</i> selective supplement, Skirrow
CBA-kan50	CBA supplemented with 50 µg/ml of kanamycin
CBA+/kan50	CBA+ supplemented with 50 µg/ml of kanamycin
cm	Centimetre
CARS	Coherent anti-stokes Raman scattering
CRS	Coherent Raman scattering
CFU	Colony forming unit
CBA	Columbia blood agar supplemented 5% defibrinated horse blood
cDNA	Complimentary deoxyribonucleic acid
CLSM	Confocal Laser Scanning Microscopy
COG	Conserved orthologous group
CFP	Cyan fluorescence protein
CDT	Cytolethal distending toxin
°C	Degree Celsius
DNA	Deoxyribonucleic acid
dNTP	Deoxyribonucleotide triphosphate
D <sub>2</sub> O	Deuterium oxide
Δω	Difference frequency
DMEM-1% FBS	DMEM supplemented with 1% fetal bovine serum
DMEM	Dulbecco's modified Eagle medium
U	Enzyme unit
ELISA	Enzyme-linked immunosorbent assays
E-CARS	Epi-detected CARS
FBS	Fetal bovine serum
F-CARS	Forward-detected CARS
FT-IR	Fourier transform infrared
GI	Gastrointestinal
gDNA	Genomic deoxyribonucleic acid
x g	g-force
GFP	Green fluorescence protein
G+C	Guanine plus cytosine
GBS	Guillain Barré syndrome

hr	Hour
hpf	Hours post-fertilisation
hpi	Hours post-infection
hyb	Hybridisation
HCl	Hydrochloric acid
IR	Infrared
kan <sup>R</sup> _cas	Kanamycin resistance cassette
kb	Kilo-bases
kDa	Kilo-dalton
kU	Kilo-unit
LSD	Least significant difference
LOS	Lipooligosaccharide
LPS	Lipopolysaccharide
LC	Liquid chromatograph
LB	Luria Bertani
MSS	Marine salt solution
µg	Microgram
µl	Micro-litre
µm	Micrometer
µM	Micro-molar
mg	Milligram
ml	Millilitre
mm	Millimetre
MQ	Milli-Q
MM	Minimal media
min	Minute
M	Molar
MHA	Muller Hinton Agar
MHB	Muller Hinton broth
MNGC	Multi-nucleated giant cell
MCS	Multiple cloning site
MOI	Multiplicity of infection
mRNA	Messenger Ribonucleic acid
ng	Nano-gram
nl	Nano-litre
nm	Nano-meter
NHP	Non-human primates
ORF	Open reading frame
OD <sub>590</sub>	Optical density at 590 nano-meter
PFA	Para-formaldehyde
P	Passage
%	Percentage
PBS	Phosphate buffered saline
PAGE	Polyacrylamide gel electrophoresis
PCR	Polymerase chain reaction
PAAR	proline-alanine-alanine-arginine
ω <sub>p</sub>	Pump frequency
Q-TOF	Quadrupole time-of-flight
RE	Restriction enzyme
RT	Reverse-transcription

rpm	Revolution per minute
RNA	Ribonucleic acid
rRNA	Ribosomal RNA
SSC	Saline-sodium-citrate
$\Omega$	sample's intrinsic molecular vibration
s	Second
NaCl	Sodium chloride
SDS	Sodium dodecyl sulfate
NaOH	Sodium hydroxide
SEM	Standard error of the mean
SRG	Stimulated Raman gain
SRL	Stimulated Raman loss
SRS	Stimulated Raman scattering
$\omega_s$	Stokes frequency
syn	synthetic
TCA	Trichloroacetic acid
TPEM	Two-photon excitation microscopy
T6SS	Type six secretion system
UoE	University of Exeter
UV	Ultraviolet
VBNC	Viable but non-culturable
V	Volt
v/v	Volume per volume
w/v	Weight per volume
WHO	World Health Organisation
YFP	Yellow fluorescence protein
YS	Yolk sac
CV	Yolk sac's circulation valley
ZF	Zebrafish
ZFE	Zebrafish embryo

**Chapter 1: Introduction to *Campylobacter* and Imaging of  
infection**

## 1.1 *Campylobacter jejuni*

*Campylobacter jejuni* is the principal bacterial cause of diarrhoeal disease in the developed world (Allos, 2001). In the course of infection, acute and self-limiting gastrointestinal illness develops and is characterized by diarrhoea, fever, and abdominal cramps (Allos, 2001). Clinical infection with *C. jejuni* and more rarely *C. coli* is called Campylobacteriosis and usually occurs after an incubation period of between two to five days following the ingestion of contaminated food or drink (Butzler and Oosterom, 1991; Dasti et al., 2010; Young et al., 2007; Zilbauer et al., 2008). An infection dose of as low as 500 organisms has been reported to cause infection in humans (Janssen et al., 2008; Young et al., 2007). Rarely, post-infection complications such as reactive arthritis, urticaria, erythema nodosum and Guillain-Barré syndrome (GBS) will occur once the primary *C. jejuni* infection has resolved (Hannu et al., 2002; Moore et al., 2005). The occurrence of GBS ranges from 0.6 to 4 cases per 100,000 (Vucic et al., 2009) and among these, *C. jejuni* infection preceding the development of GBS was reported to be approximately 30% (Allos, 2001; Hughes et al., 1999; Sivadon-Tardy et al., 2010). GBS is a type of autoimmune disease, where the immune system attacks the gangliosides on the peripheral nervous system (Israeli et al., 2010). The association between *C. jejuni* infection and GBS has made Campylobacteriosis a major public health issue (Moore et al., 2005).

### 1.1.1 Microbiology of *C. jejuni*

*Campylobacter* belongs to the epsilon class of proteobacteria (Young et al., 2007) which are spirally-curved, microaerophilic, Gram-negative bacteria (Peterson, 1994). As it shares similar morphology with *Vibrio* (spiral appearance) the organism was initially classified under the *Vibrio* genus by Theobald Smith in 1918 (Moore et al., 2005; Moore and Matsuda, 2002; Skirrow, 2006). However, in 1963, a new genus name *Campylobacter* was proposed, from the Greek "Campylo-", meaning "curved" and "bacter", meaning "rod" (Moore and Matsuda, 2002).

*Campylobacter* differs from *Vibrio* in that it utilises different carbon sources and its G+C content is also distinct (Moore et al., 2005; Moore and Matsuda, 2002). The G+C content of *C. fetus* ranges from 33-35% while *V. cholerae* ranges from 44-50% (Moore et al., 2005; Moore and Matsuda, 2002). *C. fetus* is not able to oxidise or ferment carbohydrates while *V. cholerae* can ferment glucose (Moore et al., 2005; Moore and Matsuda, 2002). *Campylobacter* is a motile organism with unipolar or dipolar flagellae (Allos, 2001). It is a slow growing organism and optimal growing temperature is 42°C under microaerophilic conditions of 5% (v/v) oxygen, 10% (v/v) carbon dioxide and 85% (v/v) nitrogen (Allos, 2001; Moore et al., 2005). Most *Campylobacter* are resistant to the antibiotics cephalothin, vancomycin, polymyxin and trimethoprim (Allos, 2001; Moore et al., 2005), and these are commonly used in selection media.

In the early days, *C. jejuni* were recovered from faecal specimens after membrane filtration (mean pore size of the filter was 0.65 µm) (Skirrow, 1977). *C. jejuni* being smaller in size was able to pass through the filter and was then plated onto non-selective media for culturing

(Skirrow, 1977). However, in this method, any bacterium that is similar or smaller in size would be able to pass through the filter as well. In 1977, owing to the naturally occurring antibiotic resistance properties of *Campylobacter*, Skirrow formulated a selective medium that contains vancomycin, polymyxin B and trimethoprim for culturing of *C. jejuni* and *C. coli* from faecal specimens (Skirrow, 1977), and the filtration procedure was abandoned. However, it has been reported that although Skirrow's medium was successful in isolation of *Campylobacter* from human faeces, when it was tested on other types of specimens from other sources (e.g. animals and avian), microorganisms other than *Campylobacter* were cultured (Bolton and Robertson, 1982), this led to development of a more refined selective medium, Preston medium, by Bolton and Robertson (Bolton and Robertson, 1982). In the Preston medium, vancomycin was replaced by rifampicin and actidione and results have shown that beside being more selective, it was also more sensitive as *Campylobacter* was isolated from more specimens as compared to Skirrow's medium (Bolton and Robertson, 1982). It has also been reported that most *C. jejuni* are able to hydrolyze hippurate, hence it is a commonly used biochemical assay used to differentiate *C. jejuni* from other bacteria (Harvey, 1980; Hébert et al., 1982).

### 1.1.2 Epidemiology and public health

The World Health Organisation (WHO) has reported that diarrhoea is a major problem around the world. Diarrhoea, a symptom of gastrointestinal infection, may last for a few days, or up to several weeks and severe diarrhoea may lead to death due to excessive water loss. Diarrhoea cases arising from gastrointestinal infections have been reported to cause 2.2 million deaths annually; the majority are children - especially those in developing countries where poor sanitation and hygiene are serious problems (Ali et al., 2003).

A vast number of pathogens, ranging from viruses to bacteria to parasites, for example protozoan and helminths, can cause diarrhoea. Among these pathogens (Ashbolt, 2004) the prevalence of *C. jejuni* induced diarrhoeal illness in both developed and developing countries; are often higher than *Salmonella* and *Shigella* induced cases (Ali et al., 2003; Allos, 2001; Blaser, 1997; Coker et al., 2002).

The prevalence of Campylobacteriosis in the United States has been estimated to be between 2.1 to 2.4 million cases in human annually (Altekruse et al., 1999). In the European Union, the reported incidence of Campylobacteriosis was higher than the reported incidence of Salmonellosis. In Germany, there are more than 60,000 reported cases annually (Allos, 2001; Dasti et al., 2010). In the United Kingdom, more than 64,000 cases of Campylobacteriosis were reported in Scotland, England and Wales in 2009. However, it was believed that the reported figure should be approximately 450,000 due to under-reporting (Strachan and Forbes, 2010). The reported figure represents a yearly rise of 30% in Scotland and 14% in England and Wales (Strachan and Forbes, 2010). *Campylobacter* is associated with approximately 5% of food-related deaths and responsible for about 17% of food-borne infections that require

hospitalisation (Dasti et al., 2010). This indicates that Campylobacteriosis is a significant public health burden.

In developed countries, the symptomatic disease Campylobacteriosis occurs in children and adults, with 2 age-peaks; first at less than a year old and a second peak at 15 to 44 years old. It had also been noted that occurrence of this disease is higher in males (Allos, 2001; Bessell et al., 2010): in developing countries, it predominantly affects young children of less than 2 years old (Ali et al., 2003; Allos, 2001; Blaser, 1997; Coker et al., 2002; Taylor et al., 1988).

*C. jejuni*, the most prevalent *Campylobacter* species causing human infection, can be found in several environmental reservoirs such as poultry and in surface water - in association with protozoans (Young et al., 2007). *C. jejuni* can be found in wild and domesticated animals for example poultry, and cattle, as normal intestinal flora. It may also be carried by household pets such as cats and dogs. Host animals can shed *C. jejuni* in faeces which may contaminate soil and surface water (Blaser, 1997). Transmission of *C. jejuni* to human could be through consumption of contaminated food and drink, for example undercooked chicken, raw milk, untreated water and barbequed foods, and through contact with infected or carrier animals (Altekruse et al., 1999).

In England and Wales, there is an annual peak in *Campylobacter* infection between May and June and an evaluation study was conducted on several factors as possible seasonal drivers: one indicated that transmission by flies could be a driving factor behind the seasonal trends (Nichols, 2005). This hypothesis was supported by studies that had shown that diarrhoea cases were reduced when flies population was controlled (Nichols, 2005). It has been suggested that due to the natural behaviour of flies, which patronise animal and human

excreta as well as food and drink for human consumption, these insects could be a vector for dissemination of the bacteria (Rosef and Kapperud, 1983). It has been proposed that flies could transmit the bacteria in one of four ways: i) carriage of bacteria on the hairs and surfaces of the fly's body; ii) bacteria sticking to the glandular hairs of the feet; iii) regurgitation of vomitus that contains bacteria; and iv) passage of bacteria through the alimentary tract which are then defecated out (Rosef and Kapperud, 1983). A study conducted by Rosef and Kapperud, showed that *C. jejuni* was isolated from 43.2% and 50.7% of the flies captured in pig and chicken farms respectively (Rosef and Kapperud, 1983).

Generally, the bacteria generally does not survive well outside the gut. It is sensitive to freezing, acidic conditions, disinfectant, oxygen and desiccation at high temperatures (Altekruse et al., 1999; Axelsson-Olsson et al., 2005). However, *C. jejuni* are often isolated from environmental water, such as wells and rivers, indicating that the bacteria has the capability of surviving in the environment. A study has shown that *C. jejuni* is able to survive within the vacuoles of *Acanthamoeba polyphaga* after internalisation (Axelsson-Olsson et al., 2005). A similar study has also demonstrated that some bacteria had entered a viable but non-culturable (VBNC) stage and were able to revert back to full culturability after passage through amoeba (Axelsson-Olsson et al., 2005). With the abundance of amoeba present in the environment, these findings suggest that the bacteria could take refuge in amoeba which act as a shield from harsh environmental conditions. Currently, isolation of *C. jejuni* from amoeba from the environment and the ability of the bacteria to infect a host after passage through amoeba have not been well reported.

### 1.1.3 Detection of *C. jejuni*

There are several approaches towards the detection of *Campylobacter*. Conventionally, detection of *C. jejuni* relied on culturing methods. The major disadvantages of culturing methodologies are: i) slow to obtain outcomes (in days) as *Campylobacters* are slow growing bacteria and phenotypic tests need to be performed for confirmation (Moore et al., 2005), ii) selection against less common species (e.g. *C. lari* and *C. upsaliensis*) (Moore et al., 2005), iii) inability to detect VBNC *Campylobacter*. In view of the various drawbacks of culturing methods for detection and diagnosis of *Campylobacter*, other more rapid approaches such as immunological-based detection, for example latex agglutination test and enzyme-linked immunosorbent assays (ELISA) and molecular-based assays, for example polymerase chain reaction (PCR) have been developed (Moore et al., 2005).

PCR is a very powerful method that can deliver fast and sensitive results. It is able to detect the presence of pathogens including those that have entered the VBNC stage unlike the culturing method. However, PCR assays: i) are usually quite expensive to perform; ii) their potential sensitivity could be limited by sample preparation steps prior to the assay (such as deoxyribonucleic acid, DNA, extraction step); iii) their performance could be hampered by factors present in the sample that inhibits the reaction from taking place; iv) they can not differentiate between live-dead cells (Moore et al., 2005). With regards to live-dead cell differentiation, enhancement of PCR to test for messenger ribonucleic acid (mRNA) could help to differentiate between live-dead cells (Moore et al., 2005).

In clinical laboratories, detection of leukocytes in faecal specimens of patients suspected of bacterial enteritis under bright-field microscopy is often a recommended test procedure.

However, the presence of leukocytes in faeces could be caused by a number of gastrointestinal pathogens such as *Salmonella* and *Campylobacter* (Paisley et al., 1982). Hence, Paisley *et al* explored on the possibility of using dark-field microscopy for the visualisation of *Campylobacter* motility (CM) as a rapid, simple, sensitive and specific methodology for diagnosis in faecal specimens (Paisley et al., 1982). However, their findings showed that the longer the time taken between CM observation and specimen collection could result in false negative outcomes, and the presence of other bacteria with similar motility, for example *Vibrio spp.* and *Pseudomonas spp.*, could lead to false positive results (Paisley et al., 1982).

#### 1.1.4 *Campylobacter jejuni* genomic information

The complete genome and plasmids sequencing of *C. jejuni* has shed some light into the factors which could participate in the bacterial pathogenesis. The bacteria has a small genome size of 1.6-2.0 megabases; and there are very few repetitive DNA sequences. (Dasti et al., 2010; Parkhill et al., 2000; Young et al., 2007). In general, the *Campylobacter* genome has only 25-33% of genes compared to *Escherichia coli*, and would likely consist of essential genes and a few auxiliary genes (Friis et al., 2010). In *C. jejuni* strain NCTC11168, the chromosome was predicted to encode 1,654 proteins and 54 stable RNAs (Parkhill et al., 2000). Around 61% of the genes are transcribed from the plus strand (Parkhill et al., 2000). There are two regions within the genome with low G+C content, and these two regions fall within the lipooligosaccharide (LOS) and extracellular polysaccharide biosynthesis cluster (Parkhill et al., 2000). It has only four repeated sequences, one of which was a ribosomal RNA operon (Parkhill et al., 2000). No functional inserted sequence element, transposons, retrons or prophages were found in the *C. jejuni* NCTC11168 genome, with the exception of Cj0752, which is similar to *Helicobacter pylori* IS605 tnpB (Parkhill et al., 2000). It was also observed that there are only a few gene operons or clusters (Parkhill et al., 2000). The presence of hypervariable sequences that consists of homopolymeric tracts was also observed (Parkhill et al., 2000; Young et al., 2007). Since the initial annotation of *C. jejuni* NCTC11168 genome in 2000, numerous literatures follows providing large amount of information. The genome of NCTC11168 was then re-analysed and re-annotated in 2007 (Gundogdu et al., 2007). The re-annotation reduces the total number of CDS from 1654 to 1643; made modification to the LOS, O-linked glycosylation and capsule loci; and added a N-linked glycosylation pathway that was not previously described (Gundogdu et al., 2007).

A plasmid, *pVir*, present in some but not all *C. jejuni* strains was previously reported to contain four open reading frames (ORF) and sequence information showed that it shared significant similarity to *H. pylori* proteins (Bacon et al., 2000). The sequence information indicated that the proteins encoded by three of the ORFs (*comB1*, *comB2* and *comB3*) are similar to *H. pylori* proteins involved in natural transformation and DNA uptake competency (Bacon et al., 2000). These proteins also shared some homology with components of a Type IV secretion system utilised by other pathogens, such as *Legionella pneumophila* and *Rickettsia prowazekii*, for transportation of proteins during intracellular survival (Bacon et al., 2000). The protein encoded by the fourth ORF (*virB11*) has the highest sequence identity with a *H. pylori* protein which is proposed to be part of a Type IV secretion system involved in virulence (Bacon et al., 2000). It was reported that *comB3* and *virB11* mutants had shown reduction in adhesion and internalisation of *C. jejuni* as compared to wild-type when infecting INT-407 cells (human embryonic intestine cells, with epithelial-like morphology) and resulting in less severe symptoms in the ferret model (Bacon et al., 2000). These plasmid encoded factors might play a part in *C. jejuni* pathogenesis; however, as only about 10% of clinical isolates harbour this plasmid, virulence must involve other mechanisms (Bacon et al., 2000; Bacon et al., 2002).

### 1.1.5 Pathogenesis of *C. jejuni*

Several factors encoded in the genome of *C. jejuni* have been identified that could participate in host cell invasion and pathogenesis (Dasti et al., 2010). Yet, unlike other diarrhoea causing pathogens, *C. jejuni* does not appear to express a large number of classical virulence factors (Dasti et al., 2010).

After gaining entry into the body system via the gastrointestinal (GI) tract, the bacteria must survive the acidic stomach environment (Butzler and Oosterom, 1991; Janssen et al., 2008) to reach and colonise the lower intestinal tract (Dasti et al., 2010). Inside the GI tract the first line of defence is formed by the mucus layer, in order to establish itself the bacteria harbours traits such as motility and a cork-screw shape to facilitate its penetration through the mucus layer and allow interaction with the epithelial cells (Young et al., 2007). The bacteria can then invade the epithelial cells via microtubule polymerisation and some strains require microfilament polymerisation as well (Young et al., 2007). The process of epithelial cells extending out pseudopods and enveloping the bacteria has been reported (Biswas et al., 2000). After internalisation the bacteria is contained within the vacuole, however its fate and activities involved in pathogenesis is still unknown (Young et al., 2007).

Two mechanisms used by *Campylobacter* during the course of infection have been proposed: the first mechanism suggested that adhesion of the bacteria to the intestine takes place followed by production of toxin that alters the intestine fluid absorption capability, which will then lead to secretory diarrhoea (Butzler and Oosterom, 1991; Janssen et al., 2008). The other mechanism proposed involved invasion and proliferation of the bacteria within the

intestinal mucosa, which would lead to inflammatory responses and eventually bloody diarrhoea (Janssen et al., 2008).

#### 1.1.5.1 Adhesion and invasion

In order to establish colonisation, factors involved in adhesion and binding are important (Dasti et al., 2010; Young et al., 2007). Several factors have been identified with adhesion or binding capability; fibronectin-binding outer membrane protein (CadF); autotransporter (CapA); periplasmic binding protein (Peb1) and surface exposed lipoprotein (JlpA). Mutagenesis has confirmed *cadF* as an important factor participating in pathogenicity (Dasti et al., 2010; Young et al., 2007). Besides binding to fibronectin that is present on the epithelial cells, CadF also activates host small GTPases Rac1 and Cdc42 leading to its internalisation by the host cell (Dasti et al., 2010).

Intracellular *C. jejuni* were observed from various tissue culture models - such as INT407 and Caco-2 cells (Dasti et al., 2010; Grant et al., 1993; Rivera-Amill et al., 2001; Wassenaar et al., 1991) - demonstrates the ability of the bacteria to invade cells. This is further strengthened with findings from experiments performed on the non-human primate *Macaca mulatta* which demonstrated that diarrhoeal disease is related to the bacteria's invasion ability (Dasti et al., 2010). However, different *C. jejuni* strains have varying ability to invade host cells (Newell et al., 1985). Several factors have been identified to play a part in this process, such as flagellum, LOS, *Campylobacter*-invasive antigens (Cia) and capsular polysaccharide.

#### 1.1.5.2 *Intracellular survival*

The ability to survive inside host cells after internalisation might be crucial in the establishment of disease. It has been reported that *C. jejuni* is able to survive inside phagocytic cells (murine peritoneal macrophages and human peripheral blood monocytes) for at least 6 days (Hickey et al., 2005; Kiehlbauch et al., 1985), whereas in the absence of phagocytic cells the bacterium lost viability after 2 days (Kiehlbauch et al., 1985). These findings suggested that phagocytosis promotes *C. jejuni* survival (Kiehlbauch et al., 1985). A separate study conducted by Day *et al* had demonstrated that a heme-containing catalase expressed in *C. jejuni*, conferring hydrogen peroxide resistance, contributed to the intracellular survivability of the bacteria within macrophages (Day et al., 2000). It has also been observed that the spiral bacteria changed morphology to a coccal form 4 to 8 hours after being internalised into vacuoles, and by 72 to 96 hours all internalised bacteria appeared in coccal form (Kiehlbauch et al., 1985). Although, this transformation process was not unique to internalised *C. jejuni* - it was observed that in the absence of phagocytic cells, the process started after 24 hours and was complete by 48 hours (Kiehlbauch et al., 1985). The intracellular coccal bacteria were recovered from phagocytic cells and were shown to be viable through culturing (Kiehlbauch et al., 1985).

Besides macrophages, *C. jejuni* has also been reported to be internalised by epithelial cells (Hep-2 cells) (De Melo et al., 1989). Like *C. jejuni* internalised by phagocytic cells, the morphology of the bacteria changed from a spiral to a coccal form inside epithelial cells (De Melo et al., 1989). However, unlike in phagocytic cells, the bacteria did not survive well. It had been observed that after 6 hours of incubation, the colony forming unit (CFU) count of internalised *C. jejuni* did not increase and after 12 hours, it dropped (De Melo et al., 1989).

The decreased CFU count coincided with the period when phagosome-lysosome fusion took place (De Melo et al., 1989): similar trends were observed by Day *et al* (2000) and Watson and Galán (2008). Day *et al* reported that the internalised bacteria underwent an initial death phase between 6 to 48 hours post-infection (hpi) (approximately 90% death), however, the survivors were able to multiply intracellularly by 72 hpi: although the total CFU count remained low (Day et al., 2000). Day *et al* had also demonstrated that, unlike in macrophages, the expression of catalase does not contribute to the survival of *C. jejuni* in epithelial cells (Day et al., 2000).

Watson and Galán observed that the total intracellular bacteria count dropped by approximately 500 fold from 4 to 24 hpi (Watson and Galan, 2008). However, further studies conducted by the team showed that the viability assessment through culturing was not a representation of true viable count as *C. jejuni* had entered the VBNC state (Watson and Galan, 2008). The bacterial cells in this state could not be enumerated by the standard culture approach. A live-dead staining method was used to determine the total number of viable intracellular *C. jejuni*, and results obtained showed that the viable number remained relatively constant between 4 to 24 hpi (Watson and Galan, 2008). Watson and Galán had also shown that when monkey kidney epithelial cell line (Cos-1) was infected with *C. jejuni*, the bacteria containing vacuoles did not fuse with lysosomes (Watson and Galan, 2008). Hence, their findings suggested that *C. jejuni* was able to survive within intestinal epithelial cells and avoid lysosome fusion (Watson and Galan, 2008). This finding contradicts previously reported work on the fate of *C. jejuni* after internalisation by epithelial cells (Day et al., 2000; De Melo et al., 1989).

In the same study, Watson and Galán also showed that the bacteria was not able to survive within bone marrow-derived macrophages as bacteria could not be recovered at 24 hpi and vacuoles containing *C. jejuni* were delivered to lysosomes (Watson and Galan, 2008). This finding again contradicts previously reported work on *C. jejuni* which had demonstrated that the bacteria could survive for at least 6 days within macrophages (Hickey et al., 2005; Kiehlbauch et al., 1985). The epithelial cells and macrophages used in Watson and Galán studies were from different sources to those previously reported, hence, it could suggest that *C. jejuni* interacts differently with host cells from different lineages.

## 1.1.6 Factors involved in virulence of *C. jejuni*

### 1.1.6.1 *Flagellum*

*C. jejuni* harbours a single unsheathed flagellum at either one or both poles (Zilbauer et al., 2008). The flagellum enables motility. Motility plays a vital role during the colonisation process. It allows the bacteria to overcome peristalsis and penetrate the mucous layer (Zilbauer et al., 2008). It has also been reported to participate in host cell invasion (Young et al., 2007). The flagellum is made up of O-linked glycosylated flagellin (Dasti et al., 2010). Defects in O-linked glycosylation lead to a loss of motility (Dasti et al., 2010). The role of flagella in invasion was originally uncertain (Novik et al., 2010), hence, *flaA* and *motA* mutants were constructed with the former being non-motile due to a lack of flagellin, and the latter, although non-motile, possessing complete flagellar structures. The results obtained demonstrated that motility is required for bacteria internalisation, but this process was not directly mediated by flagellin or proteins secreted via the flagellar apparatus, for example *ciaB* (Novik et al., 2010).

### 1.1.6.2 *LOS and capsule*

LOS and capsule are factors expressed in *C. jejuni* that might play a role in pathogenesis. Some structures of LOS in *C. jejuni* mimic human neuronal gangliosides and it was thought that this mimicry could be one of the factors leading to post-infection autoimmune disorders; such as GBS (Dasti et al., 2010; Young et al., 2007). The relatively short *O*-sidechain of the LOS has also been proposed to assist in penetration of the mucus layer inside the GI tract by

reducing the non-specific binding of the bacteria to the mucin glycoprotein (Young et al., 2007).

The potential for *C. jejuni* to synthesise capsule polysaccharide was only revealed after genome sequence information was obtained where *kps* genes, which could take part in synthesis of capsule, were identified (Karlyshev et al., 2000). The capsule on *C. jejuni* may enable serum resistance, epithelial cell adhesion, and invasion and colonisation in chicks or virulence in ferrets (Young et al., 2007; Zilbauer et al., 2008). It has been reported that capsule-deficient mutants show a reduction in invasion in *in-vitro* and ferret models, but show no differences from wild-type strain when colonising chicken gut (Zilbauer et al., 2008). This suggests that the participation of the capsule in interaction with host could be host-dependent. Besides involvement in interaction with host cells, the capsule could potentially provide protection to the bacteria against desiccation or infection by bacteriophages (Young et al., 2007).

#### 1.1.6.3 Toxins

The presence of transient watery diarrhoea leading to bloody diarrhoea suggests that bacterial toxins might play a role in this process (Dasti et al., 2010). In *C. jejuni*, cytolethal distending toxin (CDT) is the only verified toxin to date (Dasti et al., 2010). It was first identified in *C. jejuni* in 1987 (Johnson and Lior, 1988a). It is also produced by other *Campylobacter* such as *C. lari*, *C. coli*, *C. fetus* and *C. upsaliensis* (Dasti et al., 2010) and several other Gram-negative bacteria such as *Escherichia coli*, *Salmonella*, *Haemophilus ducreyi*, *Helicobacter* spp. and *Actinobacillus actinomycetemcomitans* (Cope et al., 1997; Haghjoo and Galan, 2004; Johnson and Lior, 1988b; Sugai et al., 1998; Young et al., 2000). CDT acts by arresting host

cells at G<sub>1</sub>/S or G<sub>2</sub>/M transition in the cell cycle, which prevents the cells entering mitosis and eventually leads to cell death (Young et al., 2007; Zilbauer et al., 2008). CDT is a holotoxin that is made up of 3 sub-units; CdtA, CdtB and CdtC (Dasti et al., 2010; Young et al., 2007; Zilbauer et al., 2008). CdtB is the active component of the CdtABC complex, showing DNaseI-like activity and may cause DNA damage after gaining entry to the cell nucleus (Dasti et al., 2010; Young et al., 2007), whereas CdtA and CdtC aid in the delivery of CdtB to the nucleus (Dasti et al., 2010). These two protein subunits possess lectin-like regions that are similar to the receptor-binding component of ricin - which is responsible for endocytosis (Dasti et al., 2010; Young et al., 2007). All three subunits are membrane-bound proteins, hence, CdtA and CdtC remain at the host cell membrane after delivery of CdtB subunit into the cytoplasm (Dasti et al., 2010; Zilbauer et al., 2008). Inside the cytoplasm, CdtB is transported via the Golgi apparatus to the endoplasmic reticulum and eventually gains access to the host cell nucleus; its path is aided by the nuclear localisation signal that it harbours (Dasti et al., 2010; Young et al., 2007). Although much is known about the role played by each of the subunits, the actual role of CDT in *C. jejuni* pathogenesis has not been determined, however, it has been suggested that it might be important in invasiveness and modulation of immune response (Dasti et al., 2010).

#### 1.1.6.4 *Protein secretion systems*

The active movement of protein from the site of synthesis across membranes to the exterior of the bacterial cell is an important process termed "protein secretion" (Desvaux et al., 2009). It needs to be carried out in a regulated and efficient manner. The secretion systems direct the delivery of the proteins just out of the bacterial cell into the exterior medium or into target cells (Coulthurst, 2013). This process may take place in either a one-step or two-step manner

(Coulthurst, 2013). Besides being a machinery for protein export, some secretion systems have also been shown to play a crucial role in virulence (Coulthurst, 2013). The types of secretion systems and the number of each secretion system harboured by the bacteria varies (Coulthurst, 2013).

Currently, there are eight such secretion systems - type one to eight - identified in Gram negative bacteria, Figure 1.1 (Desvaux et al., 2009). The type six secretion system (T6SS) is the most recently identified system and it secretes protein in a single step manner (Coulthurst, 2013). The type seven secretion system was previously called the chaperone-usher pathway in Gram negative bacteria (Desvaux et al., 2009). Similarly, the type eight secretion system was previously named the extracellular nucleation-precipitation pathway (Desvaux et al., 2009).

*C. jejuni* has been reported to harbour putative type two, three and four secretion systems. A typical type two secretion system comprise of a minimal of 12 proteins, and in *C. jejuni* strain 81-176, five out of the 12 proteins had been identified (Wiesner et al., 2003). The genes identified in strain 81-176 were similar to the type two secretion system genes involved in translocation of macromolecules such as pilus subunits, toxins and exoenzyme; and were suggested to promote natural transformation (Wiesner et al., 2003).

The flagellum in *C. jejuni* is also being used as a type three secretion system, involved in the secretion of *Campylobacter* invasion antigens (Cia) proteins into host cell cytosol (Neal-McKinney and Konkel, 2012). It has been reported that either one of the flagellar filament - FlaA or FlaB - is sufficient for secretion of Cia proteins via the flagellum (Konkel et al., 2004). Four Cia proteins - CiaB, CiaC, CiaD and CiaI - were secreted via the flagellum and

they played a role in secretion (CiaB), host cell invasion (CiaC), secretion of host chemokine (CiaD) and intracellular survival (CiaI) (Buelow et al., 2011; Christensen et al., 2009; Konkel et al., 1999; Neal-McKinney and Konkel, 2012; Samuelson et al., 2013).

A gene cluster consisting of 7 genes found in pVir of *C. jejuni* strain 81-176 were orthologs of *H. pylori* type four secretion system (Bacon et al., 2002). Type four secretion system had been described in various bacteria to be involved in DNA export, bacterial conjugation and protein secretion (Bacon et al., 2002).

Beside the three putative secretion systems, a T6SS had also been recently identified in *C. jejuni*.

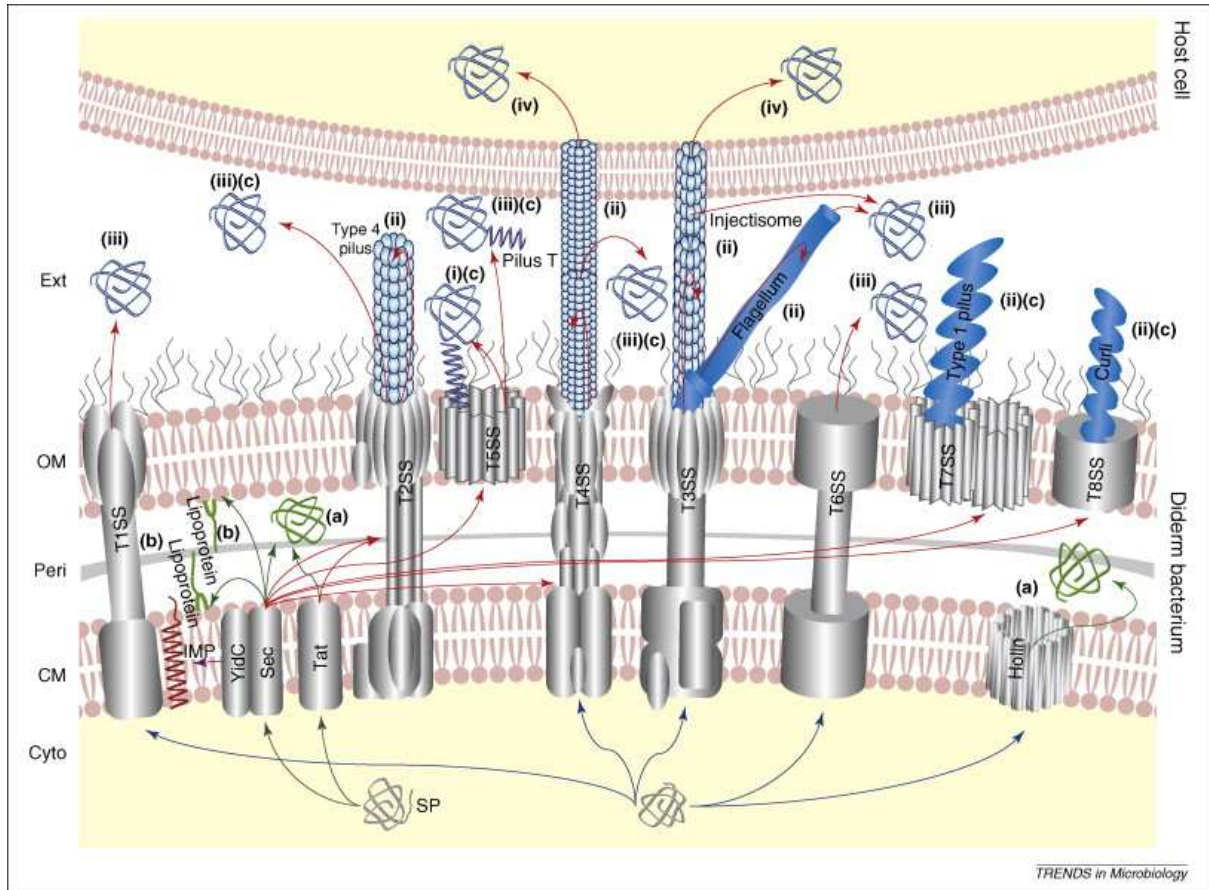


**Figure 1. 1:** Schematic representation of type I to VIII secretion systems in Gram negative bacteria. The secreted proteins could end up in four possible locations; (i) anchored to the outer membrane (OM) via Omp85 on cell surface; (ii) formed part of cell surface appendages; (iii) released into extracellular matrix (Ext); or (iv) injected into target host cell. The exported proteins could either be (a) released via cytoplasmic membrane (CM) protein into the periplasm; (b) anchored to either the cytoplasmic or outer membrane on the periplasmic side; or (c) translocated across the outer membrane. Black arrows - movement of proteins with N-terminal signal peptide (SP) targeted to cytoplasmic membrane. Blue arrows - movement of proteins without the N-terminal signal peptide. Red arrows - path of proteins towards secretion (indicated as blue proteins). Violet arrows - path of proteins towards integration as membrane protein (IMP). Green arrows - path of proteins towards exportation but not secretion (indicated as green proteins). Extracted from Desvaux *et al*, 2009.

#### 1.1.6.4.1 Type six secretion system (T6SS)

The prototypic T6SS was identified in 2006 following the study of a *vas* genes cluster in *Vibrio cholerae* (Pukatzki et al., 2006). It was shown to be involved in protein secretion and cytotoxicity towards macrophages and amoebae (Pukatzki et al., 2006). Prior to the official classification of such a system as the T6SS, gene clusters having similar functions and components had already been reported. The impaired nitrogen fixation (*imp*) locus in *Rhizobium leguminosarum* was reported to be involved in protein secretion and blocking of infection in pea plants (Bladergroen et al., 2003). The Hcp protein, a component of the T6SS, was reported a decade earlier in *V. cholerae* (Williams et al., 1996). Other components such as the *icmGCDJBF* locus in *Legionella pneumophila* (Purcell and Shuman, 1998) and *icmF* in *Salmonella enterica* (Folkesson et al., 2002) were also reported before the official T6SS classification came about. Initially, the T6SS was wrongly classified as a sub-type of T4SS due to the presence of two components - IcmF and DotU (Cascales, 2008; Filloux, 2013). The subsequent *in silico* screening of 506 bacterial genome sequences revealed that 176 T6SS loci were found in 92 different bacteria species (Boyer et al., 2009). Among the 176 T6SS loci screened, 13 conserved orthologous groups (COG) were found to be present at a frequency of more than 70 percent, which was significantly higher than other COGs screened (Boyer et al., 2009). A potentially functional T6SS would harbour the 13 COG proteins, termed "TssA to TssM", on a single locus, which make up the basic secretion apparatus (Coulthurst, 2013). A hallmark indicator for a functional T6SS in bacteria would be the presence of TssD, also commonly known as Hcp, in culture media (Pukatzki et al., 2007).

The T6SS is found mainly in Proteobacteria with the exception of the epsilon sub-group (Coulthurst, 2013). Around a third of genomes harbouring the T6SS genes were found to

have more than one T6SS cluster (Boyer et al., 2009). In *Yersinia* species 5 to 6 gene clusters of T6SS loci were identified. In *Burkholderia* species, it ranges from 2 to 6 T6SS gene clusters. In *Pseudomonas* species, 2 to 3 T6SS gene clusters have been found (Boyer et al., 2009).

In *Campylobacter* 4 components of T6SS (TssJ, TssK, TssC and TssD) were first detected in *C. concisus* cellular proteins by mass spectrometry (Kaakoush et al., 2011). There were no further reports on this secretion system in *Campylobacter* until Lertpiriyapong *et al* presented their work on a functional T6SS in *Campylobacter jejuni* in 2012 (Lertpiriyapong et al., 2012). To date, there are only two reports on functional T6SS in *Campylobacter jejuni*. In both studies, only a single copy of the T6SS locus was reported for each strain (Bleumink-Pluym et al., 2013; Lertpiriyapong et al., 2012).

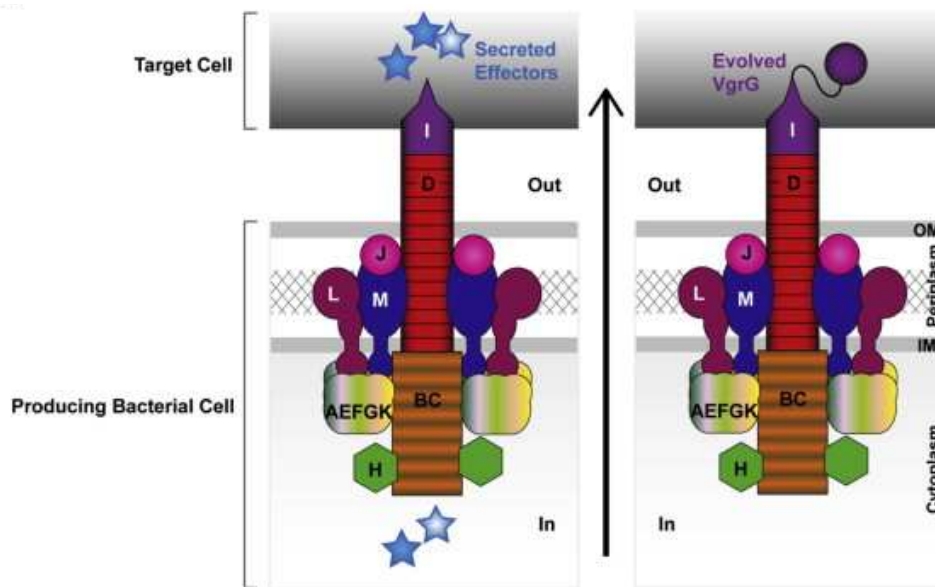


Figure 1.2: Assembly of T6SS. Left: T6SS secreting "true" effectors proteins into target cells. Right: T6SS utilising evolved VgrG to interact with target cell. Extracted from Coulthurst, 2013.

The T6SS machinery (Figure 1.1) has been commonly described as an inverted bacteriophage tail-like structure that operates in the reverse direction (Filloux, 2013; Leiman et al., 2009; Pukatzki et al., 2009; Silverman et al., 2012). Various components of T6SS, such as TssB, TssC, TssD, TssE and TssI, have been reported to have homology to bacteriophage proteins (Coulthurst, 2013; Filloux, 2013; Pukatzki et al., 2009; Silverman et al., 2012). TssD (commonly known as Hcp) and TssI (commonly known as VgrG) share structural similarity to gp19 and gp27/gp5 of bacteriophage protein (Filloux, 2013; Silverman et al., 2012). The gp19 protein is the basic unit of the phage tail tube (Filloux, 2013). A three-dimensional structure of TssD from *P. aeruginosa* showed that the protein formed hexameric units with a central channel of 40 Å (Mougous et al., 2006). These units were stacked to form a nanotube resembling the phage tail tube formed by gp19 (Leiman et al., 2009). The TssI protein of *V. cholerae* had been reported to be a fusion of phage tail protein gp27 and gp 5 at the N- and C-terminal respectively (Pukatzki et al., 2007). The phage gp27/gp5 complex is a puncturing device that creates a hole in the target cell membrane (Filloux, 2013). The gp27/gp5 complex sits at the end of the gp19 tail tube and the tail tube is sheathed by multiple copies of gp18 proteins (Filloux, 2013). Similarly in the T6SS machinery, TssI was proposed to cap the TssD tubule (Filloux, 2013; Silverman et al., 2012). It has been reported that an extension to the TssI spike, involving in attachment of effectors, was formed by proteins belonging to the proline-alanine-alanine-arginine (PAAR) repeat super-family (Shneider et al., 2013). Structural analysis of the PAAR repeat proteins bound to TssI showed that the proteins sharpen the tip of the TssI spike and plays an essential role in secretion and killing of target cells in *V. cholerae* and *Acinetobacter baylyi* (Shneider et al., 2013). The TssD tubule was sheathed by a complex made up of two proteins; TssB and TssC (Filloux, 2013; Silverman et al., 2012). The TssB/TssC complex resembles the phage gp18 (Filloux, 2013): the phage gp18 protein complex is contractile. When it contracts, it pushes the phage tail tube (gp19)

and the puncturing device (gp27/gp5) into the target cell (Filloux, 2013). The TssB/TssC complex has been reported to exist in two conformations, extended and contracted (Silverman et al., 2012). It has been suggested that the contraction of the sheath - TssB/TssC complex - provides the energy for translocation of proteins into target cells (Basler et al., 2012). With the structural similarity to phage tail structure, the assembly of TssD, TssI, TssB and TssC could potentially perform a similar structural function in the T6SS machinery. In bacteriophage, a group of proteins, gp6/gp25/gp53 formed a wedge around the gp27/gp5 puncturing device, and similarity between gp25 and TssE of T6SS has been demonstrated (Filloux, 2013).

There are other components of the T6SS machinery (TssJ, TssL and TssM), that do not have any resemblance to bacteriophage proteins (Filloux, 2013). TssM (commonly known as IcmF) is localised in the periplasm and is made up of two sub-domains (Silverman et al., 2012). It has been demonstrated to interact with TssJ - a lipoprotein anchored to the outer membrane (Kapitein and Mogk, 2013; Silverman et al., 2012). TssM also interacts with TssL - an inner membrane protein (Kapitein and Mogk, 2013; Silverman et al., 2012). TssJ has been reported to engaged in homomeric interactions and TssL has also been demonstrated to oligomerise (Silverman et al., 2012). Together, the TssL-TssM-TssJ complex forms a ring-like structure that spans the cell envelope to create a channel (Silverman et al., 2012). This trans-membrane complex forms a part of the T6SS assembly and anchors it to the cell envelope (Coulthurst, 2013). It has also been shown that TssM interacts with components of the bacteriophage tail-like structure TssB and TssD (Silverman et al., 2012). This suggests that the bacteriophage tail-like structure (TssD, TssI, TssB and TssC) of the T6SS machinery is embedded within the channel form by the TssL-TssM-TssJ complex (Kapitein and Mogk, 2013; Silverman et al., 2012). The TssB/TssC tubular complex contracts to push the TssD

tubule out of the cell (Silverman et al., 2012). The contracted TssB/TssC complex would need to disassemble and reassemble for the next round of contraction (Coulthurst, 2013; Silverman et al., 2012). The disassembly process is energy consuming and involves the AAA+-family ATPase protein, TssH (commonly known as ClpV) (Kapitein and Mogk, 2013).

In the two strains of *C. jejuni* reported to harbour a gene cluster of the T6SS, both lacks one of the core components, that is TssH (Bleumink-Pluym et al., 2013; Lertpiriyapong et al., 2012). However, although TssH is absent, the T6SS in both strains were demonstrated to be functional (Bleumink-Pluym et al., 2013; Lertpiriyapong et al., 2012). It has been reported that in the absence of TssH, the TssB/TssC complex was still able to contract to push the TssD tubule out of the cell (Zheng et al., 2011). As the complex could not disassemble due to the absence of TssH, it may render the T6SS less efficient (Zheng et al., 2011).

The T6SS has been reported to participate in the interaction of bacteria with eukaryotic cells and/or other bacterial cells within the niche in a cell-to-cell contact dependent manner (Coulthurst, 2013; Pukatzki et al., 2006; Suarez et al., 2010).

It has been reported in *V. cholerae* and *Aeromonas hydrophila* that the VgrG (TssI) component of its T6SS was involved in interacting with host cell actin (Pukatzki et al., 2007; Suarez et al., 2010). There are two types of VgrGs: canonical and evolved (Filloux, 2013). The former had no C-terminal extension, thus it was suggested that it could interact with free toxin and carry the effectors into target cell (Filloux, 2013). The evolved VgrG has an extension at the C-terminal with an effector domain and delivers the effector domain into target cells (Coulthurst, 2013; Filloux, 2013). It was thus suggested that the VgrG might play

a dual role; one in puncturing the target cell and the other in transportation of effectors (Filloux, 2013; Pukatzki et al., 2007).

In *V. cholerae*, which contains an evolved VgrG, VgrG-1 has an actin cross-linking domain (ACD) at the C-terminal (Pukatzki et al., 2007). The ACD in VgrG-1 has been shown to polymerise monomeric G-actin *in vitro* and leads to cytotoxicity in both macrophages and amoeba host (Pukatzki et al., 2007; Pukatzki et al., 2006). It was also reported that cross-linking of actin in phagocytic cells only takes place after the bacteria had been internalised which inhibited further phagocytosis (Ma et al., 2009). In an infant mouse model study the outcome of the animal challenged with *V. cholerae* lacking the ACD in VgrG-1 was shown to be similar to a non-infected control. There was no fluid accumulation, no cellular infiltration into the small intestine lumen and no induction of inflammatory responses observed (Ma and Mekalanos, 2010). The induction of the inflammatory response may enhance the survival and/or replication of *V. cholerae* in the gut (Ma and Mekalanos, 2010).

In *A. hydrophila*, another evolved VgrG was identified. Its VgrG1 has a vegetative insecticidal (VIP-2) domain at the C-terminal (Suarez et al., 2010). The VIP-2 domain possesses an ADP-ribosyltransferase activity that interacts with actin (Suarez et al., 2010). It has been reported that the VIP-2 domain of VgrG1 was responsible for the disruption of HeLa cells actin cytoskeleton, rounding up of the cell and an increase in cell apoptosis (Suarez et al., 2010). The action of VIP-2 on HeLa cells required direct contact between the bacterium and HeLa cells (Suarez et al., 2010).

In *Burkholderia* species, up to six clusters of T6SS are present (Boyer et al., 2009). T6SS-1 in *B. mallei* and *B. pseudomallei* (or named as T6SS-5 in *B. thailandensis*) has been shown to

play a role in virulence in rodent models (Burtneck et al., 2011; Schell et al., 2007; Schwarz et al., 2010). It has also been reported that T6SS-1 plays a role in facilitating actin-based motility, formation of multi-nucleated giant cell (MNGC), intracellular spreading through membrane fusion and intracellular growth (Burtneck et al., 2011; Burtneck et al., 2010; French et al., 2011). Membrane fusion required contact between intracellular bacteria and host cell membrane, and this process is facilitated by T6SS-1 (French et al., 2011). The cell-to-cell fusion and formation of MNGC in phagocytic and non-phagocytic cells has been reported as a trademark of *B. pseudomallei* infection (Harley et al., 1998; Kespichayawattana et al., 2000). In *B. cenocepacia*, it has been demonstrated that T6SS is involved in the disruption of the membrane of *B. cenocepacia* containing vacuoles (Rosales-Reyes et al., 2012). The disruption of the membrane facilitates the movement of proteins secreted by T2SS into the cytoplasm of macrophages, thereby ensuring bacterial survival inside macrophages (Rosales-Reyes et al., 2012).

In *C. jejuni*, the presence of T6SS in strain ATCC 43431 has been shown to increase the susceptibility of the bacteria to deoxycholic acid - a bile salt found in human intestine (Lertpiriyapong et al., 2012). In the same strain, the T6SS was required for adherence and invasion of both human epithelial and mouse macrophage cells. It was also reported to be required for colonisation in IL-10 deficient mice (Lertpiriyapong et al., 2012). In another study, the T6SS of another strain, strain 108, caused hemolysis of red blood cells in a contact dependent manner (Bleumink-Pluym et al., 2013). The efficiency of T6SS in the lysis of RBC was affected by the presence of the bacterium capsule polysaccharide (Bleumink-Pluym et al., 2013). The T6SS did not facilitate the bacterium in escaping from the vacuole in Caco-2 cells and did not cause cytotoxicity towards mouse macrophages (Bleumink-Pluym et al., 2013).

Besides interacting with host cells, some T6SS have been reported to act against other bacterial cells. For example, in *P. aeruginosa*, its HI-T6SS has been demonstrated to transport three toxins, Tse 1 to 3, into neighbouring bacterial cells (Russell et al., 2011). Tse1 and Tse3, a peptidoglycan amidase and a muramidase respectively, work at the periplasm of Gram negative cells and degrade the peptidoglycan (Russell et al., 2011). Tse2 is a cytoplasmic acting toxin that might inhibit growth in prokaryotic cells (Hood et al., 2010). The effects of the three toxins are neutralised by their respective immunity proteins, Tsi 1 to 3 (Hood et al., 2010; Russell et al., 2011). *P. aeruginosa* producing Tse1-3 also produce Tsi1-3 at the same time (Hood et al., 2010; Russell et al., 2011). Consequently, Tse1-3 is injected into neighbouring cells, which are killed if they do not have the ability to produce immunity protein - Tsi1-3. Similar mechanisms of the utilisation of toxins and immunity proteins have been reported in other bacteria, such as *V. cholerae*, *B. thailandensis* and *Serratia marcescens* (Coulthurst, 2013; Filloux, 2013). This anti-bacterial mechanism might help a bacterium to compete with other bacteria in a host or environmental niche, shaping the composition of the microbial population in a particular niche or within mixed species biofilm (Filloux, 2013).

The *C. jejuni* strain 108 was co-cultured with *E. coli* DH5 $\alpha$  and T6SS-negative *C. jejuni* strain 81116. It was reported that the T6SS-positive strain 108 had no growth advantage over bacterial strains without T6SS (Bleumink-Pluym et al., 2013). This indicates that the T6SS in strain 108 is unlikely to be involved in interaction with other bacteria.

### 1.1.7 Animal models

A good animal model is essential in understanding of disease and the patho-physiology of an infection. In understanding Campylobacteriosis, an ideal animal model should be able to reproduce the disease as it would occur in humans; the route of infection used should be similar to natural occurrence in humans, challenge dosage should be low, there should be reproducible results and cost of using the model is economical (Ruiz-Palacios et al., 1981). Several animal models that have been explored for understanding Campylobacteriosis are summarised in Table 1.1.

**Table 1.1: Summary on the pros and cons of various animal models.**

<b>Animal model</b>	<b>Pros</b>	<b>Cons</b>	<b>Reference</b>
<b>Bovine</b>	<ul style="list-style-type: none"> <li>▪ Exhibit diarrhoea via oral route</li> </ul>	<ul style="list-style-type: none"> <li>▪ Inoculum size not defined</li> <li>▪ High cost and maintenance</li> </ul>	<ul style="list-style-type: none"> <li>▪ Jones and Little, 1931a</li> </ul>
<b>Canine and feline</b>		<ul style="list-style-type: none"> <li>▪ Did not develop diarrhoea via oral route</li> </ul>	<ul style="list-style-type: none"> <li>▪ Prescott and Karmali, 1978</li> </ul>
<b>Avian</b>	<ul style="list-style-type: none"> <li>▪ Watery diarrhoea in young chicks via oral route</li> </ul>		<ul style="list-style-type: none"> <li>▪ Ruiz-Palacios <i>et al</i>, 1981</li> <li>▪ Sanyal <i>et al</i>, 1984</li> </ul>
<b>Murine</b>	<ul style="list-style-type: none"> <li>▪ Knock-out technology available</li> </ul>	<ul style="list-style-type: none"> <li>▪ Did not present similar clinical symptoms as in human infection</li> <li>▪ Presented gastroenteritis only in infant mice via intra-peritoneal route</li> </ul>	<ul style="list-style-type: none"> <li>▪ Young <i>et al</i>, 2007</li> <li>▪ Janssen <i>et al</i>, 2008</li> </ul>
<b>Newborn piglets</b>	<ul style="list-style-type: none"> <li>▪ Exhibit clinical and histological damages similar to human infection</li> <li>▪ Lack competing intestinal flora and maternal antibodies</li> </ul>	<ul style="list-style-type: none"> <li>▪ High cost and maintenance</li> </ul>	<ul style="list-style-type: none"> <li>▪ Babakhani <i>et al</i>, 1993</li> </ul>
<b>Ferret</b>	<ul style="list-style-type: none"> <li>▪ Able to colonise and induce human-like symptoms</li> </ul>	<ul style="list-style-type: none"> <li>▪ High cost and maintenance</li> <li>▪ No knock-out technology</li> </ul>	<ul style="list-style-type: none"> <li>▪ Young <i>et al</i>, 2007</li> <li>▪ Janssen <i>et al</i>, 2008</li> </ul>
<b>Rabbit</b>		<ul style="list-style-type: none"> <li>▪ Procedure involved surgery due to the use of a removable intestine tie</li> </ul>	<ul style="list-style-type: none"> <li>▪ Janssen <i>et al</i>, 2008</li> </ul>
<b>Non-human primate (NHP)</b>	<ul style="list-style-type: none"> <li>▪ Exhibit pathology and symptoms similar to human infection</li> </ul>	<ul style="list-style-type: none"> <li>▪ High cost and maintenance</li> </ul>	<ul style="list-style-type: none"> <li>▪ Jones <i>et al</i>, 2006</li> <li>▪ Russell <i>et al</i>, 1989</li> </ul>
<b><i>Galleria mellonella</i></b>	<ul style="list-style-type: none"> <li>▪ Ease of manipulation</li> <li>▪ Low cost and maintenance</li> <li>▪ Ethically acceptable</li> </ul>	<ul style="list-style-type: none"> <li>▪ Genome not sequenced</li> <li>▪ Limited genetic traceability</li> <li>▪ Lack mutagenesis methods</li> <li>▪ Does not have adaptive immunity</li> <li>▪ Long time to monitor killing</li> <li>▪ Oral route not possible</li> </ul>	<ul style="list-style-type: none"> <li>▪ Champion <i>et al</i>, 2010</li> </ul>

#### 1.1.7.1 *Bovine*

One of the earliest studies was conducted by Jones *et al.* They fed faeces from spontaneously infected cows exhibiting severe diarrhoea to calves and managed to induce similar disease outcomes (Jones and Little, 1931a). Pure cultures were isolated from the experimentally infected calves and then fed to other calves. These calves also developed similar diarrhoea and enteritis (Jones and Little, 1931a). In these studies, they observed that the jejunum was the primary locus of the infection. When the disease became chronic, the entire small intestine would be affected (Jones and Little, 1931b). Before the proposal of a new genus “*Campylobacter*”, the bacteria Jones *et al* worked on was classified as “*Vibrio*” and they noticed the slight differences in the morphology (length, number of coils, depth of coils) of the bacteria compared to the closely related groups (*Vibrio*): as the primary focus of infection for this bacteria was lesions in the jejunum, they proposed the name *Vibrio jejuni* (Jones et al., 1931). The disease progression in calves was reproducible in the studies conducted by Jones *et al* - and it also exhibited traits observed during human infection such as bloody diarrhoea, however, the inoculum size was not defined. At this point it was not clear if the calves would exhibit similar disease outcomes when challenged with a lower dosage. The cost of maintaining the calves as infection models would be high. These factors render calves as models less attractive.

#### 1.1.7.2 *Canine and feline*

Following Jones *et al*, another group tried to explore infection models using kittens and puppies. They were not successful as the animals failed to develop diarrhoea after being fed with the bacteria at a dose much higher than the amount that would evoke disease in humans

(Prescott and Karmali, 1978). The testing of the gnotobiotic dog as an infection model has also been reported. However, the diseases developed were milder compared to outcomes in human infection (Prescott et al., 1981). The cats and dogs models explored were not able to reproduce the disease outcomes as it would proceed in humans, thus were not considered to be good models.

#### 1.1.7.3 *Avian*

As avian species, especially chickens, are common reservoirs for *C. jejuni*, the possibility of using it as a model has been explored. It was reported that 36 to 72 hour old chicks develop watery diarrhoea with small oral inoculums, and the occurrence rate was high and reproducible, indicating that young chickens were highly susceptible to the bacteria (Ruiz-Palacios et al., 1981; Sanyal et al., 1984). Further reports state that older chickens were more resistant to the bacteria challenge thus avoiding diarrhoea (Ruiz-Palacios et al., 1981). Since *C. jejuni* does not cause disease symptoms in chickens, and is often regarded as a commensal bacteria, chickens are not the best models to use to understand pathogenesis mechanisms. However, they do remain a good model for the study of *C. jejuni* colonisation, for example *in vivo* survival (persistency) mechanisms (Janssen et al., 2008).

#### 1.1.7.4 *Murine*

Mice are commonly used for the study of bacteria infections. When used for Campylobacteriosis studies the results obtained were inconsistent. The animals did not present similar clinical symptoms to human infection (Young et al., 2007). There were successful attempts to induce gastroenteritis in infant mice through intra-peritoneal injection.

In these successful models the route of infection used was not the natural route (via ingestion), and the innate immune system of the mice had not fully developed, thus rendering them unsuitable model for studying immunological response (Janssen et al., 2008). A major advantage of the murine model is that the technology for creation of mice with defined deletions in innate or adaptive immunity components (e.g. NF- $\kappa$ B, IL-10, Nramp1 or MyD88 deficient mice) is established, thus this could help to elucidate the host factors involved in host protection (Janssen et al., 2008).

#### 1.1.7.5 Swine

Newborn piglets deprived of colostrum, have shown to be a model for *C. jejuni* pathogenesis studies (Babakhani et al., 1993). Piglets orally challenged with *C. jejuni* exhibited clinical and histological damages similar to human infection (Babakhani et al., 1993). In this model *C. jejuni* was observed to be internalised within the intestinal cells and the disruption of microvilli in the affected area was also observed (Babakhani et al., 1993). The competitive advantages of fucose transport and FeoB-mediated ferrous iron acquisition in *C. jejuni* during colonisation has also been demonstrated using colostrum deprived piglet infection model (Naikare et al., 2006; Stahl et al., 2011). The newborn piglet lacks a competing intestinal flora and, being deprived of colostrums, maternal antibodies are also absent (Babakhani et al., 1993). These are two advantageous features of this model, alongside the similarities of the swine digestive system to human system, makes it the preferred model for studying of Campylobacteriosis (Babakhani et al., 1993). However, the cost of using this model is high.

#### 1.1.7.6 *Ferret, rabbit and NHP*

Some other animal models have been explored including ferret, rabbit and NHPs (Janssen et al., 2008; Young et al., 2007). In ferrets, *C. jejuni* was able to colonise and induce human-like symptoms, but the cost involved in the use of this model is high and knock-out technology for ferrets is not as established as in the murine models. This makes them a less attractive model for studies investigating host factor involvement (Young et al., 2007). There is another potential complication for use of ferrets. As wild ferrets prey on chicks they could acquire relative resistance to Campylobacteriosis (Janssen et al., 2008).

The rabbit model explored used a removable intestinal tie in adult rabbit, thus this procedure required surgery, hence was not commonly used (Janssen et al., 2008).

NHPs challenged with *C. jejuni* were shown to exhibit pathology and symptoms similar to human infection, colonisation, shedding in faeces and diarrhoea. Also results were reproducible (Jones et al., 2006; Russell et al., 1989). Unfortunately, NHPs are a very expensive as models.

#### 1.1.7.7 *Invertebrates*

In recent years, there has been interest in the use of invertebrates as a surrogate for vertebrate animal models. The attractive factors of using invertebrate systems are the ease of manipulation, lower cost and maintenance, and ethical acceptability (Mukherjee et al., 2010; Mylonakis et al., 2005). Larvae of *Galleria mellonella* (common name: Greater Wax Moth), have been used in several pathogenesis studies of human pathogens; for example

*Pseudomonas aeruginosa*, *Bacillus cereus* and *Listeria spp.* ((Mukherjee et al., 2010). It has also been demonstrated that larvae of *Galleria mellonella* are susceptible to *C. jejuni* infection. This host system has successfully been used to identify a new virulence factor (Champion et al., 2010), yet there are some limitations on the use of *Galleria mellonella*; i) the genome of this organism has not been sequenced, so it has limited genetic tractability; ii) there is a lack of well-established methods in mutant generation; iii) it does not have an adaptive immune system; iv) it requires a relatively long time to monitor the killing of larvae; v) there is an inability to assess oral infections (Mukherjee et al., 2010; Mylonakis et al., 2005).

#### 1.1.7.8 Zebrafish embryo as a possible infection model for Campylobacteriosis study

Zebrafish (ZF) have gained popularity for studying host-pathogen interactions studies. Successful models had been established for a range of pathogens including *Salmonella enterica* serovar Typhimurium (van der Sar et al., 2003), *Bacillus subtilis* (Phelps and Neely, 2005), *Mycobacterium* (Davis et al., 2002) and *Pseudomonas* (Clatworthy et al., 2009).

In *Mycobacterium* studies, disease progression in mouse models differs to that seen in human infection as granulomas were not observed (Wang, 2010). However, infected ZF embryos (ZFE) formed granulomas similar to those seen in human tuberculosis (Pozos and Ramakrishnan, 2004) making it an attractive model for study on granuloma formation. It has been reported that with the use of the ZFE model, granulomas had been shown to form when only innate immunity was developed - in the absence of adaptive immunity (Davis et al., 2002). Real-time imaging of infected ZFE had shown that the bacteria could be disseminated either through direct transfer between macrophages via the membrane tethers or when the

"clean" macrophage picks up bacteria that remained associated with dead macrophages (Davis et al., 2002).

Another study, which involved looking at *Salmonella* Typhimurium pathogenesis, ZFE were infected with wild-type cells and a lipopolysaccharide (LPS) mutant. The LPS mutant showed attenuation indicating the role of LPS in pathogenesis. In this study, real-time visualisation of infected embryos showed that some of the bacteria were lysed inside macrophages, but most of the bacteria remained viable and were able to replicate. Extracellular bacteria cells were observed to have migrated to remote regions where they replicated and formed micro-colonies. This finding addressed and answered a long standing anomaly with regards to the site of multiplication for *S. Typhimurium* in host organisms (van der Sar et al., 2003).

To date, there is no report on the use of ZFE as an infection model for *Campylobacter*. With the seemingly numerous advantages of ZFE models it would be worthwhile exploring the possibility. The infection model could perhaps help to answer a long standing question on the interaction between *C. jejuni* and monocytes *in vivo* (Young et al., 2007).

ZF provide several advantages as a model organism. They are relatively cheap to work with in terms of cost and maintenance; similar to invertebrate models. Also the storage space required for maintaining infected fish or embryos is minimal. ZF have a similar immune system (innate and adaptive) to human and other vertebrates (Phelps and Neely, 2005). They are easy to handle and its embryo develops outside the adult. The *ex vivo* embryo allows disease pathogenesis to be studied at different developmental stages as the immune systems establish in the organism (Phelps and Neely, 2005). Studies can be conducted at the 26

somites stage (~22 hours post-fertilisation, hpf), where macrophage-like cells are found within the yolk-sac (Herbomel et al., 1999) - also at later stages, when primitive granulocytes start to circulate (at 48 hpf) (Lieschke et al., 2001), or when mature neutrophils are found in different tissues (at 72 hpf) (Willett et al., 1999). Macrophages and neutrophils form an important part of the innate immunity system and macrophages in ZFE were shown to be involved in the clearing of bacteria inoculated into the embryo (Herbomel et al., 1999). Adaptive immunity does not mature until 4 to 6 weeks post fertilisation (Clatworthy et al., 2009). As innate immunity establishes prior to adaptive immunity in ZF development (Phelps and Neely, 2005), and with its *ex vivo* embryo development, it is possible to study host-pathogen interactions in ZFE at stages when only innate immunity is involved. This is not possible in other animal models. The participation of adaptive immunity could be studied when embryos are allowed to grow into adulthood (Phelps and Neely, 2005).

ZFE remains transparent for the first three weeks of their development and this property makes live and real-time visualisation of bacteria inside ZFE possible (Phelps and Neely, 2005). For example, colonisation of fluorescent labelled fish pathogen, *Vibrio anguillarum*, could be visualised in real-time and this was used to study mode and site of entry of this pathogen (O'Toole et al., 2004). The optical transparency property also allows real-time monitoring of interactions between bacteria and host immune cells (Davis et al., 2002; van der Sar et al., 2003).

ZF are genetically tractable with the ability to create transgenic lines by both forward and reverse genetic approaches (Howe et al., 2013). Its forward genetics surpasses reverse genetics due to its lack of embryonic stem cells and homologous recombination (Pozos and Ramakrishnan, 2004). Genetic manipulation tools are available for ZF. Specific host genes

could be knocked down to have a better understanding of their roles played during host-pathogen interaction. Transgenic lines with fluorescently tagged immune cells, such as GFP-expressing neutrophils and mCherry-expressing macrophage, are also available (Gray et al., 2011). They are used to track interaction between pathogen and host immune cells in real-time. GFP-neutrophils have been used to demonstrate its interaction with *Staphylococcus aureus* at 2 hours after the bacteria was inoculated into the embryo (Prajsnar et al., 2008). In addition, transient knockdown of specific host genes is achievable with the use of morpholinos (Nasevicius and Ekker, 2000; Trede et al., 2004).

The bacterium of interest is commonly inoculated into ZFE through microinjection. The blood stream, for example axial vein (van der Sar et al., 2003), yolk-sac circulation valley (Clatworthy et al., 2009) or yolk-sac (Prajsnar et al., 2008) are common sites of inoculation. Due to its low cost and minimal maintenance requirement, it makes the screening of large number of strains or mutants feasible. A major drawback to large-scale screening is that it is labour intensive. The embryos will continue to develop throughout the microinjection process. It is crucial to have all the embryos infected at developmental stage as close to each other as possible. This limits the number of embryos that can be injected within a set time frame. Automating the injection process would be a solution to this issue. It has been reported that an automated robotic microinjection system could inoculate 15 ZFE per minute and the embryos survival rate was 98% (Wang et al., 2007).

A point to note is that ZFE survive best in water temperatures ranging between 22°C to 33°C (Tobin et al., 2012). The embryos are commonly incubated at 28°C post-bacteria challenge. The incubation temperature might affect the expression of some temperature regulated bacterial virulence genes (Prajsnar et al., 2008).

## 1.2 Imaging of infection

The concept of direct observation of *C. jejuni* is advantageous as it can avoid the lengthy wait during culturing as well as multiple procedural steps from setting up immune and molecular-based assays. Fluorescence microscopy is a commonly used technique for cell visualisation (Rodriguez et al., 2006). However, the sample to be analysed would need to be fluorescing which often requires the introduction of a fluorescence molecule. The introduction of fluorescence is an invasive process; it might alter molecular properties, distribution and functionality of the target; it also raises the problem of quenching and photo-bleaching (Rodriguez et al., 2006): a non-invasive and chemically selective microscopy technique would be preferable - this was made possible with the coupling of vibrational spectroscopy (which includes Raman scattering) with an optical microscope known as "Raman microscopy" (Rodriguez et al., 2006). In this project, the two techniques (fluorescence and Raman microscopy) were used for the interrogation of interactions between bacteria and host cells or organisms.

### 1.2.1 Brief history of microscopy techniques

Microscopy aids the viewing of objects not visible to naked eyes. The first light microscope was most probably made in 1590 by Zaccharias Janssen and Hans Janssen. In later years, Antony van Leeuwenhoek (Parker, 1965) used the microscope to see small living structures such as yeast and protozoan. Robert Hooke described the presence of "cells" in cork after viewing under the microscope (Gest, 2005). After this, many researchers began to build more complex and powerful microscopes with a typical magnification of 1,000 times i.e. 100 times magnification from objective and 10 times magnification from eye piece. However, the resolving capability of light microscopy was restricted by the wavelength of white light, hence structures smaller than half the light wavelength (e.g.  $<0.25 \mu\text{m}$ ), could not be visualised (Barer, 1974). This criterion is actually due to Rayleigh, which specifies the minimum separation required between two light sources in order to obtain resolved image.

The limitation of white light microscopy has led to the development of higher resolution microscopes. This was achieved by moving away from the use of white light to electron beam in the development of electron microscopy in 1931 (Cosslett, 1962). Electron microscopy uses beams of electrons with a wavelength one hundred-thousandth of the white light wavelength, and when focused on a cell, the electrons will either be absorbed or scattered by the components within the cell and this is captured on to an electron sensitive plate as an image detector (Barer, 1974). Although this technology enables visualisation of structures of much smaller size, down to one angstrom, it requires extensive sample preparation and so, unlike light microscopy, it is not able to visualise real-time changes within the cell. Thus, although light microscopy does not have high resolving power, it remains the most widely used technique for microbial visualisation.

Along the lineage of optical microscopy development, several enhancements have been made to enable better visualisation of different types of samples. For example, phase contrast microscopy has enabled better visualisation of cells without staining; fluorescence microscopy enabled the visualisation of compounds either using their intrinsic fluorescence or, after the attachment of a fluorescent label. The resolution of the light microscope was maximised through the development of Confocal Laser Scanning Microscopy (CLSM) in 1978 by Thomas and Christoph Cremer (Cremer and Cremer, 1978). By passing the light through a pinhole, scattered light collection is minimised and three dimensional image stacks can be obtained by scanning the pinhole in three dimensions over the sample.

In 1989 Denk *et al.* (Denk et al., 1990) filed a patent on the invention of a new type of fluorescence microscope after integrating a laser scanning microscope and a mode-locked laser (generating pulses of near-infrared light), the "two-photon excitation microscopy (TPEM)". It has been demonstrated that TPEM is superior to CLSM as it allows imaging from thicker specimens and restricts photo-bleaching or photo-damage to the focal plane thereby allowing frequent interval of long period interrogation of the specimen (Periasamy et al., 1999; Squirrell et al., 1999). The limitation of this technology is that it is only suitable for fluorescent imaging and can not be used on highly pigmented specimens or specimens that absorb near-infrared light (Masters and So, 2004).

Raman scattering is the inelastic scattering of light due to excitation of vibrational modes in the target molecules. The spectrum emitted provides a chemical fingerprint of a material. The possibility of imaging the distribution of a particular bond in a sample has long been recognised, but Raman scattering is very weak and the imaging times were at first too long to

make this practicable. Coherent excitation of the vibrations offers increased sensitivity and a shift in paradigm took place when Duncan *et al.* (Duncan et al., 1982) used coherent anti-Stokes Raman scattering (CARS) in a microscopic system in 1982. However, its use in biological specimens did not take off until two decades later, when laser systems and techniques had developed (Rodriguez et al., 2006). This technique now provides a non-invasive, chemical selective and quantitative approach to imaging biological specimens, especially in living cells, which was not achievable in the previously discussed microscopy technologies.

The most recent development in imaging is the super-resolution microscopy. It is a form of light microscopy where live-cell imaging and three dimension reconstruction of the sample are possible (Huang et al., 2009); and had overcome the diffraction limit and is able to generate images down to 25 nm, a resolution close to that of electron microscopy (Biteen and Moerner, 2010). This is achieved by several approaches, namely: structured illumination, reduction of point spread function and activation of single fluorophore (Bhuvanendran et al., 2014).

Table 1.2 summarises characteristics of various microscopy techniques.

**Table 1.2: Summary on the characteristics of microscopy techniques**

<b>Type of Microscopy</b>	<b>Characteristics</b>
<b>White light</b>	<ul style="list-style-type: none"> <li>• Specimens need to be stained to provide contrast</li> <li>• Unable to perform live cell imaging unless with the use of intravital dyes</li> <li>• Features smaller than 0.25 <math>\mu\text{m}</math> cannot be visualised</li> </ul>
<b>Phase-contrast</b>	<ul style="list-style-type: none"> <li>• Specimens does not need to be stained</li> <li>• Able to perform live cell imaging</li> <li>• Features smaller than 0.25 <math>\mu\text{m}</math> cannot be visualised</li> </ul>
<b>Fluorescence</b>	<ul style="list-style-type: none"> <li>• Specimens need to be fluorescing</li> <li>• Specimens subjected to photo-bleaching and photo-cytotoxicity</li> <li>• Able to perform live cell imaging</li> <li>• Features smaller than 0.25 <math>\mu\text{m}</math> cannot be visualised</li> </ul>
<b>Confocal</b>	<ul style="list-style-type: none"> <li>• Specimens need to be fluorescing</li> <li>• Specimens subjected to photo-bleaching and photo-toxicity</li> <li>• Able to perform live cell imaging</li> <li>• Able to perform optical sectioning</li> <li>• Features smaller than 0.25 <math>\mu\text{m}</math> cannot be visualised</li> </ul>
<b>Two-photon</b>	<ul style="list-style-type: none"> <li>• Specimens need to be fluorescing</li> <li>• Specimens subjected to lesser extend photo-bleaching and photo-cytotoxicity as compare to Confocal</li> <li>• Able to perform optical sectioning</li> <li>• Able to image thicker specimens as compare to Confocal</li> <li>• Features smaller than 0.25 <math>\mu\text{m}</math> cannot be visualised</li> </ul>
<b>Electron</b>	<ul style="list-style-type: none"> <li>• Specimens need to be stained</li> <li>• Unable to perform live cell imaging</li> <li>• Able to image features down to one angstrom</li> </ul>
<b>Raman base</b>	<ul style="list-style-type: none"> <li>• Specimens do not need to be stained</li> <li>• Able to perform live cell imaging</li> <li>• Not subjected to photo-bleaching and photo-toxicity</li> <li>• Able to perform optical sectioning</li> <li>• Features detectable is dependent on the strength of the chemical bond vibrational signals</li> </ul>
<b>Super-resolution</b>	<ul style="list-style-type: none"> <li>• Able to perform live cell imaging</li> <li>• Able to perform three dimension reconstruction</li> <li>• Resolution down to 25 nm, close to electron microscopy</li> </ul>

### 1.2.2 Fluorescence microscopy

When fluorophores within a specimen are excited with incident light, they absorb the light energy and enter a singlet excited state. In this state the excited molecule is unstable and will have to emit the excess energy gain in order to return to its ground state. Energy is lost through vibration and release light energy in the form of fluorescence (Webb and Brown, 2013). There are three fundamental properties of a fluorophore: i) its ability to absorb light energy at a given wavelength; ii) the percentage of absorbed light energy released as fluorescence; iii) its photo-stability when in the excited state (Webb and Brown, 2013). An important drawback on the use of fluorophores is photo-bleaching. It occurs when the excited molecule enters triplet state resulting in non-reversible destruction of the fluorophore as it cannot cycle between ground and excited states. The triplet state also generates oxygen radicals that destroys the fluorophores and is toxic to living cells (Webb and Brown, 2013).

The first observation of fluorescence was made by Sir John Frederik William Herschel in 1845 when he observed that a colourless and transparent quinine solution exhibited a vivid blue colour when the solution was illuminated and observed under certain incident lights (Renz, 2013). In 1852, George Stokes observed that a mineral (fluorspar) emitted red light when illuminated with blue light and the emitted light was at a wavelength longer than the light used to excite it. He termed this observation "fluorescence" and the shift in wavelength as "Stokes shift" (Ghiran, 2011).

Along with the discovery of fluorescence properties in substances, improvement towards better image resolution in microscopy was also on-going. In 1873 Ernst Abbe demonstrated the limitation of using transmitted light and around 1886 the highest practical numerical

aperture of objective was achieved (Ghiran, 2011; Renz, 2013). The first fluorescence microscope was built by Carl Zeiss and Carl Reichert at the beginning of the twentieth century. In 1929 Ellinger and Hirt switched to the use of reflected light instead of transmitted light for visualisation of living organisms. They treated the live organism with fluorescent compounds, illuminated it with UV light and using interposed filters between the objective and eyepiece to reflect incident rays and transmit red-shift fluorescence light. Their approach set the foundation for modern fluorescence microscopy. Ways to label specimens with fluorophores were explored and in the early 1940s the development of fluorescent tagged antibodies was an important step forward for fluorescence labelling and microscopy. A major drawback of fluorescence labelling are that fluorophores attached to biological molecules might alter the properties or functions of the biological molecules (Rodriguez et al., 2006). By the 1990s, with the advancement of cloning technology, cloning of GFP, as well as development of its spectral variants, were made possible (Renz, 2013). To date epi-fluorescence microscopy and CLSM are two of the most commonly used type of fluorescence microscopy.

### 1.2.3 Vibrational spectroscopy

When light interacts with matter, the photons can either be absorbed or scattered (Petry et al., 2003). Absorption usually occurs when infrared (IR) and ultraviolet (UV) light sources are used (Petry et al., 2003). The absorption of IR photons will result in excitation of vibrational modes in molecules while absorption of UV photons will excite molecules to undergo electronic transition followed by emission of radiation, termed "fluorescence" (Petry et al., 2003). When light is scattered; the majority of the photons will be scattered with the same wavelength as the light source; this is known as "elastic scattering" (Petry et al., 2003). However, a small percentage of the photons will scatter in an inelastic manner where the frequencies of the scattered photons differs from that of the light source; this effect is termed the "Raman effect" or "Raman scattering" (Petry et al., 2003). This effect was first reported in 1928 (Raman and Krishnan, 1928).

Vibrational spectroscopy is based on the photoexcitation of chemical bonds on molecules (Rodriguez et al., 2006) and measures the vibrational energy of the excited bonds (Huang et al., 2004). When light is shone onto a molecule, electrons within the molecule move into an excited state. The distribution of electrons around the atomic nuclei become distorted and this leads to various types of chemical bond resonance such as bending, stretching and rotating (Rodriguez et al., 2006). The chemical bond resonant frequencies are independent of the electric field applied, but when the applied electric field matches a particular resonant frequency a significant amount of the energy will be absorbed which will then be distributed to other parts of the molecule, or released as low energy photons (Rodriguez et al., 2006). There are two widely used techniques in vibrational spectroscopy (Huang et al., 2004); i) fourier transform infrared (FT-IR) spectroscopy; ii) Raman spectroscopy. The main

difference between these two is that FT-IR measures absorption of light while Raman spectroscopy measures Raman scattering (Huang et al., 2004). IR requires long wavelengths to excite a sample. Water molecules present in the sample will absorb strongly thereby masking potential frequencies of interest (Müller and Zumbusch, 2007; Rodriguez et al., 2006). These factors cause IR to have poor spatial resolution this method is thus less favourable for biological imaging (Downes and Elfick, 2010; Müller and Zumbusch, 2007; Rodriguez et al., 2006). Raman spectroscopy, on the other hand, is relatively unaffected by the presence of water molecules, because the vibrational modes of water are relatively weak and well-defined so it is able to generate sharper, more distinguishable spectra of specific molecules (Huang et al., 2004).

#### 1.2.4 Raman spectroscopy

Raman spectroscopy is a non-invasive and label-free (Downes and Elfick, 2010) technique that uses light source in the visible or near infrared regions to excite a sample (Rodriguez et al., 2006). When a molecule absorbs energy from the light source (photons) it goes into an excited state and returns rapidly to a lower energy state that is above original ground state and still consists of vibrational energy. This is achieved by the emission of photons that are longer in wavelength as compared to the initial light source.

The Raman spectrum generated from excitation of chemical bonds is unique to each biological sample, therefore it could be used as a “chemical fingerprint” to differentiate between samples (Huang et al., 2004). By coupling the spectrometer to an optical microscope spectra can be obtained with cell-scale spatial resolution (Huang et al., 2010). In the Raman microscope a laser replaces the normal white light as the photon source and is focused on the sample through the microscope objective lens (Huang et al., 2004). Raman micro-spectroscopy is a non-invasive and non-destructive spectroscopic technique for acquisition of chemical signals from a small volume, such as single bacterial cell, and it provides the phenotypic classification with minimal physiological interference (Huang et al., 2004; Huang et al., 2010). It has been shown to discriminate between different bacteria species and differentiates between different stages of growth within each species tested (Huang et al., 2004). By obtaining spectra from a single cell it should be possible to distinguish between cells at different growth stages could enable the use of Raman microscopy for interrogation of metabolically active and dormant cells during host-pathogen interaction. These beneficial qualities of vibration spectroscopy could also potentially enable the examination of micro-organisms in their natural habitat (Huang et al., 2004).

The limitation is that because the Raman signal is so weak, long imaging times are required. More recent advances, for example, the development of CARS and stimulated Raman scattering (SRS) (Freudiger et al., 2011), may be able to overcome this.

### 1.2.5 Coherent Raman scattering (CRS) microscopy

CRS is a non-linear optical process - that is it has a non-linear dependence on the intensity of incoming light; and produce a coherent radiation. Through excitation with short pulses, this process can be exploited to allow fast Raman imaging (Alfonso-García et al., 2014). CRS generates its image based on vibrational Raman contrast, a phenomenon initially discovered in 1962 (Alfonso-García et al., 2014; Freudiger et al., 2008). Raman contrast is used as a contrast mechanism in label-free imaging of biological samples (Alfonso-García et al., 2014; Wang, 2010). Two synchronised pulsed laser sources are required to coherently excite the sample in order to generate the CRS signals (Alfonso-García et al., 2014; Freudiger et al., 2011; Wang, 2010). The two incident beams are set at pump frequency ( $\omega_p$ ) and Stokes frequency ( $\omega_s$ ) respectively to drives the chemical bond into motion (Alfonso-García et al., 2014). When the difference in frequency ( $\Delta\omega=\omega_p-\omega_s$ ) between the pump and Stokes frequency matches the sample's intrinsic molecular vibration ( $\Omega$ ), new radiative frequencies are generated (Alfonso-García et al., 2014; Freudiger et al., 2008). These frequencies ( $\omega_p\pm\Omega$  and  $\omega_s\pm\Omega$ ) are CRS signals (Alfonso-García et al., 2014). There are four basic CRS signals; i) coherent Stokes Raman scattering -  $\omega_s-\Omega$ ; ii) coherent anti-Stokes Raman scattering (CARS) -  $\omega_p+\Omega$ ; iii) stimulated Raman gain (SRG) -  $\omega_p-\Omega=\omega_s$ ; iv) stimulated Raman loss (SRL) -  $\omega_s+\Omega=\omega_p$  (Alfonso-García et al., 2014; Freudiger et al., 2008). The two most commonly used techniques are CARS and SRS (Wang, 2010).

CARS is a version of Raman spectroscopy, hence it inherits all the beneficial capabilities of Raman spectroscopy (Rodriguez et al., 2006). Similarly, when applied to microscopic system, which uses multiple photons, it is able to perform optical sectioning capability, to distinguish from auto-fluorescence and to generate quantitative information (Robinson et al.,

2009; Rodriguez et al., 2006). There are several configurations of CARS; i) forward-detected CARS (F-CARS); ii) forward-detected polarisation CARS; iii) backward-detected or epi-detected CARS (E-CARS); iv) counter propagating CARS (Rodriguez et al., 2006). F-CARS will generate the strongest signal with features of interest being overwhelmed by non-resonant scattering, while E-CARS has reduced non-resonant background - but it loses signal strength (Rodriguez et al., 2006).

However, there are several disadvantages to CARS. In CARS a non-resonant background signal is present when there is no vibrational resonance, resulting in limited sensitivity (Freudiger et al., 2011; Saar et al., 2010). Because of its complex pattern, this background signal is very difficult to subtract from the measured signal. The shape of the spectral peaks is also distorted and the signal intensity depends nonlinearly on bond concentration (Freudiger et al., 2008; Saar et al., 2010). These shortcomings are not present in SRS (Freudiger et al., 2011; Freudiger et al., 2008; Saar et al., 2010).

The improved sensitivity of SRS is close to the shot-noise limit and signals generated scale linearly with the concentration of chemical bonds within the sample volume (Freudiger et al., 2011). SRS also avoids image artefacts due to spectral distortions or coherent signal additions and achieve Raman signal amplification by stimulated excitation. In SRG the intensity of the Stokes beam experiences a gain, while in SRL the intensity of the pump beam experiences a loss. In SRS, SRG and SRL could not occur when  $\Delta\omega$  does not match  $\Omega$ . Thus, unlike CARS, it will not exhibit a non-resonant background (Freudiger et al., 2008). These features make SRS a preferable technique for imaging infection.

### **1.3 Project aims**

The central aim of the project was to develop tools to study host-pathogen interactions in the poorly understood bacterium, *C. jejuni*. First, work was undertaken to determine the molecular make-up of bacteria using Raman spectroscopy and to use the information for imaging host-pathogen interaction during infection. The next part of the project was to establish ZFE as an optically clear animal model for *Campylobacter* and to use it for interrogating infection. As T6SS was only recently identified in some *C. jejuni* strains its roles in interaction with eukaryotic host were studied.

## **Chapter 2: Materials and methods**

## **2.1 Bacterial strains, plasmids and primers**

All the plasmids, bacterial strains, eukaryotic host strains and primers used in this study are tabulated in Tables 2.1, 2.2, 2.3 and 2.4 respectively.

**Table 2.1: List of plasmids**

<b>Plasmids</b>	<b>Descriptions</b>	<b>Sources</b>
pWM1015	Kanamycin resistance, pWM1007 $\Delta$ lacZ $\Omega$ [(T1) <sub>4</sub> -P <sub>c</sub> -gfp- $\lambda$ t0], promoter: Campylobacter consensus promoter sequence (Wosten et al., 1998) with minor modifications within non-consensus regions to minimise formation of RNA secondary structures (Miller et al., 2000)	USDA-ARS laboratory
pWM1018	Kanamycin resistance, pWM1008 $\Delta$ lacZ $\Omega$ [(T1) <sub>4</sub> -P <sub>c</sub> -yfp- $\lambda$ t0], promoter: Campylobacter consensus promoter sequence (Wosten et al., 1998) with minor modifications within non-consensus regions to minimise formation of RNA secondary structures (Miller et al., 2000)	USDA-ARS laboratory
pWM1019	Kanamycin resistance, pWM1009 $\Delta$ lacZ $\Omega$ [(T1) <sub>4</sub> -P <sub>c</sub> -cfp- $\lambda$ t0], promoter: Campylobacter consensus promoter sequence (Wosten et al., 1998) with minor modifications within non-consensus regions to minimise formation of RNA secondary structures (Miller et al., 2000)	USDA-ARS laboratory
pUC57	Ampicillin resistance, multiple cloning site (MCS) within lacZ gene, plasmid size is 2710bp	GenScript
pUC_tssD(syn)	Cloning of tssD(syn) into MCS of pUC57 by EcoRV	GenScript
pUC_tssM(syn)	Cloning of tssM(syn) into MCS of pUC57 by EcoRV	GenScript
pGEM-Teasy	Ampicillin resistance, multiple cloning site (MCS) within lacZ gene, plasmid size is 3015bp	Promega
pGEM_tssD(syn)	Cloning of tssD(syn) into MCS of pGEM-Teasy by SpeI and NdeI	GenScript
pGEM_tssM(syn)	Cloning of tssM(syn) into MCS of pGEM-Teasy by SpeI and NdeI	GenScript
pGEM_tssD(syn)::kan <sup>R</sup> _cas	Cloning of kan <sup>R</sup> _cas into tssD(syn) in pGEM_tssD(syn) by BamHI	This study
pGEM_tssM(syn)::kan <sup>R</sup> _cas	Cloning of kan <sup>R</sup> _cas into tssM(syn) in pGEM_tssM(syn) by BamHI	This study
pJMK30	Ampicillin resistance, contains a kan <sup>R</sup> _cas within BamHI sites (source of kan <sup>R</sup> _cas)	Institute of Food Research, UK

**Table 2.2: List of bacterial strains**

Strains	Descriptions	Sources
<i>S. Typhimurium</i> SL1344 wild-type	NCTC13347	Lab stock
<i>S. Typhimurium</i> SL1344 <i>fliC::gfp</i>	NCTC13347, <i>fliC::gfp</i>	Lab stock
<i>E. coli</i> RM2282	DH5- $\alpha$ , pWM1015; kanamycin resistance	USDA-ARS laboratory
<i>E. coli</i> RM2285	DH5- $\alpha$ , pWM1018; kanamycin resistance	USDA-ARS laboratory
<i>E. coli</i> RM2286	DH5- $\alpha$ , pWM1019; kanamycin resistance	USDA-ARS laboratory
<i>C. jejuni</i> Cj11168H wild-type	Hypermotile variant of sequence strain NCTC11168	LSHTM
Cj11168H/ <i>cj0079</i>	Cj11168H Cytolethal distending toxin (CDT) mutant; kanamycin resistance	Lab stock
Cj11168H/ <i>cj1132c</i> to <i>cj1152c</i>	Deletion of lipooligosaccharide (LOS) biosynthesis region; Cj11168H LOS mutant; kanamycin resistance	Lab stock
Cj11168H/ <i>cj1339</i>	Cj11168H aflagellate mutant; kanamycin resistance	Lab stock
Cj11168H/ <i>cj1413</i>	Deficient in capsule production; Cj11168H acapsular mutant; kanamycin resistance	Lab stock
<i>C. jejuni</i> Cj11168H CFP reporter	Cj11168H, pWM1019; kanamycin resistance	This study
<i>C. jejuni</i> Cj11168H GFP reporter	Cj11168H, pWM1015; kanamycin resistance	This study
<i>C. jejuni</i> Cj11168H YFP reporter	Cj11168H, pWM1018; kanamycin resistance	This study
<i>C. jejuni</i> Cj81-176_CP	Clinical isolate	Lab stock
<i>C. jejuni</i> Cj1 wild-type	Clinical isolate from Thailand	Lab stock
Cj1 $\Delta$ <i>tssD</i> (syn)::kan <sup>R</sup> _cas	<i>tssD</i> in Cj1 wild-type was replaced with <i>tssD</i> (syn)::kan <sup>R</sup> _cas; kanamycin resistance	This study
Cj1 $\Delta$ <i>tssM</i> (syn)::kan <sup>R</sup> _cas	<i>tssM</i> in Cj1 wild-type was replaced with <i>tssM</i> (syn)::kan <sup>R</sup> _cas; kanamycin resistance	This study
<i>E. coli</i> Top10	Cloning strain used to hold plasmids	Invitrogen
Top10 pGEM_ <i>tssD</i> (syn)	Transformed pGEM_ <i>tssD</i> (syn) into chemically competent <i>E. coli</i> Top10; ampicillin resistance	This study
Top10 pGEM_ <i>tssM</i> (syn)	Transformed pGEM_ <i>tssM</i> (syn) into chemically competent <i>E. coli</i> Top10; ampicillin resistance	This study
Top10 pGEM_ <i>tssD</i> (syn)::kan <sup>R</sup> _cas	Transformed pGEM_ <i>tssD</i> (syn)::kan <sup>R</sup> _cas into chemically competent <i>E. coli</i> Top10; ampicillin and kanamycin resistance	This study
Top10 pGEM_ <i>tssM</i> (syn)::kan <sup>R</sup> _cas	Transformed pGEM_ <i>tssM</i> (syn)::kan <sup>R</sup> _cas into chemically competent <i>E. coli</i> Top10; ampicillin and kanamycin resistance	This study

**Table 2.3: List of eukaryotic strains**

<b>Strains</b>	<b>Descriptions</b>	<b>Sources</b>
Mouse macrophage-like cells J774A.1	ATCC®TIB-67™	Lab stock
Mouse macrophage-like cells RAW264.7	ATCC®TIB-71™	Lab stock
<i>Danio rerio</i> (zebrafish) WIK wild-type	Polymorphic relative to the TU line	ARC, University of Exeter (UoE)
<i>Danio rerio</i> (zebrafish) AB <i>fms:nfsBmcherry</i> transgenic	mCherry expression in skin xanthophores and macrophages; constructed from AB wild-type	University of Sheffield

**Table 2.4: List of the primers**

<b>Primers</b>	<b>Sequences (5'→3')</b>	<b>Application in this study</b>
<i>fha</i> _In_F	TCAATGCTTTTTGCATCCAC	Checking for <i>fha</i> expression in Cj1 wild-type and Cj1Δ <i>tssM</i> (syn)::kan <sup>R</sup> _cas
<i>fha</i> _In_R	AGCGGTGATGATTGCACTTT	Checking for <i>fha</i> expression in Cj1 wild-type and Cj1Δ <i>tssM</i> (syn)::kan <sup>R</sup> _cas
FIG_B_In_F	CTCGCGATGAATTTGGAAGT	Checking for FIG00469624 expression in Cj1 wild-type and Cj1Δ <i>tssM</i> (syn)::kan <sup>R</sup> _cas
FIG_B_In_R	TCGAAGTTCTTGC GGAAAAT	Checking for FIG00469624 expression in Cj1 wild-type and Cj1Δ <i>tssM</i> (syn)::kan <sup>R</sup> _cas
Kan_out_F	CATCCTCTTCGTCTTGGTAGC	Checking kan <sup>R</sup> _cas orientation in T6SS mutants with either <i>tssD</i> _Flank_F or <i>tssM</i> _F
Kan_out_R	TTGCCTTCTGCGTCCGGTTCG	Checking kan <sup>R</sup> _cas orientation in T6SS mutants with either <i>tssD</i> _Flank_F or <i>tssM</i> _F
Southern_Probe_F	TCATCTGCCTTTTCTTCTTCG	Probe for southern blot
Southern_Probe_R	CAATTGCGGCTTTTGAAGAT	Probe for southern blot
<i>tssD</i> _Flank_F	ATGCCTTCGATCAAGTCGAG	1) Check for double crossover in Cj1Δ <i>tssD</i> (syn)::kan <sup>R</sup> _cas 2) Checking kan <sup>R</sup> _cas orientation in T6SS mutants with Kan_out_F and Kan_out_R
<i>tssD</i> _Flank_R	ATGTGGGCGGTATTTCAATG	Check for double crossover in Cj1Δ <i>tssD</i> (syn)::kan <sup>R</sup> _cas
<i>tssD</i> _In_F	CAAGCGGTGCATCTACTGAA	1) Checking for deletion of <i>tssD</i> 2) Checking for <i>tssD</i> expression in Cj1 wild-type and Cj1Δ <i>tssM</i> (syn)::kan <sup>R</sup> _cas
<i>tssD</i> _In_R	G TTCAGATCCGCCACTTGTT	1) Checking for deletion of <i>tssD</i> 2) Checking for <i>tssD</i> expression in Cj1 wild-type and Cj1Δ <i>tssM</i> (syn)::kan <sup>R</sup> _cas
<i>tssL</i> _In_F	TTTCCGCCTAAAGTTTCATCA	Checking for <i>tssL</i> expression in Cj1 wild-type and Cj1Δ <i>tssM</i> (syn)::kan <sup>R</sup> _cas
<i>tssL</i> _In_R	TTTGGAGTTGCTTTTGCTTTC	Checking for <i>tssL</i> expression in Cj1 wild-type and Cj1Δ <i>tssM</i> (syn)::kan <sup>R</sup> _cas
<i>tssM</i> _F	TCAATGCTTTTTGCATCCAC	Checking kan <sup>R</sup> _cas orientation in T6SS mutants with Kan_out_F and Kan_out_R
<i>tssM</i> _Flank_F	TTTCCGCAAGAACTTCGAG	Check for double crossover in Cj1Δ <i>tssM</i> (syn)::kan <sup>R</sup> _cas
<i>tssM</i> _Flank_R	TTTGGAGTTGCTTTTGCTTTC	Check for double crossover in Cj1Δ <i>tssM</i> (syn)::kan <sup>R</sup> _cas
<i>tssM</i> _In_F	GGCATCTTTATTGCCTCCAA	1) Checking for deletion of <i>tssM</i> 2) Checking for <i>tssM</i> expression in Cj1 wild-type and Cj1Δ <i>tssM</i> (syn)::kan <sup>R</sup> _cas
<i>tssM</i> _In_R	CGCTTCATTGCAACCTGTTA	1) Checking for deletion of <i>tssM</i> 2) Checking for <i>tssM</i> expression in Cj1 wild-type and Cj1Δ <i>tssM</i> (syn)::kan <sup>R</sup> _cas
VgrG_Contig_20_10_F	TGAGCATGGAAGGGTTAAGG	1) Confirmation for scf_30956_20_contig_1 joining to scf_30956_10_contig_1 2) Checking for <i>tssI</i> expression in Cj1 wild-type and Cj1Δ <i>tssM</i> (syn)::kan <sup>R</sup> _cas
VgrG_Contig_20_10_R	TGTCTTTGTTTTCTCCTACAAACTC	1) Confirmation for scf_30956_20_contig_1 joining to scf_30956_10_contig_1 2) Checking for <i>tssI</i> expression in Cj1 wild-type and Cj1Δ <i>tssM</i> (syn)::kan <sup>R</sup> _cas

## 2.2 Bacterial cell culture

### 2.2.1 *Escherichia coli*

*E. coli* strains were propagated on Luria Bertani (LB) agar or in LB broth. When appropriate, the media were supplemented with either 50 µg/ml ampicillin or 50 µg/ml kanamycin. The agar cultures were incubated at 37°C while broth cultures were incubated at 37°C with agitation at 200 revolution per minute (rpm). The bacterial cells were revived from -80°C storage by streaking onto LB agar, passage one (P1); the cells were not propagated beyond 6 passages.

### 2.2.2 *Salmonella* Typhimurium

*S. Typhimurium* SL1344 wild-type and *fliC::gfp* were propagated on LB agar or in LB broth. When appropriate, the bacterial were also propagated in Minimal media (MM) broth pH 5.8 or LB broth where 70% of water was replaced by deuterium oxide (D<sub>2</sub>O). The MM broth was made up of 1X M9 Minimal Salt (Sigma Product no. M6030), 10 µM Magnesium chloride, 0.16% (w/v) glycerol and 0.1% (w/v) casamino acid. The agar cultures were incubated at 37°C while broth cultures were incubated at 37°C with agitation at 200 rpm. The bacterial cells were revived from -80°C storage by streaking onto LB agar, P1; the cells were not propagated beyond 6 passages.

### 2.2.3 *Campylobacter jejuni*

*C. jejuni* Cj11168H, Cj81-176\_CP and Cj1 wild-type and mutant strains were propagated on Columbia blood agar (Oxoid, Product code: CM0331) supplemented with 5% defibrinated horse blood (Oxoid, Product code: SR0050) (CBA) and *Campylobacter* selective supplement, Skirrow (CBA+), or in Muller Hinton broth (MHB). When appropriate, the CBA+ media were supplemented with 50 µg/ml kanamycin. The agar and broth cultures were incubated at either 42°C or 37°C in a microaerobic environment of 5% oxygen, 10% carbon dioxide (CO<sub>2</sub>) and 85% Nitrogen. The bacterial cells were revived from -80°C storage by streaking onto CBA+, P1; the cells were not propagated beyond 4 passages.

The quantification of *C. jejuni* cells were performed in serial dilutions; each dilution was spotted onto Muller Hinton Agar (MHA) plates in triplicate, 10 µl per spot. The plates were then incubated at 37°C under a microaerobic environment for about 48 hours before counting.

## 2.3 Eukaryotic cell culture

### 2.3.1 Mouse macrophage-like cells J774A.1 and Raw267.4

The macrophage-like cells, J774A.1 and RAW264.7, were propagated in Dulbecco's modified Eagle medium (DMEM) supplemented with 10% heat-inactivated fetal bovine serum (FBS). The cell line cultures were maintained in a humidified incubator aerated with 5% CO<sub>2</sub>. The cell lines were sub-cultivated when they reached between 70-80% confluence, in a ratio of 1:3 to 1:6, and spent media was replaced with fresh media every two to three days. The macrophage-like cells were revived from -80°C storage by seeding into a T25 flask with 10 ml of fresh media, P1; the cells were not propagated beyond 20 passages.

### 2.3.2 Zebrafish *WIK* wild-type and *AB fms:nfsBmCherry* transgenic line

The adult zebrafish were maintained by Aquarium Research Centre (ARC) at UoE.

## 2.4 Nucleic acid extraction

### 2.4.1 Genomic DNA (gDNA)

All gDNA used in this study was extracted using Promega's Wizard<sup>®</sup> Genomic DNA Purification kit according to the manufacturer's protocol with slight modifications. When gDNA was extracted from *C. jejuni* cells, cells from CBA+ plates were picked up using a sterile cotton swabs moistened with sterile phosphate buffered saline (PBS) into 2 milli-litre (ml) micro-centrifuge tubes containing 1 ml of PBS. Cells were dislodged from the swab into the solution. Cells in suspension were collected to the bottom of each tube through centrifugation at 16.1 thousand times g-force (16,100 x g) for 5 minutes (min) at room temperature. The cell pellets were dislodged into 600 microlitre (µl) of Nuclei Lysis Solution from the extraction kit. The remaining steps of genomic DNA extraction were carried out according to the manufacturer's protocol. The concentration of the extracted gDNA was determined by Nanodrop.

### 2.4.2 Plasmid DNA

All plasmid DNA used for electroporation in this study was extracted using Promega's PureYield<sup>™</sup> Plasmid Midiprep System according to the manufacturer's protocol. The volume of overnight cultures used was 100 ml. The extracted plasmid DNA was further concentrated by ethanol precipitation. A 1/10 volume of 3M sodium acetate at pH 5.2 was added to the extracted plasmid DNA followed by addition of 2.5 volume (volume calculated

after addition of sodium acetate) of ice-cold 100% ethanol. The mixture was then incubated at -20°C for a minimum of 30 min. After this, the mixture was centrifugated at 20,000 x g at 4°C for 15 min. The supernatant was discarded and 1 ml of 70% ice-cold ethanol was added to rinse the plasmid DNA pellet. The pellet was collected at the bottom of the tube by centrifugation at 20,000 x g at 4°C for 5 min. The supernatant was discarded and the pellet was air dried. Once dried, the pellet was resuspended in nuclease-free water. The concentration of the extracted plasmid DNA was determined by Nanodrop.

Plasmids used for ligation in this study were extracted using QIAprep Spin Miniprep Kit (Qiagen, Product code: 27104) according to the manufacturer's protocol

### 2.4.3 RNA

All RNA used in this study was extracted using MP Biomedicals Fast RNA<sup>®</sup> Pro Blue kit according to the manufacturer's protocol with slight modifications. The bacterial cell suspensions in RNA*pro*<sup>™</sup> solution were transferred into a tube containing Lysing Matrix B and subjected to three beats in a Precellys machine set to 6500 rpm for 20 seconds each. The cell suspensions were chilled on ice for 5 min between each beating. The RNA pellet was resuspended in 100 µl of RNA storage solution (Ambion, Product code: AM7001) at room temperature for 5 min. The concentration of the extracted RNA was determined by Nanodrop.

## 2.5 Mutant construction

### 2.5.1 Transforming plasmids into *E. coli* Top10 cells

The transformation of One Shot<sup>®</sup> Chemically Competent *E. coli* Top10 cells from Invitrogen, TOPO TA Cloning kit was performed according to the manufacturer's protocol with slight modifications. Either 5 µl of plasmid DNA of pGEM\_ *tssD*(syn) or pGEM\_ *tssM*(syn) rehydrated according to manufacturer's protocol - or 10 µl of ligated product for pGEM\_ *tssD*(syn)::kan<sup>R</sup>\_cas or pGEM\_ *tssM*(syn)::kan<sup>R</sup>\_cas was used instead of PCR products. When appropriate, the transformed cells were cultured on LB agar supplemented with either 50 µg/ml ampicillin or 50 µg/ml kanamycin. The resulted strains were Top10 pGEM\_ *tssD*(syn), Top10 pGEM\_ *tssM*(syn), Top10 pGEM\_ *tssD*(syn)::kan<sup>R</sup>\_cas and Top10 pGEM\_ *tssM*(syn)::kan<sup>R</sup>\_cas.

### 2.5.2 *C. jejuni* fluorescence reporters

#### 2.5.2.1 Making electro-competent *C. jejuni* cells

Two to three colonies of *C. jejuni* grown on CBA+ passage 1 (P1) plates were picked and streaked onto fresh CBA+ plates, which is the second passage (P2) of the cells. P2 plates were incubated under the same conditions, at 42°C for approximately a day. Cells from P2 plates were used to inoculate four fresh CBA+ plates as a third passage (P3) to obtain lawn growth after approximately a day. Cells were harvested from four P3 plates cultured

overnight at 42 °C under microaerophilic conditions on CBA+ plates using sterile cotton swabs moistened with MHB into 2 ml micro-centrifuge tube containing 1.5 ml of MHB. Cells were then collected at the bottom of the tube by centrifugation at 11,000 x g for 5 min at 4 °C. The cell pellet was washed three times with 1 ml of ice-cold 272 millimolar (mM) sucrose containing 15% (v/v) glycerol (filtered sterilised) and centrifuged at 11,000 x g for 10 min at 4 °C. After the final wash the cell pellet was re-suspended in 1 ml of sucrose-glycerol solution and aliquoted into ice-chilled 1.5 ml micro-centrifuge tubes, 50 µl each, and stored on ice ready for the electroporation reaction.

#### 2.5.2.2 *Transformation of competent C. jejuni cells*

A total of 50 µg of plasmid DNA either pWM1015 (containing green fluorescent protein, GFP), pWM1018 (containing yellow fluorescent protein, YFP) or pWM1019 (containing cyan fluorescent protein, CFP), was added to 50 µl of electro-competent *C. jejuni* cells, mixed with gentle tapping and incubated on ice for 30 min. After 30 min incubation the mixture was transferred to an ice-chilled electroporation cuvette (BioRad, Product code: 165-2082). The cells were pulsed at 2500 volt (V) with capacitance set to 25 micro-farad and resistance set to 200 ohms using the Gene Pulser Xcell™ Total System (BioRad, Product code: 165-2660). After pulsing the cuvette was returned immediately to ice and 100 µl of ice-cold S.O.C. medium (Invitrogen, Product code: 15544-034) was added to each cuvette. The transformed cells were transferred onto CBA plates. The cuvette was rinsed with another 100 µl of S.O.C. media and transferred onto the same plate. The cells were gently spread over the surface of the agar. The agar plates were incubated in an upright position at 42 °C, under microaerophilic conditions for 5 hr.

After 5 hr of incubation 500 µl of MHB was added to each plate and cells were gently scraped off the agar surface. The cell suspension was transferred onto three CBA plates supplemented with 50 µg/ml of kanamycin (CBA-kan50 plates) with 120 µl of cell suspension each. The plates were incubated at 42 °C under microaerophilic conditions until colonies were observed, or up to 5 days. Transformed colonies formed on CBA-kan50 plates were picked and streaked on to CBA+ plates supplemented with 50 µg/ml of kanamycin (CBA+/kan50 plates) and incubated under similar conditions for 2 days. The resulting strains were Cj11168H GFP reporter, Cj11168H YFP reporter and Cj11168H CFP reporter. The fluorescence signals of transformed cells were checked under the fluorescence microscope.

### 2.5.3 *C. jejuni* Cj1 T6SS mutants

#### 2.5.3.1 Digestion of *pGEM\_tssD(syn)*, *pGEM\_tssM(syn)* and *pJMK30*

The extracted plasmids DNA was digested in a 50 µl reaction containing 1 µl of 20U/µl *Bam*HI (New England BioLabs, Product code: R0136S), 5 µl of NE Buffer 3, 0.5 µl of 10 mg/ml bovine serum albumin (BSA), either 20 µg of *pJMK30* or 5 µg of *pGEM\_tssD(syn)* or *pGEM\_tssD(syn)* and topped up with nuclease-free water to final volume. The reaction mix was incubated at 37°C for an hour. The digested products were separated in a 1% agarose gel electrophoretically. Two bands were obtained from *pJMK30*, approximately 2.6 kilo-bases (kb) and 1.5 kb respectively. The smaller band of approximately 1.5 kb, consisting of the *kan<sup>R</sup>\_cas* was excised from the gel. Single bands were obtained from *pGEM\_tssD(syn)* and

pGEM\_*tssM*(syn) respectively and were excised from the gel. The excised bands were eluted from the gel using QIAquick Gel Extraction Kit (Qiagen, Product code: 28704) according to the manufacturer's protocol, with slight modifications. An additional PE buffer wash step was incorporated and final elution was carried out with 30 µl of nuclease-free water. Purified kan<sup>R</sup>\_cas and digested pGEM\_*tssD*(syn) and pGEM\_*tssM*(syn) were quantitated using the NanoDrop 1000 spectrophotometer.

#### 2.5.3.2 *Ligation of kanR\_cas to pGEM\_tssD(syn) and pGEM\_tssM(syn) and transformation into E.coli Top10 cells*

The kan<sup>R</sup>\_cas (insert) was ligated to digested plasmids (pGEM\_*tssD*(syn) and pGEM\_*tssM*(syn) respectively). The amount of insert DNA required per 100 ng of plasmid DNA was 150 ng, calculation based on ratio of 4:1 (insert:plamid) according to the formula below:

Amount of insert =

$$(((100 \text{ ng of plasmid DNA}) \times (\text{insert size: } \sim 1.5 \text{ kb})) / (\text{plasmid size: } \sim 4 \text{ kb})) \times 4$$

The ligation reaction mixture of final volume 20 µl contained 1 µl of 1-3 U/µl of T4 DNA Ligase (Promega, Product code: M1801), 2 µl of 10X Ligase buffer, 172.5 ng of kan<sup>R</sup>\_cas, 100 ng of either digested pGEM\_*tssD*(syn) or pGEM\_*tssM*(syn) and topped up with nuclease-free water to final volume. The positive control used digested pJMK30 vector and

kan<sup>R</sup>\_cas, while the negative control was nuclease-free water. The reaction mixtures were incubated at 16°C overnight. After overnight ligation the resulting plasmids were pGEM\_*tssD*(syn)::kan<sup>R</sup>\_cas and pGEM\_*tssM*(syn)::kan<sup>R</sup>\_cas respectively. 10 µl of each plasmids was added to chemically competent *E. coli* Top 10 cells according to section 2.5.1.

### 2.5.3.3 Transformation of competent *C. jejuni* cells

50 µl of either pGEM\_*tssD*(syn)::kan<sup>R</sup>\_cas or pGEM\_*tssM*(syn)::kan<sup>R</sup>\_cas plasmid DNA was added to the electro-competent cells, then gently tapped to mix and incubated on ice for 30 min. The amount of plasmid DNA used was 6.6 µg for pGEM\_*tssD*(syn)::kan<sup>R</sup>\_cas and 10.6 µg for pGEM\_*tssM*(syn)::kan<sup>R</sup>\_cas. Electro-competent cells and electroporation were performed as described in section 2.5.2.1 and 2.5.2.2 respectively. The resulting strains were Cj1Δ*tssD*(syn)::kan<sup>R</sup>\_cas and Cj1Δ*tssM*(syn)::kan<sup>R</sup>\_cas.

## 2.6 PCR

### 2.6.1 PCR for products less than 1000 base-pairs (bp)

All primers used in this study were designed using Primer3Plus (<http://www.bioinformatics.nl/cgi-bin/primer3plus/primer3plus.cgi/>). PCR was performed in 50 µl reactions containing 0.5 µl of 5 U/µl of Taq polymerase (NEB, Product code: M0273S), 5 µl of 10X NEB Taq reaction buffer, 1 µl of 10 mM of deoxyribo-nucleotides (dNTPs), 2 µl of 10 µM of forward primer, 2 µl of 10 µM of reverse primer, 37.5 µl of nuclease-free water and 2 µl of 1/10 diluted gDNA (from wild-type or mutants), plasmid DNA or first strand complementary DNA (cDNA). The PCR reaction mixture was subjected to initial denaturation at 94°C for 10 min, followed by 35 cycles of denaturation at 94°C for 30 seconds (s), annealing at 56°C for 1 min and elongation at 72°C for 2 min, and final elongation at 72°C for 7 min. gDNA from wild-type or plasmid DNA were used as positive controls; while nuclease-free water was used as negative controls. The products were visualised under UV light after they were run electrophoretically through a 1% agarose gel.

### 2.6.2 PCR for products more than 1000 bp

PCR was performed in 50 µl reactions containing 1 µl of 1U/µl of KOD Xtreme™ Hot Start DNA polymerase (Novagen®, Product code: 71975-3), 25 µl of 2X Xtreme buffer, 2 µl of 10 mM of dNTPs, 1.5 µl of 10 µM of forward primer, 1.5 µl of 10 µM of reverse primer, 17 µl of nuclease-free water and 2 µl of 1/10 diluted gDNA (from wild-type or mutants) or plasmid

DNA. The PCR reaction mixture was subjected to initial denaturation at 94°C for 2 min, followed by 35 cycles of denaturation at 98°C for 10 s, annealing at 56°C for 30 s and elongation at 68°C for 3 to 6.5 min (depending on product size). gDNA from wild-type or plasmid DNA were used as positive controls - while nuclease-free water was used as negative controls. The products were visualised under ultra-violet (UV) light after they were run electrophoretically through a 0.8% agarose gel.

### 2.6.3 Reverse-transcription (RT) PCR

5 µg of RNA were pre-treated with TURBO DNA-free™ kit (Ambion, Product code: AM1907) according to the manufacturer's protocol. 10 µl of TURBO treated RNA was used for reverse transcription to make first strand complimentary DNA (cDNA). The first strand cDNA was made using SuperScript™ III Reverse Transcriptase (Invitrogen, Product code: 18080-093) according to the manufacturer's protocol. The first strand cDNA was then used for PCR as described above in section 2.6.1. RNA without SuperScript™ III Reverse Transcriptase treatment was used as non-RT control.

## 2.7 Southern Blot

### 2.7.1 Digestion of gDNA

The extracted gDNA of Cj1 wild-type, Cj1 $\Delta$ *tsd*(syn)::kan<sup>R</sup>\_cas and Cj1 $\Delta$ *tsm*(syn)::kan<sup>R</sup>\_cas was digested in a 50  $\mu$ l reaction containing 5  $\mu$ l of 2U/ $\mu$ l *BspCNI* (New England BioLabs, Product code: R0624S), 5  $\mu$ l of NE Buffer 4, 0.5  $\mu$ l of 10 mg/ml BSA, 0.5  $\mu$ l of 2 mM S-adenosylmethionine, 5  $\mu$ g of gDNA and topped up with nuclease-free water to final volume. The reaction mix was incubated at 25°C for an hour. The enzyme was heat inactivated at 80°C for 20 min. The digested products were separated electrophoretically in a 0.8% agarose gel.

### 2.7.2 Depurination and denaturation DNA in gel

The agarose gel was depurinated in 250 mM hydrochloric acid (HCl) until the bromophenol blue marker changed from blue to yellow at room temperature with gentle shaking. After this, the gel was rinsed twice in Milli-Q (MQ) water. The DNA in the gel was then denatured in two changes of solution containing 0.5M sodium hydroxide (NaOH) and 1.5M sodium chloride (NaCl) for 15 min each at room temperature with gentle shaking. The gel was rinsed twice again using MQ water. The denaturation process was neutralised by soaking the gel in two changes of 0.5M Tris-HCl at pH 7.5 and 1.5M NaCl for 15 min each at room temperature. Finally the gel was equilibrated in 20X saline-sodium-citrate (SSC) buffer for 10 min.

### 2.7.3 Blotting to membrane

The denatured DNA in the gel were transferred onto a positively-charged nylon membrane, Hybond N+ (Amersham, Product code: RPN119B) according to the set-up illustrated in Figure 2.1.

The DNA in the gel was transferred to the membrane overnight at room temperature. After the overnight transfer, the membrane was baked at 80°C between two dry Whatman paper for two hours (hr) and the membrane was ready for hybridisation.

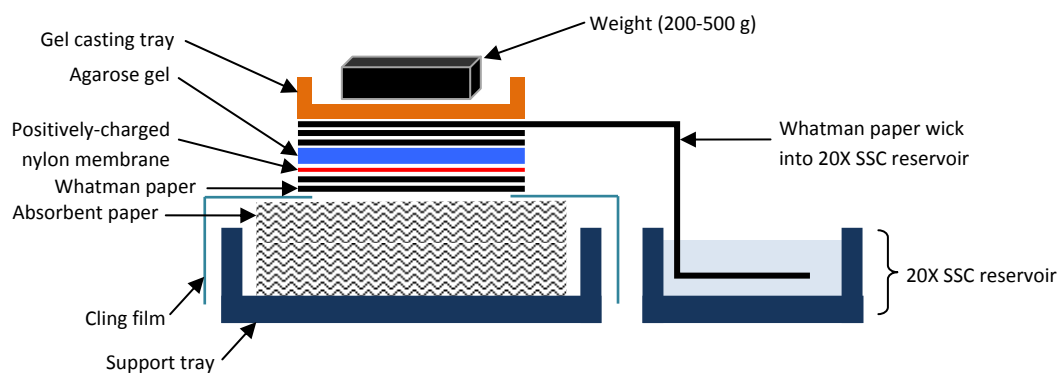


**Figure 2.1:** Set-up for transferring DNA from gel onto Hybond N+ membrane. Four pieces of Whatman paper and Hybond N+ membrane were cut to the size of the gel. A Whatman paper wick was cut to the width of the gel but extended in length, long enough to reach the 20X SSC reservoir. The gel-sized Whatman papers were soaked with 20X SSC buffer. The set-up was assembled as illustrated. Any air bubbles between the gel, membrane and Whatman paper were removed.

#### 2.7.4 Construction of a probe for the Southern blot

The probe was made using a PCR DIG Probe synthesis kit (Roche, Product code: 11636090910). The reaction mixture of final volume 50 µl contained 0.75 µl of Expand High Fidelity Enzyme mix, 5 µl of 10X DIG PCR buffer with magnesium chloride (MgCl<sub>2</sub>), 2.5 µl of 10X DIG synthesis mix, 2.5 µl of 10X dNTPs stock, 2 µl of Southern\_Probe\_F, 2 µl of Southern\_Probe\_R, 34.25 µl of nuclease-free water and 1 µl of 1/10 gDNA extracted from Cj1 wild-type cells or 1 µl of nuclease-free water as negative control. The reaction mixture was subjected to initial denaturation at 95°C for 2 min, followed by 40 cycles of denaturation at 95°C for 30 s, annealing at 56°C for 30 s and elongation at 72°C for 40 s, and final elongation at 72°C for 7 min. The products were viewed under UV light after they were run electrophoretically through a 1% agarose gel.

#### 2.7.5 Hybridisation of DIG-labelled probe to blotted membrane

The optimal hybridisation (hyb) temperature was 38.6°C, calculated based on the formula below:

$$T_m = 49.82 + 0.41(\%G+C) - 600/L$$

$$T_{hyb} = T_m - (20-25 \text{ } ^\circ\text{C})$$

- $T_m$ : melting point of probe-target hybrid  
(%G+C): % of G and C residues in probe sequence [26% for Southern\_Probe]  
L: length of hybrid in base pairs [322 bp for Southern\_Probe]  
 $T_{hyb}$ : optimal temperature for hybridisation of probe to target in DIG Easy Hyb buffer [33.6 – 38.6 °C for Southern\_Probe, used 38.6 °C]

The membrane was placed inside a hybridisation chamber (cylindrical drum) with the DNA side facing up (inwards of drum) and soaked with 25 ml of pre-warm DIG Easy Hyb buffer

and then incubated with gentle rotation in a pre-warmed oven set to 38.6°C for 30 min. 20 µl of DIG-labelled Southern\_Probe was added to 50 µl of nuclease-free water, heated to 100°C for 5 min, chilled immediately on ice and transferred to 10 ml of pre-warmed DIG Easy Hyb buffer. After the 30 min incubation of pre-hyb the pre-hyb buffer was discarded and replaced with buffer containing the Southern\_Probe. The membrane was incubated at 38.6°C overnight with gentle mixing. After overnight incubation the membrane was retrieved from the chamber into 200 ml of low stringency buffer made up of 2X SSC and 0.1% sodium dodecyl sulfate (SDS) and incubated at room temperature with shaking for 5 min. The low stringency buffer was then discarded and replaced with fresh buffer. The membrane continued to incubate in the fresh buffer for another 5 min at room temperature with shaking. After this, the membrane was transferred into high stringency buffer made up of 0.5X SSC and 0.1% SDS and pre-warmed to 65 °C. The membrane was incubated in the warmed high stringency buffer for 15 min with shaking at 65°C. The high stringency buffer was then discarded and replaced with fresh buffer. The membrane continued to incubate in the fresh buffer for another 15 min at 65°C with shaking.

#### 2.7.6 Detection of Southern\_Probe hybridised to blotted membrane

The hybridised membrane was washed and blocked using solution from the DIG Wash and Block Buffer Set (Roche, Product code: 11585762001). The membrane was transferred into 250 ml of 1X Washing Buffer with the DNA side facing up and incubated at room temperature with shaking for 2 min. The Washing Buffer was then discarded and replaced with 250 ml of 1X Blocking Buffer. The membrane was incubated in Blocking Buffer at room temperature for 30 min with shaking. The detection antibody, anti-Digoxigenin-AP

(Roche, Product code: 11093274910) was diluted 1:10,000 using 1X Blocking Buffer to a final volume of 50 ml. After the 30 min incubation in Blocking Buffer the buffer was discarded; the membrane was overlaid with 50 ml of the antibody solution and incubated for 30 min with shaking at room temperature. The antibody solution was discarded and the membrane was washed twice in 1X Washing Buffer, for 15 min each. The membrane was then equilibrated in 50 ml of 1X Detection Buffer for 3 min. After equilibration, the membrane was transferred onto a plastic film with the DNA facing up and CDP-*Star* (Roche, Product code: 12041677001) was added drop-wise onto the membrane till it was just sufficient to cover the entire surface. A second sheet of plastic film was placed over the membrane to spread the substrate evenly. The membrane sandwiched between the two plastic films was transferred to the BioRad gel imager with a ruler. The Chemi Hi Sensitivity mode was selected and the filter slider was moved to the "no filter" position. Images were captured and saved every minute between 600 and 1200 s of exposure.

## 2.8 SDS-Polyacrylamide gel electrophoresis (PAGE)

### 2.8.1 Precipitation of proteins in culture supernatant

Cj1 wild-type, Cj1 $\Delta$ *tssD*(syn)::kan<sup>R</sup>\_cas and Cj1 $\Delta$ *tssM*(syn)::kan<sup>R</sup>\_cas were cultured in 2 x 50 ml of MHB. After 24 hr incubation at 37°C, broth cultures from both flasks were pooled and transferred to two 50 ml centrifuge tubes; 47.5 ml of the culture each. Cells were collected at the bottom of the tubes by centrifugation at 11,000 x g for 15 min at 4 °C. Culture supernatants were carefully decanted into a 50ml syringe attached to 0.20 µm filter disc, and filtered into clean 50 ml tubes. Cell pellets were stored at -20°C. Proteins present in culture supernatant filtrate were extracted using trichloroacetic acid (TCA). The filtrate was split into four 50 ml centrifuge tubes, each containing 20 ml. 5 ml of 100% TCA was added to each tube and incubated on ice for 45 min to precipitate proteins present in the culture supernatant filtrate. After incubation on ice, precipitated proteins were collected at the bottom of each tube by centrifugation at 20,000 x g for 5 minutes at 4°C. The protein pellets were washed twice with ice-cold acetone, 10 ml per wash. After the second wash the pellets were dislodged into 5 ml ice-cold acetone in each tube and pooled. The precipitated proteins in the acetone suspension were collected with centrifugation. A millilitre of protein suspension was transferred to a clean 1.5 ml micro-centrifuge tube and centrifuged at 15,000 x g for 30 s at 4°C - supernatant was discarded and another millilitre of protein suspension was added to the tube. The process was repeated until the entire volume of protein suspension was spun down. After the last centrifugation acetone was discarded and the protein pellet was dried at approximately 90°C on a heat block for 30 s to 1 min. The protein pellet was rehydrated with 1 ml of PBS and stored at 4°C. The concentrations of each protein

samples were quantified by Pierce<sup>TM</sup> BCA Protein Assay kit (Thermo Scientific, Product code: 23227) according to the manufacturer's protocol with slight modifications. The volume of the protein samples used was 10  $\mu$ l and the volume of the BCA Working Reagent used per well was 180  $\mu$ l. Each protein samples was then adjusted to a concentration of 0.5 mg/ml.

### 2.8.2 Extraction of protein in cell pellet

The cell pellets (from 47.5 ml culture) of Cj1 wild-type, Cj1 $\Delta$ *tsd*(syn)::kan<sup>R</sup>\_cas and Cj1 $\Delta$ *tsm*(syn)::kan<sup>R</sup>\_cas were thawed and lysed in 2.5 ml of 1X BugBuster Protein Extraction Reagent (Novagen, Product code: 70750-3). 2.5  $\mu$ l of Benzonase<sup>®</sup> (Novagen, Product code: 70750-3) was added followed by 2.5  $\mu$ l of 1kU/ $\mu$ l of rLysozyme<sup>TM</sup> solution (Novagen, Product code: 71110-3). The mixtures were incubated at room temperature for 20 min on a rocking platform.

### 2.8.3 Separation of proteins in gel

The protein samples from culture supernatant and cell pellets were mixed with 4X NuPAGE LDS Sample Buffer (Invitrogen, Product code: NP0008) prior to loading. The final concentration of LDS Sample Buffer in each sample was 1X. The mixture was then heated at 95°C for 5 min and chilled on ice. 10-15  $\mu$ l of each mixtures was loaded into individual wells on pre-cast NuPAGE 4-12% Bis-Tris Gel 1.0 mm x 12 well (Novex, Product code: NP0322Box) assembled into a XCell SureLock<sup>®</sup> Mini-Cell according to the manufacturer's instructions. Protein markers, Perfect Protein<sup>TM</sup> Markers 10-225 kilo-Dalton (kDa) (Novagen,

Product code: 69079-3), were loaded into the first and last well on each gel, 5  $\mu$ l per well. The gels were set to run at 185 V for 35 minutes in 1X NuPAGE MES SDS Running Buffer (Invitrogen, Product code: NP0002) or until the blue dye reached the end of the gel. After electrophoresis the gel was rinsed three times in MQ water. The gel was stained with SimplyBlue™ SafeStain (Invitrogen, Product code: LC6060) according to the manufacturer's protocol. The microwave procedure was used for culture supernatant protein samples and the basic protocol was used for cellular protein samples. The images of the gel were captured using Odyssey CLx imaging system (LI-COR).

## 2.9 Mass spectrometry

### 2.9.1 Protein samples from culture supernatant

The culture supernatant protein samples were analysed by the UoE, Biosciences - Mass Spectrometry Facility. The samples were put through nano-liquid chromatography (LC) in-line with quadrupole time-of-flight (Q-TOF) 6520 (Agilent) mass spectrometer coupled to a 1200 series HPLC-Chip interface system. 1µl of each sample was loaded onto a high capacity micro C<sub>18</sub> reverse phase analytical column (Agilent Protein Identification Chip, 75µm x 150mm). The enrichment column flow rate was 3 µl/min and the analytical column flow rate was 0.3 µl/ min. Buffer A was 2% acetonitrile with 0.1% formic acid in water and buffer B was 95% acetonitrile with 0.1% formic acid in water. The peptides were separated using the following gradient, 0 min – 0% Buffer B, 9 min – 70% Buffer B, 12mins – 100% Buffer B.

Peak extraction and protein identification were carried out using Spectrum Mill MS Proteomics Workbench software (Agilent). Databases were obtained from NCBI or ExPASy, and searches were restricted to relevant species.

### 2.9.2 Protein samples from cell pellet

The stained gel containing cellular proteins was de-stained in MQ water overnight. A region on the gel containing proteins between 15 to 35 kDa was excised and sent to UoE Biosciences - Mass Spectrometry Facility for mass spectrometry analysis. As the samples were complex the digested solutions were separated using the following gradient: 0 min – 2 % Buffer B, 65 min – 30% Buffer B, 100 min – 60% Buffer B, 120 min – 100% Buffer B, 122 min – 2% Buffer B with a 7 min equilibration time.

## **2.10 Whole genome sequencing**

A fraction of extracted genomic DNA was run on 1% agarose gel to ensure that there was no degradation of the extracted genomic DNA. After quality of extracted genomic DNA was ascertained the materials were handed over to UoE Bioscience - Sequencing Facility, where they performed library preparation and ran the samples through Illumina high-throughput HiSeq 2500 with paired-end reads of 100 bp.

In brief, library preparation involved shearing genomic DNA into fragments of 200-600 bp using Covaris, ligating adaptors on to the end of each strand and attaching each strand on to an Illumina flow cell. Each strand on the flow cell was then amplified by bridge PCR on the Illumina cBot to generate a cluster of identical sequence, after which, sequencing primers were annealed and DNA was synthesised to 100 bp using fluorescent nucleotides. The incorporated nucleotide was read and bases called. When the first read was completed, the DNA clusters on the flow cell were re-generated to proceed with the sequencing of complementary strands for paired-end reads.

Data from Illumina was analysed in a standard Illumina pipeline to generate 100 bp fragments and was subjected to de-novo assembly to create contigs. The contigs were uploaded onto MG-RAST metagenomics analysis server (<http://metagenomics.anl.gov/>) for annotation.

## 2.11 Growth curve

### 2.11.1 *S. Typhimurium* SL1344 wild-type

Two to three colonies of *S. Typhimurium* grown on LB agar plates were inoculated into LB broth and incubated overnight. The optical density of the overnight culture was determined at 590 nm (OD<sub>590</sub>). The overnight culture was then diluted to obtain 40 ml of OD<sub>590</sub> approximately 0.1. 3 ml of the diluted culture were aliquoted into universal tubes and incubated. At each time-point, a tube was retrieved from the incubator and OD<sub>590</sub> was determined.

### 2.11.2 *C. jejuni* Cj1 wild-type, Cj1Δ*tsd*(syn)::kan<sup>R</sup>\_cas and Cj1Δ*tsd*(syn)::kan<sup>R</sup>\_cas

Two to three colonies of *C. jejuni* grown on CBA+ passage 1 (P1) plates were picked and streaked onto fresh CBA+ plates - which is second passage (P2) of the cells. P2 plates were incubated under the same conditions for approximately a day. Cells from P2 plates were used to inoculate third passage (P3) plates to obtain a lawn growth on fresh CBA+ plates after culturing under the same conditions for approximately a day. Cells harvested from P3 plates were dislodged into 1 ml of MHB and OD<sub>590</sub> was determined. The cell suspensions were then diluted to obtain 50ml of OD<sub>590</sub> approximately 0.1. MHB was used for the adjustment of the cell suspension, which was pre-incubated overnight at 37°C under microaerophilic conditions. The 50 ml culture was marked as fourth passage (P4). The OD<sub>590</sub> of the P4

cultures were read at the various time points. The growth curve was performed with three biological replicates.

## 2.12 Bacterial-host interaction assays

### 2.12.1 *S. Typhimurium* - macrophages infection assays

#### 2.12.1.1 *Preparation of J774A.1 cells for infection*

J774A.1 macrophage-like cells were harvested from standard T75 culturing flasks using a cell scraper. The cells were stained with trypan blue and viable cell density was determined using a haemocytometer. The cells were then seeded into 35 mm diameter  $\mu$ -Dish, with either a glass bottom (Ibidi, Product code: IB-81158) or a standard bottom (Ibidi, Product code: IB-81156) at density of  $4 \times 10^5$  cells per dish. The glass bottom  $\mu$ -Dishes were used for SRS imaging while the standard bottom  $\mu$ -Dishes were used for Confocal imaging.

The cells were allowed to attach to the bottom of the dish overnight. After overnight incubation, the cells were washed twice using L-15 media pre-warmed to 37°C.

#### 2.12.1.2 *Preparation of S. Typhimurium for infection*

SL1344 wild-type or SL1344 *fliC::gfp* were grown in LB broth or LB-D<sub>2</sub>O broth overnight. The overnight cultures were diluted to OD<sub>590</sub> of approximately 0.1 using the appropriate media, and incubated for another 2 hr, until OD<sub>590</sub> was approximately 0.5. The bacterial cell

density at OD<sub>590</sub> of 1 is equivalent to 5x10<sup>8</sup> CFU/ml. The bacterial suspension was adjusted to density of 4x10<sup>7</sup> cfu/ml in L-15 media pre-warmed to 37°C.

#### 2.12.1.3 *Infection of J774A.1 cells with S. Typhimurium*

The L-15 media in the  $\mu$ -Dishes was discarded and the monolayer J774A.1 cells were overlaid with 1 ml of bacterial suspension at density of 4x10<sup>7</sup> CFU/ml; the multiplicity of infection (MOI) was 100. The cells were incubated at 37°C for an hour after which the bacterial cell suspension was aspirated out and the J774A.1 monolayer was overlaid with 2 ml of L-15 media containing 100  $\mu$ g/ml gentamicin. At this point, the time point was set at T0. The cells were returned to the incubator for another hour. At T1 the L-15 media with 100  $\mu$ g/ml gentamicin was discarded and was replaced with 2 ml of L-15 media containing 10  $\mu$ g/ml gentamicin. The cells were imaged at T2 by SRS or fixed for Confocal imaging (refer to section 2.12.1.4).

#### 2.12.1.4 *Fixing of infected J774A.1 cells*

At T2, the media was discarded and the cells were rinsed three times with sterile PBS and overlaid with 4% para-formaldehyde (PFA) for 10 min to fix the cells. After this, the cells were then rinsed twice with PBS and washed three times in PBS with shaking for 5 min each. After the last wash, Vectashield-DAPI (Vector Laboratories, H-1200) was dropped over the cells and the  $\mu$ -Dishes were stored in the dark at 4°C ready for Confocal imaging.

## 2.12.2 *C. jejuni* - macrophages infection assays

### 2.12.2.1 *Preparation of RAW264.7 cells for infection*

RAW264.7 macrophage-like cells were harvested from standard T75 culturing flasks using a cell scraper. The cells were stained with trypan blue and viable cell density was determined using a haemocytometer. The cells were then seeded into each well of two 24-well plates at a density of  $2 \times 10^5$  cells per well. The cells were allowed to attach to the bottom of the wells overnight. After overnight incubation the cells were washed twice using DMEM supplemented with 1% FBS (DMEM-1%FBS), pre-warmed to 37°C.

### 2.12.2.2 *Preparation of Cj1 cells for infection*

Cj1 wild-type, Cj1 $\Delta$ *tsD*(syn)::kan<sup>R</sup>\_cas and Cj1 $\Delta$ *tsD*(syn)::kan<sup>R</sup>\_cas cells harvested from P3 plates and dislodged into 1 ml of MHB and OD<sub>590</sub> was determined. The cell suspension were then diluted to obtain 28 ml of OD<sub>590</sub> approximately 0.1. MHB was used for the adjustment of the cell suspension, which was pre-incubated overnight at 37 °C under microaerophilic conditions. The 28 ml culture was marked as fourth passage (P4) and was aliquoted into a 24-well plate; 1 ml per well and 1 plate per strain. The P4 cultures were incubated at 37°C under microaerophilic conditions for approximately 24 hours. After 24 hours of incubation the broth cultures from each well of the same plate were pooled. The bacterial cells were collected at the bottom of the tube by centrifugation at 11,000 x g for 5 min at room temperature. The cell pellets were resuspended in 2 ml of pre-warmed DMEM

supplemented with 1% FBS (DMEM-1% FBS). The cell suspension was then adjusted to density of  $2 \times 10^6$  CFU/ml. The bacterial cell density at OD<sub>590</sub> of 1 is equivalent to  $1 \times 10^9$  cfu/ml. The bacterial cells suspension was diluted serially and spotted on MHA plates.

#### 2.12.2.3 *Infection of RAW264.7 cells with Cj1 wild-type and T6SS mutants*

The DMEM-1% FBS in each well of the 24-well plates was discarded and the monolayer RAW264.7 cells were overlaid with 1 ml of bacterial suspension at density of  $2 \times 10^6$  CFU/ml; the multiplicity of infection (MOI) was 10. The cells were incubated at 37°C under 5% CO<sub>2</sub>.

After four hours of incubation a plate of infected RAW264.7 cells was rinsed 5 times using pre-warmed 1X PBS. The RAW264.7 cells were lysed in 0.5 ml of 1% saponin (prepared in water) for 15 min. The saponin treatment released all bacterial cells adhering to and invading the RAW264.7 cells into the saponin solution. The bacterial cell suspensions was then diluted serially and spotted on MHA plates.

After four hours of incubation another plate of infected RAW264.7 cells was rinsed three times using pre-warmed 1X PBS. After the last rinse, the RAW264.7 cells in each well were overlaid with 2 ml of DMEM-1%FBS containing 250 µg/ml of gentamicin. The cells were returned to the incubator and were further incubated at 37°C with 5% CO<sub>2</sub>. The gentamicin treatment killed all bacterial cells that were on the exterior of the macrophage cells. After two hours, the cells were rinsed three times using pre-warmed 1X PBS. The RAW264.7 cells were lysed in 0.5 ml of 1% saponin for 15 min. The saponin treatment released all bacterial

cells that had invaded the RAW264.7 cells into the saponin solution. The bacterial cell suspension was then diluted serially and spotted on MHA plates. The assays were performed with three biological replicates, each in triplicate.

### 2.12.3 *C. jejuni* - ZFE challenging assays

#### 2.12.3.1 *Preparation of ZFE for bacterial challenge*

ZF eggs were collected from the ARC in the morning and tank water was replaced with aerated 1X marine salt solution (MSS). *WIK* eggs were incubated in MSS with 0.000001% methylene blue while *AB fms:nfsB.mCherry* transgenic line eggs were incubated in MSS without methylene blue. The eggs were incubated at 28°C and unfertilised eggs were removed at 5-6 hours post-fertilisation (hpf) stages. The remaining embryos were returned to incubation till 24 hpf. At 24 hpf the chorion of the embryos was mechanically removed. After removal of chorion *WIK* wild-type embryos were placed into MSS while *AB fms:nfsB.mCherry* transgenic embryos were placed into MSS containing 75 µM of 1-phenyl 2-thiourea (PTU). The addition of PTU was to stop pigment development. The MSS with PTU was refreshed daily. At the desired stages of development (28, 30 or 52 hpf) the embryos were anaesthetised in 0.03% Tricane made in MSS. The embryos were then transferred onto a slide covered with a layer of 3% methy-cellulose.

#### 2.12.3.2 *Preparation of C. jejuni cells for challenging ZFE*

*C. jejuni* cells harvested from P3 plates were dislodged into 1 ml of MHB and OD<sub>590</sub> was determined. Cells harvested from P3 were either used for ZFE challenge or for preparing P4 cultures. For ZFE challenge the cell suspension was adjusted to OD<sub>590</sub> of approximately 10. The bacterial cell suspensions were diluted serially and spotted on MHA plates.

For P4 cultures, the cell suspensions were diluted to obtain 28 ml of OD<sub>590</sub> approximately 0.1. The bacterial suspension was aliquoted into a 24-well plate, 1 ml per well and 1 plate per strain. MHB was used for the adjustment of the cell suspension, which was pre-incubated overnight at 37°C under microaerophilic conditions. The P4 cultures were incubated at 37°C under microaerophilic conditions for approximately 24 hours. After 24 hours of incubation the broth cultures from each well of the same plate were pooled. The bacterial cells were collected at the bottom of the tube by centrifugation at 11,000 x g for 5 min at room temperature. The cell pellets were resuspended in 2 ml of PBS. The cell suspension was then adjusted to OD<sub>590</sub> of approximately 1 or 10. The bacterial cell suspensions were diluted serially and spotted on MHA plates.

#### 2.12.3.3 *Microinjection of ZFE with C. jejuni cells*

The needle for microinjection was loaded with a bacterial suspension and was calibrated on a stage micrometer. The injection pressure or time, was adjusted to obtain a droplet size of between 1-2 nl. The needle was then inserted into either the embryo's yolk sac or yolk sac circulation valley as illustrated in Figure 2.2. Two pulses were delivered per embryo. After inoculation, the embryos were rinsed out from the methyl-cellulose matrix using MSS into a clean petri dish. In general a minimum of 20 embryos were injected per set. For each experiment, two controls were incorporated: i) uninjected control - the ZFE were de-chorionated but not injected, a minimal of 5 ZFE per experiment; ii) PBS injected control - the ZFE were de-chorionated and injected with 2 pulses of PBS, a minimal of 20 ZFE per experiment. The embryos were incubated at 28°C and scored at 24 hours post-infection (hpi)

for survival or maintained up to a maximum of 5 days post-fertilisation. Embryos with observable heart beat were scored as alive - regardless of edema formation. The embryos were then killed in 70% ethanol. The actual inoculated dose was determined by delivering 50 pulses into 50  $\mu$ l PBS. The bacterial suspension were diluted serially and spotted on MHA plates.

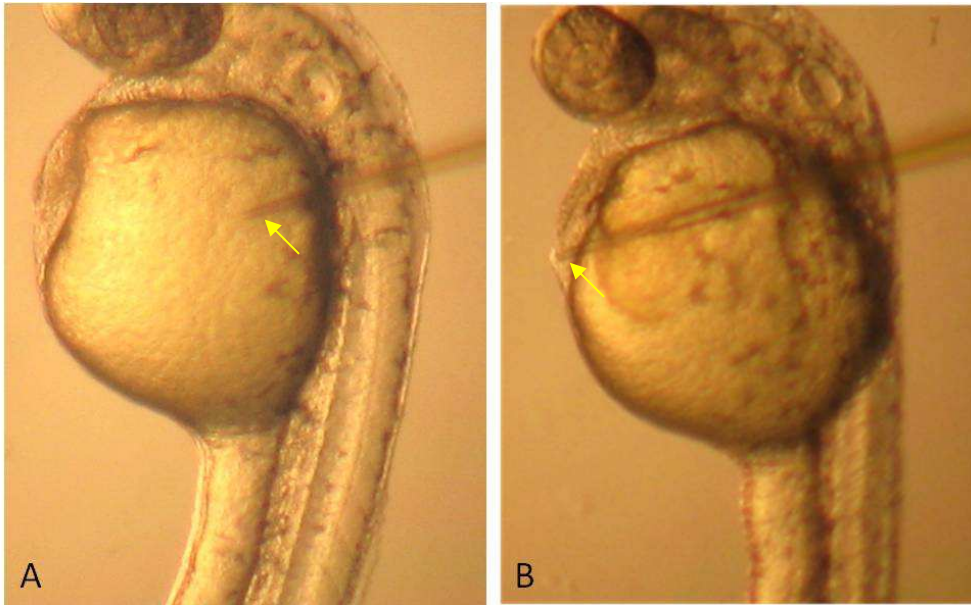


**Figure 2.2:** Site of inoculation in 28 hpf ZFE. Bacterial cells were delivered into yolk sac (A) or yolk sac circulation valley (B) via microinjection. The yellow arrows indicate the tip of the needle used for microinjection.

#### 2.12.4 *C. jejuni* - piglet challenging assays

This study was performed by Dr Paul Everest from the Institute of Infection, Immunity and Inflammation at University of Glasgow using *C. jejuni* Cj1 wild-type, Cj1 $\Delta$ *tssD*(syn)::kan<sup>R</sup>\_cas and Cj1 $\Delta$ *tssD*(syn)::kan<sup>R</sup>\_cas. Competitive index challenge was performed on two groups of animals, each consisting of 9 newborn piglets. In each group the piglets were inoculated with equal amounts of wild-type and a mutant. The wild-type strain was grown on CBA+ and mutant strains were grown on CBA+ were supplemented with 50  $\mu$ g/ml kanamycin, both strains were incubated at 37 °C in a VAIN cabinet for 48 hr. The bacteria cells from each strain was then scraped off into PBS with its optical density adjusted to 1x10<sup>8</sup> CFU/ml. The piglets were inoculated orally with an inoculation dose of approximately 1x10<sup>8</sup> CFU. Faecal samples were collected daily up to Day 5 post-infection. Faecal samples were quantified for wild-type and respective T6SS mutant by culturing.

## **2.13 Raman spectroscopy**

### **2.13.1 Raman analysis of SL1344 wild-type grown in LB, LB with 70% D<sub>2</sub>O and MM**

At each time point of the growth curve 50 ml of SL1344 wild-type cells were collected at the bottom of the tube by centrifugation at 11,000 x g for 5 min. The culture supernatant was discarded and the cell pellet was resuspended in 1 ml PBS. The cell suspension was then spun at 16,100 x g for 3 min and cells were collected at the bottom of the tube. The cell pellet was washed twice more in PBS. After the last wash, the cell pellet was placed on ice and transferred to the Raman spectrometer laboratory. Approximately 10  $\mu$ l of the moist cell pellet was spotted onto an aluminium coated glass slide. Raman shift spectra were collected between 400-4000  $\text{cm}^{-1}$  using Raman spectrometer Reinshaw RM1000. The settings used for spectrum collection were 785 nm notch, 50% laser power, 10s acquisition and 40x objective. Raman spectra were collected from a minimum of three different biological replicates and a minimum of three different focal points each.

### **2.13.2 Raman analysis of J774A.1**

J774A.1 macrophage-like cells were harvested from standard T75 culturing flasks using cell scraper into 5ml of PBS. The cells were collected at the bottom of the tube by centrifugation at 1,000 x g for 3 min. The cell pellet was washed three times in PBS. After the last wash, the cell pellet was placed on ice and transferred to the Raman spectrometer laboratory. Approximately 10  $\mu$ l of the moist cell pellet was spotted onto an aluminium coated glass slide.

Raman shift spectra were collected between 400-4000  $\text{cm}^{-1}$  using Raman spectrometer Reinshaw RM1000. The settings used for spectrum collection were 785 nm notch, 50% laser power, 10s acquisition and 40x objective. Raman spectra were collected from a minimum of three different biological replicates and a minimum of three different focal points each.

## 2.14 SRS and Confocal imaging

The J774A.1 cells infected with SL1344 wild-type or SL1344 *fliC::gfp* were imaged under SRS microscope and Confocal microscope respectively. The SRS system was built in-house by the Physics Department at UoE. The Stokes beam was fixed at 1064 nm while the pump beam was tuned to achieve as close as possible to four of the selected wavenumbers. The operation of the SRS microscope and taking of cell images were performed with help from Dr Julian Moger of Physics Department. The Confocal microscope used was ZEISS LSM 510 META. The laser was set for visualisation of GFP and DAPI.

## 2.15 Imaging of ZFE

### 2.15.1 Staining of *C. jejuni* Cj11168H with 5-(6)-carboxyfluorescein-succinylester (FITC)

Cj11168H wild-type cells were harvested from P4 cultures. The cells were collected at the bottom of the tube by centrifugation at 11,000 x g for 5 min. The cell pellet was then resuspended in 200 µl of 0.4 µg/ml FITC for 15 minutes at room temperature in the dark and with constant mixing (Agerer et al., 2004). After 15 min of incubation the cells were washed 5 times with PBS or until the supernatant no longer looked yellowish. After the final wash, the cells were resuspended in 100 µl of PBS and used for inoculation into *AB fms:nfsB.mCherry* transgenic embryos at 28 hpf.

### 2.15.2 Imaging of *AB fms:nfsB.mCherry* transgenic embryos inoculated with fluorescing Cj11168H

The *AB fms:nfsB.mCherry* transgenic embryos were inoculated with either Cj11168H GFP reporter or Cj11168H stained with FITC. The embryos were visualised at various time-points post-infection using an upright fluorescence microscope, equipped with a filter where excitation is at 472 nm, and emission at 520 nm, emission for GFP detection and another filter with excitation at 543 nm and emission at 593 nm for mCherry detection.

## **2.16 Electron microscopy (EM) for visualisation of *C. jejuni* capsule**

Cj11168H wild-type and Cj1 wild-type were cultured under two different growth conditions; i) 37 °C in MHB for 24 hr, and ii) 37 °C on CBA+ for 48 hr. Cells were then harvested for capsule detection by EM. Bacterial cells on agar cultures were picked up with a cotton swab and dislodged into 1 ml PBS. The cell suspensions from agar culture were spun down at 11,000 x g for 5 min and supernatant was discarded. 2 ml of each broth culture were spun down at 11,000 x g for 5 min, and supernatant was discarded. The cell pellets were passed to Dr Massimo Micaroni from Bio-imaging Centre at UoE for further processing and imaging under transmission EM. The samples were processed according to the protocol illustrated in Karlyshev *et al* (Karlyshev et al., 2001).

**Chapter 3: Raman microscopy of *S. Typhimurium* SL1344  
within mouse macrophage-like cells J774A.1**

## 3.1 Introduction

### 3.1.1 Raman microspectroscopy

Raman microspectrometry has been shown to discriminate between bacterial species and differentiates between different stages of growth within each species tested (Huang et al., 2004). These properties could enable the use of Raman microscopy for the interrogation of metabolically active and dormant cells during host-pathogen interactions. This could be potentially exploited for imaging based on specific chemicals in a complex matrix such as, for example, in demonstrating lipids in fresh tissues (Mansfield et al., 2013). Raman spectroscopy has been used in the detection and identification of *Campylobacter* (Lu et al., 2012). Hence, we would like to explore the possibility of using the *Campylobacter* specific chemical signature to perform label-free live imaging of bacteria within host cells. This study was initially performed using model organisms, *Salmonella* Typhimurium strain SL1344 and mouse macrophage-like cells J774A.1.

### 3.1.2 Aim of study

The aim of this study was to determine the molecular make-up of bacteria and host cells based on Raman spectroscopy and to use the information for interrogation of host-pathogen interactions. An established model, mouse macrophage-like cells infected with *Salmonella* Typhimurium was chosen for method development and testing.

## 3.2 Results

### 3.2.1 Methodologies developed for Raman spectra collection and processing

*Salmonella* Typhimurium strain SL1344 cells were grown in LB broth overnight at 37°C with shaking at 200 rpm. Mouse macrophage-like cells were cultured in T75 tissue culture flask till 70-80% confluence at 37°C with 5% CO<sub>2</sub>. Bacterial and macrophage cells were harvested from the growth vessel and washed three times in PBS. The cell pellets were spotted onto aluminium coated glass slides.

The Raman spectra of *S. Typhimurium* strain SL1344 wild-type and mouse macrophage-like cells J774A.1 were collected between 400-4000 cm<sup>-1</sup> using a Reinshaw RM1000 Raman spectrometer, equipped with a 785 nm laser, Figure 3.1. The settings used for spectrum collection were 785 nm notch, 50% laser power, 10s acquisition and 40x objective. Raman spectra were collected from a minimum of three different biological replicates and for each replicate, spectra were collected at a minimum of three different focal points. All the spectra collected were then averaged before they were used in comparisons.

The raw spectra obtained were very noisy and were smoothed using software from the Raman spectra-microscope, WIRE2.0. The smoothing algorithm in WIRE 2.0 removed most of the noise, Figure 3.1.

The baseline of each spectrum needed to be removed as well, but the smoothing algorithm was not able to perform this function. The baseline attributed to each spectrum differs according to cell types and preparations, hence, baseline subtraction was essential before different samples could be compared. This was achieved by applying an in-house developed algorithm, a Bayesian Whittaker–Henderson (BWH) smoother (Lau et al., 2012), onto smoothed spectra. The BWH algorithm was developed together with Dr Ron Yang (College of Life and Environmental Sciences, UoE). Figure 3.2 illustrates spectra before and after baseline subtraction.

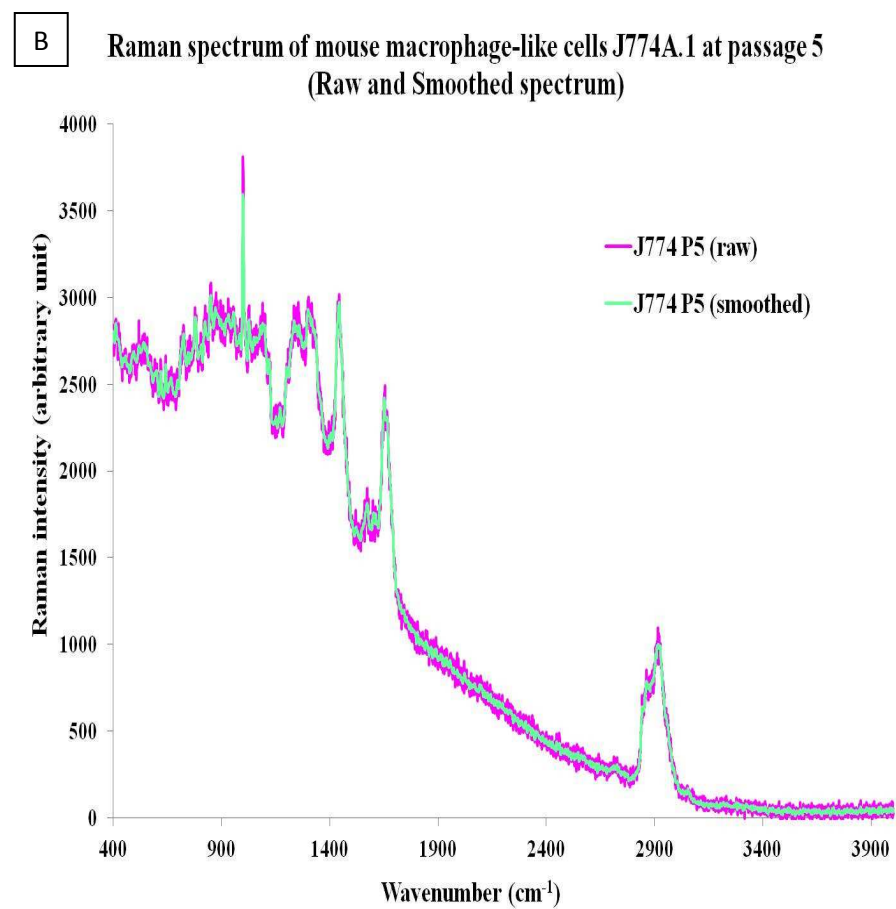
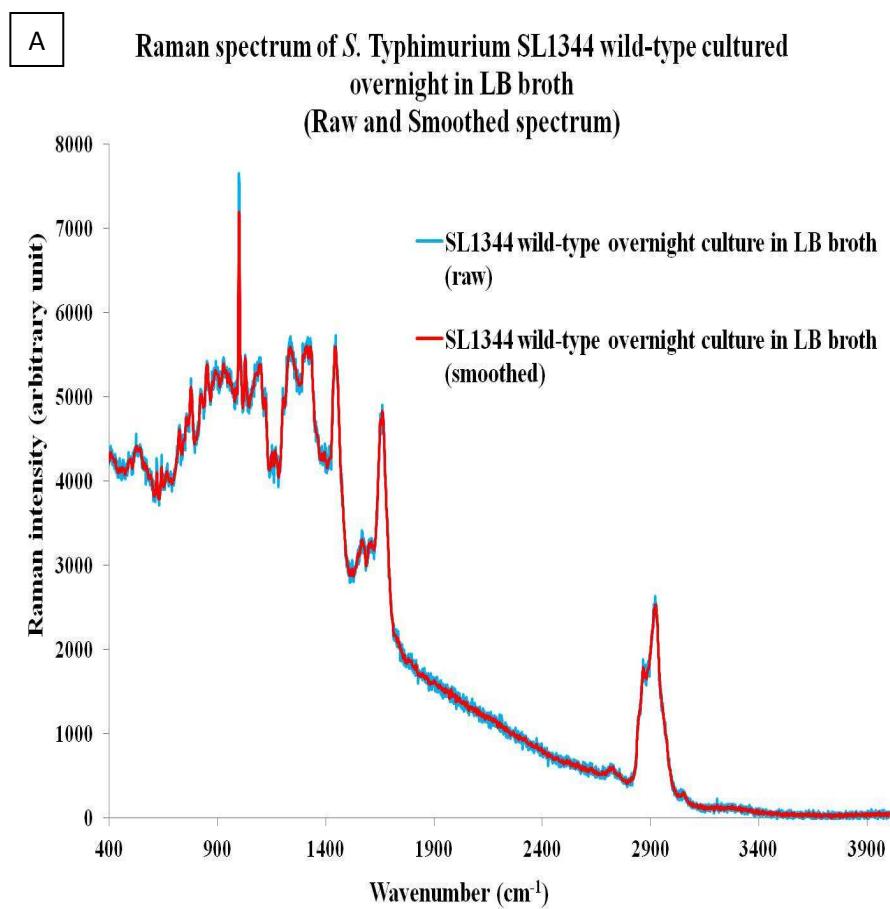


**Figure 3.1:** Raw and smoothed Raman spectrum collected from (A) *S. Typhimurium* SL1344 wild-type and (B) mouse macrophage-like cells J774A.1. Y-axis = Raman intensity (arbitrary units). X-axis = Wavenumbers (cm<sup>-1</sup>). Left: Raw (blue) and smoothed (red) Raman spectrum from *S. Typhimurium* cultured overnight in LB broth. Right: Raw (magenta) and smoothed (green) Raman spectrum from mouse macrophage-like cells J774A.1 at passage 5. Raw spectra were smoothed using WIRE 2.0.

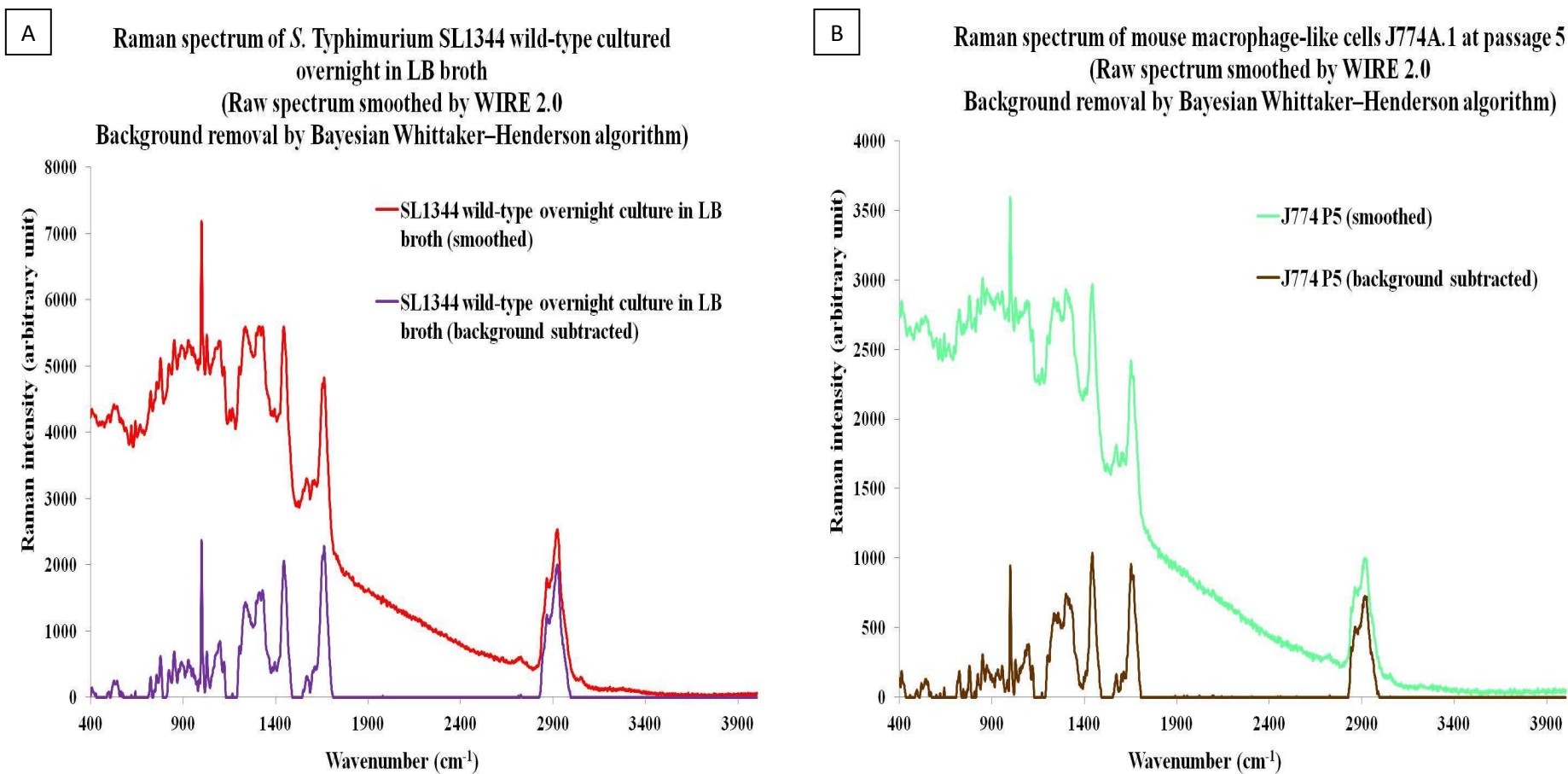


**Figure 3.2:** Smoothed and baseline subtracted Raman spectrum collected from (A) *S. Typhimurium* SL1344 wild-type and (B) mouse macrophage-like cells J774A.1. Y-axis = Raman intensity (arbitrary units). X-axis = Wavenumbers ( $\text{cm}^{-1}$ ). Left: Smoothed (red) and baseline subtracted (purple) Raman spectrum from *S. Typhimurium* cultured overnight in LB broth. Right: Smoothed (green) and baseline subtracted (brown) Raman spectrum from mouse macrophage-like cells J774A.1 at passage 5. Raw spectra were smoothed using WIRE 2.0. Baseline subtracted from smooth spectra using Bayesian Whittaker–Henderson smoother.

Raman peak intensities can be affected by the number of cells in each focal volume. Spectra collected from the same sample could result in different intensities as the cell suspension did not spread uniformly when spotted and dried on the slide. Figure 3.3 (A) provides an illustration of baseline subtracted spectra collected from a sample at different focal points. These variations between the spectra were corrected by normalisation. Each intensity value was normalised through division by total intensity integrated over the whole spectrum. Normalised spectra of the same sample are presented in Figure 3.3 (B); demonstrating that this normalisation has compensated for differences in cell concentration in the sampling volume. The normalised data could therefore be used for comparison between samples.

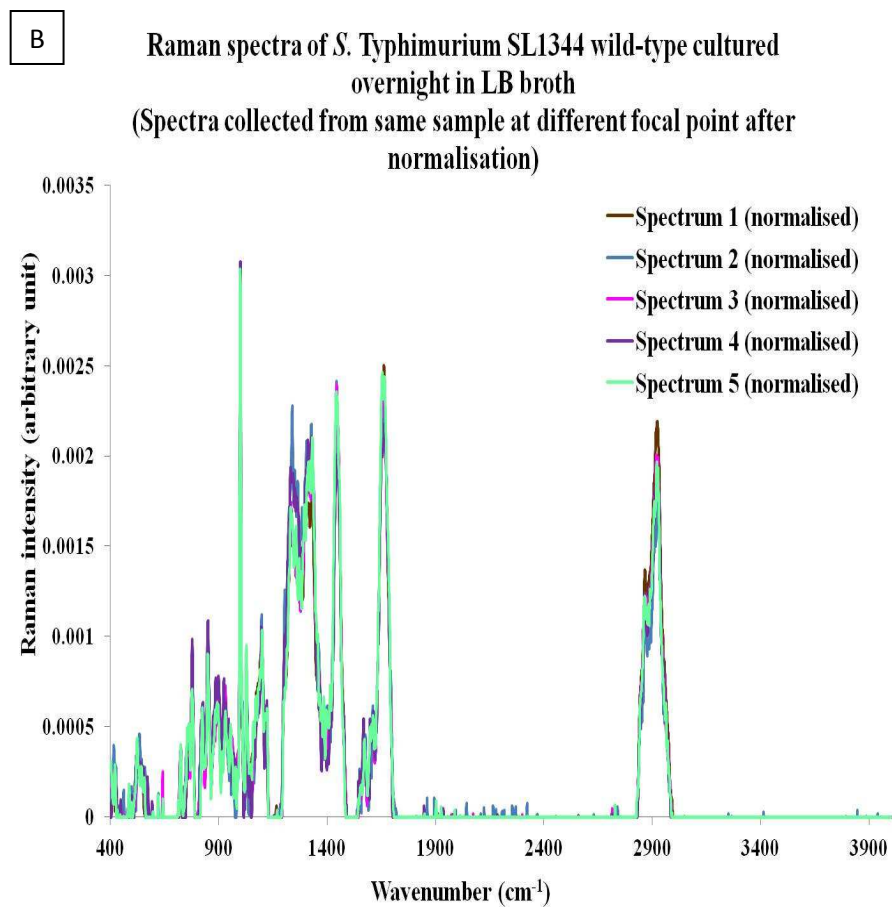
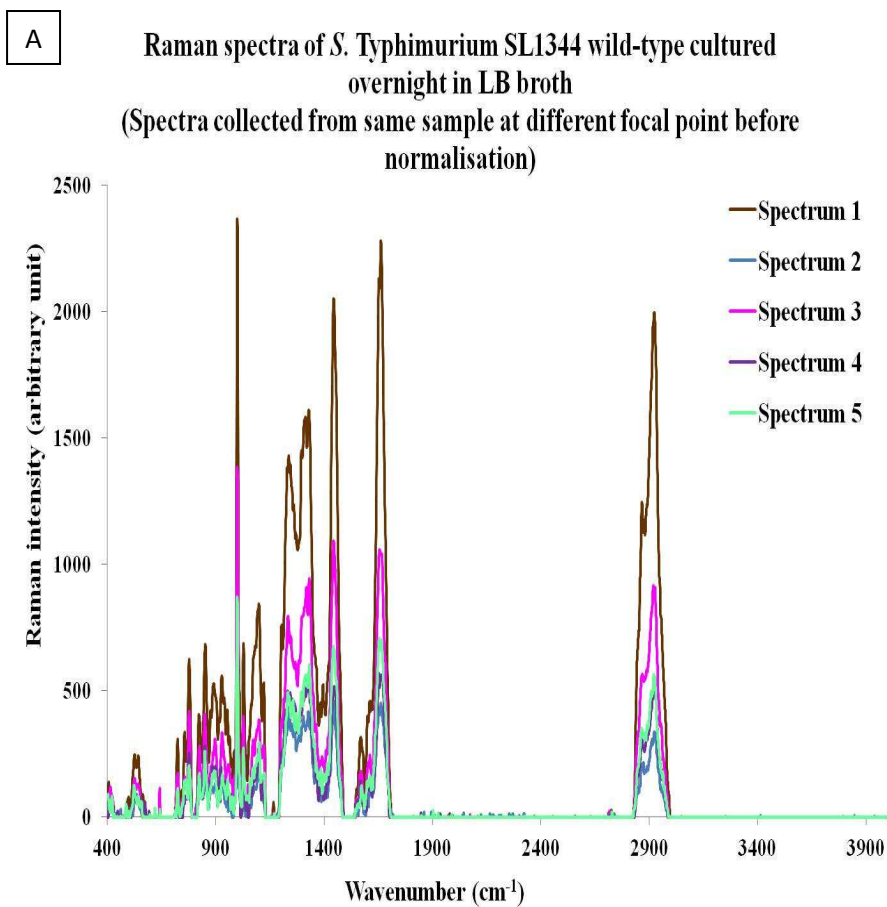


**Figure 3.3:** Raman spectra of *S. Typhimurium* SL1344 collected at different focal point, (A) before and (B) after normalisation. Y-axis = Raman intensity (arbitrary units). X-axis = Wavenumbers (cm<sup>-1</sup>). Left: 5 spectra collected from same *S. Typhimurium* sample at different focal point before normalisation. Right: Same spectra as chart on the left but after normalisation by division of each intensity value by total intensities value of respective spectrum.

### 3.2.2 Raman spectra of *S. Typhimurium* at different stages of growth

For these experiments an overnight culture of *S. Typhimurium* in LB broth was diluted and inoculated into fresh LB broth. The growth profile of the bacteria is illustrated in Figure 3.4.

At various stages of growth bacterial cells were harvested for Raman spectroscopy. The spectra obtained from various growth stages are illustrated in Figure 3.5. Profiles of cells at different growth stages were similar, but the intensities of some peaks varied. For example, cells at mid log phase gave the highest intensities at  $724\text{ cm}^{-1}$  and  $781\text{ cm}^{-1}$ , while cells at early log phase gave the highest intensities at  $810\text{ cm}^{-1}$ ,  $1477\text{ cm}^{-1}$  and  $1569\text{ cm}^{-1}$ .

### Growth curve of *S. Typhimurium* SL1344 wild-type in LB broth

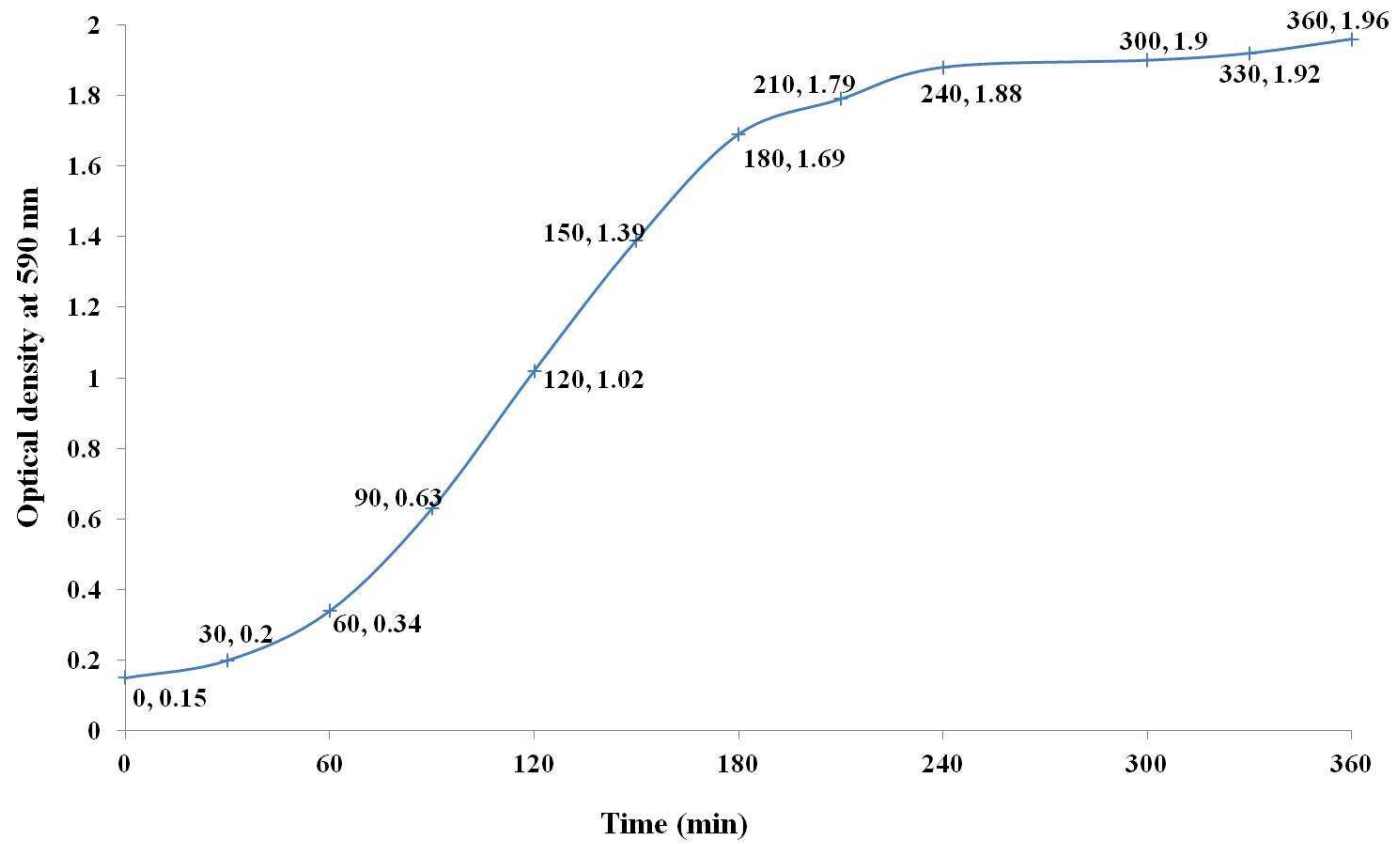


Figure 3.4: Growth curve of *S. Typhimurium* SL1344 wild-type in LB broth. The optical density of the culture was monitored at 30 min interval up to 240 minutes.

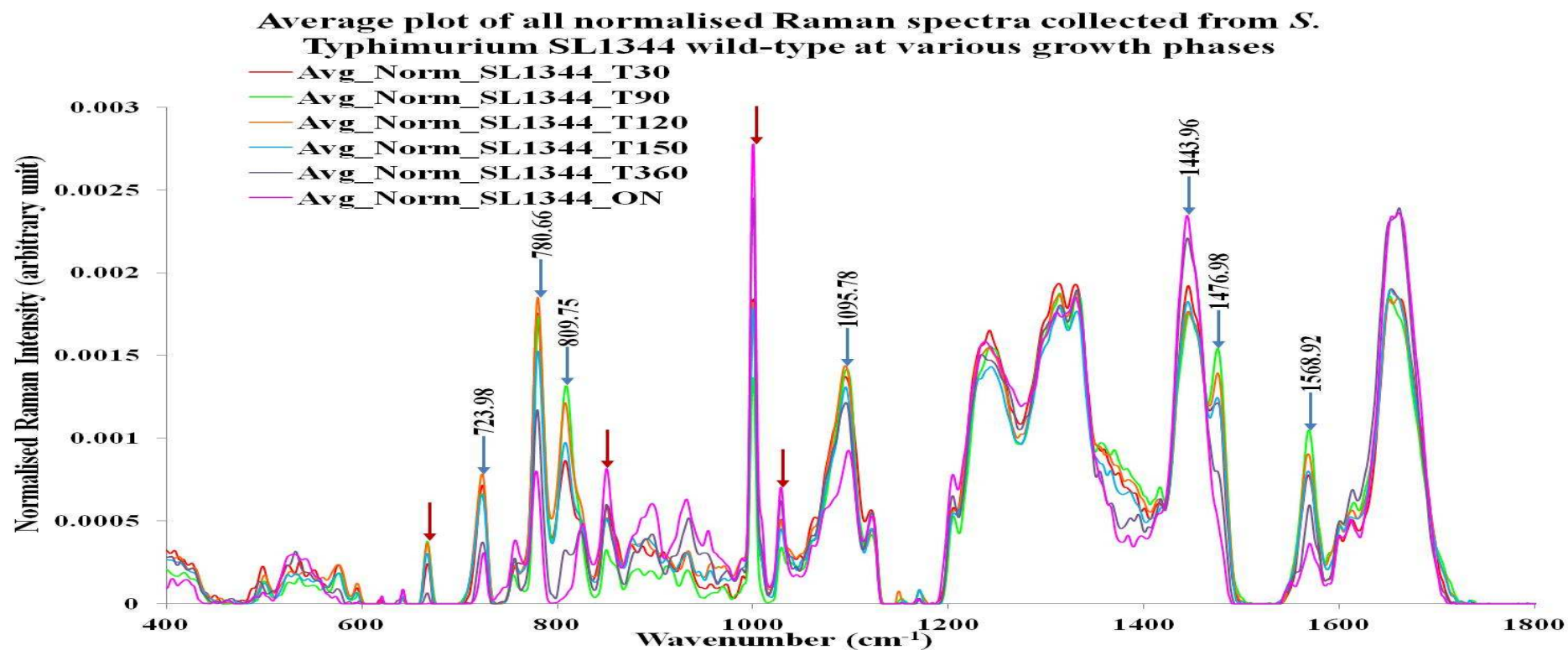


Figure 3.5: Raman spectra of *S. Typhimurium* SL1344 wild-type at various growth phases. Spectra plotted were average of all spectra collected (both technical and biological replicated). Y-axis = Normalised Raman intensity (arbitrary units). X-axis = Wavenumbers ( $\text{cm}^{-1}$ ). **Red**: Mean normalised spectrum from SL1344\_T30 representing lag phase. **Green**: Mean normalised spectrum from SL1344\_T90 representing early log phase. **Orange**: Mean normalised spectrum from SL1344\_T120 representing mid log phase. **Blue**: Mean normalised spectrum from SL1344\_T150 representing late log phase. **Purple**: Mean normalised spectrum from SL1344\_T360 representing stationary phase. **Magenta**: Mean normalised spectrum from SL1344\_ON, an overnight culture, representing late stationary phase. The **blue** arrows indicate peaks at which the wavenumbers could be selected for Raman based imaging. The **maroon** arrows indicate other peaks that had shown differences in intensities at different growth stages.

### 3.2.3 Analysis of normalised spectra and identification of wavenumbers to be used for Raman based imaging

After normalisation, spectra from each sample type collected (technical and biological replicates, minimal of 3 each) were compared by one-way ANOVA using an R programme (<http://www.r-project.org/>). Wavenumbers that had P-value  $<0.0001$  between two sample types compared were represented by vertical blue lines in Figures 3.6-10.

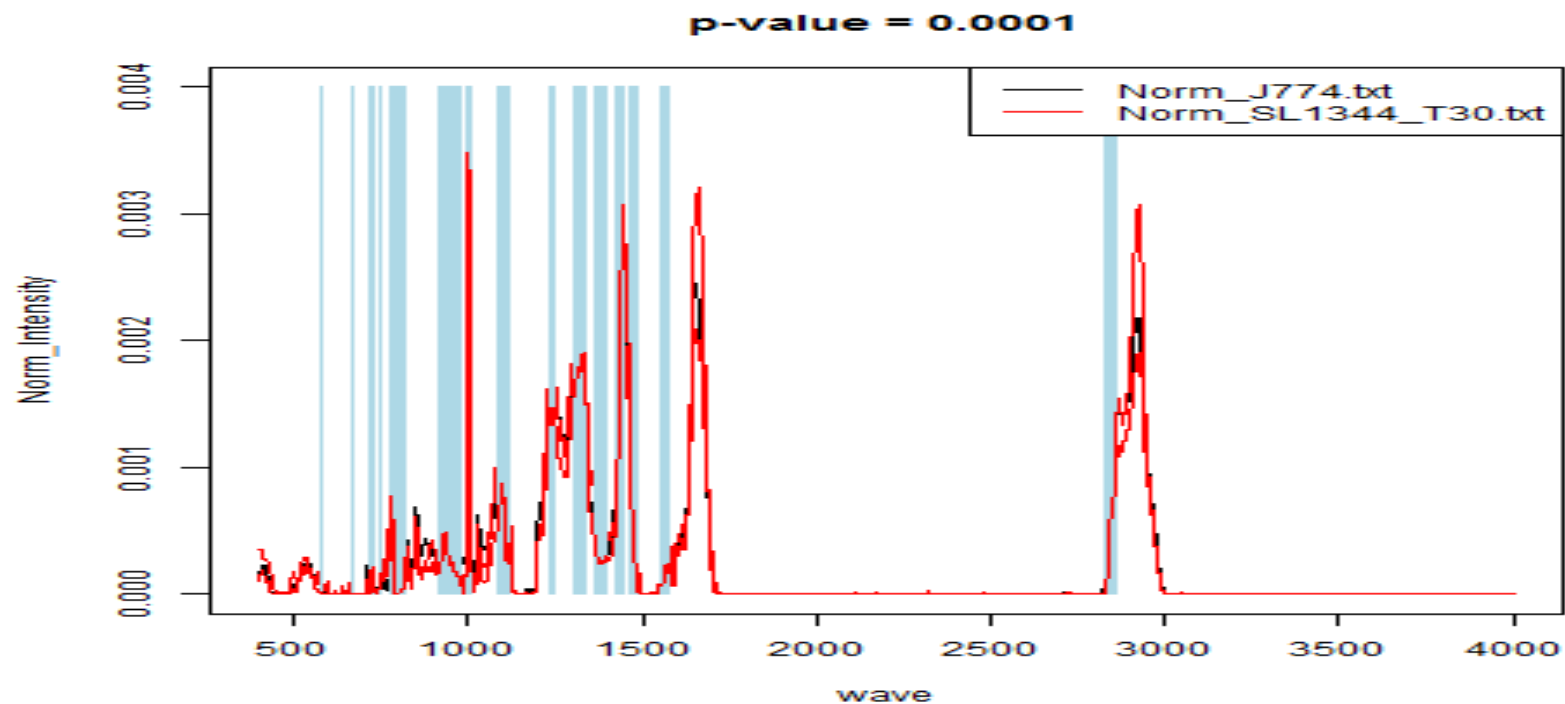


Figure 3.6: Comparison of normalised Raman spectrum collected from *S. Typhimurium* SL1344 wild-type grown in LB broth at lag phase with mouse macrophage-like cells J774A.1. Y-axis = Normalised Raman intensity (arbitrary units). X-axis = Wavenumbers ( $\text{cm}^{-1}$ ). Black: Normalised spectrum from J774A.1. Red: Normalised spectrum from SL1344. Blue: Wavenumbers at which ANOVA analysis had determine normalised intensities between J774A.1 and SL1344 to be significantly different, P-value  $\leq 0.0001$ .

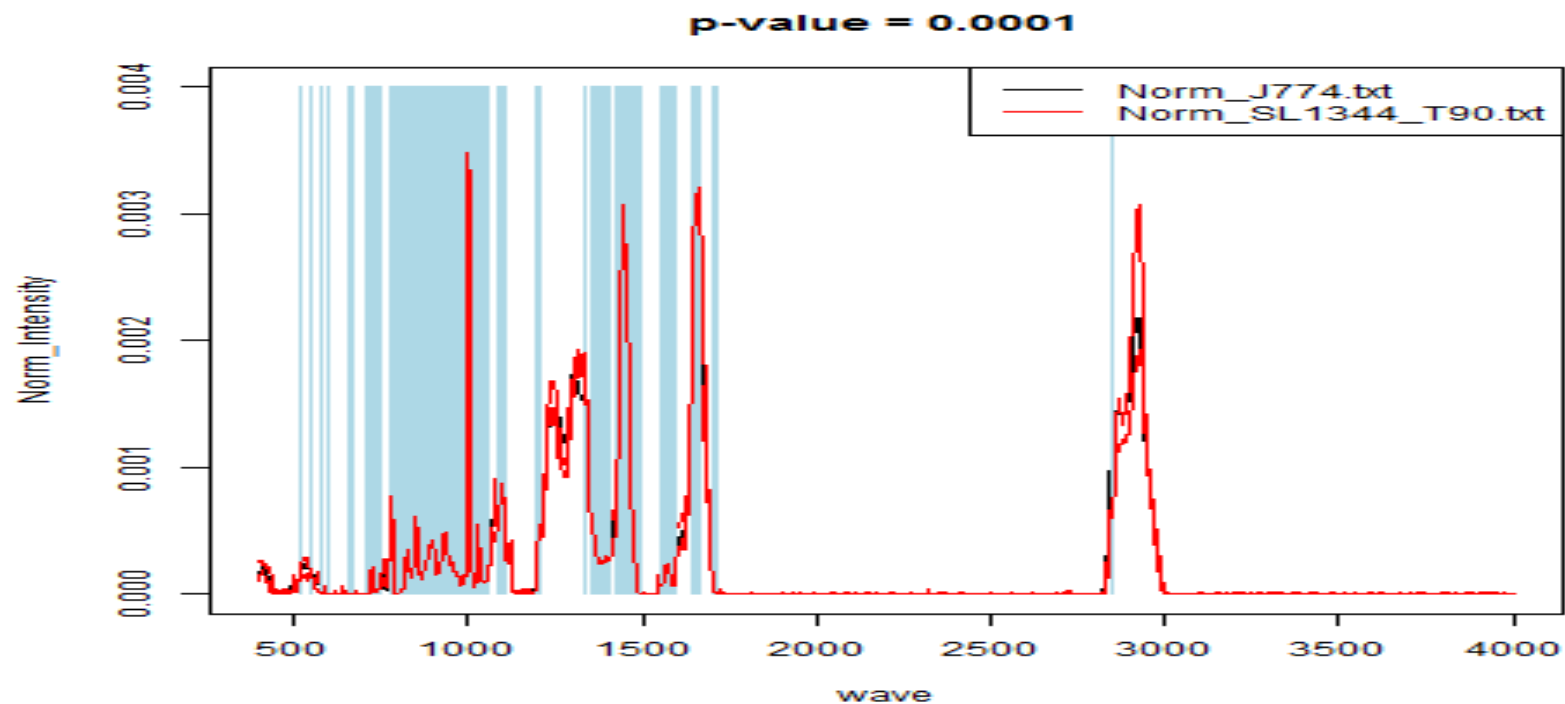


Figure 3.7: Comparison of normalised Raman spectrum collected from *S. Typhimurium* SL1344 wild-type grown in LB broth at early log phase with mouse macrophage-like cells J774A.1. Y-axis = Normalised Raman intensity (arbitrary units). X-axis = Wavenumbers ( $\text{cm}^{-1}$ ). Black: Normalised spectrum from J774A.1. Red: Normalised spectrum from SL1344. Blue: Wavenumbers at which ANOVA analysis had determine normalised intensities between J774A.1 and SL1344 to be significantly different, P-value  $\leq 0.0001$ .

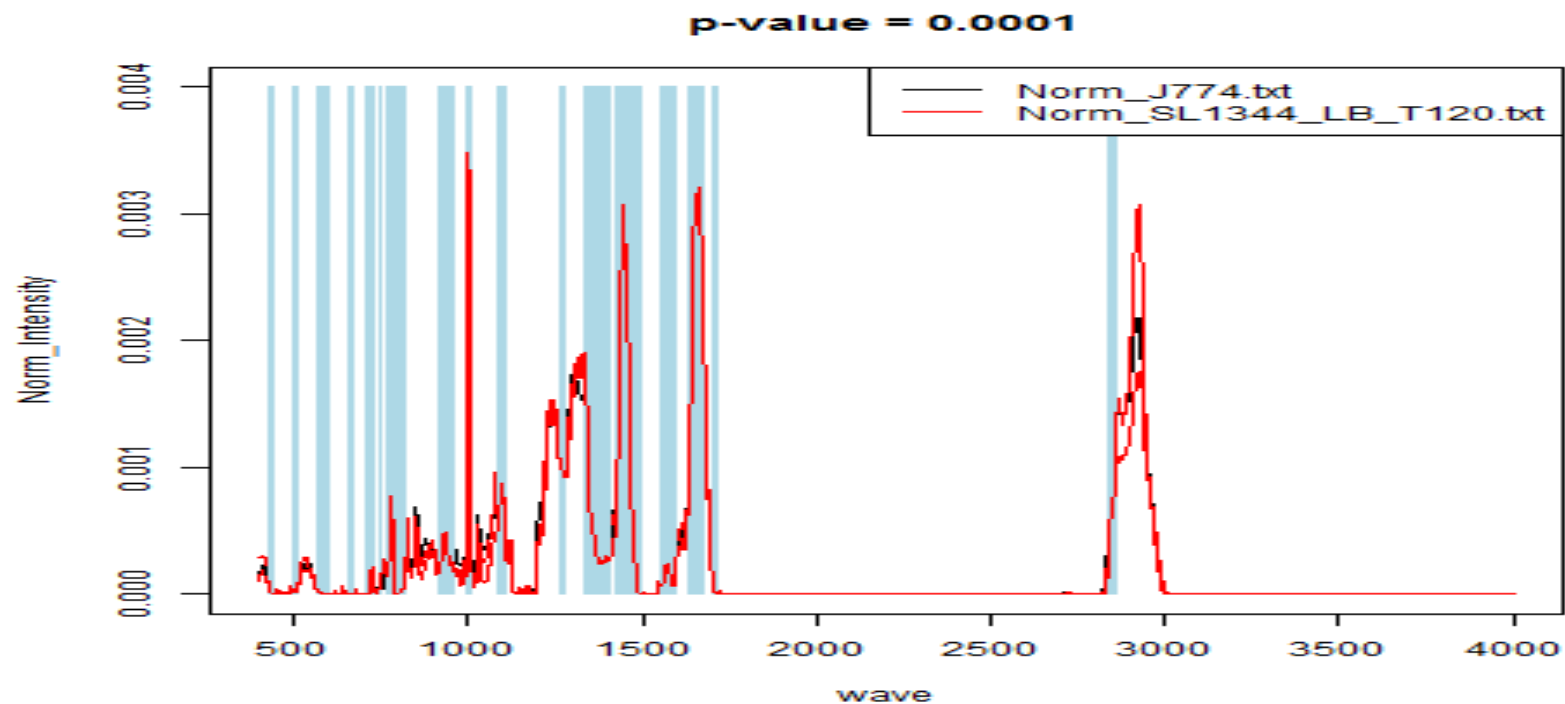


Figure 3.8: Comparison of normalised Raman spectrum collected from *S. Typhimurium* SL1344 wild-type grown in LB broth at mid log phase with mouse macrophage-like cells J774A.1. Y-axis = Normalised Raman intensity (arbitrary units). X-axis = Wavenumbers ( $\text{cm}^{-1}$ ). Black: Normalised spectrum from J774A.1. Red: Normalised spectrum from SL1344. Blue: Wavenumbers at which ANOVA analysis had determine normalised intensities between J774A.1 and SL1344 to be significantly different, P-value  $\leq 0.0001$ .

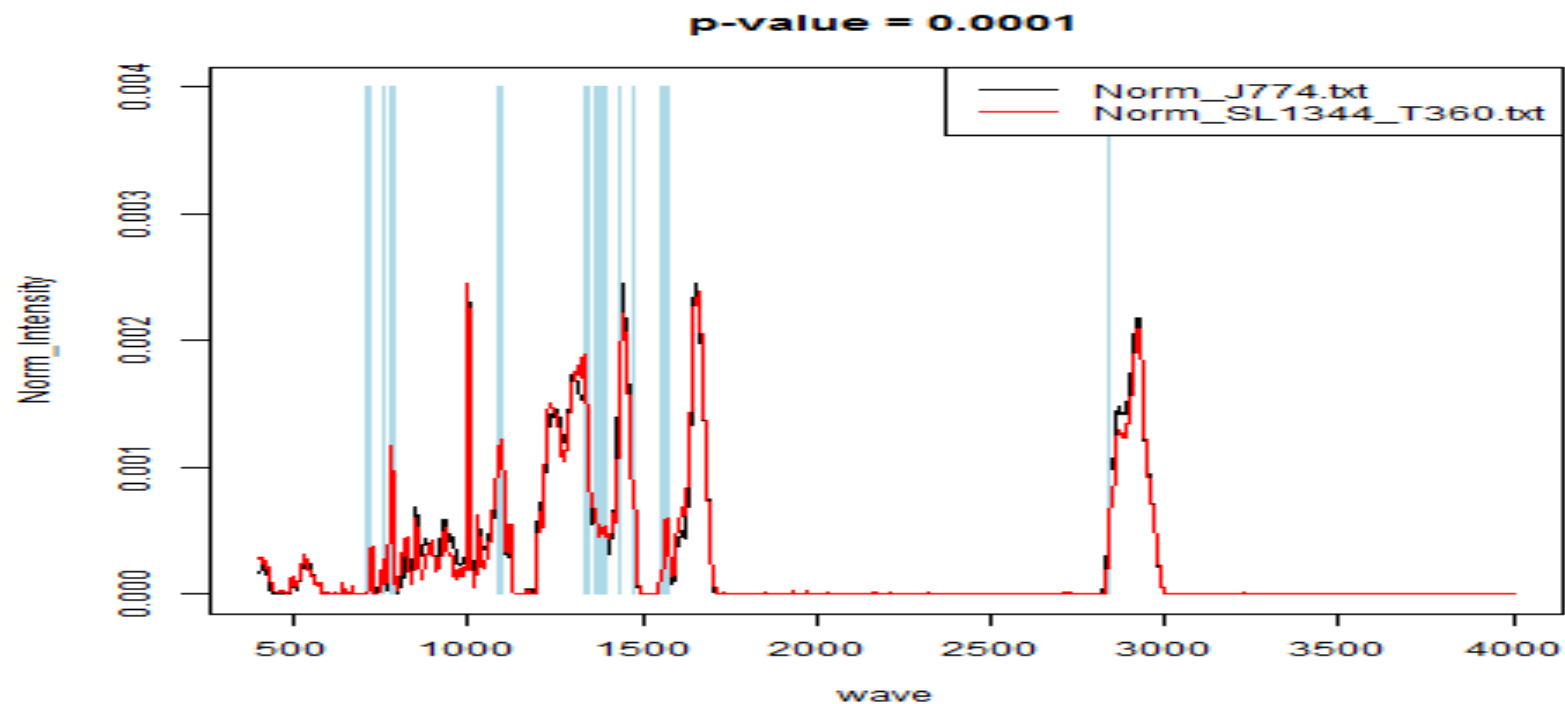


Figure 3.9: Comparison of normalised Raman spectrum collected from *S. Typhimurium* SL1344 wild-type grown in LB broth at stationary phase with mouse macrophage-like cells J774A.1. Y-axis = Normalised Raman intensity (arbitrary units). X-axis = Wavenumbers ( $\text{cm}^{-1}$ ). Black: Normalised spectrum from J774A.1. Red: Normalised spectrum from SL1344. Blue: Wavenumbers at which ANOVA analysis had determine normalised intensities between J774A.1 and SL1344 to be significantly different, P-value  $\leq 0.0001$ .

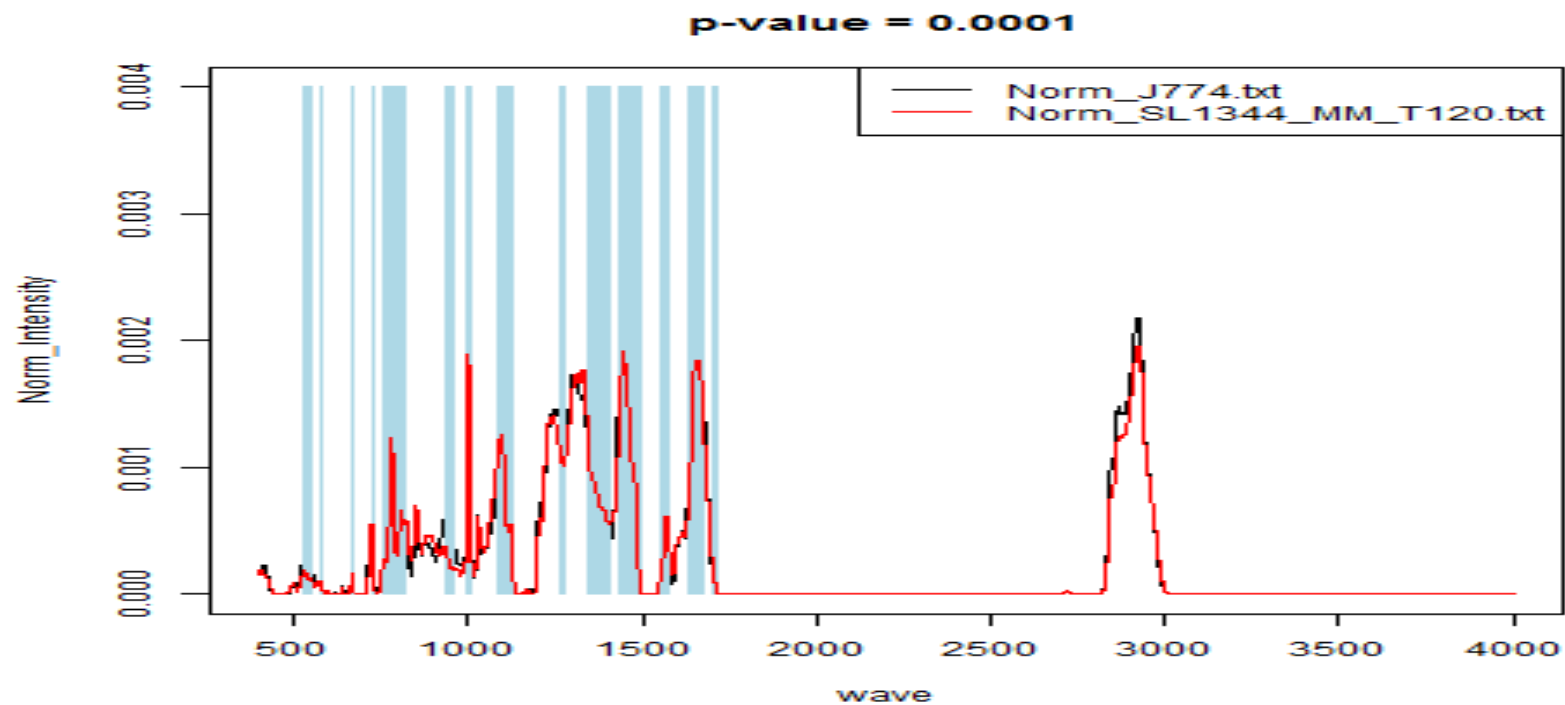


Figure 3.10: Comparison of normalised Raman spectrum collected from *S. Typhimurium* SL1344 wild-type grown in minimal media pH 5.8 broth for 120 min with mouse macrophage-like cells J774A.1. Y-axis = Normalised Raman intensity (arbitrary units). X-axis = Wavenumbers ( $\text{cm}^{-1}$ ). Black: Normalised spectrum from J774A.1. Red: Normalised spectrum from SL1344. Blue: Wavenumbers at which ANOVA analysis had determine normalised intensities between J774A.1 and SL1344 to be significantly different, P-value  $\leq 0.0001$ .

In order to establish whether it would be possible to distinguish features of the bacterial spectrum in the complex environment of the host cell, comparison spectra were obtained from a representative host cell. Normalised spectra from mouse macrophage-like cells J774A.1 were compared with spectra collected from *S. Typhimurium* SL1344 wild-type cells. SL1344 spectra were collected at different growth stages in LB broth. Spectra were also collected from cells grown in MM pH 5.8 broth for 120 min. LB mimicked the extracellular environment of intestine lumen (Balbontin et al., 2006) while MM broth mimicked the macrophage phagosomal environment (Manes et al., 2007). Figure 3.11 showed the differences in spectra obtained from SL1344 after 120 min growth in LB and MM broth with reference to J774A.1 spectrum.

Wavenumbers at which Raman signals were determined to be significantly different between macrophage cells and *S. Typhimurium* SL1344 cells are tabulated in Table 3.1.

**Average plot of all normalised Raman spectra collected from *S. Typhimurium* SL1344 wild-type grown for 120 min in LB and MM broth and mouse macrophage-like cells J774A.1**

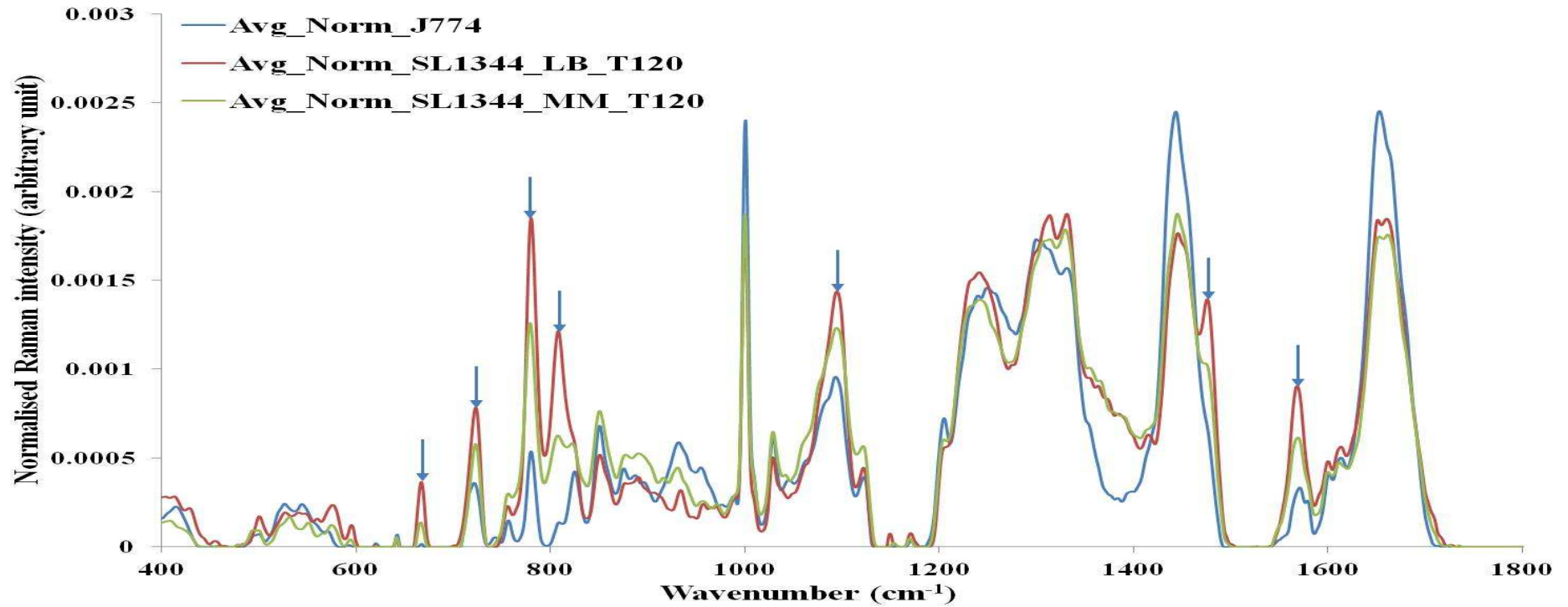


Figure 3.11: Comparison of Raman spectra from *S. Typhimurium* SL1344 wild-type grown for 120 min in LB and MM broth with mouse macrophage-like cells J774A.1. Spectra plotted were average of all spectra collected (both technical and biological replicated). Y-axis = Normalised Raman intensity (arbitrary units). X-axis = Wavenumbers (cm<sup>-1</sup>). **Blue:** Mean normalised spectrum from J774A.1. **Red:** Mean normalised spectrum from SL1344 grown in LB broth for 120 min. **Green:** Mean normalised spectrum from SL1344 grown in MM broth for 120 min. The arrows indicate differences between spectra of SL1344 grown in LB broth and MM broth.

**Table 3.1:** List of wavenumbers ranges at which Raman signals between J774A.1 cells and SL1344 cells from different growth phases were determined to be significantly different. SL1344\_T30: SL1344 at lag phase. SL1344\_T90: SL1344 at early log phase. SL1344\_T120: SL1344 at mid-log phase. SL1344\_T360: SL1344 at stationary phase. SL1344\_MM\_T120: SL1344 grown in minimal media pH 5.8 for 120 min.

<b>J774A.1 vs SL1344_T30</b>	<b>J774A.1 vs SL1344_T90</b>	<b>J774A.1 vs SL1344_T120</b>	<b>J774A.1 vs SL1344_T360</b>	<b>J774A.1 vs SL1344_MM_T120</b>
2839-2858	2843-2845	2838-2861	2841	1706-1712
2826-2837	1699-1714	1700-1718	1565-1574	1671-1677
1557-1577	1646-1667	1639-1672	1558-1559	1636-1668
1468-1488	1597-1598	1550-1595	1475-1480	1632
1428-1446	1551-1594	1467-1493	1433-1434	1553-1578
1384-1392	1468-1493	1426-1461	1376-1398	1469-1493
1368-1379	1426-1452	1343-1408	1367-1372	1431-1459
1324-1339	1353-1406	1332-1337	1332-1347	1342-1408
1308-1319	1334-1336	1264-1273	1090-1101	1262-1272
1235-1246	1198-1202	1087-1106	774-790	1129-1131
1085-1112	1088-1106	1000-1005	756-758	1123-1125
1011-1012	1053-1055	772-955	712-717	1086-1115
976-979	1043-1051	764-767		1000-1003
918-969	998-1035	744		947-954
774-820	985-991	717-730		932
774	975-979	707-709		755-822
720-727	918-969	661-673		724-727
664-670	831-905	594-599		664-671
575-582	774-821	572-586		578-583
	743-744	503-506		543-548
	718-727	434-439		525-526
	707-708			
	662-672			
	596-597			
	575-584			
	545-547			
	520-521			

Spectral data were collected from at least three independent samples and a minimum of three spectra for each sample. Biological and technical replicates were performed to increase the confidence in differences observed from spectra comparison. Spectra from different growth stages and conditions of SL1344 were compared against J774A.1 statistically by one-way ANOVA. Spectra from SL1344 at different growth stages and growth media and spectra from J774A.1 cells were then overlaid and visually compared. Six peaks were selected at which SL1344 cells had higher signal compared to J774A.1 cells. All wavenumbers shortlisted for Raman based imaging were where signals were highest for each of the selected peaks. The higher signal coming from bacterial cells could hopefully aid in discriminating bacteria cells from macrophages during imaging. The shortlisted wavenumbers and their Raman vibration attribution (if available) are summarised in Table 3.2 and indicated on spectra in Figure 3.12.

Another peak of interest was at  $2844\text{ cm}^{-1}$ , representing a C-H vibration mode which gave a strong signal from both SL1344 and J774A.1 cells. This signal could potentially be used to provide background contrast without distinguishing between cells and bacteria.

The last peak selected was the peak at  $1444\text{ cm}^{-1}$  from J774A.1 cells, because coherent Raman at low frequencies is expected to visualise the larger scale host cells rather than bacteria and hence might be used to provide control images.

**Table 3.2: List of wavenumbers selected for Raman based imaging. Ticks represent distinctive Raman signals were present in either mouse macrophage-like cells J774A.1 and *S. Typhimurium* at various growth stages and when cultured in MM.**

Cell types with higher signal	Raman vibration attribution	Wavenumbers (cm <sup>-1</sup> )	J774A.1	SL1344 Lag phase	SL1344 Early log phase	SL1344 Mid log phase	SL1344 Stationary phase	SL1344 Grown in minimal media pH 5.8 for 120 min
SL1344 and J774A.1	CH <sub>2</sub> symmetrical <sup>1</sup>	2844.40	✓	✓	✓	✓	✓	✓
SL1344		1568.92		✓	✓	✓	✓	✓
SL1344	Protein marker band <sup>2</sup>	1476.98		✓	✓	✓	✓	✓
J774A.1		1443.96	✓					
SL1344	Carbohydrate range <sup>3</sup>	1095.78		✓	✓	✓	✓	✓
SL1344	Nucleic acids (C-O-P-O-C in RNA backbone) <sup>2</sup>	809.75		✓	✓	✓		✓
SL1344	Cytosine, uracil (ring, str) <sup>2</sup>	780.66		✓	✓	✓	✓	✓
SL1344		723.98		✓	✓	✓		✓

<sup>1</sup> (Davis et al., 2003), <sup>2</sup> (Huang et al., 2010), <sup>3</sup> (Brehm-Stecher and Johnson, 2004)

**Average plot of all normalised Raman spectra collected from mouse macrophage-like cells J774A.1 and *S. Typhimurium* SL1344 wild-type at early log growth phase**

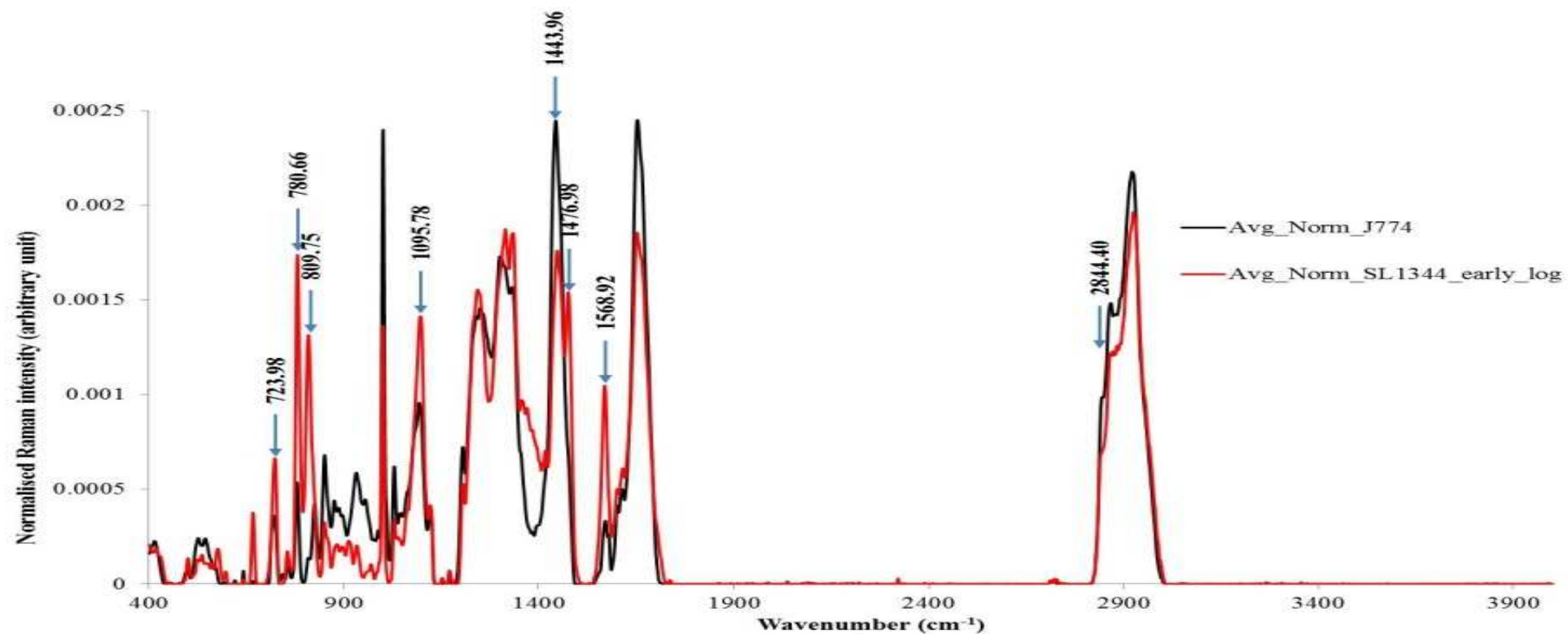


**Figure 3.12:** Overlay Raman spectra of mouse macrophage-like cells J774A.1 and *S. Typhimurium* SL1344 wild-type at early-log growth phase in LB broth. Spectra plotted were average of all spectra collected (both technical and biological replicated). Y-axis = Normalised Raman intensity (arbitrary units). X-axis = Wavenumbers (cm<sup>-1</sup>). Black: Mean normalised spectrum from J774A.1. Red: Mean normalised spectrum from SL1344. The arrows indicates peaks at which the wavenumbers were selected for Raman based imaging.

### 3.2.4 Coherent Raman based imaging

Images of *S. Typhimurium* SL1344 wild-type cells were taken at some of the selected wavenumbers using SRS microscopy. The Stokes beam was fixed at 1064 nm while the pump beam was tuned to achieve, as close as possible, to four of the selected wavenumbers. Representative images are shown in Figure 3.13, demonstrating good contrast particularly at 2841 cm<sup>-1</sup>.

Next; mouse macrophage-like J774A.1 cells were infected with either the *S. Typhimurium* SL1344 wild-type or a *S. Typhimurium* SL1344 *fliC::gfp* mutant. The *fliC::gfp* mutant enabled visualisation of bacteria cells within macrophages under Confocal microscopy, and was used to confirm the spectral identification of the bacteria. As shown in Figure 3.14, the images obtained showed that under the culture conditions employed the bacteria had invaded the host cells. Some host cells had shown to harbour one or more bacteria.

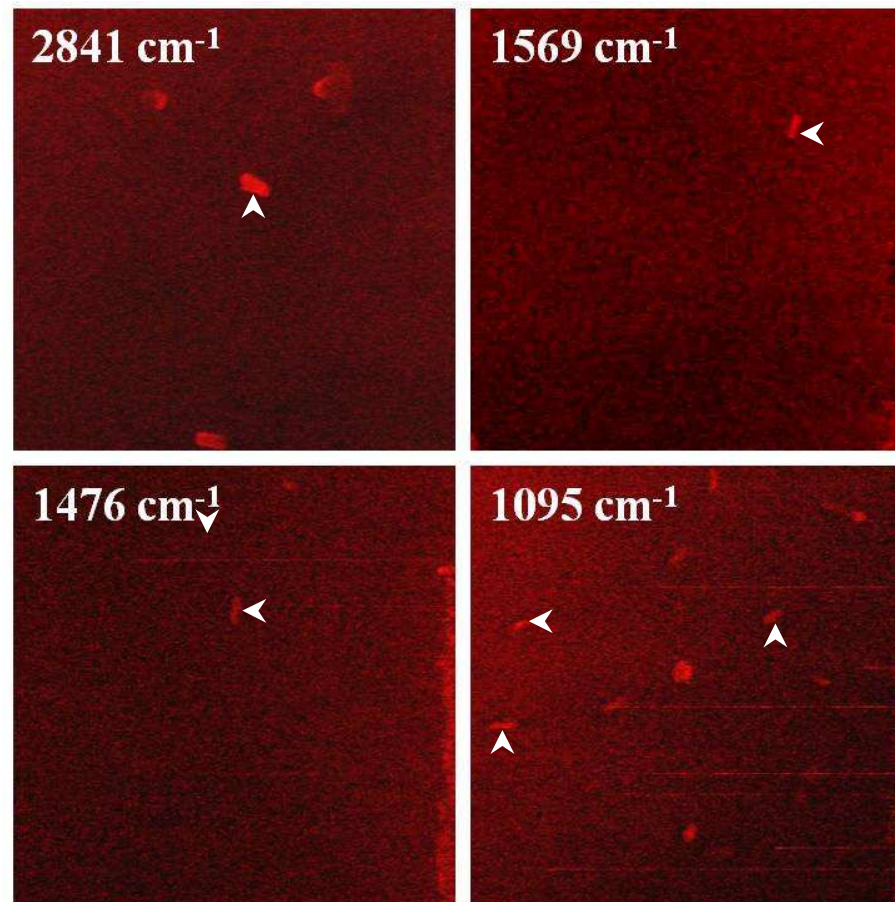
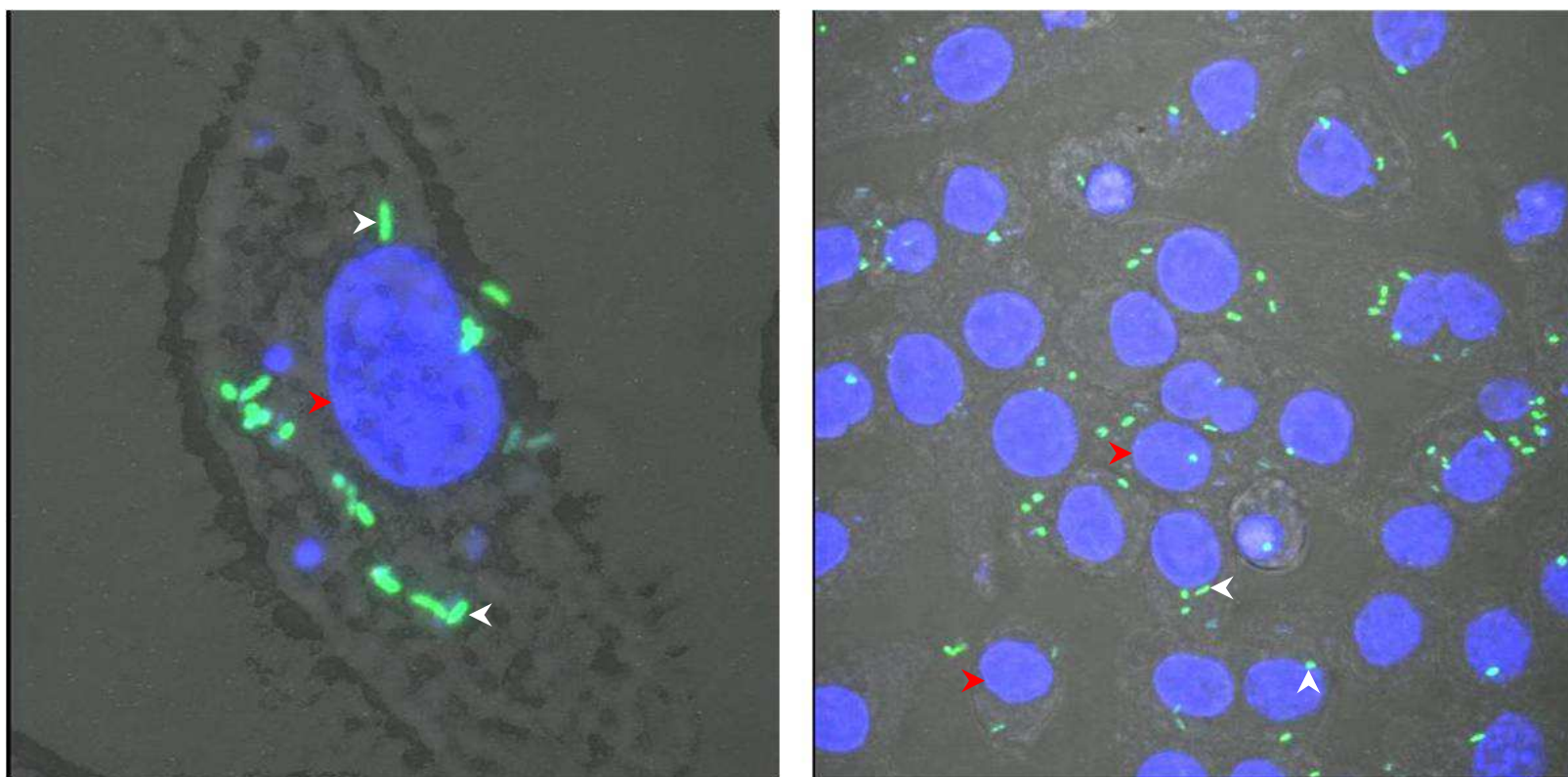


Figure 3.13: SRS images of *S. Typhimurium* SL1344 wild-type at various wavenumbers. SL1344 wild-type cells (arrowed) were at mid log phase (T120) when harvested for imaging. The cell suspension was diluted to OD<sub>590</sub> of 0.01 for imaging.



Mouse macrophage-like cells J774A.1 at 2 hr post-infection by *S. Typhimurium* SL1344 *fliC-gfp* mutant (infection duration = 1 hr, MOI=100)

Figure 3.14: Confocal images of mouse macrophage-like cells J774A.1 infected with *S. Typhimurium* SL1344 *fliC::gfp* mutant at MOI of 100. J774A.1 cells were overlaid with SL1344 *fliC::gfp* mutant for 1 hours before extracellular bacteria cells were killed by gentamicin. Macrophage cells were unstained except for nucleus stained with DAPI and fluoresced blue (red arrow). SL1344 *fliC::gfp* mutant cells fluoresced green (white arrowed). Images were taken 2 hr post-infection. Hours post-infected started together with gentamicin treatment.

Having shown that the bacteria resides within host cells by Confocal, SRS images of J774A.1 cells infected with SL1344 wild-type were taken by SRS microscopy, as shown in Figure 3.15. At each of the wavenumbers identified above features could be identified in the cells of the size expected for bacteria. However, the features were insufficiently sharp to constitute positive identification and so an alternative approach of labelling the bacteria cells with deuterium oxide was employed.

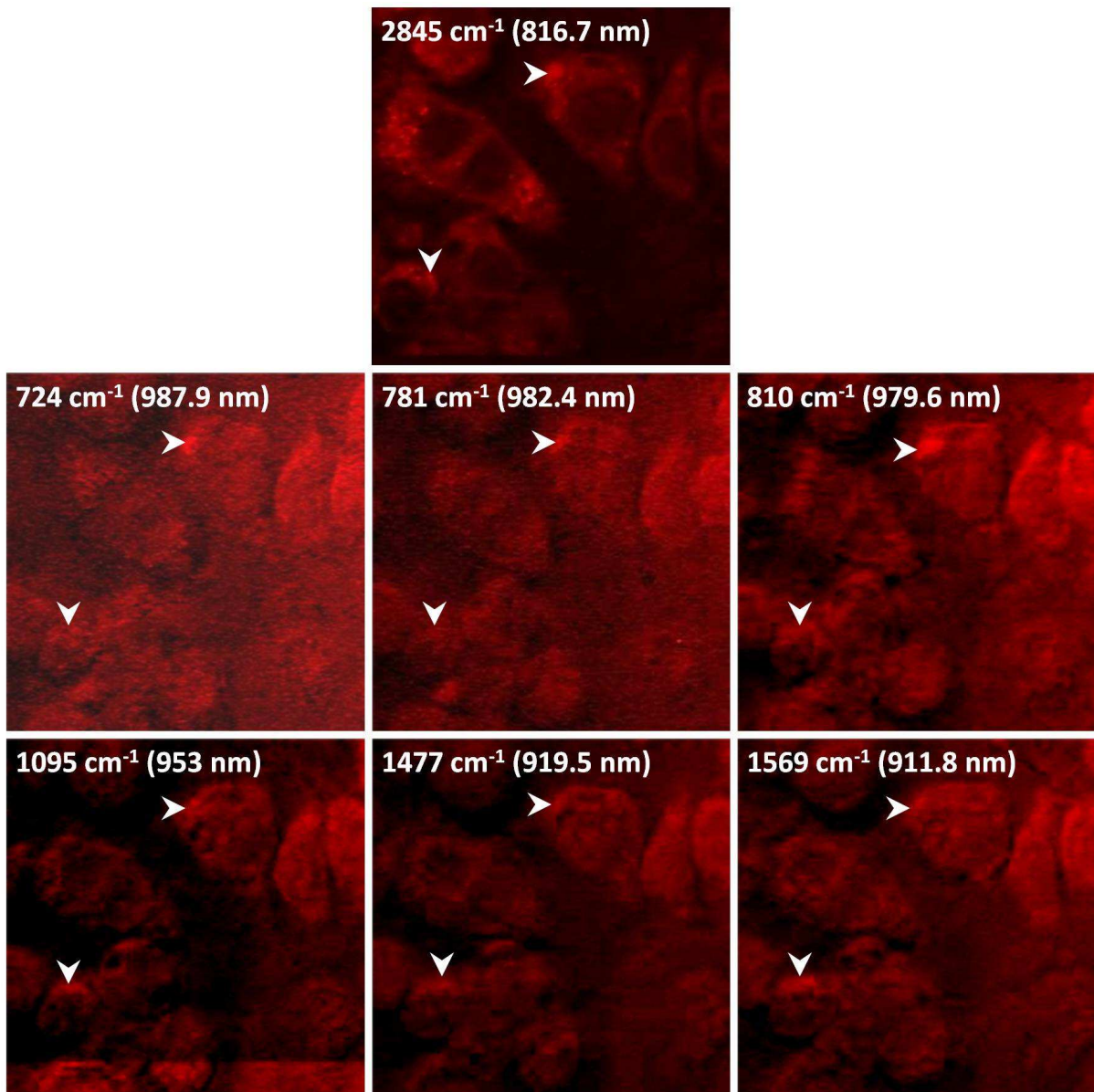


**Figure 3.15:** SRS images of mouse macrophage-like cells J774A.1 infected with *S. Typhimurium* SL1344 wild-type at MOI of 100. Images were taken between 2 to 6 hours post-infection. Stokes beam was fixed as 1064 nm while pump beam (values in brackets) was tuned to achieve closest possible to selected wavenumbers. Signals possibly coming from bacteria cells were indicated with arrows.

### 3.2.5 SRS imaging of deuterated bacteria

The lack of contrast between bacteria and host cells arises because no spectral peaks could be found in the bacteria which were not also present in the host cell. This problem was addressed by replacing C-H bond with C-D bonds which have a different vibrational frequencies. This was effected by incubating SL1344 wild-type in media where water was replaced by deuterium oxide to a percentage of 70%. The Raman spectra of SL1344 wild-type cells grown in LB or MM broth made up with 70% D<sub>2</sub>O were collected. The spectra were compared to spectra from J774A.1 cells and SL1344 cells grown in LB and MM, as shown in Figure 3.16.

The results obtained showed that culturing of SL1344 wild-type in media containing D<sub>2</sub>O gave an additional peak at 2148 cm<sup>-1</sup>. This frequency could only be found in bacterial cells grown in D<sub>2</sub>O media and not in macrophages; so it was used for SRS imaging. SRS images of SL1344 wild-type cells grown in LB made up of 70% D<sub>2</sub>O were taken at selected wavenumbers and are shown in Figure 3.17.

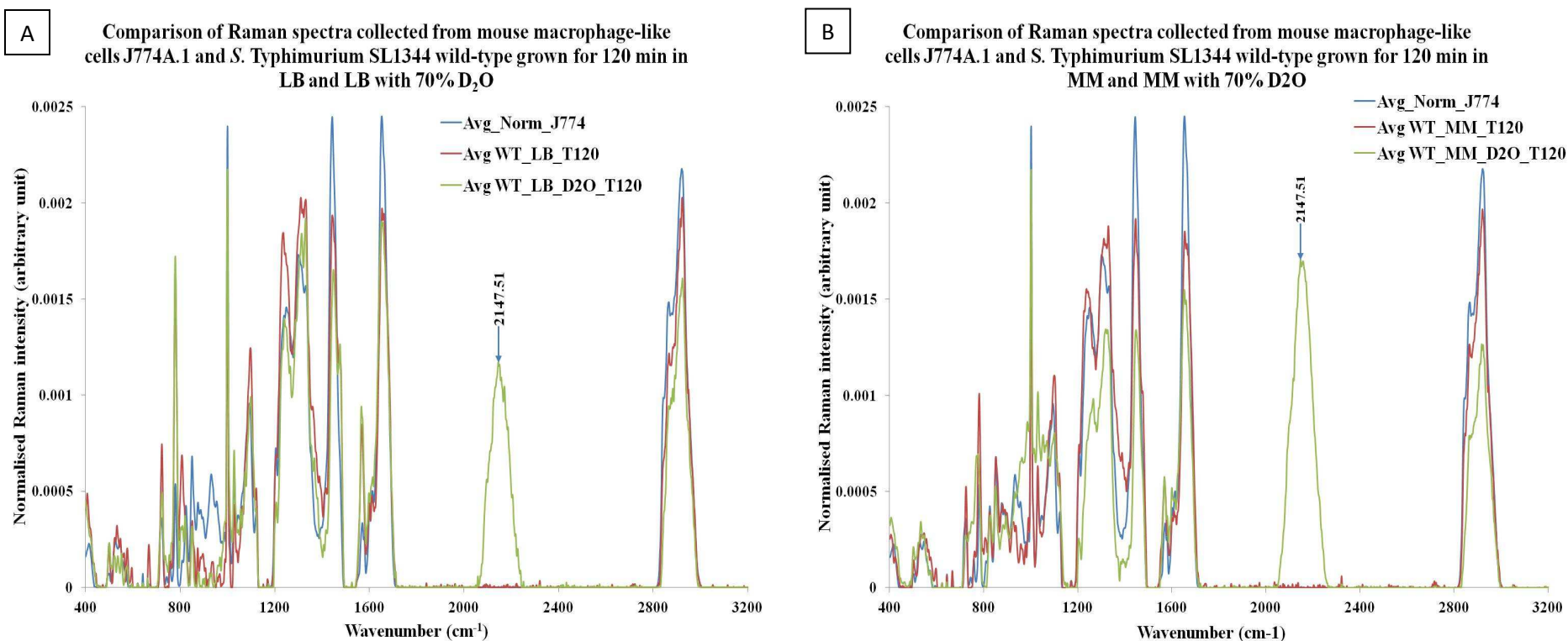


Figure 3.16: Comparison of Raman spectra from *S. Typhimurium* SL1344 wild-type grown in media with and without deuterium oxide with mouse macrophage-like cells J774A.1. Spectra plotted were average of all spectra collected (both technical and biological replicated). Y-axis = Normalised Raman intensity (arbitrary units). X-axis = Wavenumbers ( $\text{cm}^{-1}$ ). (A) **Blue**: Mean normalised spectrum from J774A.1. **Red**: Mean normalised spectrum from SL1344 grown in LB broth for 120 min. **Green**: Mean normalised spectrum from SL1344 grown in LB broth consisting of 70%  $\text{D}_2\text{O}$  for 120 min. (B) **Blue**: Mean normalised spectrum from J774A.1. **Red**: Mean normalised spectrum from SL1344 grown in MM broth for 120 min. **Green**: Mean normalised spectrum from SL1344 grown in LB broth consisting of 70%  $\text{D}_2\text{O}$  for 120 min. The arrows indicate peaks from carbon-deuterium (C-D) vibration ( $2147.51 \text{ cm}^{-1}$ ), which is only present in cells grown in media containing  $\text{D}_2\text{O}$ .

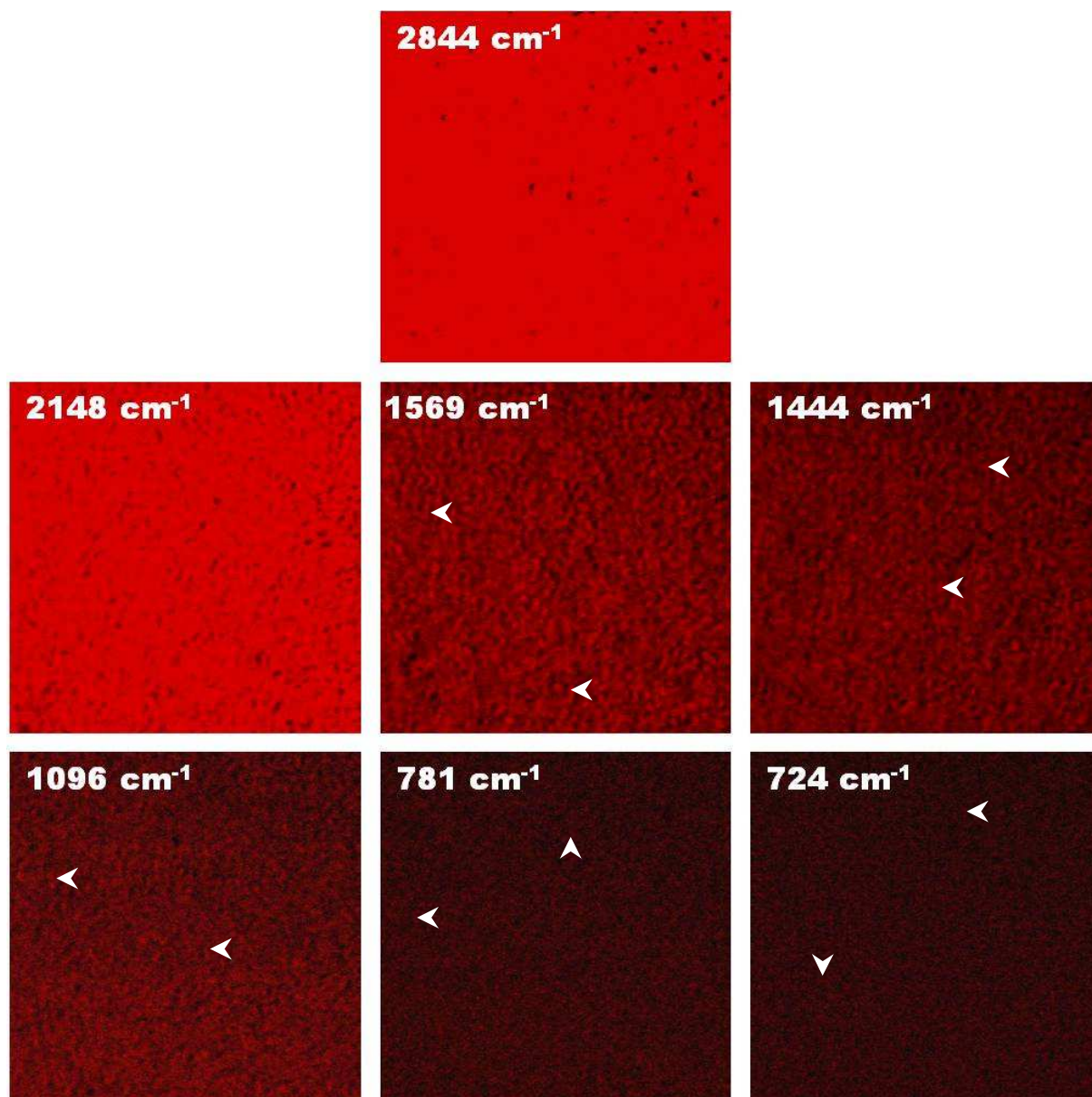
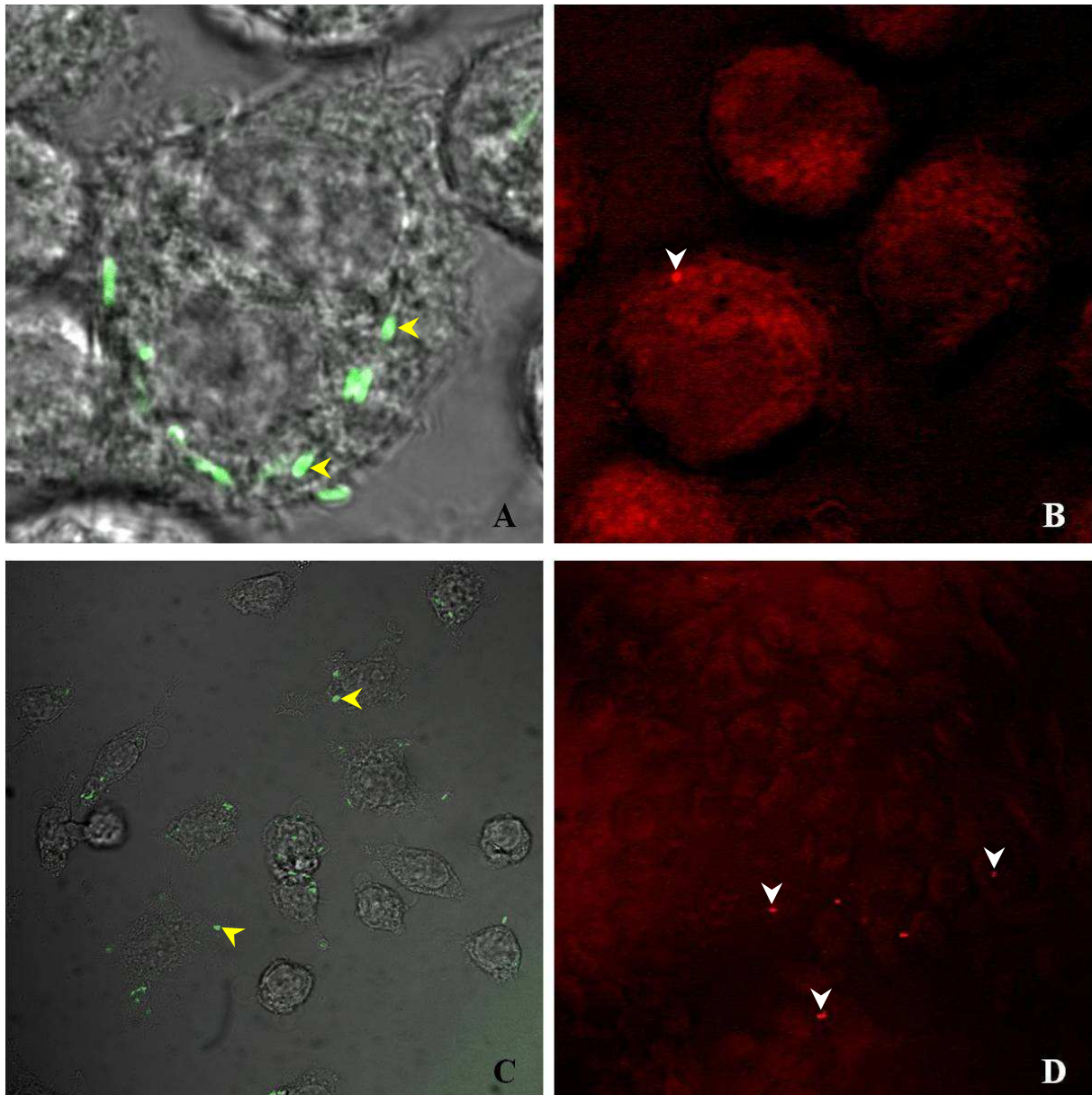


Figure 3.17: SRS images at various wavenumbers of *S. Typhimurium* SL1344 wild-type grown in LB broth made up with 70% Deuterium oxide and 30% water. SL1344 wild-type cells were at mid log phase (T120) when harvested for imaging. Stokes beam was fixed as 1064 nm while pump beam was tuned to achieve closest possible to selected wavenumbers. Cell density was  $5 \times 10^7$  cfu/ml. At  $2844 \text{ cm}^{-1}$  (C-H vibration frequency) and  $2418 \text{ cm}^{-1}$  (C-D vibration frequency), the signals were high and cell suspension was too dense and led to overexpose images. Due to the high cell density, individual cells in the remaining images were marked by arrows.

The images show that culturing of the bacteria cells in media containing D<sub>2</sub>O did not affect SRS imaging: a point to note is that although at 1444 cm<sup>-1</sup>, J774A.1 cells were shown to have a higher signal than SL1344 cells, the signal from the bacteria was strong too. Hence, it was still possible to capture bacterial images at this frequency.

SL1344 *fliC::gfp* mutant was also grown in LB consisting of 70% D<sub>2</sub>O and was used to infect J774A.1 cells. Confocal images in Figure 3.18 show that culturing in D<sub>2</sub>O containing media had not affected its ability to infect macrophages. In parallel, SL1344 wild-type cells grown in LB consisting of 70% D<sub>2</sub>O was also used to infect J774A.1 cells. Images of macrophages infected with SL1344 wild-type were captured at carbon-deuterium (C-D) frequency (Figure 3.18).



**Figure 3.18:** Mouse macrophage-like cells J774A.1 infected with *S. Typhimurium* SL1344 wild-type and *fliC::gfp* mutant grown in LB broth made up with 70% Deuterium oxide and 30% water. **A:** Confocal image of J774A.1 cells infected with SL1344 *fliC::gfp* mutant (indicated by the yellow arrows) at 30 min post-infection. **B:** SRS image at C-D frequency ( $2148\text{ cm}^{-1}$ ) of J774A.1 cells infected with SL1344 wild-type (indicated by the white arrows) at 30 min post-infection. Outlines of macrophage cells were visible and cell nuclei were the dimmer region within the macrophage cells. **C:** Confocal image of J774A.1 cells infected with SL1344 *fliC::gfp* mutant at 120 min post-infection (indicated by the yellow arrows). **D:** SRS image at C-D frequency ( $2148\text{ cm}^{-1}$ ) of J774A.1 cells infected with SL1344 wild-type (indicated by the white arrows) at 120 min post-infection. In Confocal images, bacteria cell fluoresced **green** and in SRS images, bacteria cells signal are brighter **red** against the baseline.

In Figure 3.18 (A), the bacterial cells appeared to be inside macrophage cell cytoplasm and distributed around the nucleus. Similarly, SRS images from the same time point (Figure 3.18 (B)) also showed stronger signals within the macrophage cells and around the nucleus. At 120 min post-infection, bacterial cells seemed to be sparsely distributed in both Confocal and SRS images - as shown in Figure 3.18 (C) and (D). Fewer bacterial cells were detected in SRS image (Figure 3.18 (D)).

SRS images of J774A.1 cells infected with SL1344 wild-type grown in LB consisting of 70% D<sub>2</sub>O were then taken at selected wavenumbers, as shown in Figure 3.19.

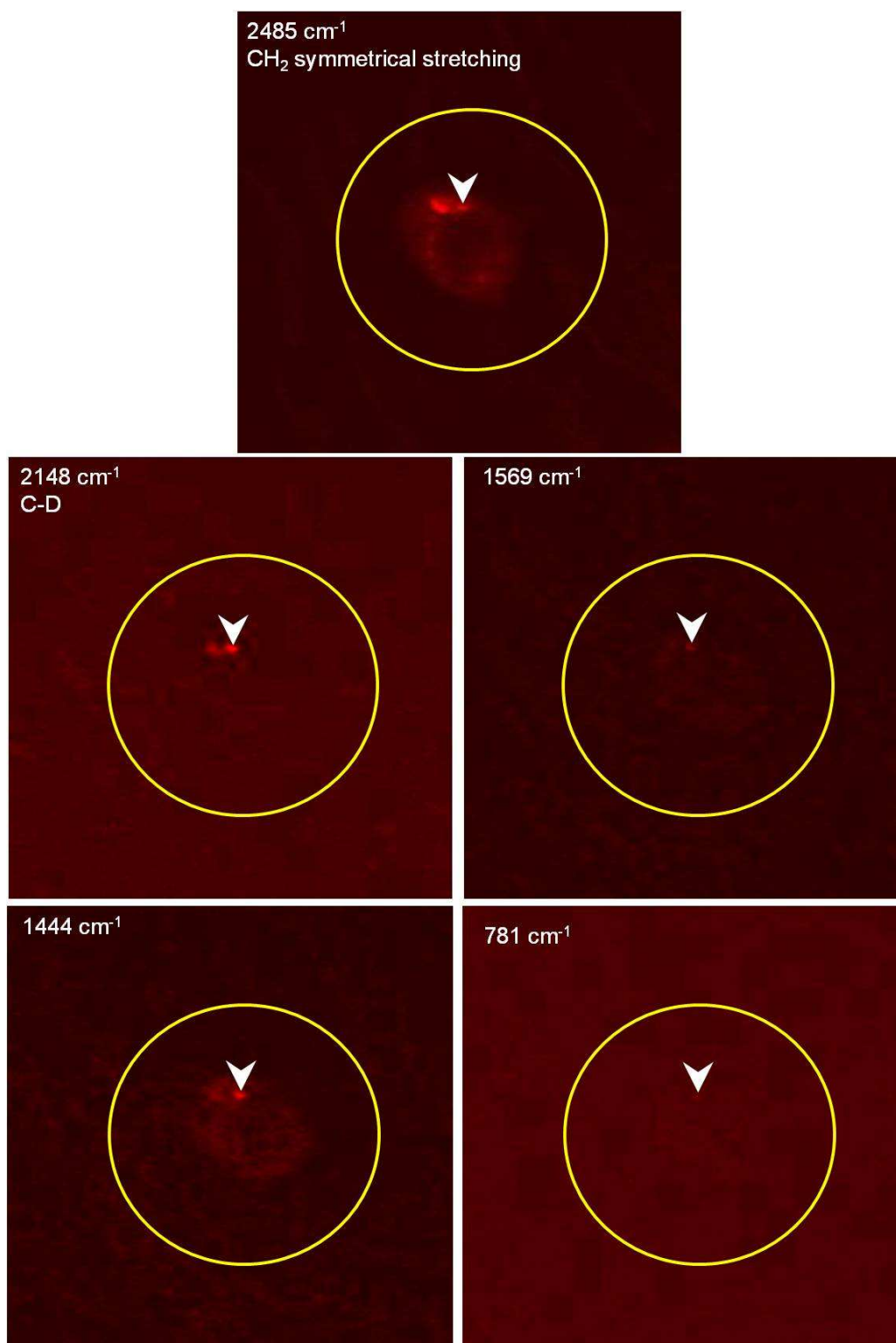


**Figure 3.19:** SRS images of mouse macrophage-like cells J774A.1 infected with *S. Typhimurium* SL1344 wild-type grown in LB broth made up with 70% Deuterium oxide and 30% water, at MOI of 100. Images were taken between 2 to 6 hours post-infection. Stokes beam was fixed as 1064 nm while pump beam was tuned to achieve closest possible to selected wavenumbers. A macrophage cell was enclosed within the yellow circle. Arrows pointing to potential signals from bacteria cells within the macrophage cell.

Regions of the size and shape expected of the bacteria were visible in images at  $2148\text{ cm}^{-1}$ . The same regions were also visible at  $1569\text{ cm}^{-1}$ ,  $1444\text{ cm}^{-1}$  and  $781\text{ cm}^{-1}$  and so these modes were most likely also to be from bacteria cells, confirming the preliminary identification made above.

Unfortunately, subsequent attempts of imaging did not yield similar outcomes. Images could only be captured at the high frequency C-H stretching region. This was due to an ongoing technical fault with the laser system which caused it to become unstable when the pump wavelength was tuned to the longer wavelengths required to access lower vibrational frequencies.

### 3.3 Discussion

A raw Raman spectrum collected from the spectrometer requires smoothing and background subtraction before useful information can be extracted from it. The smoothing process helps to reduce noise collected during the Raman spectrum acquisition and enables better resolution of spectral peaks (Ferraro et al., 2003). Spectral smoothing here were initially performed using the instrument software WIRE2.0, where Savitsky-Golay smoothing was applied. In Savitsky-Golay smoothing a weighted average of adjacent points of each point in the original spectrum was used to plot the smoothed spectrum (Ferraro et al., 2003). The smoothing process only reduced noise but not the baseline. Hence, in order for comparison of spectra collected from different samples, the baseline in each spectrum was removed.

There are several approaches available for baseline removal. It can be done either manually or automatically with an algorithm. Manual baseline removal requires user input in identifying which is a baseline and which is a signal. This is user dependent, subjective and often non-reproducible (Lau et al., 2012). The baselines of spectra collected here were subjected to baseline removal through application of an algorithm the BHW smoother, was developed in-house together with Dr Ron Yang (Lau et al., 2012).

The BHW algorithm is a Bayesian interpretation of Whittaker-Henderson's with revised fidelity. The latter is a typical Least-square error model commonly used in baseline estimation (Lau et al., 2012). The Bayesian interpretation is a learning process applied to estimate parameters for the model used (Lau et al., 2012). The BHW algorithm had been

shown to perform better than other commonly used algorithm such as Peaks, Spline, msProcess and airPLS on simulated data (Lau et al., 2012). BHW had also been shown to perform better than Spline when applied to real spectra (Lau et al., 2012).

Beside baseline issues of spectra collected, the intensity of each peak was dependent on the amount of material available in each focal volume. Within the same sample materials were distributed unevenly across the surface while drying and hence peak intensities differs between focal points. Before spectra could be combined or compared, it was important that the intensity range of each spectrum to be normalised (Ferraro et al., 2003). Each spectrum collected was normalised to achieve total area under the spectrum as 1. This is a commonly used normalisation approach especially when the spectra do not shared a common peak (Ferraro et al., 2003). The spectral processing protocol was applied to all spectra collected.

The Raman spectrum provides a chemical fingerprint of the cell being interrogated (Huang et al., 2010). This information enables differentiation between cell types (Huang et al., 2010) and is likely to be influenced by gene expression and may be regulated by factors such as: temperature, pH and nutrient availability (Huang et al., 2010). It has previously been reported that closely related species could be differentiated based on their Raman spectrum, for example different *Bacillus* species (Hutsebaut et al., 2004), *Staphylococcus epidermidis* strains and *E. coli* strains (Almarashi et al., 2012).

When the bacteria cells were actively growing, intensities at proteins ( $1477\text{ cm}^{-1}$ ) and nucleic acids ( $781\text{ cm}^{-1}$  and  $810\text{ cm}^{-1}$ ) wavenumbers were highest. However, as it entered stationary

phase, two peaks were lost, one at  $810\text{ cm}^{-1}$ . The  $810\text{ cm}^{-1}$  peak was assigned to "Cytosine, uracil (ring, str)" (Huang et al., 2010). This observation coincided with previous reported work on *Acinetobacter sp.*, *E. coli* and *Pseudomonas fluorescens* (Huang et al., 2004). The "Cytosine, uracil (ring, str)" peak was observed in the exponential phase of these cells but not at stationary phase (Huang et al., 2004). The spectra of bacteria cells collected at various growth stages differs and such information could potentially be used in future to determine physiological stages of bacteria cells. However, more work would be required to investigate further into the potential of this application. It would also require building up of spectra libraries of different bacteria, in different growth conditions and at different growth stages .

In order to achieve Raman based imaging of bacteria cells within macrophages, the differences in Raman spectrum between the two cell types were exploited. Raman spectra were collected from *S. Typhimurium* strain SL1344 grown at different growth stages and under different growth conditions. Raman spectra were also collected from mouse macrophage-like cells J774A.1, as a representative host cell.

In the initial attempt to image J774A.1 cells infected with SL1344, images were obtained at each of the selected wavenumbers, except for  $1443.96\text{ cm}^{-1}$ . Images obtained showed that signals higher than background were detected in two of the macrophage cells (Figure 3.15). The signals were detected in all the images captured at  $724\text{ cm}^{-1}$ ,  $781\text{ cm}^{-1}$ ,  $810\text{ cm}^{-1}$ ,  $1095\text{ cm}^{-1}$ ,  $1477\text{ cm}^{-1}$  and  $1569\text{ cm}^{-1}$ . These were the wavenumbers where signals were thought to be coming more strongly from bacterial cells rather than macrophage cells. The images captured suggested that the signal observed were likely to be from bacterial cells within macrophages. However, this could not be validated. Hence, although the objective of Raman

based imaging was label-free imaging, for validation, bacteria cells were required to be labelled.

In order to validate the images, the bacterial cells were required to be specifically labelled and be detectable by Raman microscopy. For this reason the approach used was to culture the bacterial cells in broth media made up with 70% of D<sub>2</sub>O. The deuterium atom will replace the hydrogen atom. This resulted in an additional molecular vibration frequency, C-D vibration. This additional peak was unique to the bacteria grown in the deuterium oxide media, and was not present in macrophage cells. When images obtained from the selected wavenumbers coincided with images from C-D frequency, it strongly suggested that the images obtained were truly from the bacteria cells.

It has been reported that microorganisms are more tolerant to deuterium oxide as compared to multicellular organisms (Hirai et al., 2010). For example, *Vibrio phosphorescens* was able to survive in prolonged contact with heavy water (Harvey, 1934). Deuterium oxide had been used in Raman based imaging to prevent heating of sample (Zumbusch et al., 1999), but not for image validation. Here, SL1344 were able to grow in media containing 70% D<sub>2</sub>O. The Raman spectra obtained showed some variations between cells grown in LB broth and in LB broth media made up with 70% of D<sub>2</sub>O; the most distinct difference is the addition of a peak at 2148 cm<sup>-1</sup> for cells grown in media containing D<sub>2</sub>O. This additional peak corresponded to C-D vibration. Although variations were observed in the Raman profile, the ability of the bacteria cells grown in media containing D<sub>2</sub>O to infect macrophages was not affected - rendering it to be suitable for imaging work.

SRS imaging of deuterium treated SL1344 in Figure 3.19 showed again that signals were detected at the same spot within macrophage cells across the selected wavenumbers. In this set of images the spot was also detected in the wavenumbers for C-D vibration. This validated the signals detected in those selected wavenumbers.

The results obtained showed that the selected wavenumbers were able to provide discriminative imaging of bacteria cells within macrophages. This is the first time that bacterial cells were distinctly imaged by SRS within macrophages based on carefully selected wavenumbers. It successfully demonstrated the potential of SRS microscopy in discriminative imaging for bacterial cells within macrophages with the selected wavenumbers. However, the quality of images was limited and further development of this approach was not possible, largely because of the instability of the laser system when operated at low frequencies which I found to be necessary. Further development of laser technology should overcome this problem and imaging of bacteria interacting with live cells in real-time and in a label-free manner could then provide more insight into bacteria and host cell interactions. It could also potentially be used to image bacteria cells within a whole organism, such as optically clear zebrafish embryos, in a label-free manner.

As reproducible results could not be obtained at present, this study was terminated and did not proceed to explore its potential use in interrogating *Campylobacter* molecular make-up for Raman based imaging. However, the ZFE infection model was established in this study as discussed in Chapter 4. Attempts in making reporter *Campylobacter* strains using

fluorescence makers had shown to be difficult (refer to Chapter 4). The resultant strains were weak in fluorescence signals, making it unsuitable to perform live-imaging to investigate interaction between the bacteria and host cells. Hence, it is important to continue to develop a label-free live-imaging technique for *Campylobacter*; the Raman based imaging provides the potential to perform live-imaging of *Campylobacter* in its native form. When the laser system for Raman based imaging matures, it could be used in the interrogation of the interaction of *Campylobacter* with host immune cells *in vivo* in a label-free manner.

**Chapter 4: Development of ZFE as an optically transparent  
infection model for *Campylobacter jejuni***

## 4.1 Introduction

### 4.1.1 Animal models for *Campylobacter*

A good animal model is essential in the understanding of disease and the patho-physiology of infection. In order to study disease an animal model should ideally be able to reproduce the disease as it would in a human host. The route of challenge used should be physiologically relevant, mimicking the natural route of infection in humans and the challenge dosage should be low. The model should produce robust, reproducible results and ideally be low cost and ethically acceptable (Ruiz-Palacios et al., 1981). Bovine, canine, feline, avian, murine and swine models have been explored for understanding Campylobacteriosis (Babakhani et al., 1993; Janssen et al., 2008; Jones and Little, 1931a, b; Jones et al., 1931; Prescott et al., 1981; Prescott and Karmali, 1978; Ruiz-Palacios et al., 1981; Sanyal et al., 1984; Young et al., 2007). However, none of these models met all the criteria stated above. For example, they are either high maintenance / cost for calves and piglets models (Jones and Little, 1931a, b; Jones et al., 1931), they do not reproduce disease outcomes observed in humans, such as in canine, feline and murine models (Prescott et al., 1981; Prescott and Karmali, 1978) or the route of infection used is not the natural route for human infection, for example in murine model (Janssen et al., 2008; Young et al., 2007).

#### 4.1.2 ZFE as infection model

ZFE have been widely used in developmental studies. This is largely because of their optical transparency properties. However, ZFE are gaining popularity in pathogen studies as model organisms for the study of disease caused by *Mycobacterium*, *Pseudomonas* and *Salmonella*, (Clatworthy et al., 2009; Davis et al., 2002; van der Sar et al., 2003; Wang, 2010). There are currently no reports on the use of ZFE as a model for Campylobacteriosis studies.

There are several advantages to ZFE as a model for infectious diseases studies, namely; i) low cost and maintenance; ii) minimal lab space requirement; iii) ease of handling; iv) *ex vivo* embryo development; v) transparency and most importantly; vi) similar immune system (innate and adaptive) to human and other vertebrates (Phelps and Neely, 2005). These features can be exploited to gain a better understanding of the interaction of *Campylobacter* with innate immunity cells, such as macrophages, *in vivo*.

#### 4.1.3 Aim of study

The aim of this study was to develop a ZFE infection model for *Campylobacter*.

## 4.2 Results

### 4.2.1 Determining the site of inoculation in ZFE for *Campylobacter* infection model

In this study *C. jejuni* strain Cj11168H was first inoculated into the ZFE yolk sac's circulation valley (CV) in embryos at 30 or 52 hpf. The bacteria were grown at 37°C or 42°C on CBA+ or in MHB. Each embryo was inoculated with approximately 2-4 nl of bacterial suspension adjusted to OD<sub>590</sub> of approximately 10. The cell density for Cj11168H wild-type cells from 24 hr broth culture at 37°C, at OD<sub>590</sub> 1 was, on average, 5x10<sup>8</sup> CFU/ml (calculated from 17 different dilution spots counts). The mean inoculum volume was set as 3 nl, hence the number of bacteria cells inoculated into each embryo was approximately 15,000 CFU. The survival of challenged embryos at 24 hpi are summarised in Table 4.1.

The conditions in which *Campylobacter* was grown had previously been shown to affect killing of *G. mellonella* (Champion et al., 2010), therefore, bacteria were cultured under different conditions; i.e. at 37°C or 42°C in broth or on agar before challenging ZFE. The results obtained showed that for CV inoculation, almost all of the embryos remained alive at 24 hpi regardless of the culturing conditions.

Next, another route of infection was investigated. Bacteria were inoculated into the yolk sac (YS) of the embryos instead of its CV. When 28 hpf embryos were challenged with OD<sub>590</sub> ~10 of Cj11168H grown at 37°C in MHB, all but one out of 93 challenged embryos were dead at 24 hpi (Table 4.2), while embryos challenged at 28 or 52 hpf with Cj11168H grown

at 42°C on CBA+ had 55% and 70% survival respectively (Table 4.2). The results obtained showed that ZFE were more susceptible when *C. jejuni* was inoculated into the YS. Hence, for all subsequent infection assays the bacteria cells were inoculated into the embryo's yolk sac.

**Table 4.1:** ZFE were challenged with *C. jejuni* Cj11168H wild-type cells that were inoculated into CV of 30 or 52 hour post-fertilisation (hpf) embryos. The bacteria were cultured at either 37°C or 42°C either on CBA+ or in MHB. Optical density of bacteria cells were adjusted to approximately OD<sub>590</sub> 10 for inoculation. A total of 4 different batches of ZFE were used. Survival percentage of challenged ZFE at 24 hpi was as tabulated.

Bacterial culture temperature (°C)	Culture media	Stage of development (hpf)	Mean optical density of bacteria cell suspension (OD <sub>590</sub> )	Number of embryos challenged	Batch number	Survival percentage at 24 hpi (%)
37	CBA+	30	10.25	25	1	100
		52	10.6	24	2	96
	MHB	30	10	25	1	100
		52	9.6	25	2	100
42	CBA+	30	10.6	20	3	100
		52	9.6	21	4	100
	MHB	30	9.8	20	3	100
		52	10.2	21	4	100

**Table 4.2:** ZFE were challenged with *C. jejuni* Cj11168H wild-type cells that were inoculated into YS of 28 or 52 hour post-fertilisation embryos. The bacteria were cultured at either 37°C or 42°C either on CBA+ or in MHB. Optical density of bacteria cells were adjusted to approximately OD<sub>590</sub> 10 for inoculation. A total of 6 different batches of ZFE were used. Survival percentage of challenged ZFE at 24 hpi was as tabulated.

Bacterial culture temperature (°C)	Culture media	Stage of development (hpf)	Mean optical density of bacteria cell suspension (OD <sub>590</sub> )	Number of embryos challenged	Batch number	Mean survival percentage at 24 hpi (%)
37	CBA+	28		Not Tested		
		52				
	MHB	28	10	93	5 to 9	2
		52		Not Tested		
42	CBA+	28	9.9	46	10 & 11	55
		52	9.65	47	10 & 11	70
	MHB	28		Not Tested		
		52				

#### 4.2.2 Determining the developmental stage of ZFE for *Campylobacter* infection model

In order to develop a ZFE infection model for *Campylobacter* embryos were challenged with bacteria at 28 hpf or 52 hpf. These developmental stages were chosen based on the expected presence of macrophages, and both macrophages and neutrophils in the organism respectively.

The ZFE were challenged with *C. jejuni*, strain Cj11168H or strain Cj81-176\_CP. The bacterial cell suspensions at an optical density of approximately 10 were inoculated into YS of 28 hpf or 52 hpf embryos. The percentage survival of the embryos at 24 hpi is summarised in Table 4.3. The results from Batch number 10 & 11 (previously presented in Table 4.2) was re-presented here for comparison with results obtained from Cj81-176\_CP.

The number of infected embryos alive at 24 hpi was lower for embryos challenged at 28 hpf as compared to those challenged at 52 hpf. This result indicates that embryos at 28 hpf were more susceptible to the infection, hence they were used for subsequent infection assays.

**Table 4.3:** ZFE were challenged with *C. jejuni* Cj11168H or Cj81-176\_CP wild-type cells that were inoculated into YS of 28 or 52 hour post-fertilisation embryos. The bacteria were cultured at 42°C either on CBA+ or in MHB. Optical density of bacteria cells were adjusted to approximately OD<sub>590</sub> 10 for inoculation. A total of 4 different batches of ZFE were used. Survival percentage of challenged ZFE at 24 hpi was as tabulated.

<i>C. jejuni</i> strain	Culture media	Stage of development (hpf)	Mean optical density of bacteria cell suspension (OD <sub>590</sub> )	Number of embryos challenged	Batch number	Mean survival percentage at 24 hpi (%)
Cj11168H	CBA+	28	9.9	46	10 & 11	55
		52	9.65	47	10 & 11	70
	MHB	28		Not Tested		
		52				
Cj81-176_CP	CBA+	28	11	40	12 & 13	40
		52	10.5	40	12 & 13	80
	MHB	28	11	40	12 & 13	48
		52	10	35	12 & 13	60

#### 4.2.3 Effects of culture conditions on infection of ZFE by *C. jejuni*

*C. jejuni* was cultured at 42°C (mimicking the chicken host environment) or 37°C (mimicking human host environment) and tested using ZFE infection model. The bacteria were also grown using two different media CBA+ and MHB.

The survival percentages of ZFE challenged at 28 or 52 hpf with agar grown or broth grown Cj81-176\_CP (Table 4.4, the data on Cj81-176\_CP was extracted from Table 4.3) were analysed by one-way ANOVA followed by uncorrected Fisher's least significant difference (LSD) test, at 95% confidence level. The results showed that differences between the survival percentages of the four groups were not significant. Based on prior observations in the *G. mellonella* model (when challenged with  $10^6$  CFU agar grown *Campylobacter* cells some larvae survived, but when challenged with same amount of broth grown *Campylobacter* cells all larvae died (Champion et al., 2010)), *Campylobacter* cells grown in broth culture were selected as the culturing condition for subsequent assays.

The results obtained showed a higher mortality when bacteria were grown at 37°C than at 42°C (Table 4.5). The data obtained was tested using t-test and the results showed the difference between the survival percentages was significant at 95% confidence (P-value = 0.016). Thus, in subsequent assays, the bacteria cells were cultured at 37°C prior to infecting ZFE.

All the results obtained were used to define the parameters for using the ZFE as an infection model for *Campylobacter* studies. The optimised ZFE infection model uses embryos at 28 hpf and *Campylobacter* cells pre-grown at 37°C in broth and inoculated into the embryo's YS.

**Table 4.4:** ZFE were challenged with *C. jejuni* Cj81-176\_CP wild-type cells that were inoculated into YS of 28 or 52 hour post-fertilisation embryos. The bacteria were cultured at 42°C either on CBA+ or in MHB. Optical density of bacteria cells were adjusted to approximately OD<sub>590</sub> 10 for inoculation. A total of 2 different batches of ZFE were used. Survival percentage of challenged ZFE at 24 hpi was as tabulated.

<i>C. jejuni</i> strain	Stage of development (hpf)	Culture media	Mean optical density of bacteria cell suspension (OD <sub>590</sub> )	Number of embryos challenged	Batch number	Mean survival percentage at 24 hpi (%)
Cj81-176_CP	28	CBA+	11	40	12 & 13	40
		MHB	11	40	12 & 13	48
	52	CBA+	10.5	40	12 & 13	80
		MHB	10	35	12 & 13	60

**Table 4.5:** ZFE were challenged with *C. jejuni* Cj11168H wild-type cells that were inoculated into YS of 28 hour post-fertilisation embryos. The bacteria cells cultured at either 37°C or 42°C in MHB. Optical density of bacteria cells were adjusted to approximately OD<sub>590</sub> 1 for inoculation. A total of 3 different batches of ZFE were used. Survival percentage of challenged ZFE at 24 hpi was as tabulated.

Bacterial culture temperature (°C)	Mean optical density of bacteria cell suspension (OD <sub>590</sub> )	Number of embryos challenged	Batch number	Mean survival percentage at 24 hpi (%)
37	1.02	60	14 to 16	32
42	0.97	60	14 to 16	57

#### 4.2.4 Effects of inoculation dose on infection of ZFE by *C. jejuni*

With the above mentioned parameters determined for the ZFE infection model, Cj11168H wild-type cells at various optical densities were used to challenge the embryos. It required approximately 4 hours to inoculate an entire set of embryos consisting of a minimum of 80 embryos. Hence, the embryos were inoculated at stages between 28-32 hpf.

Table 4.6 showed the numbers of embryos challenged for each of the inoculation dose tested. Mortalities of challenged embryos at 24 hpi are shown in Figure 4.1.

The ZFE at 28 hpf were challenged with Cj11168H wild-type cells at OD<sub>590</sub> 0.1 to 10. The cell density for Cj11168H wild-type cells at OD<sub>590</sub> 1 was, on average,  $5 \times 10^8$  cfu/ml. At OD<sub>590</sub> 10, with mean inoculum volume as 3 nl, the number of bacterial cells inoculated into each embryo was approximately 15,000 CFU. Hence the challenge doses tested were 150 CFU per ZFE (for OD<sub>590</sub> 0.1), 750 CFU per ZFE (for OD<sub>590</sub> 0.5), 1,500 CFU per ZFE (for OD<sub>590</sub> 1) and 15,000 CFU per ZFE (for OD<sub>590</sub> 10).

The mortality of the embryos increased with increasing challenge dose. Almost 100% mortality was achieved by 24 hpi when bacteria cell suspension at OD<sub>590</sub> 10 was used for inoculation. When the infection dose was reduced 100-fold to OD<sub>590</sub> 0.1, the mortality was 2.5%.

Based on the results an inoculation dose of  $OD_{590}$  at approximately 1 caused approximately 50% death and was selected for subsequent studies.

**Table 4.6:** List of the number of ZFE tested for each infection dose. ZFE were challenged with *C. jejuni* Cj11168H wild-type cells that were inoculated into YS of 28-32 hour post-fertilisation embryos. The bacteria cells were cultured at 37°C in Muller Hinton broth (MHB). Optical density of bacteria cells were adjusted to approximately OD<sub>590</sub> 0.1, 0.5, 1.0 and 10 for inoculation. A total of 5 different batches of ZFE were used. Survival percentage of challenged ZFE at 24 hpi was tabulated.

Mean optical density of bacteria cell suspension (OD <sub>590</sub> )	Number of embryos challenged	Batch number	Survival percentage at 24 hpi (%)
0.1	40	6 & 7	98
0.5	40	8 & 9	68
1	100	5 to 9	43
10	93	5 to 9	2

**Mortality at 24 hpi with *C. jejuni* strain Cj11168H wild-type at various optical densities, injected into YS of ZFE at 28-32 hpf**

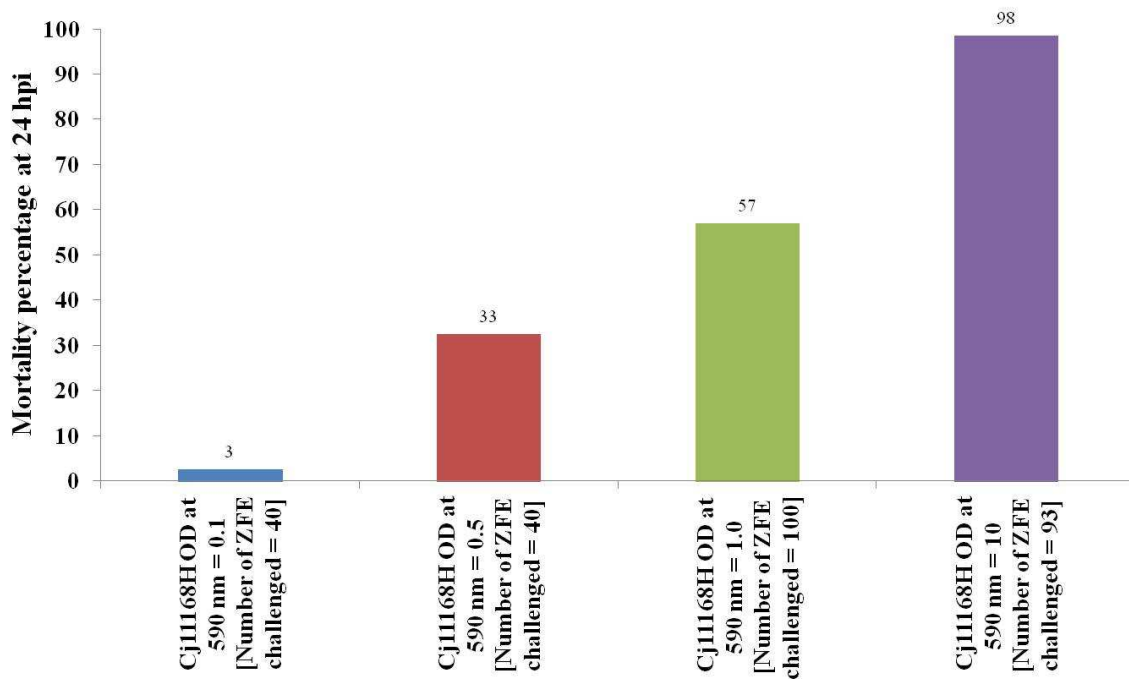


**Figure 4.1:** Mortality chart of ZFE challenged with *C. jejuni* strain Cj11168H wild-type at 24 hpi. ZFE at stages between 28-32 hpf were used. Cj11168H wild-type was cultured in MHB at 37°C for 24 hr. The optical densities of the bacterial cells were adjusted to OD<sub>590</sub> 0.1, 0.5, 1.0 and 10 respectively and were delivered into embryo's yolk-sac through micro-injection. The mortality of ZFE was dependent on the inoculation dose. Higher mortality was obtained with higher inoculation dose. At OD<sub>590</sub> of approximately 10, 99% of challenged embryos were dead by 24 hpi and at OD<sub>590</sub> of approximately 1, 57% of challenged embryos were dead by 24 hpi.

#### 4.2.5 Testing of *Campylobacter* strains and mutants using the ZFE infection model

The Cj11168H strain was used as the reference strain in the development of the ZFE infection model for *Campylobacter* studies. The model was then used to test *C. jejuni* strain Cj1, a clinical isolate from Thailand.

A total of 57 ZFE were challenged with Cj1 grown at 37°C in MHB, at OD<sub>590</sub> 1.0. The percentage of embryos survived at 24 hpi was 40%, while those challenged with Cj11168H was 33% (Table 4.7). The difference in survival percentages was tested using t-test at 95% confidence; the test result showed that the difference was not significant.

Four previously constructed Cj11168H mutants were also tested using the ZFE infection model. The four mutants were i) CDT mutant ( $\Delta cj0079$ ); ii) acapsular mutant ( $\Delta cj1413$ ); iii) aflagellate mutant ( $\Delta cj1339$ ); iv) mutant lacking the LOS biosynthesis cluster - LOS mutant ( $\Delta cj1132c$  to  $cj1152c$ ).

Table 4.8 and Figure 4.2 show the percentage survival of ZFE at 24 hpi with wild-type or mutants. The survival percentages were analysed by one-way ANOVA followed by uncorrected Fisher's LSD. The statistical analysis at 95% confidence showed that the survival percentages of the CDT mutant and the acapsular mutant were not significantly different from wild-type. ZFE challenged with the aflagellate mutant and the LOS mutant, had higher survival percentages compared to those challenged with wild-type. Statistical

analysis showed that the differences in the survival percentages were significantly different, with P-values of 0.0083 and <0.0001 respectively.

**Table 4.7:** ZFE were challenged with *C. jejuni* Cj1 or Cj11168H wild-type cells that were inoculated into YS of 28-32 hour post-fertilisation embryos. The bacteria were cultured at 37°C in MHB. Optical density of bacteria cells were adjusted to approximately OD<sub>590</sub> 1 for inoculation. A total of 2 different batches of ZFE were used. Survival percentage of challenged ZFE at 24 hpi was as tabulated.

<i>C. jejuni</i> strain	Mean optical density of bacteria cell suspension (OD <sub>590</sub> )	Number of embryos challenged	Batch number	Mean survival percentage at 24 hpi (%)
Cj1	1.0	57	17 to 18	40
Cj11168H	1.05	48	17 to 18	33

**Table 4.8:** ZFE were challenged with *C. jejuni* Cj11168H wild-type and mutants cells that were inoculated into YS of 28-32 hour post-fertilisation embryos. The bacteria were cultured at 37°C in MHB. Optical density of bacteria cells were adjusted to approximately OD<sub>590</sub> 1 for inoculation. A total of 9 different batches of ZFE were used. Survival percentage of challenged ZFE at 24 hpi was as tabulated.

<i>C. jejuni</i> strain / mutants	Mean optical density of bacteria cell suspension (OD <sub>590</sub> )	Number of embryos challenged	Number embryos alive at 24 hpi	Batch number	Mean survival percentage at 24 hpi (%)
Cj11168H wild-type	1.01	189	50	19 to 27	26
Cj11168H CDT mutant	1.03	68	18	19 to 21	26
Cj11168H acapsular mutant	0.98	60	21	24, 26 & 27	35
Cj11168H aflagellate mutant	0.995	80	36	22, 25 to 27	45
Cj11168H LOS mutant	1.03	60	57	23, 26 & 27	95

**Survival at 24 hpi with *C. jejuni* strain Cj11168H wild-type, CDT mutant, acapsular mutant, aflagellate mutant and LOS mutant, cell suspension at optical densities of approximately 1, injected into YS of ZFE at 28-32 hpf**

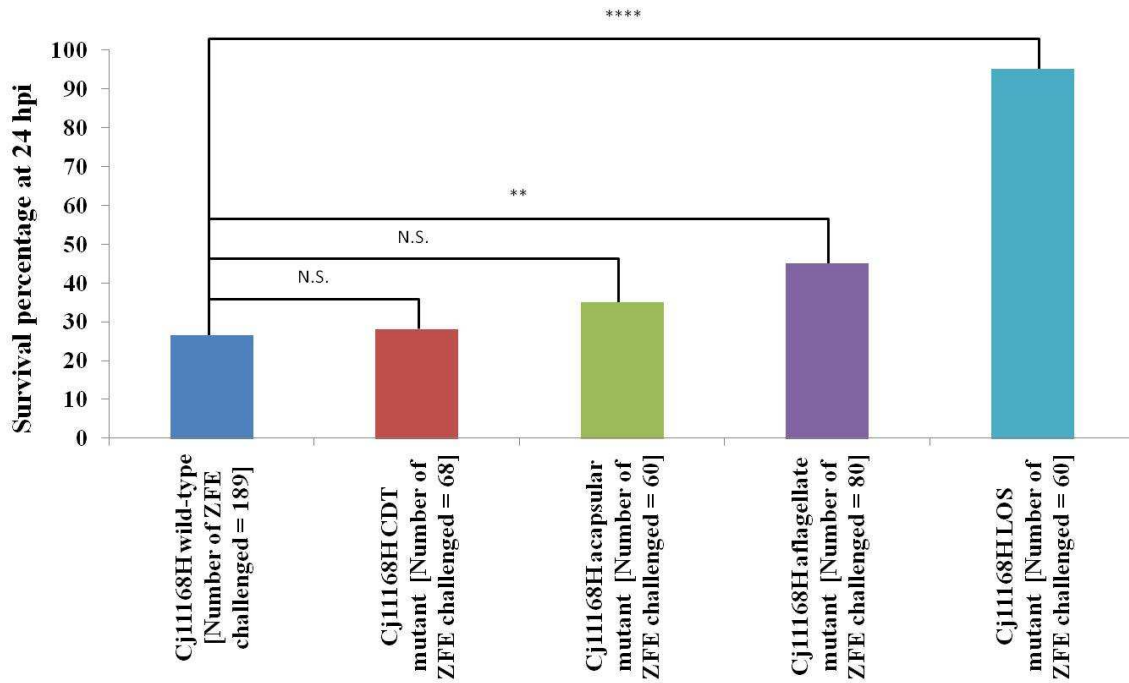


**Figure 4.2:** Survival chart of ZFE challenged with *C. jejuni* strain Cj11168H wild-type and four mutants at 24 hpi. ZFE at stages between 28-32 hpf were used. Cj11168H wild-type and mutants were cultured in MHB at 37°C for 24 hr. The optical densities of the bacterial cells were adjusted to approximately OD<sub>590</sub> 1 and were delivered into embryo's yolk-sac through micro-injection. Survival percentages of CDT mutant and acapsular mutant were not significantly different from wild-type. The survival percentages of aflagellate mutant and LOS mutant were significantly different from wild-type, with P-value of 0.0083 and <0.0001 respectively. The statistical analysis performed was one-way ANOVA followed by uncorrected Fisher's LSD.

## 4.2.6 Imaging of ZFE challenged with *C. jejuni*

### 4.2.6.1 *Bright-field imaging*

At 28 hpf the ZFE still resides within its chorion. Prior to delivering the bacteria cell suspension by micro-injection into its YS the chorion was mechanically removed. Figure 4.3 shows an image of a ZFE at 28 hpf - the insert is an embryo at the same development stage residing within its chorion. An image of uninfected embryos at 52 hpf is shown in Figure 4.4. The heart cavity and yolk sac were normal and more pigmentation could be observed on the embryo surfaces.

Most ZFE challenged with *C. jejuni* showed signs of edema in the heart cavity, YS or both by 24 hpi. Figure 4.5 provides an illustration of the various forms of edema observed in ZFE challenged with *C. jejuni*. All embryos with observable heartbeat at 24 hpi were recorded as alive. The survival data recorded includes infected embryos that had edema. Edema formation was observed in ZFE challenged with *C. jejuni* wild-type or mutant strains, with the exception of Cj11168H LOS mutant. ZFE challenged with the latter were observed to be similar to uninfected ZFE at 52 hpf. Beside edema formation, another commonly observed feature in the challenged ZFE (except for ZFE infected with Cj11168H LOS mutant) was the presence of a dark spot. It was observed to be either in the YS or at the junction of the YS and the heart cavity.

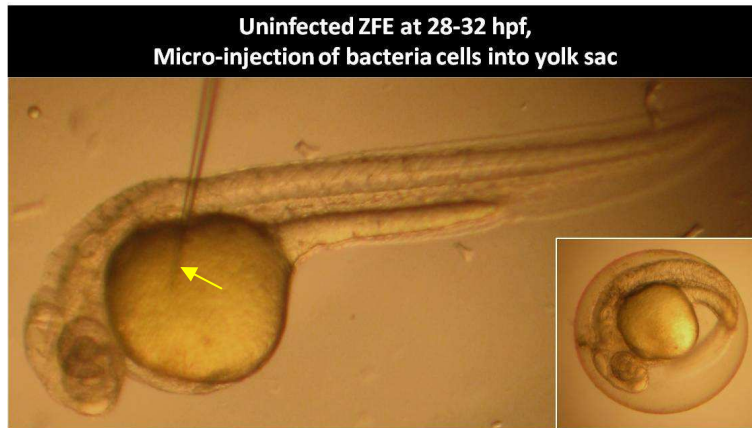


**Figure 4.3:** ZFE at 28 hpf with (insert) and without chorion. The de-chorinated embryos was embedded in 3% methyl-cellulose and glass capillary needle (indicated by the yellow arrow) was inserted into the yolk sac. 2 pulses of bacteria cell suspension, of approximately 2-4 nl were then delivered into the yolk sac through the glass capillary needle.



**Figure 4.4:** Uninfected ZFE at 52 hpf. More pigmentations (indicated by the red arrows) were observed over its surfaces, heart cavity and yolk sac is normal.

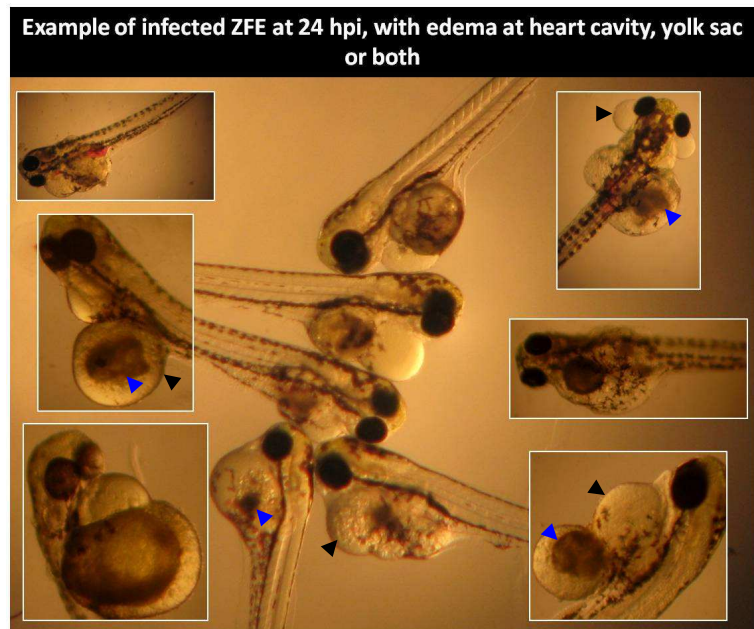


Figure 4.5: Images showing various ZFE infected with *C. jejuni*, at 24 hpi. Edema (indicated by black arrows) were observed in the infected embryos at the heart cavity, yolk sac or both. Dark spots (indicated by blue arrows) were also observed in the yolk sac or at the junction of the yolk sac and the heart cavity.

#### 4.2.6.2 *Fluorescence images*

##### 4.2.6.2.1 Reporter *C. jejuni* Cj11168H cells

Cj11168H cells were transformed by electroporation with a plasmid encoding either CFP, GFP or YFP protein (Miller et al., 2000).

In Figure 4.6 images of Cj11168H wild-type, CFP, GFP and YFP reporter are presented. The signals from the reporters in Cj11168H are very weak compared to the signals in an *E. coli* background (Figure 4.7). In both Cj11168H and *E. coli*, CFP signals crossed over and were detected in the GFP filter. In Cj11168H, the GFP signals also crossed over and were detectable in the CFP filter. However, in *E. coli* GFP signals were detected in both CFP and YFP filters. YFP signals in both Cj11168H and *E. coli* crossed over and were detected in both CFP and GFP filters.

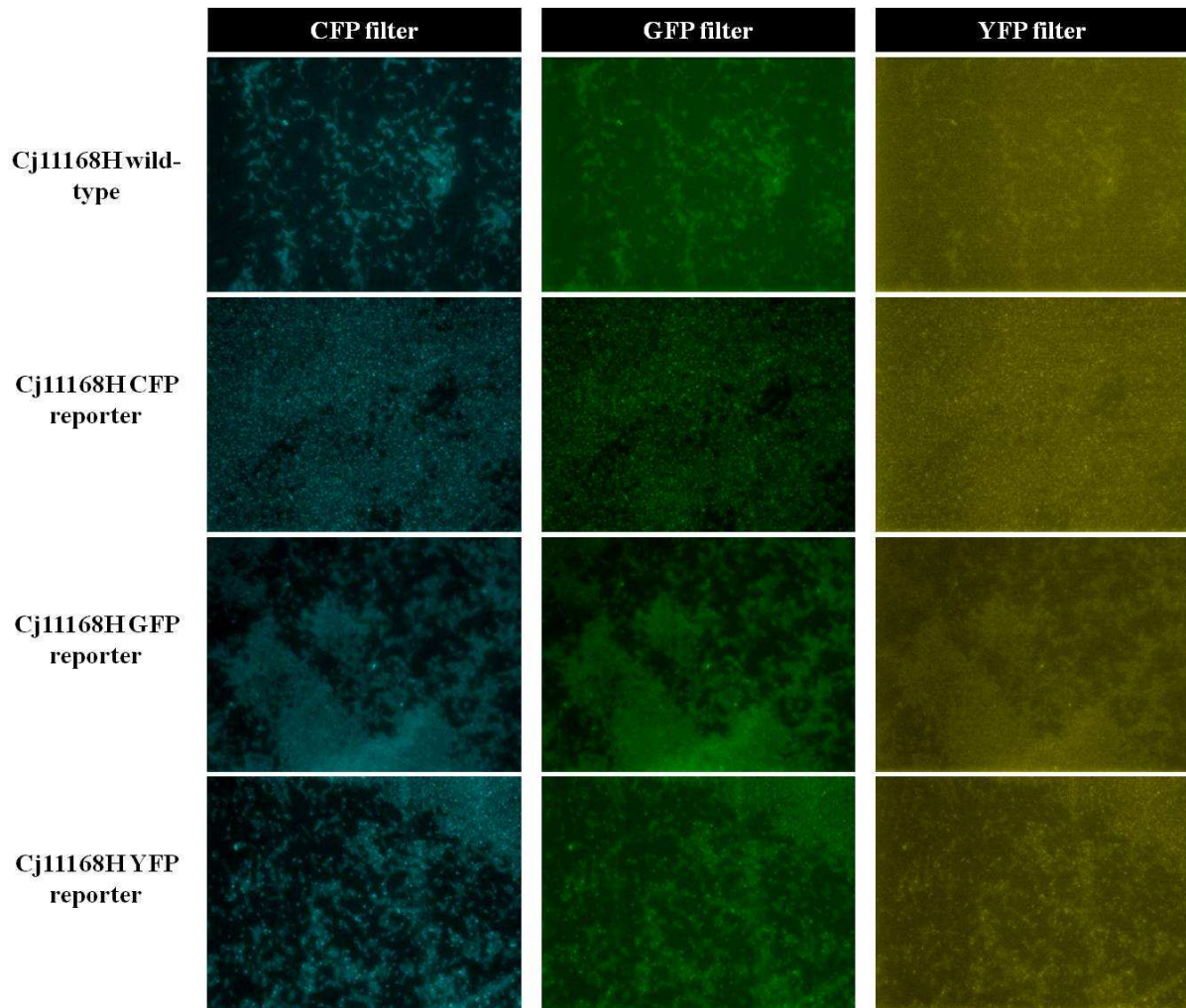


**Figure 4.6:** *C. jejuni* Cj11168H wild-type, CFP reporter, GFP reporter and YFP reporter cells. The bacteria were grown on CBA+ agar and a single colony was dislodged into 10  $\mu$ l of water on glass slide. The cells were heat fixed onto the slide. Overall, the reporter signals were weak. CFP reporter was detected under both CFP and GFP filter. GFP reporter was detected both GFP and CFP filters. YFP reporter was detected in all three filters.

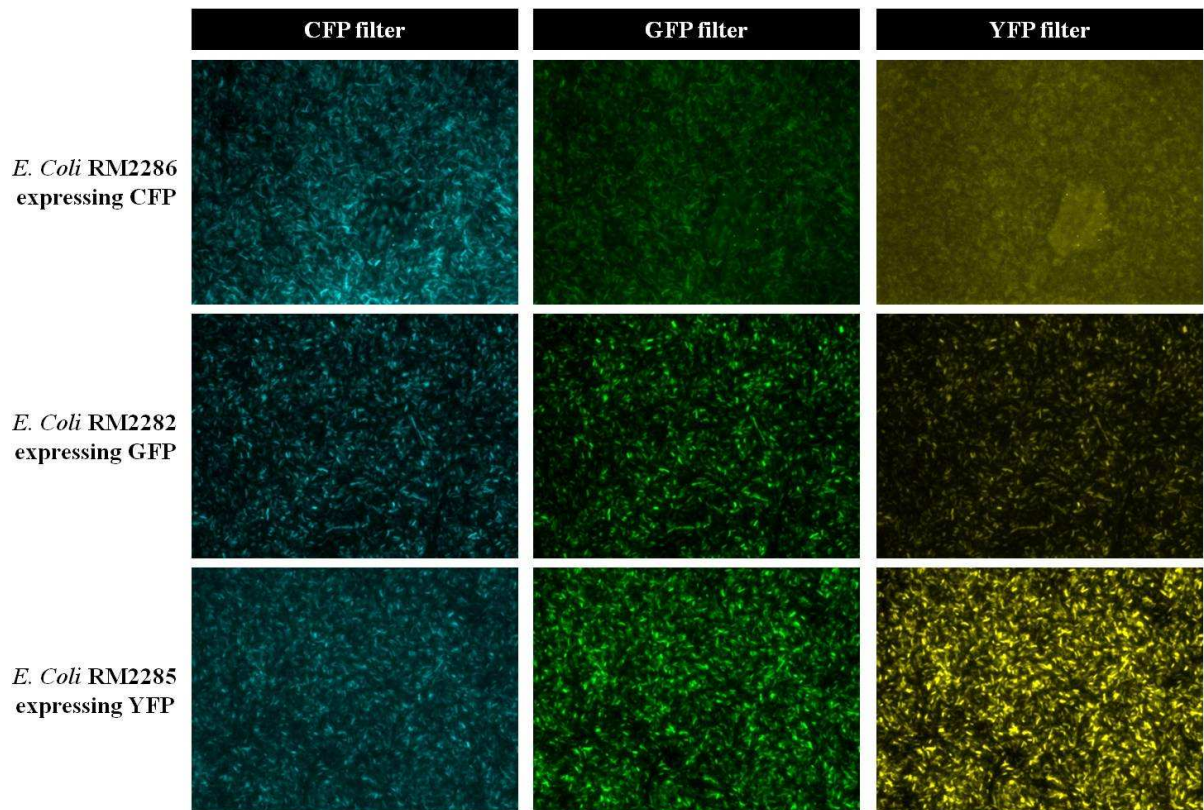


**Figure 4.7:** *E. coli* strains expressing CFP, GFP and YFP. The bacteria were grown on LB agar and a single colony was dislodged into 10  $\mu$ l of water on glass slide. The cells were heat fixed onto the slide. Overall, the reporter signals were strong. CFP reporter was detected under both CFP and GFP filter. GFP reporter and YFP reporter was detected in all three filters.

A transgenic line of zebrafish expressing mCherry as a reporter in macrophages, was kindly provided by University of Sheffield (Gray et al., 2011). The transgenic line with fluorescently tagged immune cells (mCherry-expressing macrophages) was used to track interaction between the bacteria and the immune cells in real-time.

The mCherry-macrophage ZFE were inoculated at 28 hpf with GFP-Cj11168H (Figure 4.8). The images were taken using live embryos between 0-3 hpi. This set of embryos was inoculated with a higher infection dose at  $OD_{590} \sim 13$ . As fluorescent signals from Cj11168H GFP reporter were not strong. The higher inoculation dose was used to enable better visualisation of the inoculated bacteria. During the first hour after inoculation a cloud of green fluorescence was visible within the yolk sac of the infected embryo (Figure 4.8, B). However, between the first and second hour, the green fluorescent cloud had dispersed (Figure 4.8, C) and by the third hour it could not be detected (Figure 4.8, D and E). It was observed that after the first hours more mCherry-macrophages were located towards the middle of the yolk sac. This was not observed in unchallenged embryos.

A second set of mCherry-macrophage ZFE were inoculated with GFP-Cj11168H at  $OD_{600} 1$ . This set of infected embryos was incubated overnight and images were taken at 22 hpi, (Figure 4.9). The images of live embryos were taken using an upright fluorescent microscope. High magnification objectives, such as 40X and above, could not be used as it would result in crushing of the live embryos. Auto-fluorescence from the embryos interfered with imaging of the GFP-Cj11168H and the use of low magnification objective did not allow detailed features to be imaged. However, there were regions within the yolk sac that showed higher fluorescent signals compared to background fluorescence. These regions coincide with the

dark spot observed under bright-field. It was also observed that mCherry macrophages were located within the vicinity of the dark spots. This is an indication that macrophages were recruited to the dark spot where the bacterial cells were potentially located. The current imaging approach was not able to determine if the macrophages were interacting with the bacterial cells or if the bacterial cells within the dark spot observed were still viable.

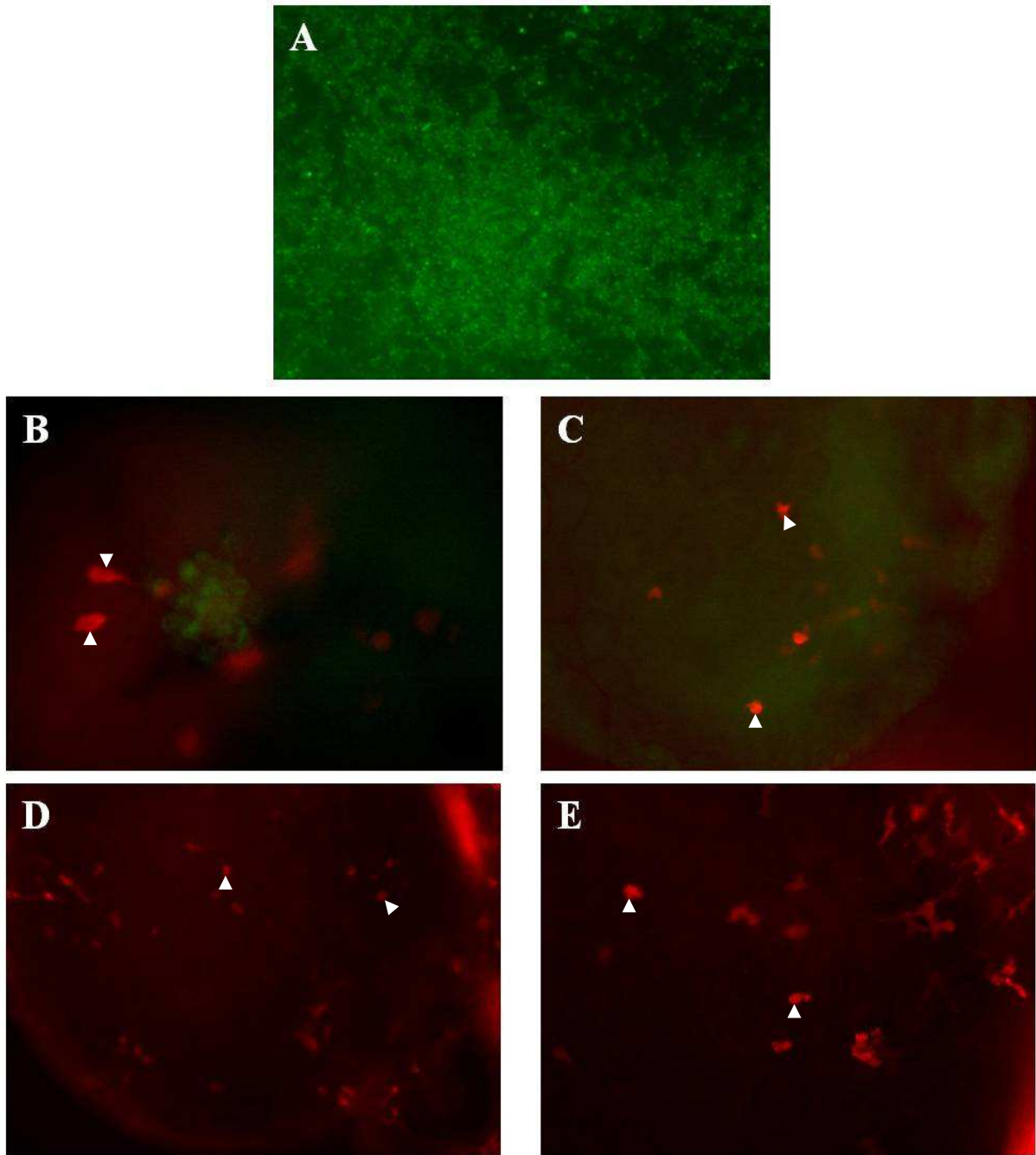


**Figure 4.8:** Images of Cj11168H GFP reporter cells and yolk sac of infected mCherry-macrophage ZFE. **A:** *C. jejuni* Cj11168H GFP reporter cells at OD<sub>600</sub> 13, image taken with 100X objective. **B:** Transgenic ZFE with mCherry-expressing macrophages infected with *C. jejuni* Cj11168H GFP reporter cells at OD<sub>600</sub> 13, image taken between 0-1 hpi with 20X objective. Green - Cj11168 GFP reporter cells and Red (indicated by white arrows) - mCherry macrophages. **C:** Transgenic ZFE with mCherry-expressing macrophages infected with *C. jejuni* Cj11168H GFP reporter cells at OD<sub>600</sub> 13, image taken between 1-2 hpi with 10X objective. Green - Cj11168 GFP reporter cells and Red (indicated by white arrows) - mCherry macrophages. **D and E:** Transgenic ZFE with mCherry-expressing macrophages infected with *C. jejuni* Cj11168H GFP reporter cells at OD<sub>600</sub> 13, image taken between 1-3 hpi with 10X objective. Red (indicated by white arrows) - mCherry macrophages.

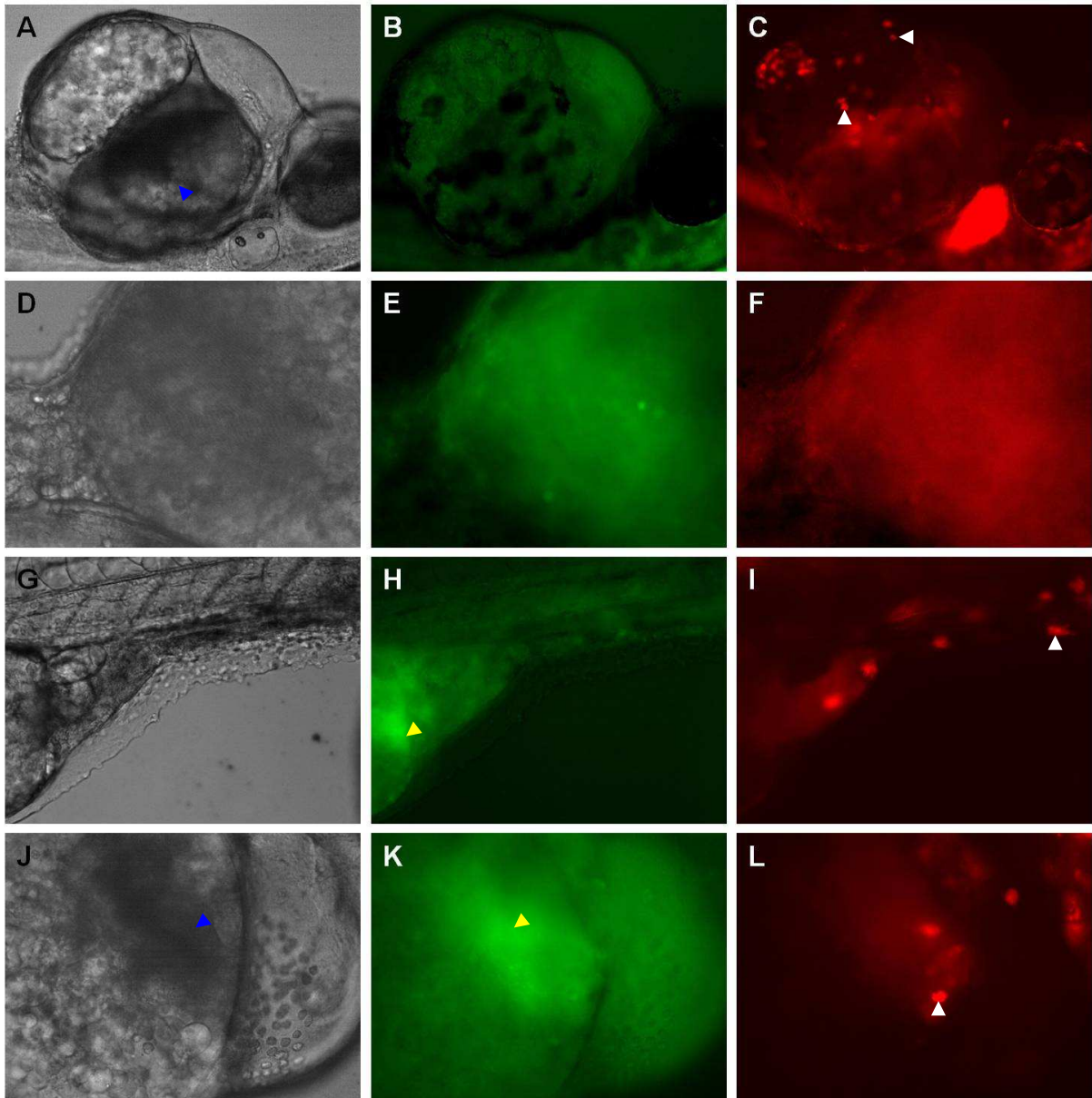


**Figure 4.9:** Images of yolk sac regions taken at 22 hpi of mCherry-macrophage ZFE infected with *C. jejuni* Cj11168H GFP reporter cells at OD<sub>600</sub> 1. A, D, G and J: Imaged taken at bright-field. Dark regions within yolk sac were indicated by blue arrows. B, E, H and K: Images taken using GFP filter. Regions with stronger green fluorescence were indicated by yellow arrows. C, F, I and L: Images taken using mCherry filter. mCherry macrophages were indicated by white arrows. A-C: images taken using 10X objective. D-L: Images taken using 20X objective.

#### 4.2.6.2.2 FITC labelled *C. jejuni* Cj11168H cells

As the Cj11168H GFP reporter did not have a strong fluorescent signal staining of *Campylobacter* cells was explored. Cj11168H wild-type cells were stained in 0.4 µg/ml of FITC for 15 minutes at room temperature with constant mixing (Agerer et al., 2004). The FITC stained bacteria cells gave a strong fluorescent signal, Figure 4.10.

A total of 24 ml of Cj111668H wild-type broth culture were stained with FITC. After washing, the cells were re-suspended in 100 µl of PBS and were used to inoculate mCherry-macrophages ZFE. The infected ZFE were monitored for up to 52 hpi (Figure 4.11). The FITC signal was strong and dispersed within the yolk sac. However, this staining approach could not be used to address the issue of determining if the bacteria are still viable or not. Furthermore, it is not a good approach for studying bacteria and macrophage interactions as the binding of the dye to the bacterial cell would have modified or masked the structures on the bacteria cell surfaces that might be important for interaction with host cells. In Figure 4.11 (G and I) the bright-field image showed a dark spot was present in the embryo's YS and the mCherry images showed that mCherry expressing macrophages gathered around the dark spot. This was, as previously observed when Cj11168H GFP reporter images were taken.

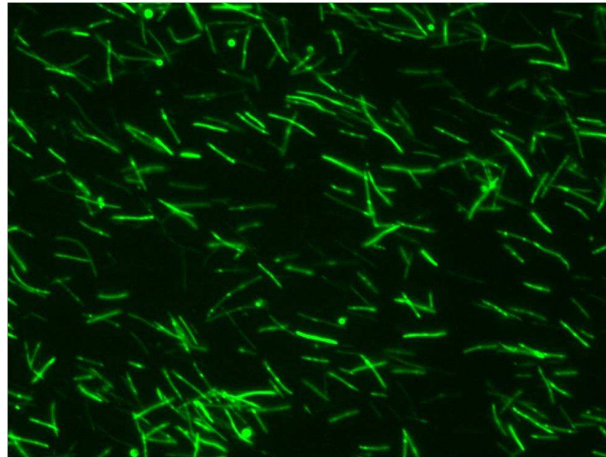


**Figure 4.10:** Broth grown Cj11168H wild-type cells ( $OD_{600} \sim 10$ ) were stained with  $0.4 \mu\text{g/ml}$  5-(6)-carboxyfluorescein-succinylester for 15 min, with constant mixing at room temperature. The stained cells were washed thrice in PBS before visualisation under fluorescence microscope using 100X objective.

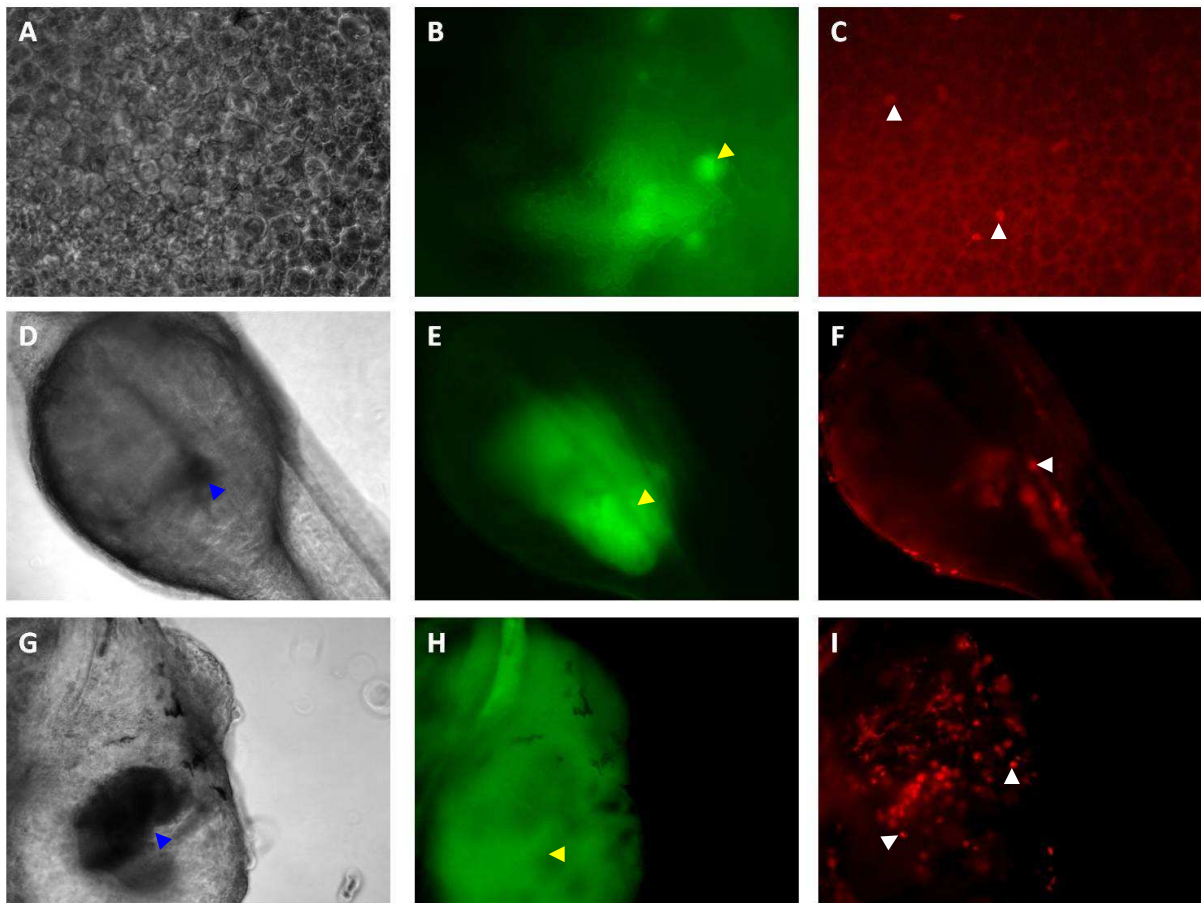


**Figure 4.11:** mCherry-macrophage ZFE infected with Cj11168H wild-type cells stained with FITC. A-C: Images taken at 1 hpi using 20X objective. A - Bright-field, B - GFP filter and C - mCherry filter. D-F: Images taken at 22 hpi using 10X objective. D - Bright-field, E - GFP filter and F - mCherry filter. G-I: Images taken at 52 hpi using 10X objective. G - Bright-field, H - GFP filter and I - mCherry filter. mCherry macrophages were indicated by white arrows. Dark regions within yolk sac were indicated by blue arrows. Regions with stronger green fluorescence were indicated by yellow arrows.

### 4.3 Discussion

ZFE infection models have been established for several pathogens. In these studies the pathogen of interest was inoculated into the ZFE by micro-injection into the axial vein (van der Sar et al., 2003), yolk sac circulation valley (Clatworthy et al., 2009) or yolk sac (Prajsnar et al., 2008). Inoculation into the yolk sac could be done at any ZFE developmental stage. However, injection into the circulation valley, was only possible when the blood circulation system was established - which is around 30 hpf. Inoculation into the circulation valley would potentially allow the bacteria to travel within the blood circulation to other parts of the body, whereas inoculation into the yolk sac should result in the bacteria remaining localised.

*Campylobacter* is not a natural pathogen for zebrafish, hence it was important to determine if the pathogen was able to establish an infection in ZFE. The yolk sac's circulation valley is a point where blood returning from the body and tail of the embryo flows freely to the heart and is re-circulated (Clatworthy et al., 2009). When bacteria were injected into the circulation valley, it enter the circulation, thereby mimicking bacteraemia (Prajsnar et al., 2008). It was reported that *P. aeruginosa* inoculated into the circulation valley of 28 hpf ZFE was lethal to the embryos.

Unlike the *P. aeruginosa* ZFE infection model inoculation of *C. jejuni* into circulation valley was not lethal. Nonetheless, the results obtained were similar to those seen in a *S. aureus* ZFE infection model. In the study, it was reported that 100% of the infected embryos were alive at 48 hpi when *S. aureus* was inoculated into the circulation valley of the embryo

(Prajsnar et al., 2008). However, when it was inoculated into the yolk sac, 100% mortality was achieved at a lower infecting dose (Prajsnar et al., 2008). It was suggested that survival of embryos inoculated into the circulation valley could be due to the ZFE host defence mechanism either controlling or clearing the challenge (Prajsnar et al., 2008). When inoculated into the yolk sac *S. aureus* grew within the site of inoculation, and injection into the circulation valley led to systemic infection (Prajsnar et al., 2008).

It is not clear what happens to *C. jejuni* after inoculation into the circulation valley or the yolk sac. Attempts to recover *Campylobacter* cells post-infection were not successful. A problem faced was the presence of other bacteria from the embryos that were able to grow on selective agar that contained Skirrow supplement. The other challenge was low or no recovery of *Campylobacter* cells from infected embryos. It could either be due to the bacteria being killed by the embryo's defence mechanism, or the bacteria switching into VBNC state and thereby were not quantifiable by cfu counts.

The *ex vivo* embryo allows disease pathogenesis to be studied at different developmental stages as the immune system becomes established in the organism (Phelps and Neely, 2005). Macrophage-like cells are found within the yolk-sac after ~22 hpf (Herbomel et al., 1999); primitive granulocytes circulate the embryo by 48 hpf (Lieschke et al., 2001), while mature neutrophils are found in tissues by 72 hpf (Willett et al., 1999). Macrophages and neutrophils form an important part of the innate immunity system and macrophages in ZFE have been shown to be involved in the clearing of bacteria inoculated into the embryo (Herbomel et al., 1999).

The ZFE were tested at 2 different stages of development (28 hpf and 52 hpf) and results obtained were similar to ZFE infected with *P. aeruginosa* at 28 hpf and 50 hpf (Clatworthy et al., 2009). The survival rates of embryos when challenged at 52 hpf were higher compared to those infected at 28 hpf. This is because at 52 hpf the embryos were potentially more immuno-competent since both macrophages and granulocytes (neutrophils) had appeared and were functional (Clatworthy et al., 2009; Herbomel et al., 1999; Le Guyader et al., 2008; Lieschke et al., 2001). The interaction of *C. jejuni* with monocytes *in vivo* is still an unanswered question (Young et al., 2007). Hence, ZFE at 28 hpf, where only macrophages are present, is a good developmental stage at which to study this interaction.

*Campylobacter* is exposed to different temperatures, from chickens to humans, throughout its infection cycle. While inside the chicken intestine, bacteria is exposed to 42°C. Upon entry into human host, the temperature will be at 37°C. The temperature in which bacteria reside will affect its cellular process (Hurme and Rhen, 1998) - some genes might be switched either on or off to adapt to the new environment.

In this study Cj11168H wild-type cells were grown at 37°C or 42°C prior to inoculating into ZFE. It was recorded that embryos infected with *Campylobacter* grown at 37°C had a higher mortality rate. The difference in mortality rate observed could be due to differential gene expression when the bacteria were exposed to the two different temperatures.

A proteomic study conducted on *Campylobacter* grown at 37°C or 42°C both on agar and in broth showed that various categories of proteins were differentially expressed (Zhang et al., 2009). The proteins shown to be differentially expressed were either involved in; i) metabolism; ii) stress defences; iii) iron acquisition; iv) regulator system or v) cell structures (Zhang et al., 2009). It was reported that some proteins were uniquely expressed when *Campylobacter* was grown at 37°C and might play a part in human host adaptation (Zhang et al., 2009). This might explain the observations made in ZFE infection.

Besides, the proteomics study, the effect of culturing temperature on growth, chemotaxis, motility and adherence/invasion of epithelial cells has also been reported. Culturing of *Campylobacter* at 37°C was shown to be more favourable for growth and chemotaxis (Khanna et al., 2006). The motilities of *Campylobacter* grown at 37°C or 42°C were reported to be strain dependent. Cj81116 was more motile at 42°C, whereas environmental isolate *C. jejuni* M1 showed no significant differences in motility between the two temperatures tested (Aroori et al., 2013). *Campylobacter* grown at 37°C has also been demonstrated to exhibit enhanced adherence/invasion of human epithelial cells (Aroori et al., 2013; Konkel et al., 1992). In order to investigate further the difference observed in ZFE, motilities, transcriptomics and proteomics studies could be performed on Cj1168H wild-type grown under the two different temperatures.

The percentage of embryo death post challenged was dependent on the inoculation dose. When comparing the inoculation dose of *C. jejuni* used to challenged ZFE to a *S. aureus* ZFE infection model (bacteria inoculated into yolk sac), the ZFE were more susceptible to *S. aureus*. However, when compared to a *P. aeruginosa* infection model (bacteria inoculated

into yolk sac's circulation valley), the ZFE were more susceptible to *C. jejuni*. The infection dose of different bacteria will be different. It has been reported that infection doses of bacteria are dependent on the molecules the pathogen use to facilitate its infection in each host (Leggett et al., 2012). If the molecules work in close proximity of the bacteria, then fewer bacteria will be required to establish an infection (Leggett et al., 2012). Contrary to this, when the molecules act on sites at a distance away from the bacteria, then a higher number of the bacteria would be required to establish an infection - a matter of concentration over distance (Leggett et al., 2012).

An important outcome from the infection dose study was that ZFE could be killed in a dose dependent manner. With that knowledge, this model could be used to screen *Campylobacter* isolates or mutants for its virulence or attenuation in ZFE. An additional advantage to the ZFE model was its ability to use organismal death as the hard end-point (Prajsnar et al., 2008). This is often not possible in other model organisms.

The ZFE model was used to screen four *C. jejuni* Cj11168H mutants. These mutants were previously tested using the *G. mellonella* model (Champion et al., 2010).

In the ZFE model the CDT mutant was not attenuated. Survival percentage between this mutant and wild-type strain was the same. This is different from observations made in the *G. mellonella* model where CDT mutant had shown significant attenuation (Champion et al., 2010). It suggests that CDT does not have any role in establishing infection in ZFE.

The acapsular mutant although showed a higher percentage of survival when compared to wild-type, the difference was not significant. Similarly, in the *G. mellonella* model, enhance survival of this mutant was observed but was not significant ( $P>0.5$ ) when compared to wild-type strain (Champion et al., 2010). The slight increase in survival observed in both model suggests that capsule might play a role in infection. It has been reported that it is unusual for *Campylobacter*, an intestinal pathogen, to have capsule and its actual role was not well defined (Guerry et al., 2012) although it has a role in serum resistance (Keo et al., 2011) and modulates host immune responses (Maue et al., 2013).

The aflagellate mutants tested had showed a significant higher percentage of survival when compared to wild-type. In the *G. mellonella* model, the survival percentage of larvae challenged with this mutant was also significant higher ( $P<0.5$ ) when compared to wild-type (Champion et al., 2010). This indicates that flagella in *Campylobacter* play a role in establishing infection in both ZFE and *G. mellonella*. The flagella is an important export apparatus for Cia (*Campylobacter* invasion antigens) proteins which play a role in invasion of epithelial cells (Konkel et al., 2004).

The LOS mutant was highly attenuated in the ZFE and this is similar to observations in the *G. mellonella* model (Champion et al., 2010). This indicates that LOS plays a vital role in virulence in both model organisms. LOS of *Campylobacter* has been reported to play a part in serum resistance and adherence and invasion of epithelial cells (Young et al., 2007).

The variation in survival observed when the embryos were infected with different *Campylobacter* mutants shows the potential of using ZFE as an infection model for screening mutants. The ZFE has been used as an infection model for mutant screening in other pathogens such as *Salmonella* Typhimurium (van der Sar et al., 2003) and *Listeria monocytogenes* (Levraud et al., 2009). Besides these various advantages stated previously, the ability to perform high throughput screening makes ZFE an attractive model for *Campylobacter* studies (Phelps and Neely, 2005; Wang et al., 2007).

However, before going full scale into using the ZFE model, an important point to note is that ZFE could not be maintained at 37°C; hence, upon inoculation into the embryo the bacteria will be incubated inside the embryo at 28°C. As *Campylobacter* is able to grow at temperatures between 30°C to 47°C (Aroori et al., 2013) its ability to survive at 28°C will need to be addressed. It has also been observed that quality of the embryos varies from batch to batch. For example, when tested at OD<sub>590</sub> of 1 in Batch 16-20 the survival rate of the embryo was 43%. When different batches were tested with the same input the survival percentages changed. For example, for Batches 21 to 22, it was 31.25% and for Batches 23-31, it dropped to 26.46%. In order to overcome the batch to batch issue, a reference strain, such as Cj11168H wild-type, should always be included in each infection assay involving strains or mutants screening.

An important advantage of ZFE was that it stays optically transparent during the first three weeks of its development (Phelps and Neely, 2005). This property allows images of embryos to be taken. Real-time imaging to track bacteria injected in ZFE had been reported for various pathogens (Clatworthy et al., 2009; Davis et al., 2002; Rounioja et al., 2012; van der

Sar et al., 2003). In all these real-time imaging studies a strong fluorescent reporter strain was made to allow tracking of the bacteria inside the embryo. A major challenge faced in the imaging of *Campylobacter* within the embryo was the lack of a strong fluorescent reporter strain.

Plasmids comprising of CFP, GFP or YFP reporter gene fused with *Campylobacter* promoter were obtained from its USDA-ARS laboratory (Miller et al., 2000) and transformed into Cj11168H. Unfortunately, the fluorescence signal in Cj11168H reporter were not strong. In order to obtain a stronger reporter Cj11168H wild-type cells were stained with FITC prior to inoculation into ZFE. Although the FITC signal was strong, it was dispersed inside the yolk sac and remained strong after 2 days. The images obtained were not able to determine if the bacteria were still alive with the dye bound to them, or dead with the dye freely dispersed inside the yolk sac.

The bright-field images showed formation of edema at either the yolk or heart cavity or both in infected embryos. Edema formation had not been reported in other pathogens using ZFE as an infection model. It will be interesting to investigate further to determine what bacterial or host factors caused this phenomenon.

Another observation was that infected embryos developed a dark spot in the yolk sac or at the junction of yolk sac and heart cavity. In fluorescent-based imaging mCherry macrophages were seen at the same location as the dark spot seen in bright-field images. In Figure 4.9 the GFP signal was also stronger at the same location as the dark spot and the mCherry

macrophages. This suggests that the dark spot observed in bright-field images may be aggregations of bacteria and macrophages. What is happening within the dark spot? This is an important question that still needs to be addressed. It is unfortunate that higher magnification could not be achieved with the upright fluorescent microscope used. However, this demonstrated the potential of using ZFE to interrogate the interaction of *Campylobacter* with macrophages *in vivo*.

Real-time imaging to monitor interaction of macrophages with bacteria cells might be possible with a different microscope system, for example a multi-photon inverted microscope. The multi-photon microscope will be able to perform optical sectioning of thick tissues (such as ZFE) and due to its laser system, will be less detrimental to the cells (Masters and So, 2004). An inverted microscope would allow higher magnification objectives to be used without the fear of crushing the live embryos. However, before that could be done a stronger *Campylobacter* reporter will be needed.

**Chapter 5: Identification of T6SS and construction of T6SS  
mutants in *Campylobacter jejuni***

## 5.1 Introduction

### 5.1.1 Identification of T6SS

A component of the T6SS, Hcp, was reported as early as 1996 in *V. cholerae* (Williams et al., 1996) and since then other components such as the *icmGCDJBF* locus in *Legionella pneumophila* (Purcell and Shuman, 1998), and *icmF* in *Salmonella enterica* (Folkesson et al., 2002), have also been reported. The classification of the secretion system as Type VI secretion system was in 2006 after the *vas* genes cluster was found in *Vibrio cholerae* (Pukatzki et al., 2006). The T6SS is found mainly in Proteobacteria, with the exception of the epsilon sub-group. Around a third of genomes harbouring the T6SS were found to have multiple copies (Boyer et al., 2009). For example, *Yersinia* species can have 5 to 6 copies of T6SS loci, *Burkholderia* species between 2 to 6 copies and *Pseudomonas* species 2 to 3 copies (Boyer et al., 2009).

A functional T6SS in *Campylobacter* was first suspected when 4 components of T6SS (*tssJ*, *tssK*, *tssC* and *tssD*) were detected after mass spectrometry analysis of *C. concisus* cellular proteins (Kaakoush et al., 2011). However, no further work on the potential T6SS in *Campylobacter* was reported until Lertpiriyapong *et al* presented their work on a functional T6SS in *C. jejuni* (Lertpiriyapong et al., 2012). To date, there are only two reports on functional T6SS in *C. jejuni* - and both report a single copy of T6SS (Bleumink-Pluym et al., 2013; Lertpiriyapong et al., 2012).

The identification of a potentially functional T6SS was based on the presence of 13 COGs of protein on a single locus. The 13 COGs were identified by Boyer *et al* after screening a total of 506 complete genome sequences. The 506 complete genome consist of 176 T6SS loci from 92 different bacteria (Boyer et al., 2009). The 13 core COGs were present within T6SS loci at a frequency of more than 70 percent, which was significantly higher than other COGs screened (Boyer et al., 2009). A hallmark indicator for functional T6SS in bacteria harbouring T6SS locus is the presence of TssD in culture media (Pukatzki et al., 2007).

### 5.1.2 Mutagenesis in *Campylobacter*

Early work on *Campylobacter* was handicapped by a lack of tools to make mutants. However, a breakthrough was made when Labigne-Roussel *et al* constructed the shuttle vector, pILL550. This allowed the introduction of foreign DNA into *Campylobacter* via conjugation (Labigne-Roussel et al., 1987). Subsequently, a conjugative suicide vector, pILL560, was constructed. It was similar to pILL550 but was unable to replicate in *Campylobacter* after the removal of *Campylobacter* replication sequences (Labigne-Roussel et al., 1988). The suicide plasmid was constructed to include a *C. jejuni* 16s rRNA gene at the multiple cloning site (MCS). A kanamycin resistance cassette was inserted within the 16s rRNA gene to disrupt it. The suicide plasmid containing the disrupted 16s rRNA gene, pILL545, was transferred into *C. jejuni* via conjugation. The kanamycin resistance cassette was shown to have integrated into the chromosome at the target gene region (a double crossover event) and the plasmid was lost in cells when grown on selective plates (Labigne-Roussel et al., 1988). The work of Labigne-Roussel *et al* set the background for

*Campylobacter* mutagenesis, and Miller *et al* demonstrated its ability to be transformed by electroporation (Miller et al., 1988).

### 5.1.3 Aim of study

The aim of this study was to identify a T6SS in *C. jejuni* strains isolated from Thailand and to construct T6SS mutants for future work.

## 5.2 Results

### 5.2.1: Identification of T6SS in *Campylobacter jejuni* strain Cj1

*C. jejuni* strains isolated from patients in Thailand were sequenced using the Illumina HiSeq 2500 with 100 bp paired end reads. The 100 bp reads were subjected to de-novo assembly to create contigs. The contigs were then uploaded onto MG-RAST metagenomics analysis server (<http://metagenomics.anl.gov/>) for annotation. Annotation of contigs from the various *C. jejuni* strains being sequenced revealed that strain Cj1 harbours a cluster of genes consisting of T6SS core orthologs (Pukatzki et al., 2006).

Two contigs from Cj1 were found to include genes that could encode components of a T6SS. Contig scf\_30956\_20\_contig\_1 (20905 bps in length) contained 12 genes which are likely to be components of a T6SS. Contig scf\_30956\_10\_contig\_1 (963 bps) had a partial gene which could encode for a T6SS component, *tssI*. The stop codon of *tssI* was within this contig but not its start codon. Table 5.1 is the annotation output from MG-RAST for the two contigs.

**Table 5.1: Summary of *C. jejuni* strain Cj1 contig scf\_30956\_10\_contig\_1 and contig scf\_30956\_20\_contig\_1 annotation from MG-RAST.**

Contig ID	Location	Start	Stop	Strand	Function	Evidence codes
scf_30956_10_contig_1	scf_30956_10_contig_1_12_908	12	908	+	VgrG protein	isu;USS-DB-7 isu;Type_VI_secretion_systems
scf_30956_20_contig_1	scf_30956_20_contig_1_47_3469	47	3469	+	FIG00470311: hypothetical protein	ff
scf_30956_20_contig_1	scf_30956_20_contig_1_3480_4781	3480	4781	+	FIG00469624: hypothetical protein	ff
scf_30956_20_contig_1	scf_30956_20_contig_1_5684_4785	5684	4785	-	hypothetical protein	
scf_30956_20_contig_1	scf_30956_20_contig_1_9208_5681	9208	5681	-	IcmF-related protein	isu;Type_VI_secretion_systems
scf_30956_20_contig_1	scf_30956_20_contig_1_9326_9841	9326	9841	+	hypothetical protein	
scf_30956_20_contig_1	scf_30956_20_contig_1_10869_10096	10869	10096	-	Outer membrane protein ImpK/VasF, OmpA/MotB domain	icw(2);USS-DB-7 icw(3);Type_VI_secretion_systems
scf_30956_20_contig_1	scf_30956_20_contig_1_12263_10866	12263	10866	-	Uncharacterized protein ImpJ/VasE	icw(5);USS-DB-7 icw(6);Type_VI_secretion_systems
scf_30956_20_contig_1	scf_30956_20_contig_1_12719_12273	12719	12273	-	Type VI secretion lipoprotein/VasD	icw(7);Type_VI_secretion_systems
scf_30956_20_contig_1	scf_30956_20_contig_1_12845_14092	12845	14092	+	Uncharacterized protein ImpA	icw(3);USS-DB-7 icw(3);Type_VI_secretion_systems
scf_30956_20_contig_1	scf_30956_20_contig_1_14161_14646	14161	14646	+	Uncharacterized protein ImpB	isu;USS-DB-7 isu;Type_VI_secretion_systems
scf_30956_20_contig_1	scf_30956_20_contig_1_14648_16102	14648	16102	+	Uncharacterized protein ImpC	icw(5);USS-DB-7 icw(5);Type_VI_secretion_systems
scf_30956_20_contig_1	scf_30956_20_contig_1_16105_16497	16105	16497	+	Uncharacterized protein similar to VCA0109	icw(2);USS-DB-7 icw(2);Type_VI_secretion_systems
scf_30956_20_contig_1	scf_30956_20_contig_1_16494_18215	16494	18215	+	Protein ImpG/VasA	icw(1);USS-DB-7 icw(1);Type_VI_secretion_systems
scf_30956_20_contig_1	scf_30956_20_contig_1_18212_19120	18212	19120	+	Uncharacterized protein ImpH/VasB	icw(4);USS-DB-7 icw(4);Type_VI_secretion_systems

Two genes encoded in contig scf\_30956\_20\_contig\_1 were annotated as hypothetical proteins. Sequences of these two proteins were search against the National Centre for Biotechnology Information Conserved Domains Database (<http://www.ncbi.nlm.nih.gov/Structure/cdd/wrpsb.cgi>). The search showed that Scf\_30956\_20\_contig\_1\_5684\_4785 consisted of T6SS forkhead-associated (*Fha*) domain (E-value = 4.87e-14). Scf\_30956\_20\_contig\_1\_9326\_9841 was identified as T6SS hemolysin co-regulated protein (Hcp) (E-value: 3.32e-68).

T6SS components of Cj1 annotated by MG-RAST were assigned to a standardised nomenclature for T6SS and COGs, Table 5.2.

The scf\_30956\_10\_contig\_1 contig that comprised a partial *tssI* gene was aligned *in silico* with contig scf\_30956\_20\_contig\_1 using Clone Manager version 7 ([http://www.scied.com/pr\\_cmbas.htm](http://www.scied.com/pr_cmbas.htm)). The alignment showed a homology block of 42 bps between the two contigs. The homology block was at the 3' end of contig scf\_30956\_20\_contig\_1 and 5' end of contig scf\_30956\_10\_contig\_1, as illustrated in Figure 5.1.

**Table 5.2:** Assignment of T6SS components in *C. jejuni* strain Cj1 as annotated by MG-RAST to standardised T6SS nomenclature.

Contig and Location	Function	<i>tss</i> assignment	COGs
scf_30956_10_contig_1_12_908	VgrG protein	<i>tssI</i>	3501
scf_30956_20_contig_1_47_3469	FIG00470311: hypothetical protein	-	
scf_30956_20_contig_1_3480_4781	FIG00469624: hypothetical protein	-	
scf_30956_20_contig_1_5684_4785	hypothetical protein; <i>fha</i> domain	-	3456
scf_30956_20_contig_1_9208_5681	IcmF-related protein	<i>tssM</i>	3523
scf_30956_20_contig_1_9326_9841	hypothetical protein; <i>hcp</i>	<i>tssD</i>	3157
scf_30956_20_contig_1_10869_10096	Outer membrane protein ImpK/VasF, OmpA/MotB domain	<i>tssL</i>	3455
scf_30956_20_contig_1_12263_10866	Uncharacterized protein ImpJ/VasE	<i>tssK</i>	3522
scf_30956_20_contig_1_12719_12273	Type VI secretion lipoprotein/VasD	<i>tssJ</i>	3521
scf_30956_20_contig_1_12845_14092	Uncharacterized protein ImpA	<i>tssA</i>	3515
scf_30956_20_contig_1_14161_14646	Uncharacterized protein ImpB	<i>tssB</i>	3516
scf_30956_20_contig_1_14648_16102	Uncharacterized protein ImpC	<i>tssC</i>	3517
scf_30956_20_contig_1_16105_16497	Uncharacterized protein similar to VCA0109	<i>tssE</i>	3518
scf_30956_20_contig_1_16494_18215	Protein ImpG/VasA	<i>tssF</i>	3519
scf_30956_20_contig_1_18212_19120	Uncharacterized protein ImpH/VasB	<i>tssG</i>	3520

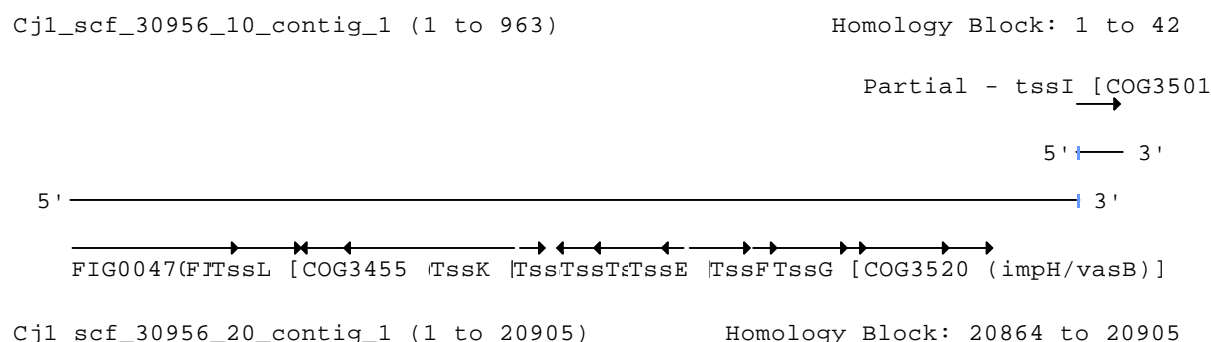


**Figure 5.1:** Alignment of *C. jejuni* strain Cj1 contig scf\_30956\_10\_contig\_1 with contig scf\_30956\_20\_contig\_1 in Clone Manager version 7. The comparison showed a region of 42 bps overlap between the two contigs. The last 42 bps of contig scf\_30956\_20\_contig\_1 is in homology with the first 42 bps of contig scf\_30956\_10\_contig\_1.

Sequences from both contigs were joined *in silico*. The start codon of *tssI* was identified within contig scf\_30956\_20\_contig\_1 and the complete *tssI* gene was mapped. The *in silico* fusion of the two contigs was verified with PCR. A forward primer binding to contig scf\_30956\_20\_contig\_1 and a reverse primer binding to contig scf\_30956\_10\_contig\_1 generated a product of 701 bps, which is the correct size (Figure 5.2). These results verified that the fusion of the two contigs *in silico* was correct.

The putative T6SS locus in Cj1 included 12 out of 13 T6SS core COGs (Table 5.2). However, COG0542 corresponding to *tssH* (also known as *clpV*), which belongs to a subtype of the ATPase AAA+ family (Schlieker et al., 2005), was missing from the Cj1 T6SS genes cluster.

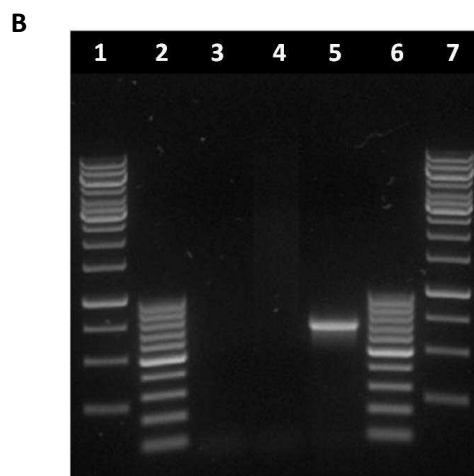
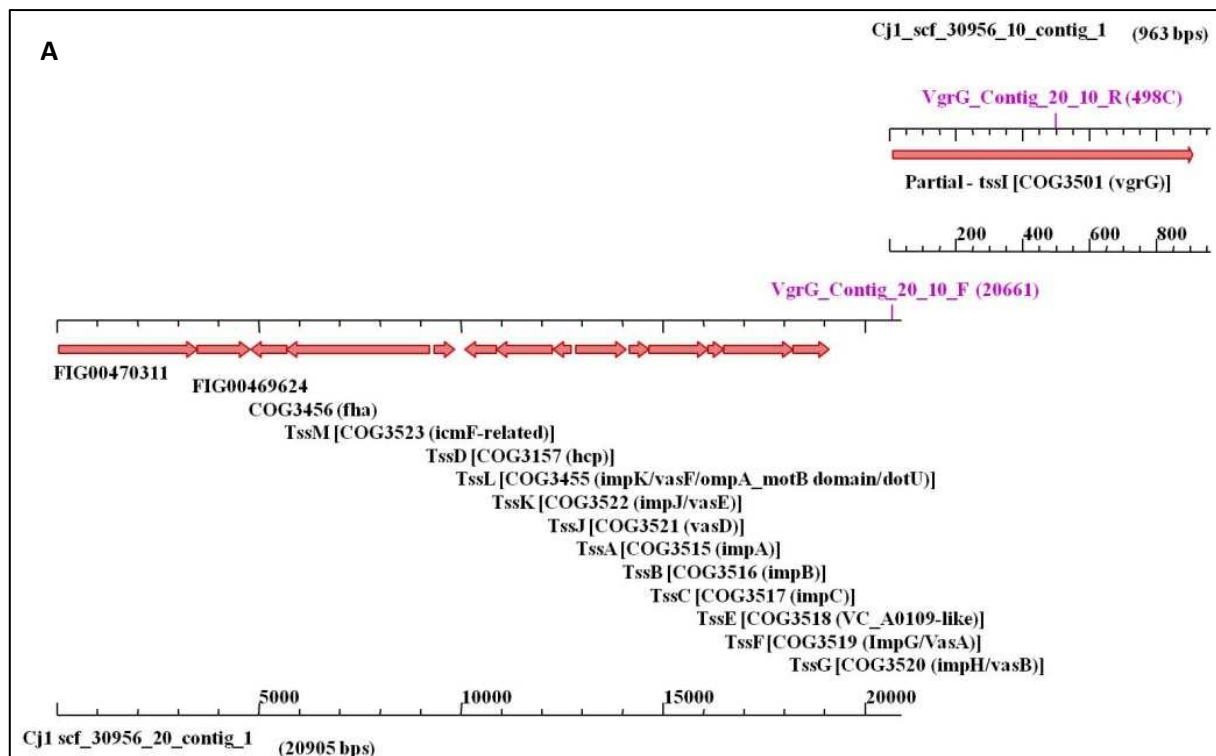


**Figure 5.2:** PCR confirmation of the fusion of contig scf\_30956\_10\_contig\_1 with contig scf\_30956\_20\_contig\_1 as predicted *in silico*. **A:** Position of primers pair used; forward primer - VgrG\_Contig\_20\_10\_F on Cj1\_scf\_30956\_20\_contig\_1 (at position 20661bp) and reverse primer - VgrG\_Contig\_20\_10\_R on Cj1scf\_30956\_10\_contig\_1 (at position 498C bp). **B:** PCR products of the primers pair used. Lane 1 and 7: GeneRuler™ 1kb DNA ladder (Fermentas); Lane 2 and 6: GeneRuler™ 100 bp DNA ladder; Lane 3: No template control; Lane 4: *C. jejuni* strain 11168H genomic DNA; Lane 5: *C. jejuni* strain Cj1 genomic DNA. An expected product of 701 bps was obtained from Cj1 genomic DNA.

### 5.2.2 Gene organisation of T6SS in *Campylobacter jejuni* strain Cj1

Sequence information from the fusion of two contigs was used to map the gene organisation of the Cj1 putative T6SS locus using Clone Manager (Figure 5.3).

The gene organisation of T6SS locus in Cj1 was similar to the two reported *C. jejuni* strains, ATCC 43431 and 108 (Bleumink-Pluym et al., 2013; Lertpiriyapong et al., 2012).

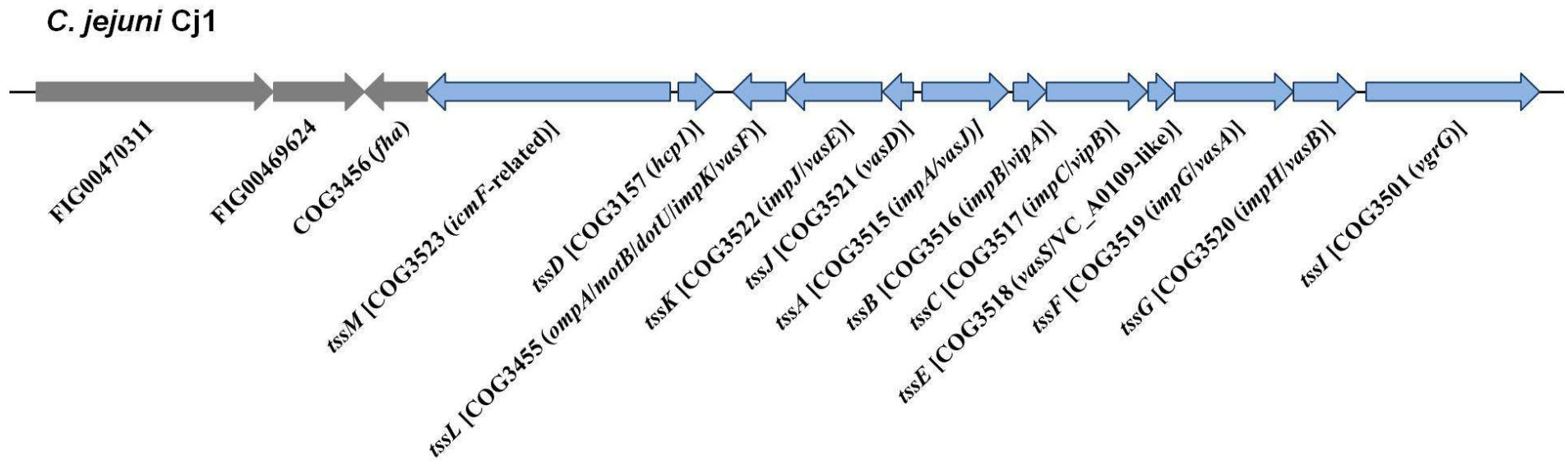


Figure 5.3: Gene organisation of putative T6SS locus in *C. jejuni* strain Cj1. The genes on the locus were assigned with standardised T6SS nomenclature; COGs number and alternative gene name were provided in brackets.

### 5.2.3 Functionality of T6SS in *Campylobacter jejuni* strain Cj1

The genomic DNA sequence of Cj1 *tssD* was translated *in silico* into an amino acid sequence. The TssD protein sequence was provided to commercial company Perbio. They input the sequence into their Antigen Profiler software and identified three regions within the protein sequence as likely antigenic peptides. The results from the Antigen Profiler are presented in Figure 5.4.

Among the three peptides identified by Antigen Profiler, DKTELLKVSMSYRK, was recommended as the best option for Western Blot and immuno-fluorescence applications. The selected peptide for Cj1 TssD was synthesised and used as an antigen for immunisation in a rabbit host.

Unfortunately, after additional boosting and extension of the immunisation protocol, the highest titre obtained was only 1:3200. The failure to generate antibodies against Cj1 TssD peptide led to an inability to use Western Blot for detection of TssD in Cj1 culture supernatant as a functionality test for T6SS in Cj1.

# Antigen Profiler

## Custom Antigen Information

**Designed For:** Sok Kiang Lau\_Cj1\_Hcp  
**Accession:** Q4HDG3  
**Sequence:** Length: 171 amino acids.  
**Gene Symbol:** CCOA0139  
**Protein Name:** Hcp protein  
**Target Species:** Campylobacter coli RM2228

## Protein Sequence and Features

MAEPAFIKIE GSTQGLISSG ASTEASIGNR **RYKSGHEDEIMAE** AQEVSHIVTV 50  
 EVDQQSGQPS GQRVHKPEEF TCSLNKSVPL LYNALTKGER LPTVEVHWER 100  
 TATSGGSEHF **FTTKLEDATITNIELIMPNA** QESSNHDKTE **LLKVSMSYRK** 150  
 VVWEHTAAGT **SGSDDWREGKA** 171

## Antigen Peptide Candidates

Name	Peptide	Position	Length
CCOA0139-30:43	RYKSGHEDEIMAE	30	14
CCOA0139-137:150	DKTELLKVSMSYRK	137	14
CCOA0139-158:171	AGTSGSDDWREGKA	158	14

## Graphical Analysis

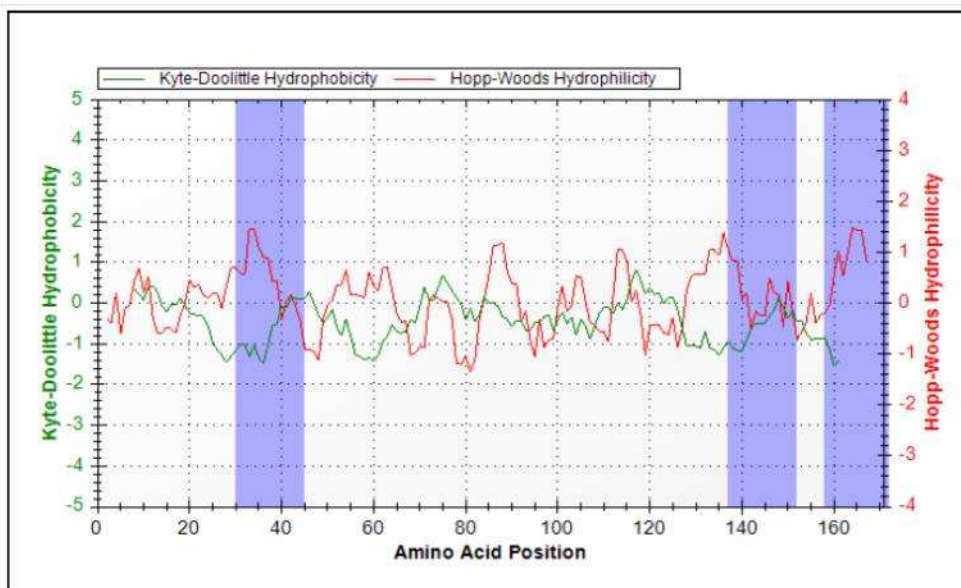


**Figure 5.4:** Report from Antigen Profiler provided by Perbio. Cj1 TssD protein sequence was analysed for peptides suitable for generation of antibodies that could be used for both Western blot and immunofluorescence applications. The location of the peptides within the sequence was shown in the section on Protein Sequence and Features. Three peptides were identified as suitable candidates and their sequences were shown in the Antigen Peptide Candidates table. The hydrophobicity and hydrophilicity chart of the Cj1 TssD was presented in the Graphical Analysis section. The regions of suitable candidates were highlight in blue.

In view of the fact that no antibodies were available for Western blot, mass spectrometry was used instead to detect secreted T6SS components in culture supernatant. Complex protein extracts would not be suitable for direct mass spectrometry analysis without fractionation. Hence, proteins precipitated from culture supernatant were run on SDS-PAGE (Figure 5.5). The gel image was shown to Dr Hannah Florance from UoE - Mass Spectrometry Facility and the proteins were confirmed to be suitable for nano-LC coupled to QTOF mass spectrometry analysis. The mass spectrometry output data was analysed using Spectrum Mill MS Proteomics Workbench software by Agilent.

A total of 14 *C. jejuni* proteins were identified in Cj1 culture supernatant sample (Table 5.3). The proteins detected were mostly flagellar associated proteins. TssD was also among the 14 proteins detected but no other T6SS components were detected. The TssD detected had a calling of 5 distinct peptides and coverage of 40.9% of its amino acid sequence (Table 5.3). The presence of TssD in culture media is a hallmark indicator that the T6SS in bacteria harbouring T6SS genes cluster is functional (Pukatzki et al., 2007). Hence, the detection of TssD in Cj1 culture supernatant strongly suggests that the secretory mechanism of T6SS in Cj1 is functional.

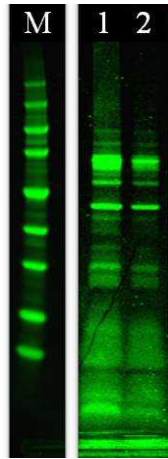


**Figure 5.5:** Analysis of *C. jejuni* strain Cj1 culture supernatant by SDS-PAGE. Proteins in Cj1 24 hr old culture media were precipitated using TCA and run on NuPAGE® 4-12% Bis-Tris Gel (Novex®), at 200 V for 35 minutes in MES buffer. The gel was stained with SimplyBlue™ SafeStain (Invitrogen) and imaged with Odyssey® CLx infra-red imager (LI-COR). Lane M: Perfect Protein™ Markers, 10-225 kDa (Novagen®); Lane 1: 3.75 µg Cj1 culture supernatant TCA protein precipitate; and Lane 2: 1.875 µg Cj1 culture supernatant TCA protein precipitate.

**Table 5.3: Mass spectrometry data on the analysis of *C. jejuni* strain Cj1 culture supernatant TCA protein precipitate.**

Group number	Spectra number	Distinct peptides number	Distinct summed MS/MS search score	% amino acid coverage	Mean peptide spectral intensity	Protein molecular weight (da)	Species	Database accession number	Protein Name
1	15	11	160.6	<a href="#">29.2</a>	3.15E+05	59337	CAMJU	<a href="#">I6ZA17</a>	Flagellin A (Fragment)
2	9	6	77.33	<a href="#">12.4</a>	1.51E+05	69981	CAMJU	<a href="#">H8BLU8</a>	Flagellar capping protein
<b>3</b>	<b>9</b>	<b>5</b>	<b>76.65</b>	<b><a href="#">40.9</a></b>	<b>3.66E+05</b>	<b>18807</b>	<b>CAMJU</b>	<b><a href="#">B5QJ70</a></b>	<b>Secreted protein Hcp</b>
4	5	3	47.02	<a href="#">28.0</a>	5.65E+05	11023	CAMJU	<a href="#">H7X9T0</a>	Putative periplasmic cytochrome C
5	5	3	36.72	<a href="#">7.4</a>	2.03E+05	46406	CAMJU	<a href="#">A5KG76</a>	Major outer membrane protein
6	3	2	34.41	<a href="#">10.4</a>	1.77E+05	21925	CAMJU	<a href="#">H7X5W9</a>	Putative uncharacterized protein
7	3	2	25.17	<a href="#">10.4</a>	3.30E+05	26574	CAMJJ	<a href="#">A1VZ75</a>	Flagellin subunit protein FlaC
8	2	2	19.48	<a href="#">16.5</a>	1.25E+05	13620	CAMJU	<a href="#">A5KF91</a>	Possible flagellar protein
9	1	1	17.1	<a href="#">2.2</a>	1.25E+05	58409	CAMJU	<a href="#">D2N0U0</a>	Flagellar hook protein flgE
10	1	1	16.84	<a href="#">4.8</a>	1.42E+05	27527	CAMJU	<a href="#">H7ZT60</a>	Putative uncharacterized protein
11	1	1	16.51	<a href="#">10.3</a>	1.81E+05	12192	CAMJU	<a href="#">H7XE85</a>	Putative uncharacterized protein
12	2	1	16.43	<a href="#">15.7</a>	4.34E+05	14179	CAMJU	<a href="#">A5KGY8</a>	Putative uncharacterized protein
13	2	1	13.11	<a href="#">2.9</a>	1.03E+05	45098	CAMJU	<a href="#">A5KF24</a>	Elongation factor Tu
14	1	1	12.4	<a href="#">4.9</a>	1.26E+04	28820	CAMJU	<a href="#">A5KH72</a>	Probable ABC-type amino-acid transporter periplasmic solute-binding protein

## 5.2.4 T6SS mutants in *Campylobacter jejuni* strain Cj1

### 5.2.4.1 Construction of *tssD* and *tssM* mutants in Cj1

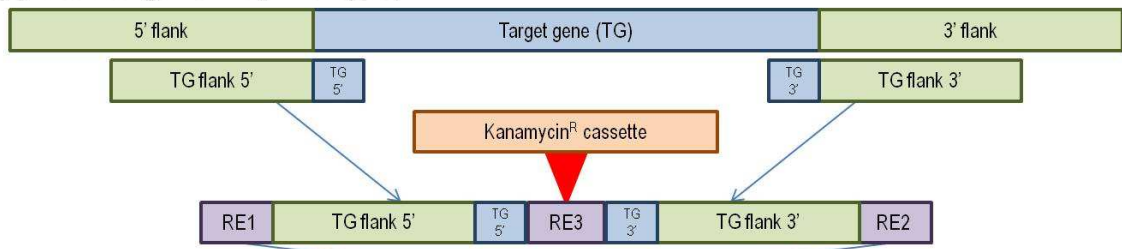
The genes encoding two components of the T6SS system in Cj1, *tssD* and *tssM*, were selected for inactivation and replacement with a gene cassette conferring kanamycin resistance.

A synthetic construct was designed for each of the target genes. It consisted of 7 sections; i) restriction enzyme site 1 (RE1) - *SpeI*, for sub-cloning into pGEM-Teasy vector; ii) TG flank 5': 450 bp region flanking 5' end of target gene; iii) TG 5': 50 bp region of target gene at 5' end; iv) restriction enzyme site 3 (RE3) - *BamHI*, for insertion of kanamycin resistance cassette; v) TG 3': 50 bp region of target gene at 3' end; vi) TG flank 3': 450 bp region flanking 3' end of target gene; vii) restriction enzyme site 2 (RE2) - *NdeI*, for sub-cloning into pGEM-Teasy. The design of the construct is illustrated in Figure 5.6. The detailed descriptions of the designed cloning fragments, i) *tssD*(syn) and ii) *tssM*(syn), are tabulated in Table 5.4.

The cloning fragments were synthesised by GenScript using their standard vector, pUC57 and sub-cloned into the multiple cloning site (MCS) of pGEM-Teasy, at *SpeI* and *NdeI* sites. The resulting plasmids were pGEM\_*tssD*(syn) and pGEM\_*tssM*(syn).

A plasmid (pJMK30) containing a kanamycin resistance cassette ( $\text{kan}^{\text{R}}_{\text{cas}}$ ) was kindly provided by Dr Mark Reuter from the Institute of Food Research, UK (van Vliet et al., 1998). The  $\text{kan}^{\text{R}}_{\text{cas}}$  was digested from pJMK30 using *Bam*HI (Karlyshev and Wren, 2005) and cloned into the suitably digested pGEM\_*tssD*(syn) and pGEM\_*tssM*(syn) respectively. The resultant plasmids pGEM\_*tssD*(syn):: $\text{kan}^{\text{R}}_{\text{cas}}$  and pGEM\_*tssM*(syn):: $\text{kan}^{\text{R}}_{\text{cas}}$  had a  $\text{kan}^{\text{R}}_{\text{cas}}$  sandwiched between the 50 bp from start codon and 50 bp to stop codon of the respective target genes - as illustrated by in the mutant genome in Figure 5.6. The list of plasmids used in this study is tabulated in Table 5.5.

*Campylobacter* genome (wild-type)



**Synthetic construct design:**

Target gene and flanking regions synthesised

- TG flank 5': 450 bp region flanking 5' end of target gene
- TG flank 3': 450bp region flanking 3' end of target gene
- TG 5': 50 bp region at the 5' end of target gene
- TG 3': 50 bp region at the 3' end of target gene

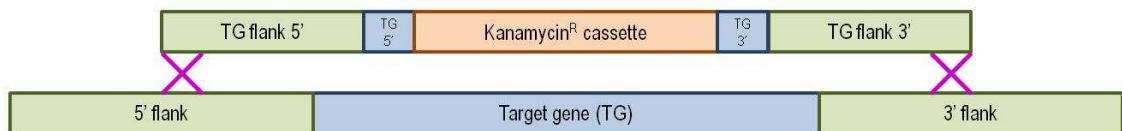
Restriction enzyme (RE) sites incorporated for cloning

- RE1 & 2 for cloning into pGEM-Teasy vector
- RE3 for insertion of Kanamycin<sup>R</sup> cassette

**Primer pairs (P) were designed within:**

1. Flanking regions (5' & 3') outside of synthetic construct: **1F & 1R**
2. TG flank 5' & 3' regions within synthetic construct: **2F & 2R**
3. Kanamycin<sup>R</sup> cassette: **3F & 3R**
4. Knock-out region of target gene: **4F & 4R**

**Double crossover**



*Campylobacter* genome (mutant)

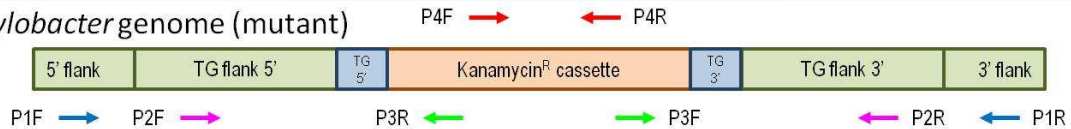


**Figure 5.6: Construction of *Cj1tssD* and *tssM* mutants.** A synthetic construct was made up of 7 sections: i) RE1 - *SpeI* restriction enzyme site (for sub-cloning into pGEM-Teasy vector); ii) TG flank 5' - 450 bp region flanking 5' end of target gene; iii) TG 5' - 50 bp region of target gene at 5' end; iv) RE3 - *BamHI* restriction enzyme site (for insertion of kan<sup>R</sup>\_cas); v) TG 3' - 50 bp region of target gene at 3' end; vi) TG flank 3' - 450 bp region flanking 3' end of target gene; and vii) RE2 - *NdeI* restriction enzyme site (for sub-cloning into pGEM-Teasy). The construct was synthesised and dropped into pGEM-Teasy vector. A kan<sup>R</sup>\_cas could be dropped into the construct at RE3. The construct carrying a kan<sup>R</sup>\_cas could then be integrated into the genome in a double crossover event. The resulted genome of the mutant will be as illustrated in *Campylobacter* genome (mutant). Four primers pairs were designed to check for orientation of kanamycin resistance cassette inserted and successful occurrence of double crossover event.

**Table 5.4: List of cloning fragments used in this study.**

Cloning fragments	Descriptions	Sources
<i>tssD</i> (syn)	<i>SpeI</i> :450 bp flanking 5' end of <i>tssD</i> :50 bp of <i>tssD</i> from start codon: <i>BamHI</i> :50 bp of <i>tssD</i> to stop codon:450 bp flanking 3'end of <i>tssD</i> : <i>NdeI</i>	GenScript
<i>tssM</i> (syn)	<i>SpeI</i> :450 bp flanking 5' end of <i>tssM</i> :50 bp of <i>tssM</i> from start codon: <i>BamHI</i> :50 bp of <i>tssM</i> to stop codon:450 bp flanking 3'end of <i>tssM</i> : <i>NdeI</i>	GenScript
kan <sup>R</sup> _cas	Kanmycin resistance cassette (consisting of its own promoter and <i>aphAIII</i> gene) were digested from pJMK30 at <i>BamHI</i> sites, cassette size is 1499 bp	pJMK30
<i>tssD</i> (syn)::kan <sup>R</sup> _cas	450 bp flanking 5' end of <i>tssD</i> :50 bp of <i>tssD</i> from start codon:kan <sup>R</sup> _cas:50 bp of <i>tssD</i> to stop codon:450 bp flanking 3'end of <i>tssD</i>	This study
<i>tssM</i> (syn)::kan <sup>R</sup> _cas	450 bp flanking 5' end of <i>tssM</i> :50 bp of <i>tssM</i> from start codon:kan <sup>R</sup> _cas:50 bp of <i>tssM</i> to stop codon:450 bp flanking 3'end of <i>tssM</i>	This study

**Table 5.5: List of plasmids used in this study.**

Plasmids	Descriptions	Sources
<b>pUC57</b>	Ampicillin resistance, multiple cloning site (MCS) within <i>lacZ</i> gene, plasmid size is 2710bp	GenScript
<b>pUC_ <i>tssD</i>(syn)</b>	Cloning of <i>tssD</i> (syn) into MCS of pUC57 by <i>EcoRV</i>	GenScript
<b>pUC_ <i>tssM</i>(syn)</b>	Cloning of <i>tssM</i> (syn) into MCS of pUC57 by <i>EcoRV</i>	GenScript
<b>pGEM-Teasy</b>	Ampicillin resistance, multiple cloning site (MCS) within <i>lacZ</i> gene, plasmid size is 3015bp	Promega
<b>pGEM_ <i>tssD</i>(syn)</b>	Cloning of <i>tssD</i> (syn) into MCS of pGEM-Teasy by <i>SpeI</i> and <i>NdeI</i>	GenScript
<b>pGEM_ <i>tssM</i>(syn)</b>	Cloning of <i>tssM</i> (syn) into MCS of pGEM-Teasy by <i>SpeI</i> and <i>NdeI</i>	GenScript
<b>pJMK30</b>	Ampicillin resistance, contains a kan <sup>R</sup> _cas within <i>BamHI</i> sites (source of kan <sup>R</sup> _cas)	Institute of Food Research, UK
<b>pGEM_ <i>tssD</i>(syn)::kan<sup>R</sup>_cas</b>	Cloning of kan <sup>R</sup> _cas into <i>tssD</i> (syn) in pGEM_ <i>tssD</i> (syn) by <i>BamHI</i>	This study
<b>pGEM_ <i>tssM</i>(syn)::kan<sup>R</sup>_cas</b>	Cloning of kan <sup>R</sup> _cas into <i>tssM</i> (syn) in pGEM_ <i>tssM</i> (syn) by <i>BamHI</i>	This study

The two suicide plasmids: pGEM\_ *tssD*(syn)::kan<sup>R</sup>\_cas and pGEM\_ *tssM*(syn)::kan<sup>R</sup>\_cas, were delivered into electro-competent Cj1 cells via electroporation. The wild-type target genes were then replaced by the cloning fragments *tssD*(syn)::kan<sup>R</sup>\_cas and *tssM*(syn)::kan<sup>R</sup>\_cas (Table 5.4) respectively, through a double crossover event. This resulted in two T6SS mutants in Cj1, i) Cj1Δ*tssD*(syn)::kan<sup>R</sup>\_cas and ii) Cj1Δ*tssM*(syn)::kan<sup>R</sup>\_cas. The list of strains used in this study is tabulated in Table 5.6.

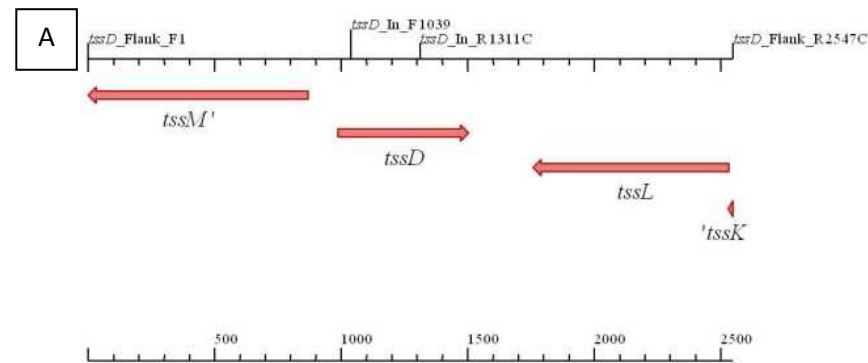
The total number of transformants obtained for each mutant was not determined. However, a total of four Cj1Δ*tssD*(syn)::kan<sup>R</sup>\_cas isolates and three Cj1Δ*tssM*(syn)::kan<sup>R</sup>\_cas were screened by PCR.

**Table 5.6: List of strains used in this study.**

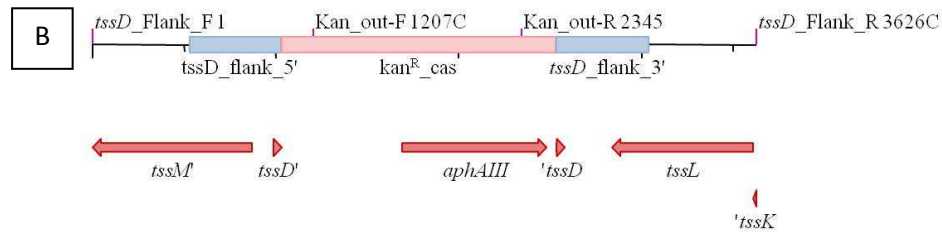
Strains	Descriptions	Sources
<i>E. coli</i> Top10	Cloning strain used to hold plasmids	Invitrogen
Top10 pGEM_ <i>tssD</i> (syn)	Transformed pGEM_ <i>tssD</i> (syn) into chemically competent Top10	This study
Top10 pGEM_ <i>tssM</i> (syn)	Transformed pGEM_ <i>tssM</i> (syn) into chemically competent Top10	This study
Top10 pGEM_ <i>tssD</i> (syn)::kan <sup>R</sup> _cas	Transformed pGEM_ <i>tssD</i> (syn)::kan <sup>R</sup> _cas into chemically competent Top10	This study
Top10 pGEM_ <i>tssM</i> (syn)::kan <sup>R</sup> _cas	Transformed pGEM_ <i>tssM</i> (syn)::kan <sup>R</sup> _cas into chemically competent Top10	This study
<i>C. jejuni</i> strain Cj1 wild-type	Clinical isolate from Thailand	Lab stock
Cj1Δ <i>tssD</i> (syn)::kan <sup>R</sup> _cas	<i>tssD</i> in Cj1 wild-type was replaced with <i>tssD</i> (syn)::kan <sup>R</sup> _cas	This study
Cj1Δ <i>tssM</i> (syn)::kan <sup>R</sup> _cas	<i>tssM</i> in Cj1 wild-type was replaced with <i>tssM</i> (syn)::kan <sup>R</sup> _cas	This study

#### 5.2.4.2 PCR screening of *tssD* and *tssM* mutants in *Cj1*

Potential *Cj1ΔtssD(syn)::kan<sup>R</sup>\_cas* isolates generated from two different plasmid sources were tested with 4 different sets of primer. Regions amplified by each set of primers are illustrated in Figure 5.7. The results obtained from primer set 1: *tssD\_Flank* forward and reverse (F+R) are shown in Figure 5.8; primer set 2: *tssD\_In* F+R in Figure 5.9; primer set 3: *tssD\_Flank* forward and *Kan\_Out* forward in Figure 5.10; and primer set 4: *tssD\_Flank* forward and *Kan\_Out* reverse in Figure 5.11.



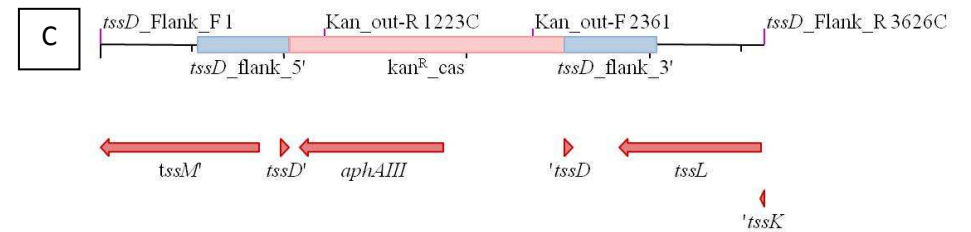
**Cj1 wild-type *tssD*\_Flank F+R (2547 bps)**



**kan<sup>R</sup>\_cas inserted in same orientation as *tssD***



**Cj1 *tssD* mutant *tssD*\_Flank F+R (3626 bps)**



**kan<sup>R</sup>\_cas inserted in opposite orientation as *tssD***



**Cj1 *tssD* mutant *tssD*\_Flank F+R (3626 bps)**

**Figure 5.7: Illustration on regions primed by each primer sets in *C. jejuni* strain Cj1 (A) wild-type and two possible constructs of *tssD* mutant: (B) kan<sup>R</sup>\_cas inserted in the same orientation as *tssD* and (C) kan<sup>R</sup>\_cas inserted in the opposite orientation as *tssD*. Primer set 1: *tssD*\_Flank forward and reverse; primer set 2: *tssD*\_In forward and reverse; primer set 3: *tssD*\_Flank forward and Kan\_out forward; and primer set 4: *tssD*\_Flank forward and Kan\_out reverse.**

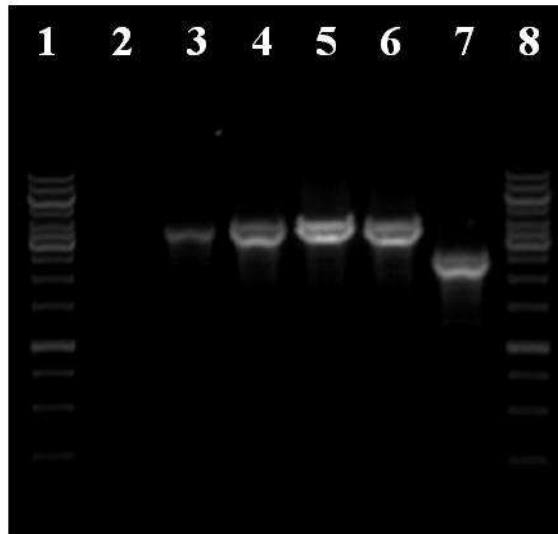


**Figure 5.8:** PCR screening of *C. jejuni* strain Cj1 *tssD* replacement mutant, *Cj1ΔtssD(syn)::kan<sup>R</sup>\_cas* with *tssD*\_Flank forward and reverse primer. Lane 1 and 8: GeneRuler™ 1kb DNA ladder (Fermentas); Lane 2: No template control; Lane 3: *Cj1ΔtssD(syn)::kan<sup>R</sup>\_cas* isolate 1 genomic DNA; Lane 4: *Cj1ΔtssD(syn)::kan<sup>R</sup>\_cas* isolate 2 genomic DNA; Lane 5: *Cj1ΔtssD(syn)::kan<sup>R</sup>\_cas* isolate 3 genomic DNA; Lane 6: *Cj1ΔtssD(syn)::kan<sup>R</sup>\_cas* isolate 4 genomic DNA; and Lane 7: *C. jejuni* strain Cj1 wild-type genomic DNA. Cj1 wild-type yielded a product of 2547 bps and *Cj1ΔtssD(syn)::kan<sup>R</sup>\_cas* yielded a product of 3626 bps.

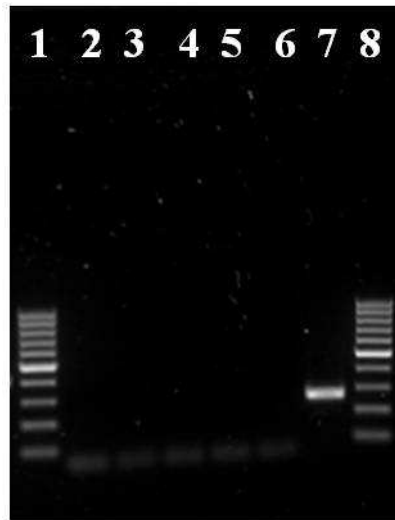


Figure 5.9: PCR screening of *C. jejuni* strain Cj1 *tssD* replacement mutant, *Cj1ΔtssD(syn)::kan<sup>R</sup>\_cas* with *tssD*\_In forward and reverse primer. Lane 1 and 8: GeneRuler™ 100 bp DNA ladder (Fermentas); Lane 2: No template control; Lane 3: *Cj1ΔtssD(syn)::kan<sup>R</sup>\_cas* isolate 1 genomic DNA; Lane 4: *Cj1ΔtssD(syn)::kan<sup>R</sup>\_cas* isolate 2 genomic DNA; Lane 5: *Cj1ΔtssD(syn)::kan<sup>R</sup>\_cas* isolate 3 genomic DNA; Lane 6: *Cj1ΔtssD(syn)::kan<sup>R</sup>\_cas* isolate 4 genomic DNA; and Lane 7: *C. jejuni* strain Cj1 wild-type genomic DNA. Cj1 wild-type yielded a product of 273 bps and *Cj1ΔtssD(syn)::kan<sup>R</sup>\_cas* yielded no product.

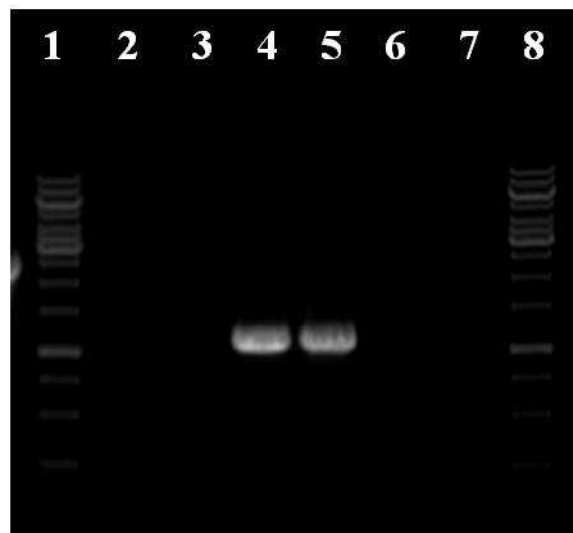


Figure 5.10: PCR screening of *C. jejuni* strain Cj1 *tssD* replacement mutant, *Cj1ΔtssD(syn)::kan<sup>R</sup>\_cas* with *tssD*\_Flank forward and Kan\_Out forward to determine orientation of kanamycin resistance cassette inserted. Lane 1 and 8: GeneRuler™ 1kb DNA ladder (Fermentas); Lane 2: No template control; Lane 3: *Cj1ΔtssD(syn)::kan<sup>R</sup>\_cas* isolate 1 genomic DNA; Lane 4: *Cj1ΔtssD(syn)::kan<sup>R</sup>\_cas* isolate 2 genomic DNA; Lane 5: *Cj1ΔtssD(syn)::kan<sup>R</sup>\_cas* isolate 3 genomic DNA; Lane 6: *Cj1ΔtssD(syn)::kan<sup>R</sup>\_cas* isolate 4 genomic DNA; and Lane 7: *C. jejuni* strain Cj1 wild-type genomic DNA. Cj1 wild-type yielded no product. *Cj1ΔtssD(syn)::kan<sup>R</sup>\_cas* isolates with kanamycin resistance cassette inserted in same orientation as *tssD* yielded a product of 1207 bps. *Cj1ΔtssD(syn)::kan<sup>R</sup>\_cas* isolates with kanamycin resistance cassette inserted in opposite orientation as *tssD* yielded no product.

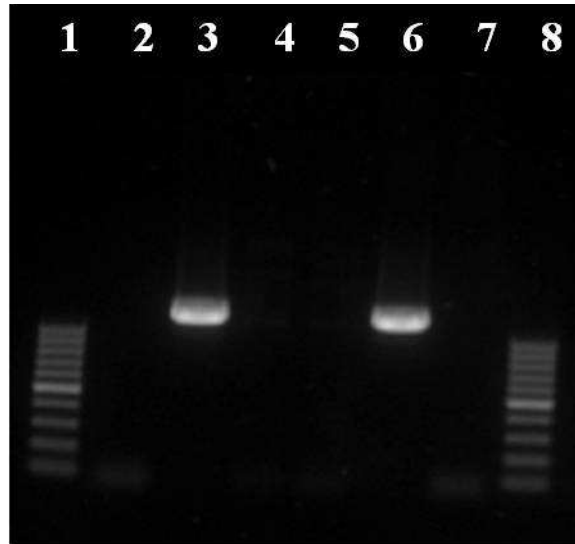
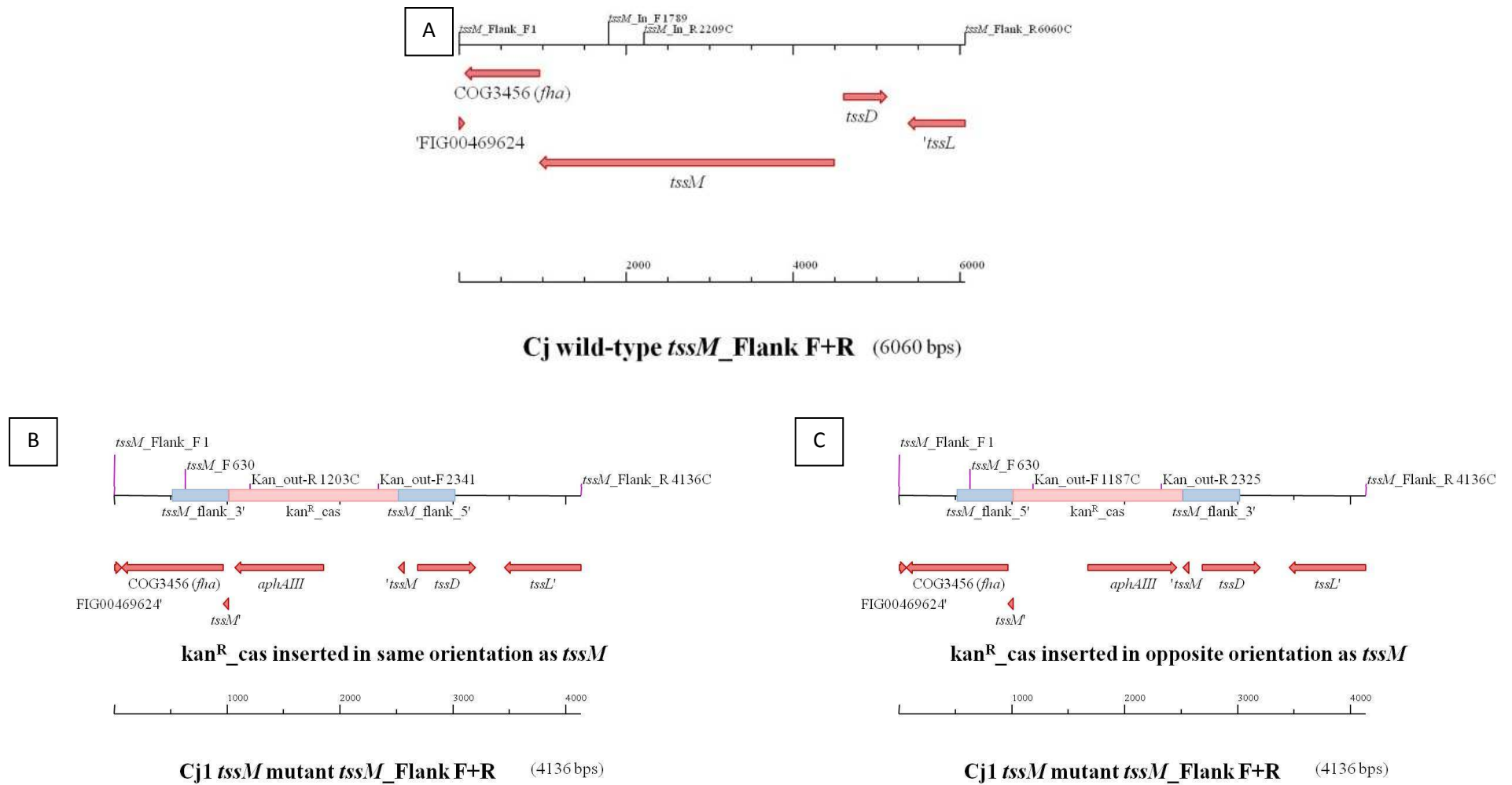


Figure 5.11: PCR screening of *C. jejuni* strain Cj1 *tssD* replacement mutant, *Cj1ΔtssD(syn)::kan<sup>R</sup>\_cas* with *tssD*\_Flank forward and Kan\_Out reverse to determine orientation of kanamycin resistance cassette inserted. Lane 1 and 8: GeneRuler™ 100 bp DNA ladder (Fermentas); Lane 2: No template control; Lane 3: *Cj1ΔtssD(syn)::kan<sup>R</sup>\_cas* isolate 1 genomic DNA; Lane 4: *Cj1ΔtssD(syn)::kan<sup>R</sup>\_cas* isolate 2 genomic DNA; Lane 5: *Cj1ΔtssD(syn)::kan<sup>R</sup>\_cas* isolate 3 genomic DNA; Lane 6: *Cj1ΔtssD(syn)::kan<sup>R</sup>\_cas* isolate 4 genomic DNA; and Lane 7: *C. jejuni* strain Cj1 wild-type genomic DNA. Cj1 wild-type yielded no product. *Cj1ΔtssD(syn)::kan<sup>R</sup>\_cas* isolates with kanamycin resistance cassette inserted in opposite orientation as *tssD* yielded a product of 1223 bps. *Cj1ΔtssD(syn)::kan<sup>R</sup>\_cas* isolates with kanamycin resistance cassette inserted in same orientation as *tssD* yielded no product.

Potential Cj1 $\Delta$ *tssM*(syn)::kan<sup>R</sup>\_cas isolates were also tested with 4 different sets of primers. Regions amplified by each set of primers are illustrated in Figure 5.12. The results obtained from primer set 1: *tssM*\_Flank forward and reverse (F+R) are shown in Figure 5.13; primer set 2: *tssM*\_In F+R in Figure 5.14; primer set 3: *tssM* forward and Kan\_Out forward in Figure 5.15; and primer set 4: *tssM* forward and Kan\_Out reverse in Figure 5.16.



**Figure 5.12:** Illustration on regions primed by each primer sets in *C. jejuni* strain Cj1 (A) wild-type and two possible constructs of *tssM* mutant: (B) *kan*<sup>R</sup>\_cas inserted in the same orientation as *tssM* and (C) *kan*<sup>R</sup>\_cas inserted in the opposite orientation as *tssM*. Primer set 1: *tssM*\_Flank forward and reverse; primer set 2: *tssM*\_In forward and reverse; primer set 3: *tssM* forward and *Kan*<sup>R</sup>\_out forward; and primer set 4: *tssM* forward and *Kan*<sup>R</sup>\_out reverse.

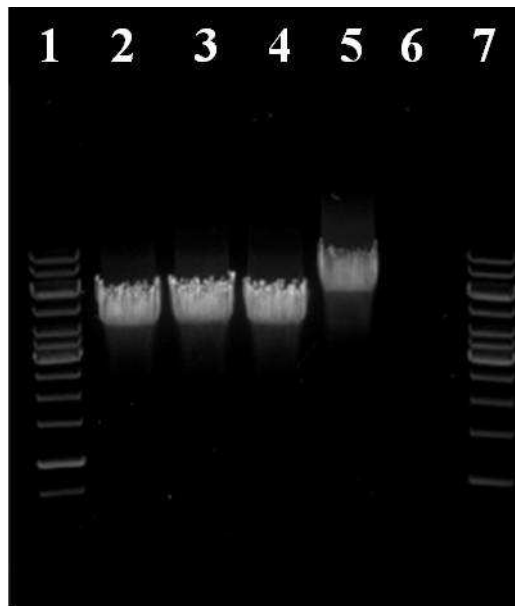


Figure 5.13: PCR screening of *C. jejuni* strain Cj1 *tssM* replacement mutant, *Cj1ΔtssM(syn)::kan<sup>R</sup>\_cas* with *tssM\_Flank* forward and reverse primer. Lane 1 and 7: GeneRuler™ 1kb DNA ladder (Fermentas); Lane 2: *Cj1ΔtssM(syn)::kan<sup>R</sup>\_cas* isolate 1 genomic DNA; Lane 3: *Cj1ΔtssM(syn)::kan<sup>R</sup>\_cas* isolate 2 genomic DNA; Lane 4: *Cj1ΔtssM(syn)::kan<sup>R</sup>\_cas* isolate 3 genomic DNA; Lane 5: *C. jejuni* strain Cj1 wild-type genomic DNA; and Lane 6: No template control. Cj1 wild-type yielded a product of 6060 bps and *Cj1ΔtssM(syn)::kan<sup>R</sup>\_cas* yielded a product of 4136 bps.

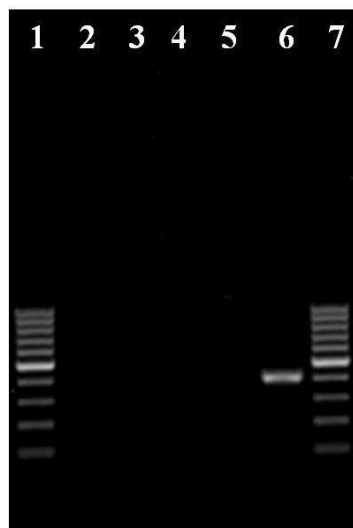


Figure 5.14: PCR screening of *C. jejuni* strain Cj1 *tssM* replacement mutant, *Cj1ΔtssM(syn)::kan<sup>R</sup>\_cas* with *tssM\_In* forward and reverse primer. Lane 1 and 7: GeneRuler™ 100 bp DNA ladder (Fermentas); Lane 2: *Cj1ΔtssM(syn)::kan<sup>R</sup>\_cas* isolate 1 genomic DNA; Lane 3: *Cj1ΔtssM(syn)::kan<sup>R</sup>\_cas* isolate 2 genomic DNA; Lane 4: *Cj1ΔtssM(syn)::kan<sup>R</sup>\_cas* isolate 3 genomic DNA; Lane 5: *C. jejuni* strain Cj1 wild-type genomic DNA; and Lane 6: No template control. Cj1 wild-type yielded a product of 421 bps and *Cj1ΔtssM(syn)::kan<sup>R</sup>\_cas* yielded no product.

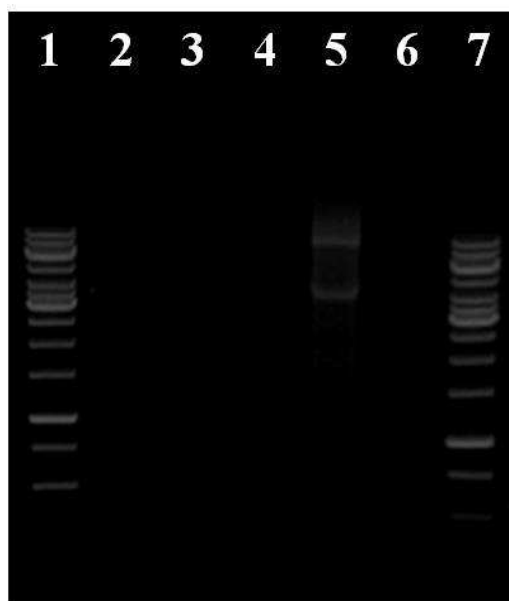


Figure 5.15: PCR screening of *C. jejuni* strain Cj1 *tssM* replacement mutant, *Cj1ΔtssM(syn)::kan<sup>R</sup>\_cas* with *tssM* forward and Kan\_Out forward to determine orientation of kanamycin resistance cassette inserted. Lane 1 and 7: GeneRuler™ 1 kb DNA ladder (Fermentas); Lane 2: *Cj1ΔtssM(syn)::kan<sup>R</sup>\_cas* isolate 1 genomic DNA; Lane 3: *Cj1ΔtssM(syn)::kan<sup>R</sup>\_cas* isolate 2 genomic DNA; Lane 4: *Cj1ΔtssM(syn)::kan<sup>R</sup>\_cas* isolate 3 genomic DNA; Lane 5: pGEM\_*tssM(syn)::kan<sup>R</sup>\_cas* plasmid DNA; and Lane 6: No template control. pGEM\_*tssM(syn)::kan<sup>R</sup>\_cas* plasmid DNA with kanamycin cassette inserted in the same orientation as *tssM* yield no product. *Cj1ΔtssM(syn)::kan<sup>R</sup>\_cas* isolates with kanamycin resistance cassette inserted in opposite orientation as *tssM* yielded a product of 558 bps. *Cj1ΔtssM(syn)::kan<sup>R</sup>\_cas* isolates with kanamycin resistance cassette inserted in same orientation as *tssM* yielded no product.

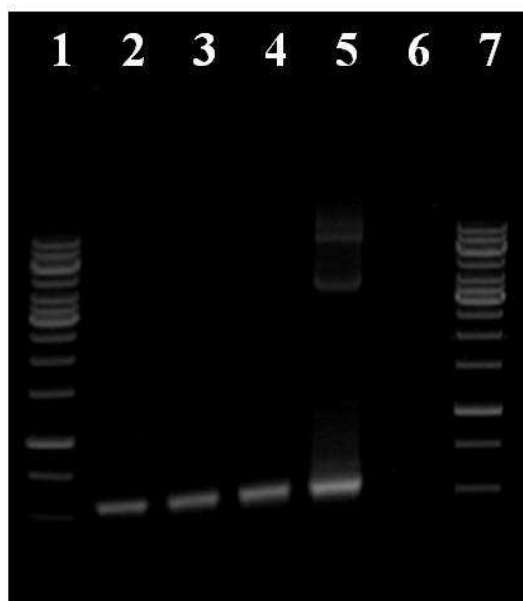


Figure 5.16: PCR screening of *C. jejuni* strain Cj1 *tssM* replacement mutant, *Cj1ΔtssM(syn)::kan<sup>R</sup>\_cas* with *tssM* forward and Kan\_Out reverse to determine orientation of kanamycin resistance cassette inserted. Lane 1 and 7: GeneRuler™ 1 kb DNA ladder (Fermentas); Lane 2: *Cj1ΔtssM(syn)::kan<sup>R</sup>\_cas* isolate 1 genomic DNA; Lane 3: *Cj1ΔtssM(syn)::kan<sup>R</sup>\_cas* isolate 2 genomic DNA; Lane 4: *Cj1ΔtssM(syn)::kan<sup>R</sup>\_cas* isolate 3 genomic DNA; Lane 5: pGEM\_*tssM(syn)::kan<sup>R</sup>\_cas* plasmid DNA; and Lane 6: No template control. pGEM\_*tssM(syn)::kan<sup>R</sup>\_cas* plasmid DNA with kanamycin cassette inserted in the same orientation as *tssM* yield a product of 574bp. *Cj1ΔtssM(syn)::kan<sup>R</sup>\_cas* isolates with kanamycin resistance cassette inserted in same orientation as *tssM* yield a product of 574 bps. *Cj1ΔtssM(syn)::kan<sup>R</sup>\_cas* isolates with kanamycin resistance cassette inserted in opposite orientation as *tssM* yield no product.

Primer sets *tssD*\_Flank and *tssM*\_Flank, which annealed to regions on the chromosome flanking the synthetic construct, generated products of different sizes between wild-type and mutants. In Cj1 wild-type, *tssD*\_Flank and *tssM*\_Flank generated products of 2547bp and 6060bp respectively. However, in Cj1 $\Delta$ *tssD*(syn)::kan<sup>R</sup>\_cas, a larger product of 3626bp was generated. The increase in size was because the kan<sup>R</sup>\_cas used to replace *tssD* was larger than the latter. In Cj1 $\Delta$ *tssM*(syn)::kan<sup>R</sup>\_cas, the product generated was 4136bp. This is a smaller product as compared to the wild-type. Here, the reduction in size was because the size of kan<sup>R</sup>\_cas was smaller than the *tssM* it replaced.

A second set of primers, *tssD*\_In and *tssM*\_In, prime to regions within the target genes. This set of primers was used in the screening to ensure that the target genes were no longer present in the genome of the mutants. There was no product from both mutants when this set of primers was used. This indicated that each target gene was lost in its respective mutant.

The PCR results obtained confirmed that double crossover had taken place in all Cj1 $\Delta$ *tssD*(syn)::kan<sup>R</sup>\_cas and Cj1 $\Delta$ *tssM*(syn)::kan<sup>R</sup>\_cas isolates.

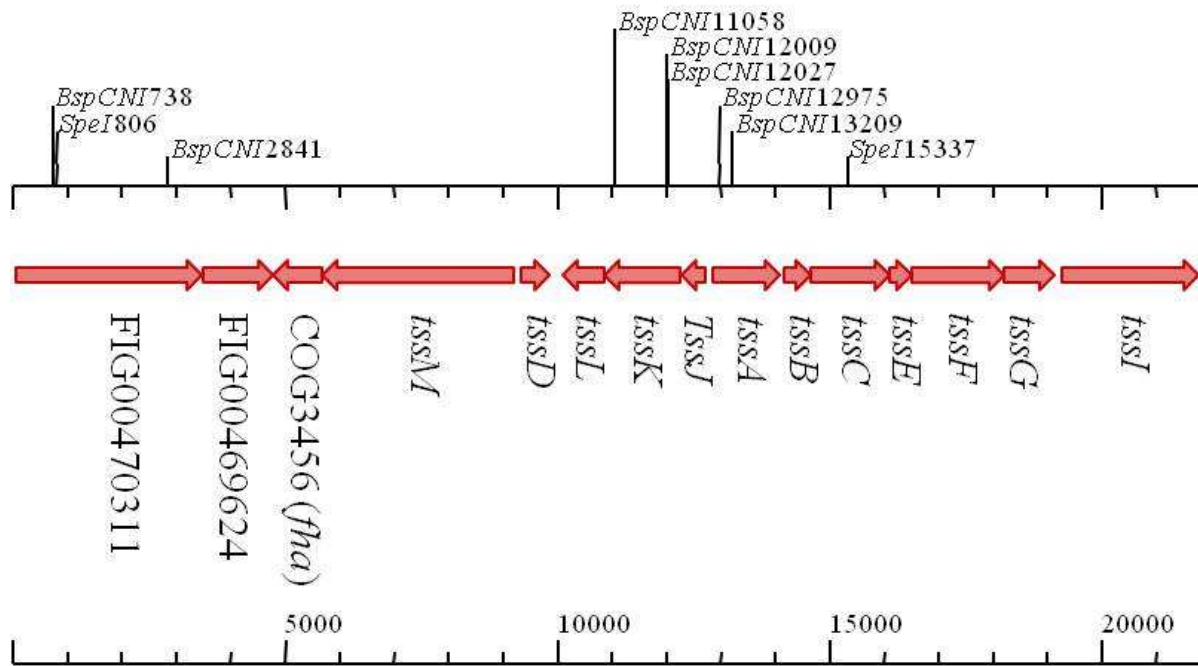
In Cj1 $\Delta$ *tssD*(syn)::kan<sup>R</sup>\_cas, two out of four isolates, isolate 2 and 3, had the kan<sup>R</sup>\_cas inserted in the same orientation as *tssD*. The Cj1 $\Delta$ *tssD*(syn)::kan<sup>R</sup>\_cas isolate 2 was selected for use in subsequent work.

In Cj1 $\Delta$ *tssM*(syn)::kan<sup>R</sup>\_cas, all isolates had the kan<sup>R</sup>\_cas inserted in the same orientation as *tssM*. The Cj1 $\Delta$ *tssM*(syn)::kan<sup>R</sup>\_cas isolate 1 was selected for use in subsequent work.

#### 5.2.4.3 Checking of *tssD* and *tssM* mutants in *Cj1* by Southern Blot

Southern blotting was also used to confirm the identity of *Cj1* $\Delta$ *tssD*(syn)::kan<sup>R</sup>\_cas and *Cj1* $\Delta$ *tssM*(syn)::kan<sup>R</sup>\_cas. The restriction enzymes sites within the T6SS gene cluster of *Cj1* wild-type and the two T6SS mutant strains were predicted. *BspCNI* and *SpeI* were not predicted to cut within the *tssD* or *tssM* or kan<sup>R</sup>\_cas (Figure 5.17 and Table 5.7). The *in silico* analysis indicated that digestion of wild-type DNA with *BspCNI* would generate a fragment of 8217 bp that contained *tssD* and *tssM*. In *Cj1* $\Delta$ *tssD*(syn)::kan<sup>R</sup>\_cas, the fragment containing *tssD*(syn)::kan<sup>R</sup>\_cas would be 9296 bp while in *Cj1* $\Delta$ *tssM*(syn)::kan<sup>R</sup>\_cas, the fragment containing *tssM*(syn)::kan<sup>R</sup>\_cas would be 6293 bp. The difference in the size of the fragments generated between wild-type and T6SS mutants was due to the insertion of kan<sup>R</sup>\_cas that had replaced the target genes.

The digested gDNA of wild-type and T6SS mutants were separated in an agarose gel (Figure 5.18) and Southern blotted using a DIG labelled probe. The probe was generated from *fha*, which is downstream to *tssM*, but within the *BspCNI* cutting sites, as illustrated in Figure 5.19. The results showed that a fragment of approximately 8217 bp in digested wild-type gDNA reacted with the probe (Figure 5.20). The probe also reacted with digested *Cj1* $\Delta$ *tssD*(syn)::kan<sup>R</sup>\_cas and *Cj1* $\Delta$ *tssM*(syn)::kan<sup>R</sup>\_cas gDNA (Figure 5.20). However, the size of the fragment reacting with the probe in *Cj1* $\Delta$ *tssD*(syn)::kan<sup>R</sup>\_cas was approximately 9296 bp while in *Cj1* $\Delta$ *tssM*(syn)::kan<sup>R</sup>\_cas, it was approximately 6293 bp. The results obtained were similar to the *in silico* analysis and thus confirmed the identities of *Cj1* $\Delta$ *tssD*(syn)::kan<sup>R</sup>\_cas and *Cj1* $\Delta$ *tssM*(syn)::kan<sup>R</sup>\_cas.



## Cj1 T6SS locus (21826 bps)

Figure 5.17: Illustration on cutting sites for BspCNI and SpeI along *C. jejuni* strain Cj1 T6SS locus.

Table 5.7: List of fragments generated from *C. jejuni* strain Cj1 wild-type T6SS locus after digestion by restriction enzymes, BspCNI and SpeI, respectively. Fragment in bold will comprise of both *tssD* and *tssM*.

Fragment	<i>BspCNI</i>	<i>SpeI</i>
<b>1</b>	2103 bp (730-2832)	<b>14531 bp (807-15337)</b>
<b>2</b>	<b>8217 bp (2833-11049)</b>	
<b>3</b>	974 bp (11050-12023)	
<b>4</b>	18 bp (12024-12041)	
<b>5</b>	948 bp (12042-12989)	
<b>6</b>	211 bp (12990-13200)	

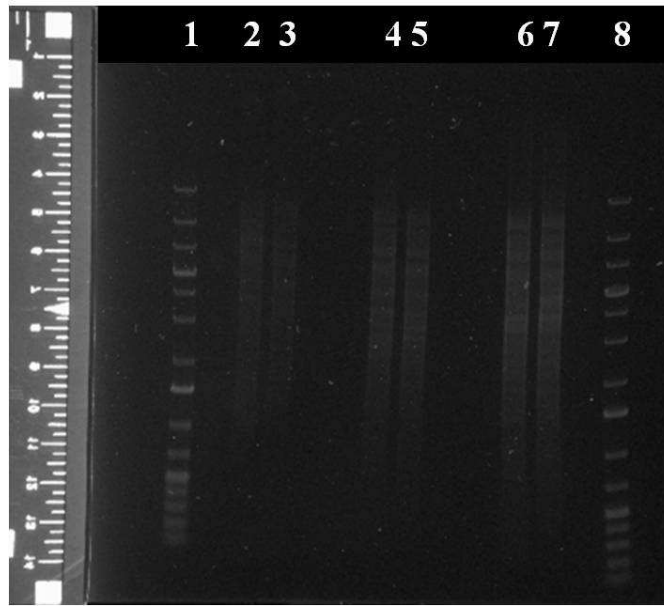
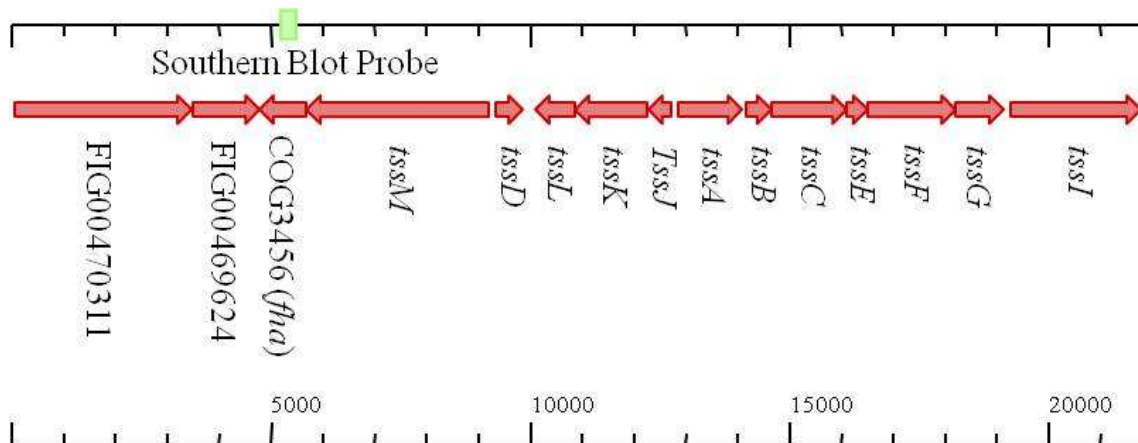


Figure 5.18: Digested of genomic DNA of *C. jejuni* strain Cj1 wild-type and T6SS mutants separated on 0.8% agarose gel and stained with SYBR® Safe stain post-electrophoresis. Lane 1 and 8: GeneRuler™ 1kb plus DNA ladder (Fermentas); Lane 2 and 3: *BspCNI* digested Cj1 wild-type genomic DNA; Lane 4 and 5: *BspCNI* digested Cj1Δ*tssM* genomic DNA; and Lane 6 and 7: *BspCNI* digested Cj1Δ*tssD* genomic DNA.



### Cj1 T6SS locus (21826 bps)

Figure 5.19: Illustration on location of Southern blot probe along *C. jejuni* strain Cj1 T6SS locus (green box).

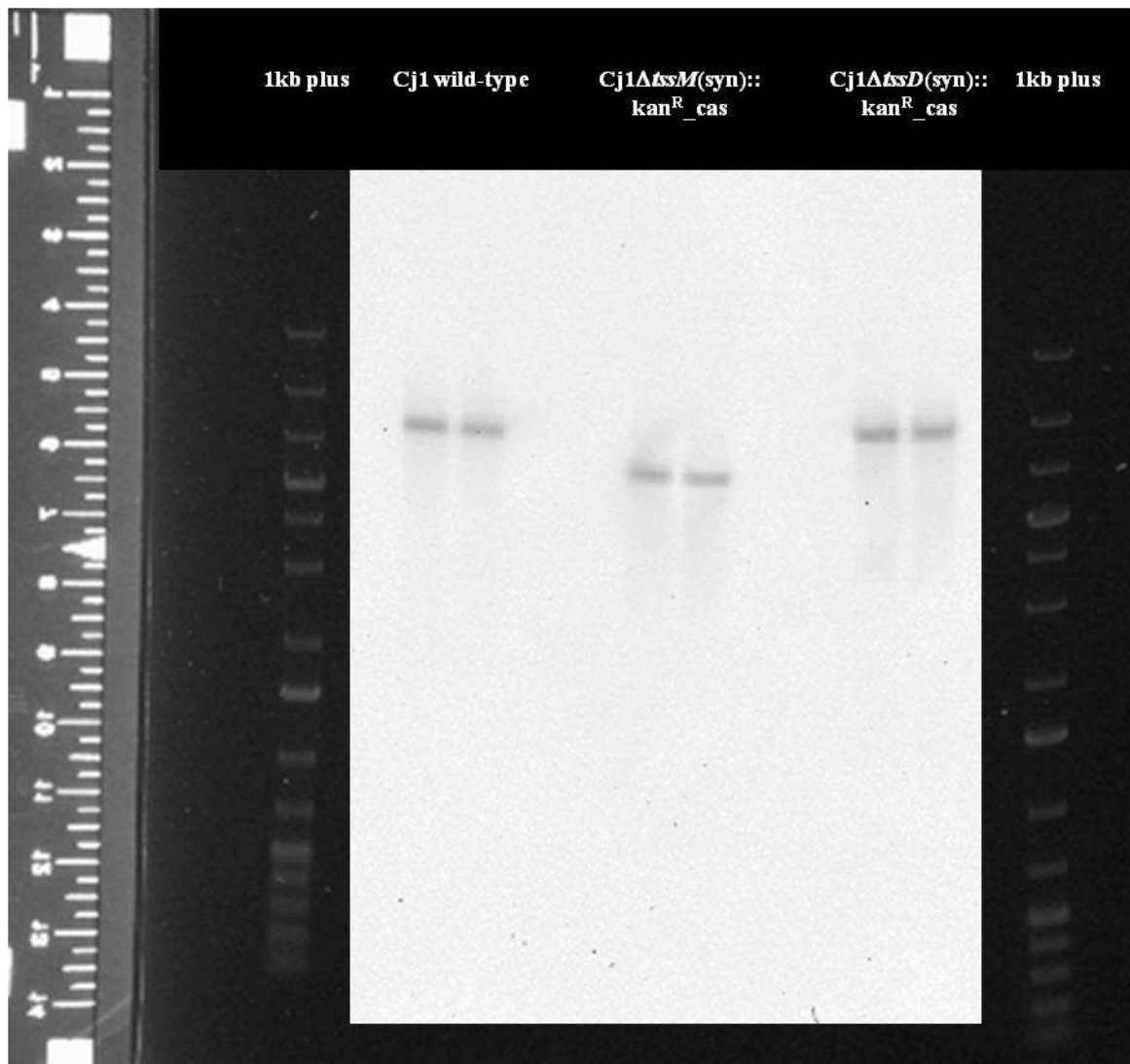


Figure 5.20: Southern blot of *BspCNI* digested genomic DNA of *C. jejuni* strain Cj1 wild-type, *Cj1ΔtssD(syn)::kan<sup>R</sup>\_cas* and *Cj1ΔtssM(syn)::kan<sup>R</sup>\_cas*. DIG-labelled probe hybridised to fragments within the T6SS genes cluster that consist of both *tssD* and *tssM*. The fragment hybridised by the probe in Cj1 wild-type was 8217 bps. The fragment hybridised by the probe in *Cj1ΔtssM(syn)::kan<sup>R</sup>\_cas* was 6293 bps. The fragment hybridised by the probe in *Cj1ΔtssD(syn)::kan<sup>R</sup>\_cas* was 9296 bps.

#### 5.2.4.4 Checking of *tssD* and *tssM* mutants in *Cj1* by sequencing

Genomic DNA of *Cj1* wild-type, *Cj1* $\Delta$ *tssD*(syn)::kan<sup>R</sup>\_cas and *Cj1* $\Delta$ *tssM*(syn)::kan<sup>R</sup>\_cas were sent for whole genome sequencing at UoE - Sequencing Facility. Similarly, sequence data were input into MG-RAST for annotation. Contigs containing genes of interest *tssD* and *tssM* were illustrated in Figure 5.21. Sequence data confirmed deletions of each target gene and the kan<sup>R</sup>\_cas was also inserted in the same transcription orientation as its respective target gene.

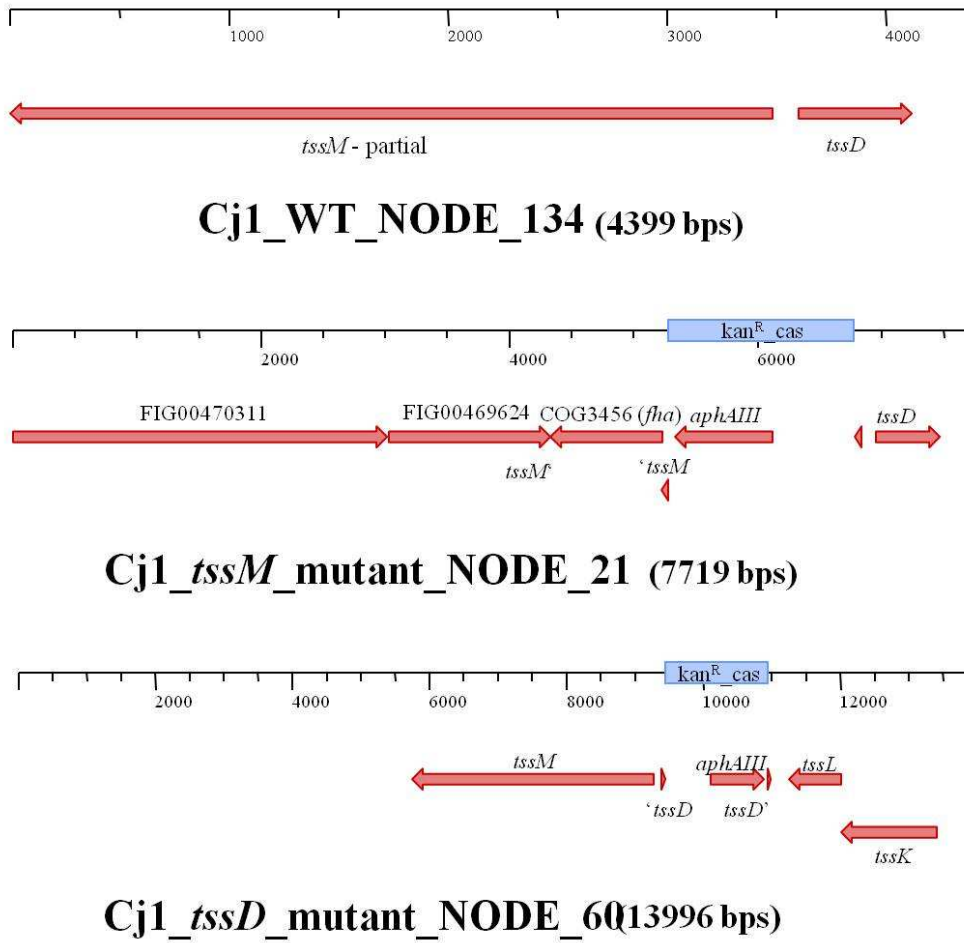


Figure 5.21: Comparison of Sequence data of *C. jejuni* strain Cj1 wild-type, *Cj1ΔtssD(syn)::kan<sup>R</sup>\_cas* and *Cj1ΔtssM(syn)::kan<sup>R</sup>\_cas*. Sequence information confirmed that *kan<sup>R</sup>\_cas* had replaced bulk of the target genes and was inserted in the same transcription orientation as its respective target gene.

#### 5.2.4.5 *Mass spectrometry of Cj1ΔtssD(syn)::kan<sup>R</sup>\_cas and Cj1ΔtssM(syn)::kan<sup>R</sup>\_cas culture supernatants*

The supernatants from 24 hr cultures of Cj1ΔtssD(syn)::kan<sup>R</sup>\_cas and Cj1ΔtssM(syn)::kan<sup>R</sup>\_cas were analysed by mass spectrometry. Similarly, protein precipitated from culture supernatant of the two mutants was run on SDS-PAGE (Figure 5.22).

TssD was not detected in either culture supernatant protein samples. To demonstrate that TssD was being made, but not secreted in Cj1ΔtssM(syn)::kan<sup>R</sup>\_cas, its cellular proteins were analysed for the presence of TssD. A cell pellet lysate of Cj1ΔtssM(syn)::kan<sup>R</sup>\_cas was separated by SDS-PAGE and the gel area between 15-35 kDa excised for analysis by mass spectrometry, Figure 5.23. A cell pellet lysate of Cj1ΔtssD(syn)::kan<sup>R</sup>\_cas, prepared in the same way as Cj1ΔtssM(syn)::kan<sup>R</sup>\_cas, was also analysed.

TssD was only detected in Cj1ΔtssM(syn)::kan<sup>R</sup>\_cas cellular protein fraction with a calling of 8 distinct peptides. The amino acid coverage was 78.3 percentage, Table 5.8. No TssD was detected in Cj1ΔtssD(syn)::kan<sup>R</sup>\_cas cell pellet.

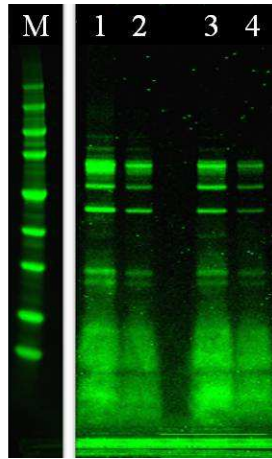


**Figure 5.22:** Analysis of *C. jejuni* strain *Cj1ΔtssD(syn)::kan<sup>R</sup>\_cas* and *Cj1ΔtssM(syn)::kan<sup>R</sup>\_cas* culture supernatant by SDS-PAGE. Proteins from 24 hr old culture media were precipitated using TCA and run on NuPAGE<sup>®</sup> 4-12% Bis-Tris Gel (Novex<sup>®</sup>), at 200 V for 35 minutes in MES buffer. The gel was stained with SimplyBlue<sup>™</sup> SafeStain (Invitrogen) and imaged with Odyssey<sup>®</sup> CLx infra-red imager (LI-COR). Lane M: Perfect Protein<sup>™</sup> Markers, 10-225 kDa (Novagen<sup>®</sup>); Lane 1: 3.75 μg *Cj1ΔtssM(syn)::kan<sup>R</sup>\_cas* culture supernatant TCA protein precipitate; Lane 2: 1.875 μg *Cj1ΔtssM(syn)::kan<sup>R</sup>\_cas* culture supernatant TCA protein precipitate; Lane 3: 3.75 μg *Cj1ΔtssD(syn)::kan<sup>R</sup>\_cas* culture supernatant TCA protein precipitate; and Lane 4: 1.875 μg *Cj1ΔtssD(syn)::kan<sup>R</sup>\_cas* culture supernatant TCA protein precipitate.

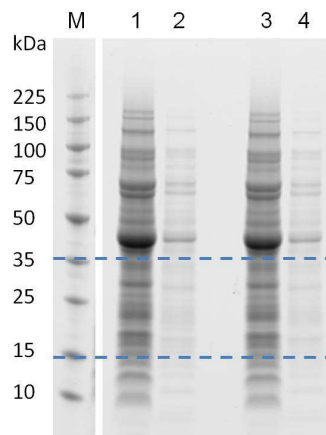


**Figure 5.23:** SDS-PAGE of *C. jejuni* strain *Cj1ΔtssD(syn)::kan<sup>R</sup>\_cas* and *Cj1ΔtssM(syn)::kan<sup>R</sup>\_cas* cell pellet lysates. Cellular protein were separated on NuPAGE<sup>®</sup> 4-12% Bis-Tris Gel (Novex<sup>®</sup>), at 200 V for 35 minutes in MES buffer. The gel was stained with SimplyBlue<sup>™</sup> SafeStain (Invitrogen) and imaged with Odyssey<sup>®</sup> CLx infra-red imager (LI-COR). Lane M: Perfect Protein<sup>™</sup> Markers, 10-225 kDa (Novagen<sup>®</sup>); Lane 1: neat *Cj1ΔtssM(syn)::kan<sup>R</sup>\_cas* cell pellet lysate; Lane 2: 1:10 *Cj1ΔtssM(syn)::kan<sup>R</sup>\_cas* cell pellet lysate; Lane 3: neat *Cj1ΔtssD(syn)::kan<sup>R</sup>\_cas* cell pellet lysate; and Lane 4: 1:10 *Cj1ΔtssD(syn)::kan<sup>R</sup>\_cas* cell pellet lysate. Lane 1 and 3 between the sizes of 15 to 35 kDa were excised for mass spectrometry analysis (between blue dash line).

**Table 5.8:** An extract of mass spectrometry data on the analysis of *C. jejuni* strain Cj1ΔtssM cell pellet lysate.

Group number	Spectra number	Distinct peptides number	Distinct summed MS/MS search score	% amino acid coverage	Mean peptide spectral intensity	Protein molecular weight (da)	Species	Database accession number	Protein Name
31	16	8	115.23	78.3	1.46E+06	18806.6	CAMJU	<a href="#">B5QJ70</a>	Secreted protein Hcp

5.2.4.6 *Checking the expression of other T6SS components by reverse transcription PCR (RT-PCR) in Cj1ΔtssM(syn)::kan<sup>R</sup>\_cas*

Total RNA extracted from 24 hr or 48 hr cultures of Cj1 wild-type or Cj1Δ*tssM*(syn)::kan<sup>R</sup>\_cas were reverse-transcribed and first strand complimentary DNA (cDNA) were analysed by PCR. The cDNA was checked against 6 genes on the T6SS locus; i) FIG00469624, ii) *fha*, iii) *tssM*, iv) *tssD*, v) *tssL*, and vi) *tssI* (Figure 5.24 to 5.29).

The results obtained showed that all genes tested were expressed by Cj1 wild-type under the culturing conditions tested. Similarly, in Cj1Δ*tssM*(syn)::kan<sup>R</sup>\_cas all gene tested with exception of *tssM* were transcribed under the growth conditions tested. This finding indicated that expression of genes along the T6SS genes cluster in Cj1Δ*tssM*(syn)::kan<sup>R</sup>\_cas was not affected by the mutation.

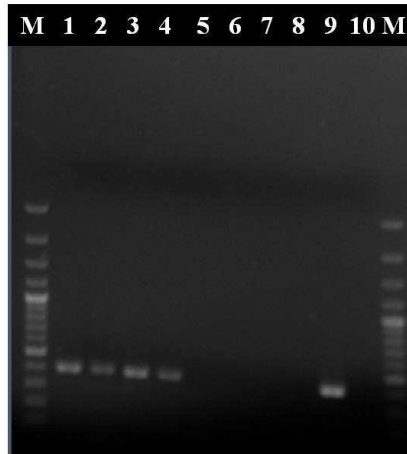


Figure 5.24: Expression of unidentified gene FIG00469624 in opposite transcriptional orientation to *tssM* by RT-PCR. RNA tested were extracted from 24 hr and 48 hr *C. jejuni* strain Cj1 wild-type and *Cj1ΔtssM(syn)::kan<sup>R</sup>\_cas* cultures. Lane M: GeneRuler™ 100 bp plus DNA ladder (Fermentas); Lane 1: Cj1 wild-type cDNA from 24 hr culture; Lane 2: Cj1 wild-type cDNA from 48 hr culture; Lane 3: *Cj1ΔtssM(syn)::kan<sup>R</sup>\_cas* cDNA from 24 hr culture; Lane 4: *Cj1ΔtssM(syn)::kan<sup>R</sup>\_cas* cDNA from 48 hr culture; Lane 5: Cj1 wild-type non-RT control from 24 hr culture; Lane 6: Cj1 wild-type non-RT control from 48 hr culture; Lane 7: *Cj1ΔtssM(syn)::kan<sup>R</sup>\_cas* non-RT control from 24 hr culture; Lane 8: *Cj1ΔtssM(syn)::kan<sup>R</sup>\_cas* non-RT control from 48 hr culture; Lane 9: Cj1 wild-type genomic DNA; and Lane 10: No template control. Transcription of FIG00469624 yielded a product of 386 bps.

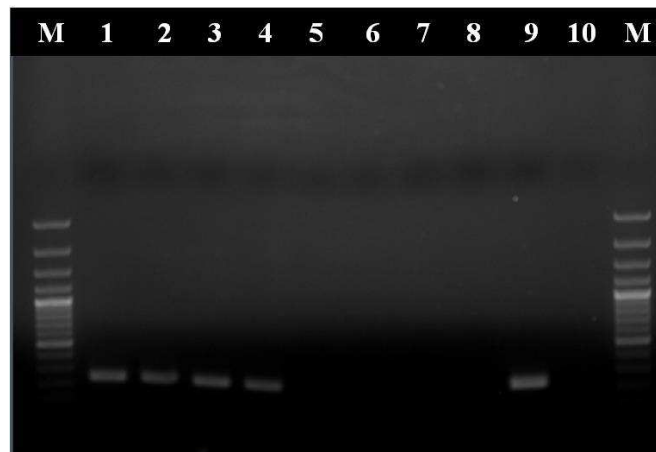


Figure 5.25: Expression of *fha* in same transcriptional orientation as *tssM* by RT-PCR. RNA tested were extracted from 24 hr and 48 hr *C. jejuni* strain Cj1 wild-type and *Cj1ΔtssM(syn)::kan<sup>R</sup>\_cas* cultures. Lane M: GeneRuler™ 100 bp plus DNA ladder (Fermentas); Lane 1: Cj1 wild-type cDNA from 24 hr culture; Lane 2: Cj1 wild-type cDNA from 48 hr culture; Lane 3: *Cj1ΔtssM(syn)::kan<sup>R</sup>\_cas* cDNA from 24 hr culture; Lane 4: *Cj1ΔtssM(syn)::kan<sup>R</sup>\_cas* cDNA from 48 hr culture; Lane 5: Cj1 wild-type non-RT control from 24 hr culture; Lane 6: Cj1 wild-type non-RT control from 48 hr culture; Lane 7: *Cj1ΔtssM(syn)::kan<sup>R</sup>\_cas* non-RT control from 24 hr culture; Lane 8: *Cj1ΔtssM(syn)::kan<sup>R</sup>\_cas* non-RT control from 48 hr culture; Lane 9: Cj1 wild-type genomic DNA; and Lane 10: No template control. Transcription of *fha* yielded a product of 236 bps.

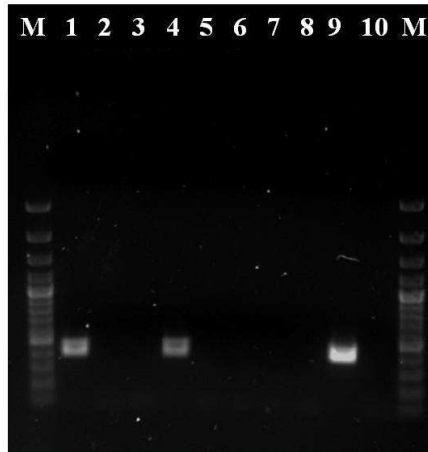


Figure 5.26: Expression of *tssM* by RT-PCR. RNA tested were extracted from 24 hr and 48 hr *C. jejuni* strain Cj1 wild-type and *Cj1ΔtssM(syn)::kan<sup>R</sup>\_cas* cultures. Lane M: GeneRuler™ 100 bp plus DNA ladder (Fermentas); Lane 1: Cj1 wild-type cDNA from 24 hr culture; Lane 2: *Cj1ΔtssM(syn)::kan<sup>R</sup>\_cas* cDNA from 48 hr culture; Lane 3: *Cj1ΔtssM(syn)::kan<sup>R</sup>\_cas* cDNA from 24 hr culture; Lane 4: Cj1 wild-type cDNA from 48 hr culture; Lane 5: Cj1 wild-type non-RT control from 24 hr culture; Lane 6: Cj1 wild-type non-RT control from 48 hr culture; Lane 7: *Cj1ΔtssM(syn)::kan<sup>R</sup>\_cas* non-RT control from 24 hr culture; Lane 8: *Cj1ΔtssM(syn)::kan<sup>R</sup>\_cas* non-RT control from 48 hr culture; Lane 9: Cj1 wild-type genomic DNA; and Lane 10: No template control. Transcription of *tssM* yielded a product of 421 bps.

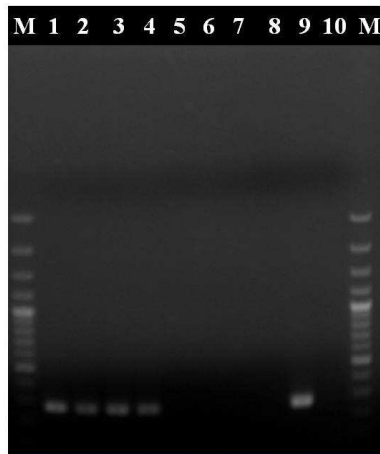


Figure 5.27: Expression of *tssD* in opposite transcriptional orientation to *tssM* by RT-PCR. RNA tested were extracted from 24 hr and 48 hr *C. jejuni* strain Cj1 wild-type and *Cj1ΔtssM(syn)::kan<sup>R</sup>\_cas* cultures. Lane M: GeneRuler™ 100 bp plus DNA ladder (Fermentas); Lane 1: Cj1 wild-type cDNA from 24 hr culture; Lane 2: Cj1 wild-type cDNA from 48 hr culture; Lane 3: *Cj1ΔtssM(syn)::kan<sup>R</sup>\_cas* cDNA from 24 hr culture; Lane 4: *Cj1ΔtssM(syn)::kan<sup>R</sup>\_cas* cDNA from 48 hr culture; Lane 5: Cj1 wild-type non-RT control from 24 hr culture; Lane 6: Cj1 wild-type non-RT control from 48 hr culture; Lane 7: *Cj1ΔtssM(syn)::kan<sup>R</sup>\_cas* non-RT control from 24 hr culture; Lane 8: *Cj1ΔtssM(syn)::kan<sup>R</sup>\_cas* non-RT control from 48 hr culture; Lane 9: Cj1 wild-type genomic DNA; and Lane 10: No template control. Transcription of *tssD* yielded a product of 273 bps.

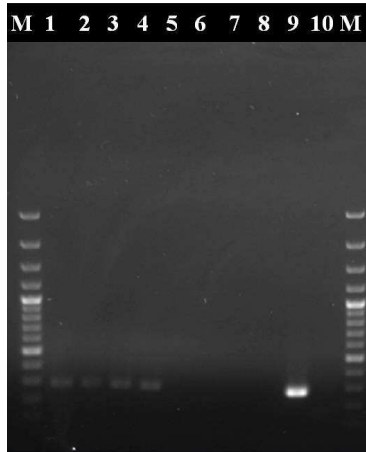


Figure 5.28: Expression of *tssL* in same transcriptional orientation as *tssM* by RT-PCR. RNA tested were extracted from 24 hr and 48 hr *C. jejuni* strain Cj1 wild-type and *Cj1ΔtssM(syn)::kan<sup>R</sup>\_cas* cultures. Lane M: GeneRuler™ 100 bp plus DNA ladder (Fermentas); Lane 1: Cj1 wild-type cDNA from 24 hr culture; Lane 2: Cj1 wild-type cDNA from 48 hr culture; Lane 3: *Cj1ΔtssM(syn)::kan<sup>R</sup>\_cas* cDNA from 24 hr culture; Lane 4: *Cj1ΔtssM(syn)::kan<sup>R</sup>\_cas* cDNA from 48 hr culture; Lane 5: Cj1 wild-type non-RT control from 24 hr culture; Lane 6: Cj1 wild-type non-RT control from 48 hr culture; Lane 7: *Cj1ΔtssM(syn)::kan<sup>R</sup>\_cas* non-RT control from 24 hr culture; Lane 8: *Cj1ΔtssM(syn)::kan<sup>R</sup>\_cas* non-RT control from 48 hr culture; Lane 9: Cj1 wild-type genomic DNA; and Lane 10: No template control. Transcription of *tssL* yielded a product of 276 bps.

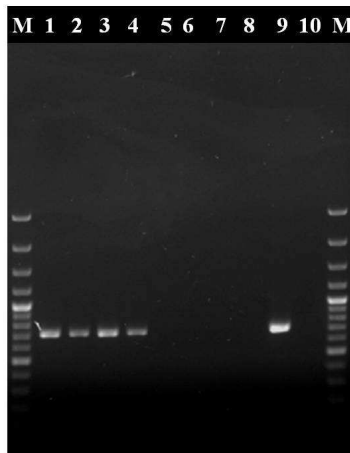


Figure 5.29: Expression of *tssI* in opposite transcriptional orientation to *tssM* by RT-PCR. RNA tested were extracted from 24 hr and 48 hr *C. jejuni* strain Cj1 wild-type and *Cj1ΔtssM(syn)::kan<sup>R</sup>\_cas* cultures. Lane M: GeneRuler™ 100 bp plus DNA ladder (Fermentas); Lane 1: Cj1 wild-type cDNA from 24 hr culture; Lane 2: Cj1 wild-type cDNA from 48 hr culture; Lane 3: *Cj1ΔtssM(syn)::kan<sup>R</sup>\_cas* cDNA from 24 hr culture; Lane 4: *Cj1ΔtssM(syn)::kan<sup>R</sup>\_cas* cDNA from 48 hr culture; Lane 5: Cj1 wild-type non-RT control from 24 hr culture; Lane 6: Cj1 wild-type non-RT control from 48 hr culture; Lane 7: *Cj1ΔtssM(syn)::kan<sup>R</sup>\_cas* non-RT control from 24 hr culture; Lane 8: *Cj1ΔtssM(syn)::kan<sup>R</sup>\_cas* non-RT control from 48 hr culture; Lane 9: Cj1 wild-type genomic DNA; and Lane 10: No template control. Transcription of *tssI* yielded a product of 701 bps.

### 5.3 Discussion

The T6SS is the most recently identified secretion system (Coulthurst, 2013). An analysis of 506 available genome sequences identified 176 T6SS genes clusters distributed across 92 different bacteria (Boyer et al., 2009). It is commonly found in Proteobacteria except for the epsilon sub-group (Coulthurst, 2013). Among the different bacteria harbouring the T6SS, about a third of them had been found to have more than one T6SS gene cluster, ranging from two to six clusters (Boyer et al., 2009). It has been reported that the T6SS is involved in the interactions of its parent organism with either eukaryotic cells, other prokaryotic cells or both (Coulthurst, 2013). The interaction with eukaryotic cells could help the bacteria to establish an infection in the host organism, for example, in the case of *V. cholerae* (Ma and Mekalanos, 2010). On the other hand, interactions with other prokaryotic cells could help the bacteria to establish its population within a mixed species environment, such as biofilm (Filloux, 2013). The T6SS system had also been found in two strains of *C. jejuni*, ATCC 43431 and an intestinal isolate 108 (Bleumink-Pluym et al., 2013; Lertpiriyapong et al., 2012). Both strains have been reported to have only one cluster of the T6SS genes (Bleumink-Pluym et al., 2013; Lertpiriyapong et al., 2012). Hence, it was of interest to find out if the patients isolates obtained in Thailand carry any T6SS gene clusters.

Among the 5 isolates screened by genome sequencing, only one of them, strain Cj1, contains a cluster of genes for T6SS components. The putative T6SS genes cluster in Cj1 had only 12 out of 13 T6SS core COGs. COG0542 corresponding to *tssH* (also known as *clpV*) is absent. This is consistent with the T6SS genes clusters reported in ATCC 43431 and 108, as both strains also lacks *tssH* (Bleumink-Pluym et al., 2013; Lertpiriyapong et al., 2012). The

arrangement of the genes within the cluster of Cj1 is similar to that of ATCC 43431 (Lertpiriyapong et al., 2012).

The missing component in all three *C. jejuni* T6SS, TssH, belongs to a sub-type of the ATPase AAA+ family - suggested as an energy provider for the secretion system (Schlieker et al., 2005). TssH had also been shown to interact with the contractile sheath-like tubular structure formed by two other core components of the T6SS, TssB and TssC (also known as VipA and VipB, respectively). TssH provides the energy required for the disassembly of the TssB/TssC tubules (Kapitein and Mogk, 2013). The disassembled TssB and TssC return to the cytosol pool and new tubules can be formed (Basler et al., 2012; Bönemann et al., 2009). It has been reported that TssH is not required for assembly of the T6SS (Zheng et al., 2011). Hence, the TssB/TssC tubule could still be assembled in the absence of TssH. However, after the first contraction, the tubule needs to be disassembled and reassembled before the next contraction can occur. Without the aid of TssH in its disassembly, the TssB/TssC tubules could only deliver its "goods" once and that could potentially lessen the efficacy of T6SS (Zheng et al., 2011).

A point to note was that MG-RAST annotation picked up another protein belonging to the ATPase AAA+ family (ClpB) in a different Cj1 contig (scf\_30956\_6\_contig\_1). It is possible that ClpB complements the absence of TssH in the T6SS. In *Rhizobium leguminosarum* *tssH* was absent from the T6SS (previously known as *imp*) cluster. In this case, it was suggested that the T6SS utilised a protein from *clpV* gene found in other part of the genome (Filloux et al., 2008).

Although TssH is absent in both reported strains it has been demonstrated that the T6SS in them were functional (Bleumink-Pluym et al., 2013; Lertpiriyapong et al., 2012). Functionalities of the systems were marked by the secretion of TssD into the culture supernatants (Bleumink-Pluym et al., 2013; Lertpiriyapong et al., 2012; Pukatzki et al., 2007).

A hallmark indicator for a functional T6SS in bacteria is the presence of TssD in culture media (Pukatzki et al., 2007). TssD was detected in the culture supernatant of Cj1 cells grown in MHB for approximately 24 hr at 37°C under microaerophilic conditions. Successful detection of TssD in the culture supernatant suggested that T6SS in Cj1 is functional. This finding coincided with the two other *C. jejuni* strains ATCC 43431 and 108 (Bleumink-Pluym et al., 2013; Lertpiriyapong et al., 2012).

It had been reported that secretion of TssD in *C. jejuni* strain 108 was evident under most growth conditions (Bleumink-Pluym et al., 2013). This differs from other bacterial species where secretion of TssD was dependent on environmental cues (Bernard et al., 2010). In this study TssD was detected in culture supernatant when Cj1 was grown for 24 hr at 37°C in broth media. Previous work by a visiting researcher had shown that *tssD* and *tssI* were expressed when Cj1 was grown in broth at 37°C but not when the cells were grown at 42°C. This information suggested that expression of T6SS in Cj1 might be temperature dependent. All subsequent assays conducted on Cj1 were performed using broth cultures grown at 37°C.

Currently, there are two main strategies for making mutants in *Campylobacter*: insertion or insertion-deletion approach. The insertion approach disrupts the reading frame of the target gene by inserting an antibiotic resistance cassette (Coward et al., 2006; Labigne-Roussel et al., 1988). As for insertion-deletion approach, either all or most of the target gene is deleted and replaced by an antibiotic cassette (Coward et al., 2006; Hansen et al., 2007; Weerakoon and Olson, 2008). To date, two antibiotic resistance cassettes are commonly used in *Campylobacter* cloning work. They are the kanamycin resistance cassette and the chloramphenicol resistance cassette. The kanamycin resistance cassette was derived from *C. coli* plasmid pIP1433 (Labigne-Roussel et al., 1987), while the chloramphenicol cassette was from *C. coli* plasmid pNR9589 (Wang and Taylor, 1990). The availability of two different cassettes provides the flexibility of mutating two different genes within the same strain (Yao et al., 1993).

In this study, two components of T6SS, *tssD* and *tssM* were selected for disruption. The *tssD* gene was suggested to be involved in the formation of the needle-like structure of the secretion system (Zhou et al., 2012). It had also been suggested to play a role modulating host cell cytokine production or cytoskeleton rearrangement (Zhou et al., 2012). *tssM* consisting of trans-membrane domains (Filloux et al., 2008) was thought to play a role in anchoring the T6SS assembly to the cell membrane (Coulthurst, 2013; Lertpiriyapong et al., 2012). The deletion of the two selected genes might result in disruption of T6SS functionality in Cj1 and thus the mutants could be used to better understand the role played by T6SS in this strain.

The strategy used for constructing the *tssD* and *tssM* mutants is the insertion-deletion approach. In these mutants 50 bps of the target gene at 5' end and 3' end was retained, while the intervening region was deleted and replaced by a kan<sup>R</sup>\_cas. The retention of the 50 bps of the target gene at each end should ensure that expression of neighbouring genes is not affected by the mutation.

Transcriptional orientation of kan<sup>R</sup>\_cas was also checked. It was reported that when the inserted antibiotic cassette was in a different orientation from the target gene it might result in a polar effect (van Vliet et al., 1998). Both the Cj1Δ*tssD*(syn)::kan<sup>R</sup>\_cas and Cj1Δ*tssM*(syn)::kan<sup>R</sup>\_cas mutants used in subsequent work have the cassette inserted in the same orientation as its target gene.

In most published reports, functionality of T6SS was tested by Western blotting to determine the presence of TssD in culture supernatant. However, due to the lack of antibodies against Cj1 TssD functionality of T6SS in Cj1Δ*tssD*(syn)::kan<sup>R</sup>\_cas and Cj1Δ*tssM*(syn)::kan<sup>R</sup>\_cas mutants were determined using mass spectrometry. Both culture supernatant and cell pellet lysate (partial, 15-35 kDa) from the two mutants were tested. TssD was only detected in the cell lysate of Cj1Δ*tssM*(syn)::kan<sup>R</sup>\_cas. The results showed that the disruption of *tssD* in Cj1Δ*tssD*(syn)::kan<sup>R</sup>\_cas had resulted in no production of TssD. The production of TssD in Cj1Δ*tssM*(syn)::kan<sup>R</sup>\_cas was not affected by the disruption of *tssM*. However, the protein could not be secreted into the culture supernatant. This indicates that the disruption of *tssM* had affected the secretion ability of the T6SS. This finding supports the suggestion that TssM anchors the apparatus of T6SS onto the membrane in order to facilitate secretion

(Coulthurst, 2013; Lertpiriyapong et al., 2012). It has also been reported that mutation of *tssM* prevented secretion of TssD in other bacterial species (Pukatzki et al., 2006; Wu et al., 2008; Zheng and Leung, 2007).

Transcriptomics analysis of the *tssM* mutant, Cj1Δ*tssM*(syn)::kan<sup>R</sup>\_cas shown that genes upstream and downstream of *tssM*, in both transcriptional orientations, were not affected by the insertion-deletion mutation. Hence, any phenotypic differences observed between Cj1 wild-type and Cj1Δ*tssM*(syn)::kan<sup>R</sup>\_cas are unlikely to be due to polar effects. The Cj1 wild-type, Cj1Δ*tssD*(syn)::kan<sup>R</sup>\_cas and Cj1Δ*tssM*(syn)::kan<sup>R</sup>\_cas mutants were tested in various infection assays and results obtained are presented in Chapter 6.

Two T6SS mutants were made in this study, however, no complemented strains were made. It is important to construct complemented strains for each mutant made. The mutant could be complemented by insertion of a copy of the wild-type gene into the mutant. When the complemented strain exhibits phenotypes similar to wild-type strain it confirms that the different phenotypes observed in mutant strains were a direct effect of the disrupted gene and not due to other factors, such as polar effects.

Several shuttle vectors had been made to incorporate either one of the antibiotic resistance cassettes into *Campylobacter* (Labigne-Roussel et al., 1987; Yao et al., 1993). These shuttle plasmids could also be used for gene delivery, such as reporter genes (e.g. antibiotic resistance or fluorescence reporter genes) or wild-type genes in complementation analysis (Malik-Kale et al., 2007; Miller et al., 2000; Mixter et al., 2003; Yao et al., 1993). For

complementation, the wild type gene together with its native promoter was amplified by PCR and inserted into a shuttle vector; downstream of an antibiotic resistance cassette (Fields and Thompson, 2008; Malik-Kale et al., 2007).

It has been reported that several shuttle vectors could not be introduced into various *C. jejuni* strains which includes the typed strain Cj11168 (Karlyshev and Wren, 2005). Besides using shuttle vectors, genes delivery into *Campylobacter* could also be done via an insertional system (Karlyshev and Wren, 2005; Kim et al., 2008). When it is used to complement a mutant, the wild-type gene, together with its native promoter, is cloned into a suicide vector. The suicide vector consists of a chromosomal sequence that will be directed towards either rRNA genes (Karlyshev and Wren, 2005) or a pseudogene, cj0046 (Kim et al., 2008). The complement suicide vectors carry an antibiotic resistance cassette that is different from the one used in the making of the mutant (Yao et al., 1993). The wild-type target gene would then be incorporated into the bacterial chromosome at the directed sites: rRNA genes or cj0046. An insertional system has also been used to deliver the fluorescence reporter gene, *gfp*, into *C. jejuni* rRNA genes (Karlyshev and Wren, 2005).

The *tssD* and *tssM* mutants made in this study used a kanamycin resistance cassette as the marker. In order to complement the two mutants, either the shuttle vector or the insertional system approach could be applied. For both approaches chloramphenicol resistance cassette would be the alternative marker used. However, for the shuttle vector approach, it is dependent on shuttle vectors being introduced into Cj1. In terms of the insertional system, the genome analysis of Cj1 showed that it has the pseudogene cj0046, hence complementation into this pseudogene, would be possible.

## **Chapter 6: Role of T6SS in *C. jejuni* strain Cj1**

## 6.1 Introduction

### 6.1.1 Role of T6SS

There have been numerous reports on the different roles played by T6SS in various bacteria, which mainly classify it into two main categories. One was a mechanism targeting a eukaryotic host, while the other involved a mechanism against other prokaryotic cells. An anti-eukaryotic role has been reported in various bacteria, for example, *V. cholerae* and *Pseudomonas aeruginosa* (Pukatzki et al., 2006; Purcell and Shuman, 1998; Sana et al., 2012; Schwarz et al., 2010). An anti-prokaryotic role has been demonstrated in *Burkholderia thailandensis*, *P. aeruginosa* and *V. cholerae* (MacIntyre et al., 2010; Sana et al., 2012; Schwarz et al., 2010). The role of the T6SS in both scenarios is to ensure bacterial survival in the host or in the environment. The T6SS in *V. anguillarum* has also been demonstrated to be involved in modulating general stress response regulators (Weber et al., 2009).

The T6SS in *C. jejuni* was previously reported to be involved in bacterial survival in deoxycholic acid and the adhesion and invasion of epithelial and macrophage cells (Lertpiriyapong et al., 2012). It has also been shown to have cytotoxic effects towards red blood cells, in a contact dependent manner and in the absence of capsule (Bleumink-Pluym et al., 2013).

### 6.1.2 Aim of study

The aim of this study was to determine involvement of T6SS in *in vitro* cell growth and eukaryotic host infection.

## 6.2 Results

### 6.2.1 Growth rate of *C. jejuni* strain Cj1 wild-type and its T6SS mutants

Cj1 wild-type, Cj1 $\Delta$ *tssD*(syn)::kan<sup>R</sup>\_cas and Cj1 $\Delta$ *tssM*(syn)::kan<sup>R</sup>\_cas were cultured in broth at 37 °C under microaerophilic conditions. The starter cultures were prepared to OD<sub>590</sub> of approximately 0.1. The OD<sub>590</sub> of the cultures were monitored over 120 hours. Figure 6.1 shows mean OD<sub>590</sub> readings of wild-type and T6SS mutants strains from four independent experiments and the standard error of the mean (SEM).

Growth of both T6SS mutants was slower as compared to wild-type. The cell density obtained by Cj1 $\Delta$ *tssD*(syn)::kan<sup>R</sup>\_cas by stationary phase was significantly lower than wild-type. However, mean cell optical density of Cj1 $\Delta$ *tssM*(syn)::kan<sup>R</sup>\_cas after 48 hr, although lower than wild-type, was not significantly different.

**Growth curve of *C. jejuni* Cj1 wild-type, Cj1 $\Delta$ tssD(syn)::kan<sup>R</sup>\_cas and Cj1 $\Delta$ tssM(syn)::kan<sup>R</sup>\_cas in Muller Hinton broth, incubated at 37 °C in static**

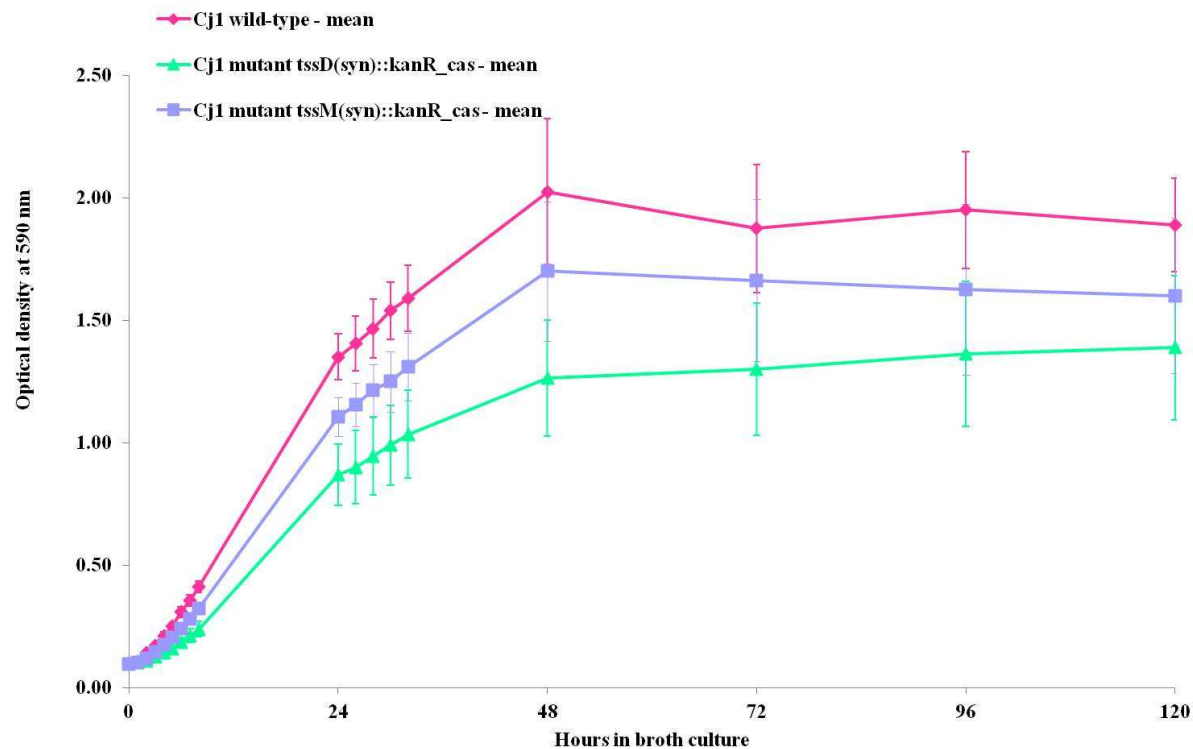


**Figure 6.1:** Growth curve of *C. jejuni* strain Cj1 wild-type, Cj1 $\Delta$ tssD(syn)::kanR\_cas and Cj1 $\Delta$ tssM(syn)::kanR\_cas. Cell were inoculated into 50 ml of broth to OD590 of approximately 0.1. The cultures were incubated at 37 °C under microaerophilic conditions for up to 120 hr. OD590 of the three strains were plotted against time. Each strain was plotted based on mean values. Error bars represent SEM. Mean values and SEM were calculated from four individual experiments. Growth curve of Cj1 wild-type is shown by pink line with diamond markers. Growth curve of Cj1 $\Delta$ tssD(syn)::kanR\_cas is shown by green line with triangle markers. Growth curve of Cj1 $\Delta$ tssM(syn)::kanR\_cas is shown by lavender line with square markers.

## 6.2.2 The adhesion and invasion of macrophages by *C. jejuni* strain Cj1 wild-type and T6SS mutants

Mouse macrophage-like cells RAW264.7 were infected with Cj1 wild-type Cj1 $\Delta$ *tssD*(syn)::kan<sup>R</sup>\_cas and Cj1 $\Delta$ *tssM*(syn)::kan<sup>R</sup>\_cas at MOI of approximately 10. The data was analysed in GraphPad Prism version 6. A two-way ANOVA using Fisher's LSD test was performed at a 90% confidence interval for comparison of Cj1 wild-type with Cj1 $\Delta$ *tssD*(syn)::kan<sup>R</sup>\_cas and Cj1 $\Delta$ *tssM*(syn)::kan<sup>R</sup>\_cas respectively. Figure 6.2 shows the percentage of bacterial cells that adhered to macrophage cells or that invaded macrophage cells. The data presented were mean values from 3 individual experiments and SEM.

The percentage of bacterial cells adhering to and/or invading macrophage cells was very low - less than 1 % for wild-type and T6SS mutants. The percentage of wild-type cells adhering to macrophage cells was 0.70%, and 0.38% had invaded them. In comparison, Cj1 $\Delta$ *tssD*(syn)::kan<sup>R</sup>\_cas achieved 0.93% adherence and 0.48% invasion of macrophage cells, while Cj1 $\Delta$ *tssM*(syn)::kan<sup>R</sup>\_cas obtained 0.94% adherence and 0.54% invasion. The mean percentage of Cj1 $\Delta$ *tssD*(syn)::kan<sup>R</sup>\_cas and Cj1 $\Delta$ *tssM*(syn)::kan<sup>R</sup>\_cas that adhered to macrophage cells was significantly higher than that of Cj1 wild-type (P-value = 0.0088 and 0.0071, respectively). Mean percentage of Cj1 $\Delta$ *tssM*(syn)::kan<sup>R</sup>\_cas that had invaded macrophage cells was also significantly higher compared to Cj1 wild-type with P-value = 0.0684.

**Percentage of *C. jejuni* strain Cj1 wild-type, Cj1 $\Delta$ tssD(syn)::kan<sup>R</sup>\_cas and Cj1 $\Delta$ tssM(syn)::kan<sup>R</sup>\_cas cells adhered to or invaded mouse macrophage-like cells RAW264.7**

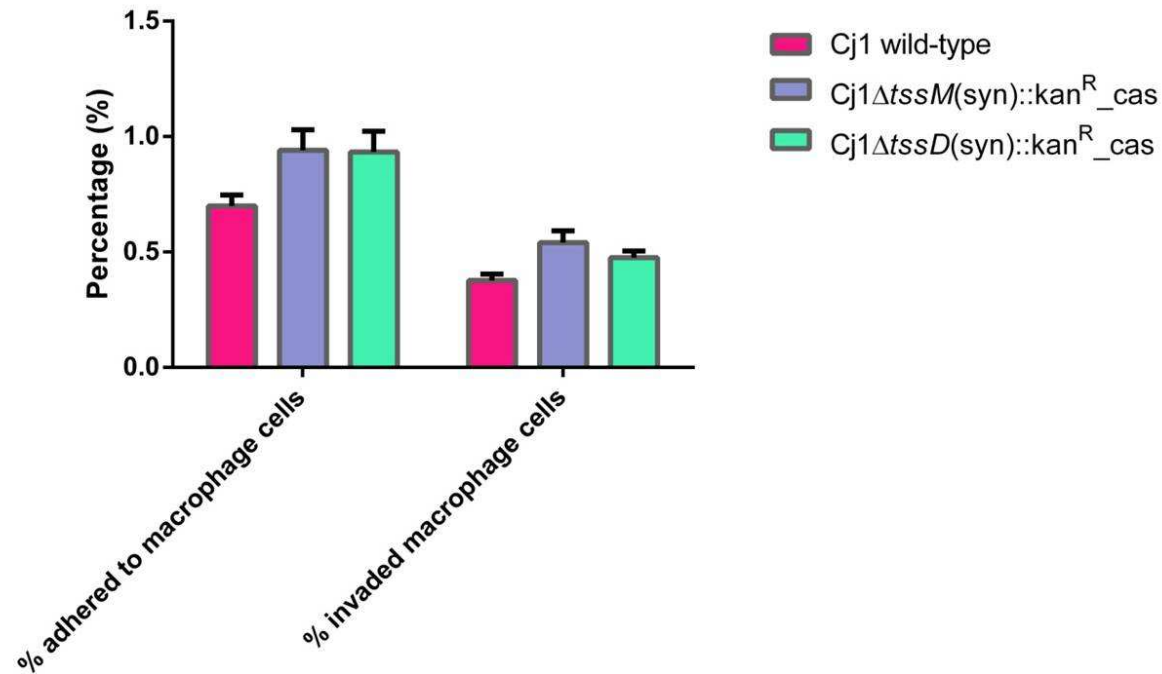


**Figure 6.2:** Percentage of *C. jejuni* strain Cj1 wild-type, Cj1 $\Delta$ tssD(syn)::kan<sub>R\_cas</sub> and Cj1 $\Delta$ tssM(syn)::kan<sub>R\_cas</sub> adhered to or invaded mouse macrophage cells RAW264.7. Cj1 wild-type, Cj1 $\Delta$ tssD(syn)::kan<sub>R\_cas</sub> and Cj1 $\Delta$ tssM(syn)::kan<sub>R\_cas</sub> used were cultured in MHB at 37 °C for 24 hr. The MOI for the assay was approximately 10. Percentage of bacterial cells adhered to macrophages were enumerated at 4 hpi. Percentage of bacterial cells that had invaded macrophages were enumerated after additional 2 hr of gentamicin treatment, at 6 hpi. The graph was plotted with mean and SEM values from three independent experiments, each with 3 replicates. Error bars represent SEM. Mean percentage of Cj1 wild-type: i) adhered to macrophage cells was 0.70 % (SEM = 0.047) and ii) invaded macrophage cells was 0.38 % (SEM = 0.027). Mean percentage of Cj1 $\Delta$ tssD(syn)::kan<sub>R\_cas</sub>: i) adhered to macrophage cells was 0.93 % (SEM = 0.090) and ii) invaded macrophage cells was 0.48 % (SEM = 0.028). Mean percentage of Cj1 $\Delta$ tssM(syn)::kan<sub>R\_cas</sub>: i) adhered to macrophage cells was 0.94 % (SEM = 0.090) and ii) invaded macrophage cells was 0.54 % (SEM = 0.051).

### 6.2.3 Infection of 28 hpf ZFE with Cj1 wild-type and T6SS mutants

ZFE were challenged with Cj1 wild-type, Cj1 $\Delta$ *tssD*(syn)::kan<sup>R</sup>\_cas and Cj1 $\Delta$ *tssM*(syn)::kan<sup>R</sup>\_cas at embryo stages between 28 to 32 hpf. The challenge doses were between 1500 to 7000 cfu per embryo. In each experiment the number of ZFE challenged by each strain was 20. The data was analysed in GraphPad Prism version 6. One-way ANOVA using Fisher's LSD test was performed with a 90% confidence interval for comparison of Cj1 wild-type with Cj1 $\Delta$ *tssD*(syn)::kan<sup>R</sup>\_cas and Cj1 $\Delta$ *tssM*(syn)::kan<sup>R</sup>\_cas respectively. Figure 6.3 shows the survival chart of infected embryos at 24 hpi. The data presented were mean values from 6 individual experiments and SEM.

Results obtained showed that 39% of ZFE infected with Cj1 wild-type survived at 24 hpi, with SEM value of 3.005. The survival percentage of Cj1 $\Delta$ *tssD*(syn)::kan<sup>R</sup>\_cas was very similar to Cj1 wild-type at 38 % with SEM value of 6.280. ZFE infected with Cj1 $\Delta$ *tssM*(syn)::kan<sup>R</sup>\_cas had the highest survival percentage of 54 % with SEM value of 6.760. The analysis showed that there was no significant differences between Cj1 wild-type and Cj1 $\Delta$ *tssD*(syn)::kan<sup>R</sup>\_cas. However, there was a significant difference between the survival percentage of Cj1 wild-type and Cj1 $\Delta$ *tssM*(syn)::kan<sup>R</sup>\_cas (P-value = 0.0952).

**Survival Chart at 24 hours post-infection**  
***C. jejuni* strain Cj1 wild-type, Cj1 $\Delta$ tssD(syn)::kan<sup>R</sup>\_cas and**  
**Cj1 $\Delta$ tssM(syn)::kan<sup>R</sup>\_cas were injected into yolk sac of *D. rerio* embryos at stages**  
**between 28-32 hours post-fertilisation**

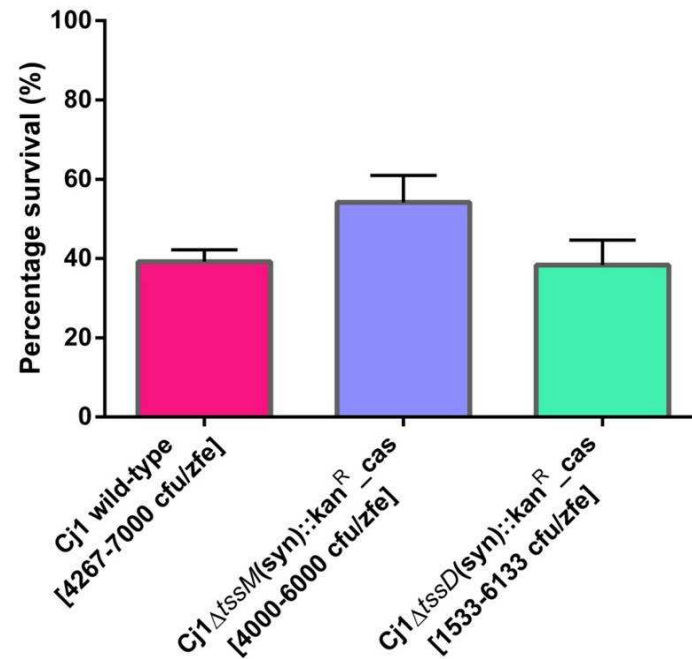


**Figure 6.3:** Survival chart of ZFE infected with *C. jejuni* strain Cj1 wild-type, Cj1 $\Delta$ tssD(syn)::kan<sup>R</sup>\_cas and Cj1 $\Delta$ tssM(syn)::kan<sup>R</sup>\_cas at 24 hpi. ZFE at stages between 28-32 hpf were used. Cj1 wild-type, Cj1 $\Delta$ tssD(syn)::kan<sup>R</sup>\_cas and Cj1 $\Delta$ tssM(syn)::kan<sup>R</sup>\_cas used were cultured in MHB at 37 °C for 24 hr. The bacterial cells were delivered into embryo's yolk-sac through micro-injection. The infection dose ranged between 1500 - 7000 cfu per embryo. The graph was plotted with mean values from six independent experiments. Error represents SEM. Mean survival rate Cj1 wild-type set was 39 % (SEM = 3.005). Mean survival rate Cj1 $\Delta$ tssD(syn)::kan<sup>R</sup>\_cas set was 38 % (SEM = 6.280). Mean survival rate Cj1 $\Delta$ tssM(syn)::kan<sup>R</sup>\_cas set was 54 % (SEM = 6.760).

#### 6.2.4 Infection of newborn piglets with Cj1 wild-type and T6SS mutants

This study was performed at the Institute of Infection, Immunity and Inflammation at University of Glasgow using *C. jejuni* Cj1 wild-type, Cj1 $\Delta$ tsd(syn)::kan<sup>R</sup>\_cas and Cj1 $\Delta$ tsm(syn)::kan<sup>R</sup>\_cas. Competitive index challenge was performed on two groups of animals - each consisting of 9 piglets. In each group, the piglets were inoculated with equal amount of wild-type and a mutant. Faecal samples were collected daily up to Day 5 post-infection. Faecal samples were quantified for wild-type and respective T6SS mutant by culturing. No bacterial cells were recovered by culture from faecal samples collected from Day 1 to 4. Bacterial counts recovered from Day 5 faecal samples are presented in Figure 6.4.

On Day 5 in Group A, Cj1 $\Delta$ tsm(syn)::kan<sup>R</sup>\_cas faecal count was at Log<sub>10</sub>(5.46), which was lower than the inoculated dose of Log<sub>10</sub>(8.4). It was also lower compared to the Cj1 wild-type count of Log<sub>10</sub>(10.13). In fact, Cj1 wild-type count had increased slightly on Day 5 from Log<sub>10</sub>(8.8) to Log<sub>10</sub>(10.13). In Group B, bacterial counts recovered from both Cj1 wild-type and Cj1 $\Delta$ tsd(syn)::kan<sup>R</sup>\_cas were comparable at Log<sub>10</sub>(10.371) and Log<sub>10</sub>(10.246) respectively. The counts for both were higher than the inoculated dose as Cj1 $\Delta$ tsd(syn)::kan<sup>R</sup>\_cas was inoculated at Log<sub>10</sub>(8.5).

Newborn piglets competitive index challenge using *C. jejuni* strain Cj1 wild-type, Cj1 $\Delta$ tssD(syn)::kan<sup>R</sup>\_cas and Cj1 $\Delta$ tssM(syn)::kan<sup>R</sup>\_cas  
 Incoculation dose on Day 0 and bacterial count recovered from faecal samples collected on Day 5 post-infection

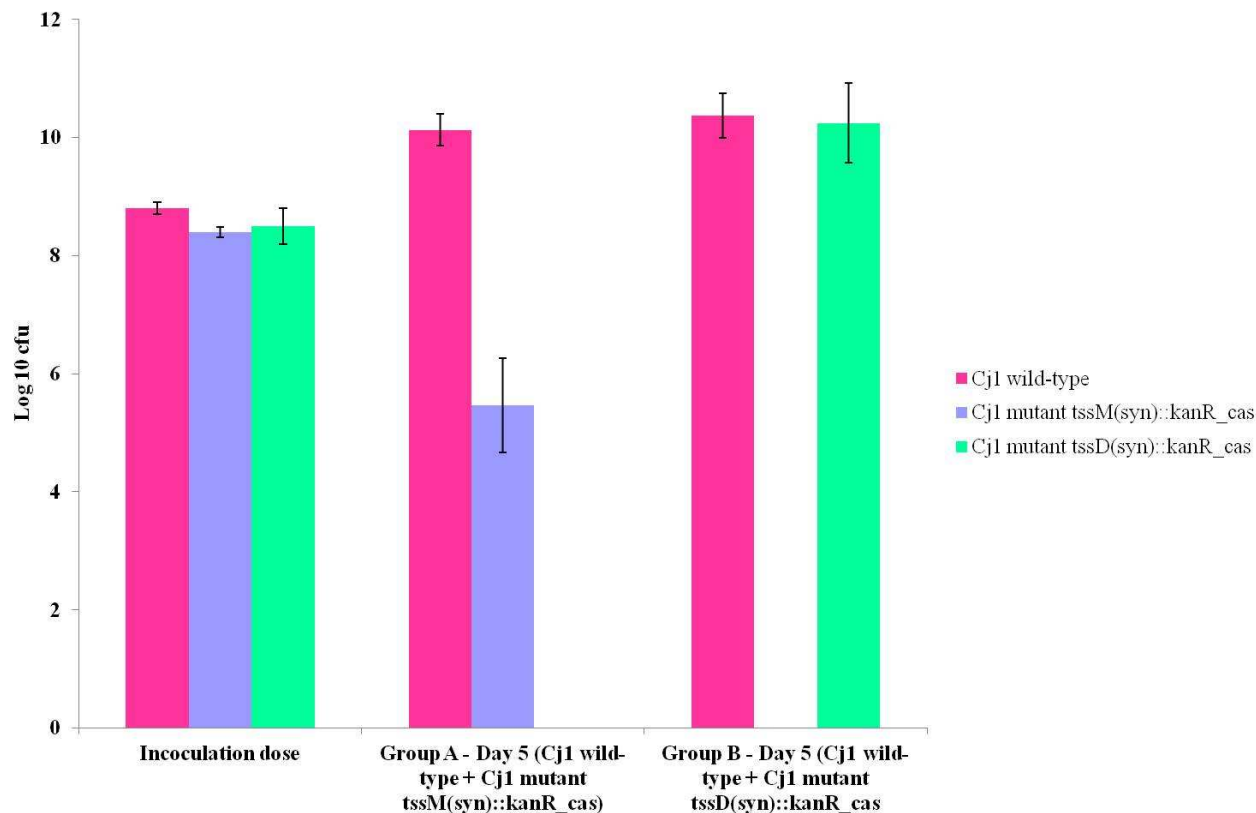
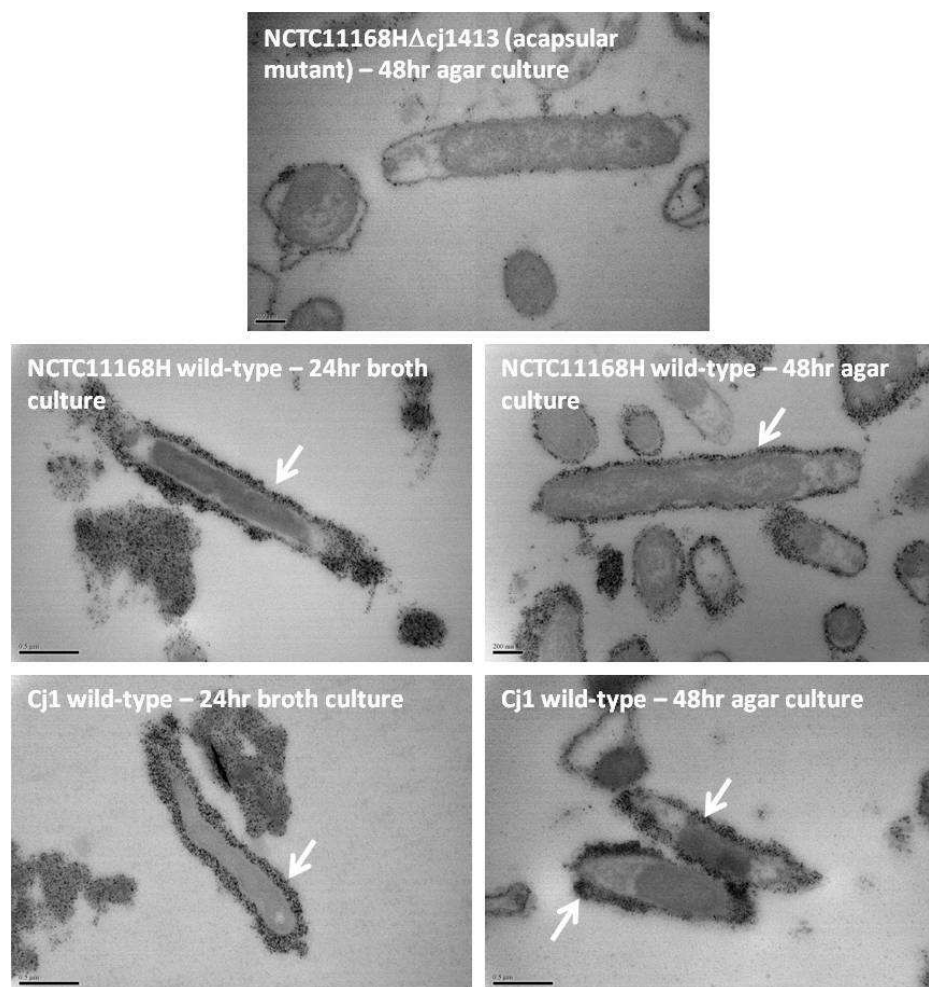


Figure 6.4: Competitive index challenge performed on 2 groups of newborn piglets, 9 animals in each group. Group A was challenged with approximately equal amount of *C. jejuni* strain Cj1 wild-type and Cj1 $\Delta$ tssM(syn)::kan<sup>R</sup>\_cas. Group B was challenged with approximately equal amount of Cj1 wild-type and Cj1 $\Delta$ tssD(syn)::kan<sup>R</sup>\_cas. Inoculation dose for Cj1 wild-type was Log<sub>10</sub>(8.8), Cj1 $\Delta$ tssM(syn)::kan<sup>R</sup>\_cas was Log<sub>10</sub>(8.4) and Cj1 $\Delta$ tssD(syn)::kan<sup>R</sup>\_cas was Log<sub>10</sub>(8.5). In Group A, count on Day 5 post-infection for Cj1 wild-type was Log<sub>10</sub>(10.13) and for Cj1 $\Delta$ tssM(syn)::kan<sup>R</sup>\_cas was Log<sub>10</sub>(5.46). In Group B, count on Day 5 post-infection for Cj1 wild-type was Log<sub>10</sub>(10.371) and for Cj1 $\Delta$ tssD(syn)::kan<sup>R</sup>\_cas was Log<sub>10</sub>(10.246). Error bars represent standard deviation.

### 6.2.5 Detection of capsule in Cj1 wild-type under two growth conditions

It has been reported that the presence of capsule could hinder T6SS machinery in *C. jejuni* (Bleumink-Pluym et al., 2013). It was unclear if capsule was produced in Cj1 strains under the growth conditions used. Cj1 wild-type was cultured under two different growth conditions; i) 37 °C in MHB for 24 hr; ii) 37 °C on CBA+ for 48 hr. Cells were then harvested for capsule detection. Culturing in MHB was the growth condition used in most studies, such as growth curve, ZFE infection and macrophage cells adhesion and invasion. Cells grown on CBA+ was used for piglets challenge.

Capsule was detected in Cj1 wild-type cultured under both growth conditions. Thickness of capsule varied from cell to cell but cells cultured in broth seemed to have a thicker layer of capsule as compared to agar grown cells.



**Figure 6.5:** Electron micrograph of *C. jejuni* cell stained with Alcain Blue for capsule detection. Positive control for Alcain Blue staining: *C. jejuni* strain NCTC11168H wild-type. Negative control for Alcain Blue staining: *C. jejuni* strain NCTC11168HΔcj1413 (acapsular mutant). Capsule stained by Alcain Blue were the black deposits around the cell (white arrow), which was not present in acapsular mutant (NCTC11168HΔcj1413). Capsule was detected in both NCTC11168 and Cj1 wild-type cultured in broth and on agar. Cells grown in broth had thicker capsule as compared to those grown on agar.

### 6.3 Discussion

It has been previously reported that T6SS promotes host cell adhesion and invasion in *V. parahaemolyticus* and avian pathogenic *E. coli* (APEC) (de Pace et al., 2011; de Pace et al., 2010; Yu et al., 2012). Similar observations have been made in a recent study conducted with the *C. jejuni* strain ATCC 43431 (Lertpiriyapong et al., 2012).

In this study Cj1 wild-type cells were used to infect macrophages. The percentages of Cj1 wild-type adhering to or invading mouse macrophage-like cells RAW264.7 were lower than reported in *C. jejuni* strain ATCC 43431 wild-type (Lertpiriyapong et al., 2012). This result could be due to inherent differences in adhesion and invasion ability between the two strains. It has been suggested that the presence of capsule would affect the functionality of the T6SS (Bleumink-Pluym et al., 2013). Hence, the presence of capsule on Cj1 wild-type was investigated. Capsule was detected in Cj1 wild-type (Figure 6.5) when it was cultured in broth. The growth conditions tested for capsule presence here are the same as conditions used to culture the Cj1 wild-type cells prior to using it for the macrophage assays. Thus, a lower amount of adhered Cj1 wild-type could be due to the presence of capsule. The presence of capsule and its effect on *C. jejuni* strain ATCC 43431 was not investigated. Therefore, no direct comparison could be made.

With the current cloning techniques and tools available it is possible to first make an acapsular mutant in Cj1 and then to construct a double mutant targeting the T6SS in the Cj1 acapsular mutant. For example, a kanamycin resistance marker could be used for

construction of the first mutant and a chloramphenicol resistance marker could be used in the construction of the second mutation within the same strain (Yao et al., 1993). The availability of T6SS mutants in an acapsular background would facilitate the study of T6SS functionality without its interference from the bacterial capsule.

It has been previously reported that in both *V. parahaemolyticus* and APEC the disruption of *tssD* and *tssM* led to a reduction in adhesion and invasion of epithelial cells, HeLa and CaCo2 cells (de Pace et al., 2011; de Pace et al., 2010; Yu et al., 2012). For APEC, disruption of *tssD* did not affect its intra-macrophage survival, but when *tssM* was disrupted intra-macrophage survival had decreased (de Pace et al., 2011; de Pace et al., 2010).

The number of bacterial cells adhering to and/or invading macrophage cells was significantly higher for both Cj1 $\Delta$ *tssD*(syn)::kan<sup>R</sup>\_cas and Cj1 $\Delta$ *tssM*(syn)::kan<sup>R</sup>\_cas when compared to Cj1 wild-type. These findings contradicted results previously reported for *C. jejuni* strain ATCC 43431. It has been reported that disruption of *tssD* or *tssM* in *C. jejuni* strain ATCC 43431 resulted in a reduction of host cell adhesion and invasion (Lertpiriyapong et al., 2012).

In another report, an insertional mutation of *icmF* (equivalent to *tssM*) of *V. cholerae* had resulted in enhanced adhesion to intestinal epithelial cells (Das et al., 2002). Disruption of *tssM* could prevent assembly of T6SS machinery on the cell membrane and cause changes in the bacterial surface structures (Das et al., 2002). A similar change might rendered Cj1 $\Delta$ *tssM*(syn)::kan<sup>R</sup>\_cas to adhere and possibly invade macrophages more efficiently.

Differences observed between T6SS mutants constructed from the two strains could be due to inherent strain differences or presence of capsule. It could also be that the role played by T6SS in both strains differs.

*C. jejuni* strain Cj1 wild-type and its T6SS mutants were put through two different animal models: zebrafish embryo model, and piglet model. In both models Cj1 $\Delta$ tssM(syn)::kan<sup>R</sup>\_cas was shown to be attenuated, but not Cj1 $\Delta$ tssD(syn)::kan<sup>R</sup>\_cas. Attenuation observed in Cj1 $\Delta$ tssM(syn)::kan<sup>R</sup>\_cas indicates that T6SS in Cj1 might have a role to play in establishing infection in both animal models. The T6SS mutants were also put through the *G. mellonella* model, however the results obtained were not presented here. This is because when 2 batches of larvae were infected with a lethal dose of the reference strain, *C. jejuni* NCTC11168H, 80-100% of the larvae survived after 24 hours post-infection. This is in contrast to previously reported rate of no survival by 24 hours post-infection (Champion et al., 2010). Since the *G. mellonella* model was not performing as it should when infected with the reference strain, the results obtained for larvae infected with Cj1 wild-type and its T6SS mutants were inconclusive., thus were not included for comparison with the ZFE and piglet models.

It has also been suggested that reduced virulence of a T6SS mutant observed in a higher eukaryotic host might not be directly linked to anti-eukaryotic activity (Coulthurst, 2013). It could be because the mutant was less able to compete with endogenous micro-flora or its wild-type strain in competitive studies (Coulthurst, 2013). The attenuation of Cj1 $\Delta$ tssM(syn)::kan<sup>R</sup>\_cas observed in the piglet model could not be due to its inability to compete against endogenous micro-flora as the newborn piglets do not have gut flora. The attenuation observed was also unlikely to be a result of competition against wild-type cells.

This was because, *Cj1ΔtssD(syn)::kan<sup>R</sup>\_cas*, being the slowest in terms of growth rate among the three strains, was recovered in the same amount as *Cj1* wild-type cells in the piglet competitive index study. On the same note, the cell densities achieved by *Cj1ΔtssM(syn)::kan<sup>R</sup>\_cas* by stationary phase were not significantly different from that of *Cj1* wild-type.

In the ZFE model, *Cj1ΔtssM(syn)::kan<sup>R</sup>\_cas* was not challenged together with *Cj1* wild-type cells, hence, the attenuation observed was unlikely to be due to its inability to compete against *Cj1* wild-type strain. With regards to competition against endogenous flora the existence of micro-flora in ZFE at 28-32 hpf would be minimal, hence once again, the attenuation observed was unlikely to be due to out-competition of *Cj1ΔtssM(syn)::kan<sup>R</sup>\_cas* by the micro-flora communities.

TssD has previously been shown to form hexameric rings and assemble into nano-tubes (Ballister et al., 2008; Mougous et al., 2006). This tube-like structure was suggested to be a conduit of the T6SS assembly on the bacterial cell surface (Filloux et al., 2008). It might be involved in transportation of other T6SS effectors out into the environment or host cell (Filloux et al., 2008). The loss of TssD in *Cj1ΔtssD(syn)::kan<sup>R</sup>\_cas* did not alter its virulence in both animal models. This suggests that either T6SS remain functional in *Cj1ΔtssD(syn)::kan<sup>R</sup>\_cas*, or TssD does not play a role in virulence. The only difference observed between *Cj1ΔtssD(syn)::kan<sup>R</sup>\_cas* and wild-type is in the enhanced ability of the former to adhere to macrophage cells.

It has been reported that TssB and TssC formed a complex of contractile sheath-like structure and was involved in secretions of effectors from the bacterial cell (Coulthurst, 2013). It has been suggested that the TssB/TssC complex was involved in guiding T6SS effector proteins to secretion channels (Bröms et al., 2013). The complex was also reported to be essential for secretion of TssD (Lin et al., 2013). This process was achieved when the complex wrapped around tube-like structure formed by TssD and contracted to push the latter across the bacterial membrane (Lin et al., 2013). Thus, in the absence of TssD, it was uncertain if the TssB/TssC complex continued to push proteins across the bacterial membrane to maintain T6SS functionality. The identity of other T6SS components involved in retaining the bacterial virulence in Cj1Δ*tssD*(syn)::kan<sup>R</sup>\_cas, also remained uncertain.

The observed attenuation of Cj1Δ*tssM*(syn)::kan<sup>R</sup>\_cas was supported by similar observations made in IL-10-deficient mice infected with *tssM* mutant of *C. jejuni* strain ATCC 43431 (Lertpiriyapong et al., 2012). At 30 days post-infection, *C. jejuni* strain ATCC 43431 *tssM* mutants were detected in a lesser number of mice (Lertpiriyapong et al., 2012). The amount of bacterial cells detected in both cecum and faeces samples were also lower as compared to wild-type (Lertpiriyapong et al., 2012).

TssM has been reported to be located in the inner membrane and consists of both cytosolic and periplasmic domains (Bönemann et al., 2009). A Walker A motif conferring ATPase function was identified in the cytosolic domain of TssM (Bönemann et al., 2009). It has been reported that TssM was the energising components for TssD secretion (Ma et al., 2012). Cj1 T6SS lacked the commonly known energising component TssH - knocking out *tssM* in Cj1 might partially or entirely disable the secretion system. Beside its potential role as energy

provider, TssM might also be a key component in assembling and anchoring the T6SS apparatus to the cell membrane (Coulthurst, 2013; Lertpiriyapong et al., 2012). In its absence, the secretion system might not be able to assemble or anchor to the cell membrane which may render the system partially or entirely non-functional. Again, with the potential for disrupting the assembly of the system, surface structures of the bacterial might be altered as well (Das et al., 2002). This could have affected the interaction of bacteria with host immune cells, as shown in the macrophage adhesion and invasion assays performed.

It is important to note that the studies conducted here were with T6SS mutant strains. There were no complemented strains constructed and tested. In order to confirm the observations made, especially in the attenuation of *Cj1ΔtssM(syn)::kan<sup>R</sup>\_cas*, it is important to complement the mutants. This serves to check if the observed phenotype could be restored to wild-type with complementation. The various approaches for complementation were discussed in Chapter 5.

## **Concluding remarks**

In this project, the interactions between *C. jejuni* and host cells were studied.

Initially, I explored the use of Raman spectroscopy to determine the molecular make-up of bacteria cells with a view towards using this information to interrogate host-pathogen interactions. The exploratory work was carried out using an established model of mouse macrophage-like cells infected with *S. Typhimurium*. SRS images of *S. Typhimurium* within macrophage cells were obtained using selected wavenumbers. There are several reports on bacteria detection, imaging and sorting in complex matrixes, for example in biofilms (Beier et al., 2012; Li et al., 2012), and the imaging of eukaryotic cells (Downes and Elfick, 2010), using the Raman spectroscopy technique. In a study conducted by Neugebauer *et al.*, they stated good signal-to-noise Raman images were recorded from formaldehyde fixed endothelial cell infected with *S. aureus* and statistical analysis of the Raman maps acquired were able to resolved host's nucleus and individual bacteria cells (Neugebauer et al., 2012). However, no Raman images on the infected endothelial cells were presented in the publication. The SRS images from live bacteria within macrophages presented here are the first of its kind. Unfortunately, in subsequent imaging attempts, the quality of the images at the lower frequencies were poor and no features could be identified. This was mainly due to the instability of the laser system used. The study with Raman based imaging was not extended to *C. jejuni* after the exploratory work on *S. Typhimurium*. Nonetheless, this exploratory work had shown a potential for this technique to be used for future work on interrogation of host-pathogen interactions. Besides using the Raman spectroscopy technique for label-free real-time imaging, potentially, Raman spectra could be obtained from a single bacteria cell residing within a eukaryotic host cell over time. Data processed from the spectra collected will then provide information on molecular changes taking place inside the bacteria. The labelling of bacteria cells with deuterium oxide in this study was used for imaging,

however, this labelling technique could also be applied for monitoring cell metabolism. Neugebauer *et al.* also reported the use of digital holographic microscopy to perform live cell imaging of *S. aureus* within endothelial cells. It is a phase contrast technique and was able to capture images of the infected endothelial cell at high spatial resolution in a label-free, non-destructive and non-contact manner (Neugebauer *et al.*, 2012). This could be another technique to explore for real-time imaging of *Campylobacter*.

In order to better understand the interaction of *C. jejuni* with its host, a new animal model of infection which would allowed real-time imaging was developed. *C. jejuni* was able to establish an infection in ZFE and the death of challenged embryo was shown to be dose-dependent. The ZFE model was used to screen several mutants and strains. The different *C. jejuni* mutants used to challenge ZFE had showed differences in their virulence in this model and together with its low cost of maintenance and ease of handling, the ZFE is a suitable infection model for *C. jejuni* strains and mutants screening. Optical transparency is the other key property of ZFE that allows the tracking of bacterial cells throughout the whole organism and monitoring of bacterial interactions with host immune cells. A GFP labelled *C. jejuni* was constructed in this study to exploit the advantage provided by ZFE in real-time imaging. However, due to the low fluorescence level of GFP tagged in the constructed *C. jejuni* the migration of the bacteria within the host organism could not be tracked and the images obtained were not able to reveal interactions between the bacteria and ZFE immune cells - in this case mCherry tagged macrophages. The ability to track the bacteria cells and its interaction with host immune cells especially with macrophages would help to address the debating issue on the fate of the bacteria after being taken up by macrophages - does it survive or not within macrophages (Hickey *et al.*, 2005; Kiehlbauch *et al.*, 1985; Watson and Galan, 2008)? When a strongly fluorescing *C. jejuni* is available, and with the use of an

inverted fluorescent microscope that allows higher magnification and without damaging the ZFE - such as a Confocal or Two-photon microscopy - real-time imaging could be performed to track the migration of the bacteria from the site of infection as well as to capture bacterial interactions with immune cells. This would then provide an insight into how *C. jejuni* interacts with a whole host organism; a new dimension to the study of Campylobacteriosis that is not possible in other animal models. The weak fluorescence in the GFP constructed in this study could potentially be due to the promoter used resulting in weak transcriptions. The transcription level could be checked by relative-quantification real-time PCR, for example, against a house-keeping gene. If the cause of weak fluorescence was due to the promoter, then a stronger promoter could be used instead. It would also be worth looking into integration of the gene encoding GFP - together with a strong promoter, into genome rRNA genes or a pseudogene, for example, cj0046.

The T6SS was recently reported in several Proteobacteria including *C. jejuni*. A clinical strain (Cj1) isolated from Thailand was sequenced in this project and a gene cluster consisting of 12 out of 13 T6SS core COGs was identified. When a bacteria - harbouring the T6SS genes - was cultured under suitable conditions for the expression of the T6SS, it has been suggested that the detection of TssD in culture supernatant indicates a functional T6SS (Pukatzki et al., 2007). In the culture supernatant of Cj1, TssD was detected thus suggested that the secretion mechanism of T6SS in Cj1 is functional. Two T6SS mutants in Cj1 targeting deletion of *tssD* or *tssM* respectively were constructed: Cj1 $\Delta$ *tssD*(syn)::kan<sup>R</sup>\_cas and Cj1 $\Delta$ *tssM*(syn)::kan<sup>R</sup>\_cas. TssD was suggested to form the 'needle' structure of the secretion system and was wrapped around by TssB/TssC complex (Filloux et al., 2008; Lin et al., 2013). It is not known if the secretion mechanism of the T6SS remains functional in its

absence. The TssM component of the T6SS was suggested to be a key component in anchoring the apparatus into the cell membrane (Das et al., 2002). In its absence other components could not be assembled or anchored, resulting in disruption of the secretion mechanism. In this study TssD was detected in cell lysate, but not in culture supernatants of *tssM* deleted mutant of Cj1. This finding demonstrated that the deletion of *tssM* had disrupted the secretion mechanism of T6SS in Cj1.

Both the *tssD* and *tssM* deletion mutants showed significant increase in adherence to the macrophages, but only Cj1 $\Delta$ *tssM*(syn)::kan<sup>R</sup>\_cas showed significant increase in invasion - indicating that the T6SS played a negative role in host cells adhesion and invasion. When the T6SS mutants were used for challenge in ZFE and piglet models, only Cj1 $\Delta$ *tssM*(syn)::kan<sup>R</sup>\_cas was attenuated.

In the adhesion and invasion assays, the *tssD* deletion mutant showed an increase in adhesion but not invasion of the macrophages. On the contrary, *tssM* deletion mutant showed increased adhesion and invasion. When TssD was absent (in *tssD* deletion mutant) or not secreted (in *tssM* deletion mutant), adhesion to macrophages was increased. This showed that TssD may play a part in preventing adherence of the bacteria to macrophages. In the *tssM* deletion mutant, where the T6SS was disrupted, an increase in invasion was observed. In the *tssD* deletion mutant, where the T6SS could possibly remain functional, invasion was not significantly different from wild type. This suggests that TssD is unlikely to participate in resisting invasion of macrophages and other components of the secretion system could be the one playing a part in resisting invasion.

The *tssM* deletion mutant showed enhanced engulfment by host macrophages and reduced virulence observed in both animal models, while for *tssD* deletion mutant, the bacteria was likely to resist uptake by macrophages and thus remained as virulent as wild-type as demonstrated in the two animal models. Overall, the findings suggested that the role of T6SS in Cj1 could be in resisting uptake by macrophages for the bacteria survival in host organisms. The full mechanisms utilised by the bacteria in establishing an infection and whether it involves T6SS remains to be answered.

The growth of rates both the *tssD* and *tssM* deletion mutants were slower when compared to wild type - *tssD* deletion mutant being the slowest in growth and had the lowest cell density at stationary stage. The difference in growth rate is unlikely to be the contributing factor for the attenuated phenotype observed in *tssM* deletion mutant. This is because although *tssD* deletion mutant is the slowest in growth, when challenged in piglets together with wild type cells the amount of *tssD* deletion mutant recovered from challenged piglet at Day 5 were higher than input dose and was also approximately the same amount as wild-type cells.

A point of note is that the host cells or animal models challenge were not performed with complemented strains. So, in order to be conclusive with regards to the phenotype observed in the two mutants, the assays need to be repeated using complemented strains. The infection assays performed with the piglets were competitive index challenge. The main advantage of such challenge is that two strains tested were subjected to the same host organism, however a major drawback is that there might be a competition in growth between the two strains used

and one might be stronger in growth and out competes the other. If this happens, the outcomes recorded might not be a true indication of one strain being more virulent than the other.

In this project, T6SS in Cj1 has been demonstrated to play a role against eukaryotic cells. As it seems that there is only one T6SS in *Campylobacter*, it would be interesting to find out if the T6SS has an anti-prokaryotic role as well. Currently, the T6SS has shown to be expressing under the growth condition tested. It would also be interesting to look into environmental factors regulating its expression, for example, temperature, pH and nutrient level.

Overall, this project has revealed the potential of using Raman based techniques to perform live-imaging of bacteria cells within infected macrophage cells. A new animal model, ZFE, was developed for Campylobacteriosis study that can used for screening of strains and mutants. The potential of using ZFE in fluorescence based live-imaging was also demonstrated. The investigations into the role of the recently identified T6SS in *C. jejuni* shows its involvement in adhesion and invasion of macrophage cells and its virulence in both ZFE and piglet models.

## **References**

Agerer, F., Waeckerle, S., and Hauck, C.R. (2004). Microscopic quantification of bacterial invasion by a novel antibody-independent staining method. *Journal of microbiological methods* 59, 23-32.

Alfonso-García, A., Mittal, R., Lee, E.S., and Potma, E.O. (2014). Biological imaging with coherent Raman scattering microscopy: a tutorial. *BIOMEDO* 19, 071407-071407.

Ali, A.M., Qureshi, A.H., Rafi, S., Roshan, E., Khan, I., Malik, A.M., and Shahid, S.A. (2003). Frequency of *Campylobacter jejuni* in diarrhoea/dysentery in children in Rawalpindi and Islamabad. *J Pak Med Assoc* 53, 517-520.

Allos, B.M. (2001). *Campylobacter jejuni* Infections: update on emerging issues and trends. *Clin Infect Dis* 32, 1201-1206.

Almarashi, J.F.M., Kapel, N., Wilkinson, T.S., and Telle, H.H. (2012). Raman Spectroscopy of Bacterial Species and Strains Cultivated under Reproducible Conditions. *Spectroscopy: An International Journal* 27.

Altekruse, S.F., Stern, N.J., Fields, P.I., and Swerdlow, D.L. (1999). *Campylobacter jejuni*--an emerging foodborne pathogen. *Emerg Infect Dis* 5, 28-35.

Aroori, S.V., Cogan, T.A., and Humphrey, T.J. (2013). The effect of growth temperature on the pathogenicity of *Campylobacter*. *Current microbiology* 67, 333-340.

Ashbolt, N.J. (2004). Microbial contamination of drinking water and disease outcomes in developing regions. *Toxicology* 198, 229-238.

Axelsson-Olsson, D., Waldenstrom, J., Broman, T., Olsen, B., and Holmberg, M. (2005). Protozoan *Acanthamoeba polyphaga* as a potential reservoir for *Campylobacter jejuni*. *Appl Environ Microbiol* 71, 987-992.

Babakhani, F.K., Bradley, G.A., and Joens, L.A. (1993). Newborn piglet model for campylobacteriosis. *Infect Immun* 61, 3466-3475.

Bacon, D.J., Alm, R.A., Burr, D.H., Hu, L., Kopecko, D.J., Ewing, C.P., Trust, T.J., and Guerry, P. (2000). Involvement of a plasmid in virulence of *Campylobacter jejuni* 81-176. *Infect Immun* 68, 4384-4390.

Bacon, D.J., Alm, R.A., Hu, L., Hickey, T.E., Ewing, C.P., Batchelor, R.A., Trust, T.J., and Guerry, P. (2002). DNA sequence and mutational analyses of the pVir plasmid of *Campylobacter jejuni* 81-176. *Infect Immun* 70, 6242-6250.

Bacon, D.J., Szymanski, C.M., Burr, D.H., Silver, R.P., Alm, R.A., and Guerry, P. (2001). A phase-variable capsule is involved in virulence of *Campylobacter jejuni* 81-176. *Molecular microbiology* 40, 769-777.

Balbontin, R., Rowley, G., Pucciarelli, M.G., Lopez-Garrido, J., Wormstone, Y., Lucchini, S., Garcia-Del Portillo, F., Hinton, J.C., and Casadesus, J. (2006). DNA adenine methylation regulates virulence gene expression in *Salmonella enterica* serovar Typhimurium. *Journal of bacteriology* 188, 8160-8168.

- Ballister, E.R., Lai, A.H., Zuckermann, R.N., Cheng, Y., and Mougous, J.D. (2008). In vitro self-assembly of tailorable nanotubes from a simple protein building block. *Proceedings of the National Academy of Sciences of the United States of America* *105*, 3733-3738.
- Barer, R. (1974). Microscopes, microscopy, and microbiology. *Annual review of microbiology* *28*, 371-389.
- Basler, M., Pilhofer, M., Henderson, G.P., Jensen, G.J., and Mekalanos, J.J. (2012). Type VI secretion requires a dynamic contractile phage tail-like structure. *Nature* *483*, 182-186.
- Beier, B.D., Quivey, R.G., and Berger, A.J. (2012). Raman microspectroscopy for species identification and mapping within bacterial biofilms. *AMB Express* *2*, 35.
- Bernard, C.S., Brunet, Y.R., Gueguen, E., and Cascales, E. (2010). Nooks and crannies in type VI secretion regulation. *Journal of bacteriology* *192*, 3850-3860.
- Bessell, P.R., Matthews, L., Smith-Palmer, A., Rotariu, O., Strachan, N.J., Forbes, K.J., Cowden, J.M., Reid, S.W., and Innocent, G.T. (2010). Geographic determinants of reported human *Campylobacter* infections in Scotland. *BMC Public Health* *10*, 423.
- Bhuvanendran, S., Salka, K., Rainey, K., Sreetama, S.C., Williams, E., Leeker, M., Prasad, V., Boyd, J., Patterson, G.H., Jaiswal, J.K., and Colberg-Poley, A.M. (2014). Superresolution imaging of human cytomegalovirus vMIA localization in sub-mitochondrial compartments. *Viruses* *6*, 1612-1636.
- Biswas, D., Itoh, K., and Sasakawa, C. (2000). Uptake pathways of clinical and healthy animal isolates of *Campylobacter jejuni* into INT-407 cells. *FEMS Immunol Med Microbiol* *29*, 203-211.
- Biteen, J.S., and Moerner, W.E. (2010). Single-molecule and superresolution imaging in live bacteria cells. *Cold Spring Harbor perspectives in biology* *2*, a000448.
- Bladergroen, M.R., Badelt, K., and Spaink, H.P. (2003). Infection-blocking genes of a symbiotic *Rhizobium leguminosarum* strain that are involved in temperature-dependent protein secretion. *Molecular plant-microbe interactions : MPMI* *16*, 53-64.
- Blaser, M.J. (1997). Epidemiologic and clinical features of *Campylobacter jejuni* infections. *J Infect Dis* *176 Suppl 2*, S103-105.
- Bleumink-Pluym, N.M., van Alphen, L.B., Bouwman, L.I., Wosten, M.M., and van Putten, J.P. (2013). Identification of a functional type VI secretion system in *Campylobacter jejuni* conferring capsule polysaccharide sensitive cytotoxicity. *PLoS Pathog* *9*, e1003393.
- Bolton, F.J., and Robertson, L. (1982). A selective medium for isolating *Campylobacter jejuni/coli*. *J Clin Pathol* *35*, 462-467.
- Bönemann, G., Pietrosiuk, A., Diemand, A., Zentgraf, H., and Mogk, A. (2009). Remodelling of VipA/VipB tubules by ClpV-mediated threading is crucial for type VI protein secretion. *The EMBO journal* *28*, 315-325.

- Boyer, F., Fichant, G., Berthod, J., Vandenbrouck, Y., and Attree, I. (2009). Dissecting the bacterial type VI secretion system by a genome wide in silico analysis: what can be learned from available microbial genomic resources? *BMC genomics* 10, 104.
- Brehm-Stecher, B.F., and Johnson, E.A. (2004). Single-cell microbiology: tools, technologies, and applications. *Microbiol Mol Biol Rev* 68, 538-559.
- Bröms, J.E., Ishikawa, T., Wai, S.N., and Sjostedt, A. (2013). A functional VipA-VipB interaction is required for the type VI secretion system activity of *Vibrio cholerae* O1 strain A1552. *BMC microbiology* 13, 96.
- Buelow, D.R., Christensen, J.E., Neal-McKinney, J.M., and Konkel, M.E. (2011). *Campylobacter jejuni* survival within human epithelial cells is enhanced by the secreted protein CiaI. *Molecular microbiology* 80, 1296-1312.
- Burtnick, M.N., Brett, P.J., Harding, S.V., Ngugi, S.A., Ribot, W.J., Chantratita, N., Scorpio, A., Milne, T.S., Dean, R.E., Fritz, D.L., *et al.* (2011). The cluster 1 type VI secretion system is a major virulence determinant in *Burkholderia pseudomallei*. *Infect Immun* 79, 1512-1525.
- Burtnick, M.N., DeShazer, D., Nair, V., Gherardini, F.C., and Brett, P.J. (2010). *Burkholderia mallei* cluster 1 type VI secretion mutants exhibit growth and actin polymerization defects in RAW 264.7 murine macrophages. *Infect Immun* 78, 88-99.
- Butzler, J.P., and Oosterom, J. (1991). *Campylobacter*: pathogenicity and significance in foods. *Int J Food Microbiol* 12, 1-8.
- Cascales, E. (2008). The type VI secretion toolkit. *EMBO reports* 9, 735-741.
- Champion, O.L., Karlyshev, A.V., Senior, N.J., Woodward, M., La Ragione, R., Howard, S.L., Wren, B.W., and Titball, R.W. (2010). Insect infection model for *Campylobacter jejuni* reveals that O-methyl phosphoramidate has insecticidal activity. *J Infect Dis* 201, 776-782.
- Christensen, J.E., Pacheco, S.A., and Konkel, M.E. (2009). Identification of a *Campylobacter jejuni*-secreted protein required for maximal invasion of host cells. *Molecular microbiology* 73, 650-662.
- Clatworthy, A.E., Lee, J.S., Leibman, M., Kostun, Z., Davidson, A.J., and Hung, D.T. (2009). *Pseudomonas aeruginosa* infection of zebrafish involves both host and pathogen determinants. *Infect Immun* 77, 1293-1303.
- Coker, A.O., Isokpehi, R.D., Thomas, B.N., Amisu, K.O., and Obi, C.L. (2002). Human campylobacteriosis in developing countries. *Emerg Infect Dis* 8, 237-244.
- Cope, L.D., Lumbley, S., Latimer, J.L., Klesney-Tait, J., Stevens, M.K., Johnson, L.S., Purven, M., Munson, R.S., Jr., Lagergard, T., Radolf, J.D., and Hansen, E.J. (1997). A diffusible cytotoxin of *Haemophilus ducreyi*. *Proceedings of the National Academy of Sciences of the United States of America* 94, 4056-4061.
- Cosslett, V.E. (1962). Electron microscopy: introduction. *British medical bulletin* 18, 179-182.

Coulthurst, S.J. (2013). The Type VI secretion system - a widespread and versatile cell targeting system. *Research in microbiology* 164, 640-654.

Coward, C., Grant, A.J., Swift, C., Philp, J., Towler, R., Heydarian, M., Frost, J.A., and Maskell, D.J. (2006). Phase-variable surface structures are required for infection of *Campylobacter jejuni* by bacteriophages. *Appl Environ Microbiol* 72, 4638-4647.

Cremer, C., and Cremer, T. (1978). Considerations on a laser-scanning-microscope with high resolution and depth of field. *Microsc Acta* 81, 31-44.

Das, S., Chakraborty, A., Banerjee, R., and Chaudhuri, K. (2002). Involvement of in vivo induced icmF gene of *Vibrio cholerae* in motility, adherence to epithelial cells, and conjugation frequency. *Biochemical and biophysical research communications* 295, 922-928.

Dasti, J.I., Tareen, A.M., Lugert, R., Zautner, A.E., and Gross, U. (2010). *Campylobacter jejuni*: a brief overview on pathogenicity-associated factors and disease-mediating mechanisms. *Int J Med Microbiol* 300, 205-211.

Davis, A.P., Ma, G., and Allen, H.C. (2003). Surface vibrational sum frequency and Raman studies of PAMAM G0, G1 and acylated PAMAM G0 dendrimers. *Analytica Chimica Acta* 496, 117-131.

Davis, J.M., Clay, H., Lewis, J.L., Ghori, N., Herbomel, P., and Ramakrishnan, L. (2002). Real-time visualization of *Mycobacterium*-macrophage interactions leading to initiation of granuloma formation in zebrafish embryos. *Immunity* 17, 693-702.

Day, W.A., Jr., Sajecki, J.L., Pitts, T.M., and Joens, L.A. (2000). Role of catalase in *Campylobacter jejuni* intracellular survival. *Infect Immun* 68, 6337-6345.

De Melo, M.A., Gabbiani, G., and Pechere, J.C. (1989). Cellular events and intracellular survival of *Campylobacter jejuni* during infection of HEp-2 cells. *Infect Immun* 57, 2214-2222.

de Pace, F., Boldrin de Paiva, J., Nakazato, G., Lancellotti, M., Sircili, M.P., Guedes Stehling, E., Dias da Silveira, W., and Sperandio, V. (2011). Characterization of IcmF of the type VI secretion system in an avian pathogenic *Escherichia coli* (APEC) strain. *Microbiology* 157, 2954-2962.

de Pace, F., Nakazato, G., Pacheco, A., de Paiva, J.B., Sperandio, V., and da Silveira, W.D. (2010). The type VI secretion system plays a role in type 1 fimbria expression and pathogenesis of an avian pathogenic *Escherichia coli* strain. *Infect Immun* 78, 4990-4998.

Denk, W., Strickler, J.H., and Webb, W.W. (1990). Two-photon laser scanning fluorescence microscopy. *Science* 248, 73-76.

Desvaux, M., Hebraud, M., Talon, R., and Henderson, I.R. (2009). Secretion and subcellular localizations of bacterial proteins: a semantic awareness issue. *Trends in microbiology* 17, 139-145.

Downes, A., and Elfick, A. (2010). Raman spectroscopy and related techniques in biomedicine. *Sensors* 10, 1871-1889.

- Duncan, M.D., Reintjes, J., and Manuccia, T.J. (1982). Scanning coherent anti-Stokes Raman microscope. *Opt Lett* 7, 350-352.
- Ferraro, J.R., Nakamoto, K., and Brown, C.W. (2003). Chapter 5 - Analytical Chemistry. In *Introductory Raman Spectroscopy (Second Edition)*, J.R. Ferraro, K. Nakamoto, and C.W. Brown, eds. (San Diego: Academic Press), pp. 267-293.
- Fields, J.A., and Thompson, S.A. (2008). *Campylobacter jejuni* CsrA mediates oxidative stress responses, biofilm formation, and host cell invasion. *Journal of bacteriology* 190, 3411-3416.
- Filloux, A. (2013). The rise of the Type VI secretion system. *F1000prime reports* 5, 52.
- Filloux, A., Hachani, A., and Bleves, S. (2008). The bacterial type VI secretion machine: yet another player for protein transport across membranes. *Microbiology* 154, 1570-1583.
- Folkesson, A., Lofdahl, S., and Normark, S. (2002). The *Salmonella enterica* subspecies I specific centisome 7 genomic island encodes novel protein families present in bacteria living in close contact with eukaryotic cells. *Research in microbiology* 153, 537-545.
- French, C.T., Toesca, I.J., Wu, T.H., Teslaa, T., Beaty, S.M., Wong, W., Liu, M., Schroder, I., Chiou, P.Y., Teitell, M.A., and Miller, J.F. (2011). Dissection of the *Burkholderia* intracellular life cycle using a photothermal nanoblade. *Proceedings of the National Academy of Sciences of the United States of America* 108, 12095-12100.
- Freudiger, C.W., Min, W., Holtom, G.R., Xu, B., Dantus, M., and Xie, X.S. (2011). Highly specific label-free molecular imaging with spectrally tailored excitation stimulated Raman scattering (STE-SRS) microscopy. *Nature photonics* 5, 103-109.
- Freudiger, C.W., Min, W., Saar, B.G., Lu, S., Holtom, G.R., He, C., Tsai, J.C., Kang, J.X., and Xie, X.S. (2008). Label-free biomedical imaging with high sensitivity by stimulated Raman scattering microscopy. *Science* 322, 1857-1861.
- Friis, C., Wassenaar, T.M., Javed, M.A., Snipen, L., Lagesen, K., Hallin, P.F., Newell, D.G., Toszeghy, M., Ridley, A., Manning, G., and Ussery, D.W. (2010). Genomic characterization of *Campylobacter jejuni* strain M1. *PloS one* 5, e12253.
- Gest, H. (2005). The remarkable vision of Robert Hooke (1635-1703): first observer of the microbial world. *Perspect Biol Med* 48, 266-272.
- Ghiran, I.C. (2011). Introduction to fluorescence microscopy. *Methods in molecular biology* 689, 93-136.
- Grant, C.C., Konkel, M.E., Cieplak, W., Jr., and Tompkins, L.S. (1993). Role of flagella in adherence, internalization, and translocation of *Campylobacter jejuni* in nonpolarized and polarized epithelial cell cultures. *Infect Immun* 61, 1764-1771.
- Gray, C., Loynes, C.A., Whyte, M.K., Crossman, D.C., Renshaw, S.A., and Chico, T.J. (2011). Simultaneous intravital imaging of macrophage and neutrophil behaviour during inflammation using a novel transgenic zebrafish. *Thrombosis and haemostasis* 105, 811-819.

- Guerry, P., Poly, F., Riddle, M., Maue, A.C., Chen, Y.H., and Monteiro, M.A. (2012). *Campylobacter* polysaccharide capsules: virulence and vaccines. *Frontiers in cellular and infection microbiology* 2, 7.
- Gundogdu, O., Bentley, S.D., Holden, M.T., Parkhill, J., Dorrell, N., and Wren, B.W. (2007). Re-annotation and re-analysis of the *Campylobacter jejuni* NCTC11168 genome sequence. *BMC genomics* 8, 162.
- Haghjoo, E., and Galan, J.E. (2004). *Salmonella typhi* encodes a functional cytolethal distending toxin that is delivered into host cells by a bacterial-internalization pathway. *Proceedings of the National Academy of Sciences of the United States of America* 101, 4614-4619.
- Hannu, T., Mattila, L., Rautelin, H., Pelkonen, P., Lahdenne, P., Siitonen, A., and Leirisalo-Repo, M. (2002). *Campylobacter*-triggered reactive arthritis: a population-based study. *Rheumatology (Oxford)* 41, 312-318.
- Hansen, C.R., Khatiwara, A., Ziprin, R., and Kwon, Y.M. (2007). Rapid construction of *Campylobacter jejuni* deletion mutants. *Letters in applied microbiology* 45, 599-603.
- Harley, V.S., Dance, D.A., Drasar, B.S., and Tovey, G. (1998). Effects of *Burkholderia pseudomallei* and other *Burkholderia* species on eukaryotic cells in tissue culture. *Microbios* 96, 71-93.
- Harvey, E.N. (1934). Biological effect of heavy water. *Biological Bulletin* 66, 91-96.
- Harvey, S.M. (1980). Hippurate hydrolysis by *Campylobacter fetus*. *J Clin Microbiol* 11, 435-437.
- Hébert, G.A., Hollis, D.G., Weaver, R.E., Lambert, M.A., Blaser, M.J., and Moss, C.W. (1982). 30 years of campylobacters: biochemical characteristics and a biotyping proposal for *Campylobacter jejuni*. *J Clin Microbiol* 15, 1065-1073.
- Herbomel, P., Thisse, B., and Thisse, C. (1999). Ontogeny and behaviour of early macrophages in the zebrafish embryo. *Development* 126, 3735-3745.
- Hickey, T.E., Majam, G., and Guerry, P. (2005). Intracellular survival of *Campylobacter jejuni* in human monocytic cells and induction of apoptotic death by cytolethal distending toxin. *Infect Immun* 73, 5194-5197.
- Hirai, K., Tomida, M., Kikuchi, Y., Ueda, O., Ando, H., and Asanuma, N. (2010). Effects of deuterium oxide on *Streptococcus mutans* and *Pseudomonas aeruginosa*. *The Bulletin of Tokyo Dental College* 51, 175-183.
- Hood, R.D., Singh, P., Hsu, F., Guvener, T., Carl, M.A., Trinidad, R.R., Silverman, J.M., Ohlson, B.B., Hicks, K.G., Plemel, R.L., *et al.* (2010). A type VI secretion system of *Pseudomonas aeruginosa* targets a toxin to bacteria. *Cell host & microbe* 7, 25-37.
- Howe, K., Clark, M.D., Torroja, C.F., Tarrance, J., Berthelot, C., Muffato, M., Collins, J.E., Humphray, S., McLaren, K., Matthews, L., *et al.* (2013). The zebrafish reference genome sequence and its relationship to the human genome. *Nature* 496, 498-503.

- Huang, B., Bates, M., and Zhuang, X. (2009). Super-resolution fluorescence microscopy. *Annual review of biochemistry* 78, 993-1016.
- Huang, W.E., Griffiths, R.I., Thompson, I.P., Bailey, M.J., and Whiteley, A.S. (2004). Raman microscopic analysis of single microbial cells. *Anal Chem* 76, 4452-4458.
- Huang, W.E., Li, M., Jarvis, R.M., Goodacre, R., and Banwart, S.A. (2010). Shining light on the microbial world the application of Raman microspectroscopy. *Adv Appl Microbiol* 70, 153-186.
- Hughes, R.A., Hadden, R.D., Gregson, N.A., and Smith, K.J. (1999). Pathogenesis of Guillain-Barre syndrome. *J Neuroimmunol* 100, 74-97.
- Hurme, R., and Rhen, M. (1998). Temperature sensing in bacterial gene regulation--what it all boils down to. *Molecular microbiology* 30, 1-6.
- Hutsebaut, D., Maquelin, K., De Vos, P., Vandenabeele, P., Moens, L., and Puppels, G.J. (2004). Effect of culture conditions on the achievable taxonomic resolution of Raman spectroscopy disclosed by three *Bacillus* species. *Anal Chem* 76, 6274-6281.
- Israeli, E., Agmon-Levin, N., Blank, M., Chapman, J., and Shoenfeld, Y. (2010). Guillain-Barre Syndrome-A Classical Autoimmune Disease Triggered by Infection or Vaccination. *Clin Rev Allergy Immunol*.
- Janssen, R., Krogfelt, K.A., Cawthraw, S.A., van Pelt, W., Wagenaar, J.A., and Owen, R.J. (2008). Host-pathogen interactions in *Campylobacter* infections: the host perspective. *Clin Microbiol Rev* 21, 505-518.
- Johnson, W.M., and Lior, H. (1988a). A new heat-labile cytolethal distending toxin (CLDT) produced by *Campylobacter* spp. *Microb Pathog* 4, 115-126.
- Johnson, W.M., and Lior, H. (1988b). A new heat-labile cytolethal distending toxin (CLDT) produced by *Escherichia coli* isolates from clinical material. *Microb Pathog* 4, 103-113.
- Jones, F.R., Baqar, S., Gozalo, A., Nunez, G., Espinoza, N., Reyes, S.M., Salazar, M., Meza, R., Porter, C.K., and Walz, S.E. (2006). New World monkey *Aotus nancymae* as a model for *Campylobacter jejuni* infection and immunity. *Infect Immun* 74, 790-793.
- Jones, F.S., and Little, R.B. (1931a). The Etiology of Infectious Diarrhea (Winter Scours) in Cattle. *J Exp Med* 53, 835-843.
- Jones, F.S., and Little, R.B. (1931b). Vibrionic Enteritis in Calves. *J Exp Med* 53, 845-851.
- Jones, F.S., Orcutt, M., and Little, R.B. (1931). *Vibrios* (*Vibrio jejuni*, N.Sp.) Associated with Intestinal Disorders of Cows and Calves. *J Exp Med* 53, 853-863.
- Kaakoush, N.O., Deshpande, N.P., Wilkins, M.R., Raftery, M.J., Janitz, K., and Mitchell, H. (2011). Comparative analyses of *Campylobacter concisus* strains reveal the genome of the reference strain BAA-1457 is not representative of the species. *Gut pathogens* 3, 15.
- Kapitein, N., and Mogk, A. (2013). Deadly syringes: type VI secretion system activities in pathogenicity and interbacterial competition. *Current opinion in microbiology* 16, 52-58.

- Karlyshev, A.V., Linton, D., Gregson, N.A., Lastovica, A.J., and Wren, B.W. (2000). Genetic and biochemical evidence of a *Campylobacter jejuni* capsular polysaccharide that accounts for Penner serotype specificity. *Molecular microbiology* 35, 529-541.
- Karlyshev, A.V., McCrossan, M.V., and Wren, B.W. (2001). Demonstration of polysaccharide capsule in *Campylobacter jejuni* using electron microscopy. *Infect Immun* 69, 5921-5924.
- Karlyshev, A.V., and Wren, B.W. (2005). Development and application of an insertional system for gene delivery and expression in *Campylobacter jejuni*. *Appl Environ Microbiol* 71, 4004-4013.
- Keo, T., Collins, J., Kunwar, P., Blaser, M.J., and Iovine, N.M. (2011). *Campylobacter* capsule and lipooligosaccharide confer resistance to serum and cationic antimicrobials. *Virulence* 2, 30-40.
- Kespichayawattana, W., Rattanachetkul, S., Wanun, T., Utaisincharoen, P., and Sirisinha, S. (2000). *Burkholderia pseudomallei* induces cell fusion and actin-associated membrane protrusion: a possible mechanism for cell-to-cell spreading. *Infect Immun* 68, 5377-5384.
- Khanna, M.R., Bhavsar, S.P., and Kapadnis, B.P. (2006). Effect of temperature on growth and chemotactic behaviour of *Campylobacter jejuni*. *Letters in applied microbiology* 43, 84-90.
- Kiehlbauch, J.A., Albach, R.A., Baum, L.L., and Chang, K.P. (1985). Phagocytosis of *Campylobacter jejuni* and its intracellular survival in mononuclear phagocytes. *Infect Immun* 48, 446-451.
- Kim, J.S., Li, J., Barnes, I.H., Baltzegar, D.A., Pajaniappan, M., Cullen, T.W., Trent, M.S., Burns, C.M., and Thompson, S.A. (2008). Role of the *Campylobacter jejuni* Cj1461 DNA methyltransferase in regulating virulence characteristics. *Journal of bacteriology* 190, 6524-6529.
- Konkel, M.E., Corwin, M.D., Joens, L.A., and Cieplak, W. (1992). Factors that influence the interaction of *Campylobacter jejuni* with cultured mammalian cells. *Journal of medical microbiology* 37, 30-37.
- Konkel, M.E., Kim, B.J., Rivera-Amill, V., and Garvis, S.G. (1999). Bacterial secreted proteins are required for the internalization of *Campylobacter jejuni* into cultured mammalian cells. *Molecular microbiology* 32, 691-701.
- Konkel, M.E., Klena, J.D., Rivera-Amill, V., Monteville, M.R., Biswas, D., Raphael, B., and Mickelson, J. (2004). Secretion of virulence proteins from *Campylobacter jejuni* is dependent on a functional flagellar export apparatus. *Journal of bacteriology* 186, 3296-3303.
- Labigne-Roussel, A., Courcoux, P., and Tompkins, L. (1988). Gene disruption and replacement as a feasible approach for mutagenesis of *Campylobacter jejuni*. *Journal of bacteriology* 170, 1704-1708.
- Labigne-Roussel, A., Harel, J., and Tompkins, L. (1987). Gene transfer from *Escherichia coli* to *Campylobacter* species: development of shuttle vectors for genetic analysis of *Campylobacter jejuni*. *Journal of bacteriology* 169, 5320-5323.

- Lau, S.K., Winlove, P., Moger, J., Champion, O.L., Titball, R.W., Yang, Z.H., and Yang, Z.R. (2012). A Bayesian Whittaker–Henderson smoother for general-purpose and sample-based spectral baseline estimation and peak extraction. *Journal of Raman Spectroscopy* *43*, 1299-1305.
- Le Guyader, D., Redd, M.J., Colucci-Guyon, E., Murayama, E., Kissa, K., Briolat, V., Mordelet, E., Zapata, A., Shinomiya, H., and Herbomel, P. (2008). Origins and unconventional behavior of neutrophils in developing zebrafish. *Blood* *111*, 132-141.
- Leggett, H.C., Cornwallis, C.K., and West, S.A. (2012). Mechanisms of pathogenesis, infective dose and virulence in human parasites. *PLoS Pathog* *8*, e1002512.
- Leiman, P.G., Basler, M., Ramagopal, U.A., Bonanno, J.B., Sauder, J.M., Pukatzki, S., Burley, S.K., Almo, S.C., and Mekalanos, J.J. (2009). Type VI secretion apparatus and phage tail-associated protein complexes share a common evolutionary origin. *Proceedings of the National Academy of Sciences of the United States of America* *106*, 4154-4159.
- Lertpiriyapong, K., Gamazon, E.R., Feng, Y., Park, D.S., Pang, J., Botka, G., Graffam, M.E., Ge, Z., and Fox, J.G. (2012). *Campylobacter jejuni* type VI secretion system: roles in adaptation to deoxycholic acid, host cell adherence, invasion, and in vivo colonization. *PLoS one* *7*, e42842.
- Levraud, J.P., Disson, O., Kissa, K., Bonne, I., Cossart, P., Herbomel, P., and Lecuit, M. (2009). Real-time observation of listeria monocytogenes-phagocyte interactions in living zebrafish larvae. *Infect Immun* *77*, 3651-3660.
- Li, M., Xu, J., Romero-Gonzalez, M., Banwart, S.A., and Huang, W.E. (2012). Single cell Raman spectroscopy for cell sorting and imaging. *Current opinion in biotechnology* *23*, 56-63.
- Lieschke, G.J., Oates, A.C., Crowhurst, M.O., Ward, A.C., and Layton, J.E. (2001). Morphologic and functional characterization of granulocytes and macrophages in embryonic and adult zebrafish. *Blood* *98*, 3087-3096.
- Lin, J.S., Ma, L.S., and Lai, E.M. (2013). Systematic dissection of the agrobacterium type VI secretion system reveals machinery and secreted components for subcomplex formation. *PLoS one* *8*, e67647.
- Louwen, R., Heikema, A., van Belkum, A., Ott, A., Gilbert, M., Ang, W., Endtz, H.P., Bergman, M.P., and Nieuwenhuis, E.E. (2008). The sialylated lipooligosaccharide outer core in *Campylobacter jejuni* is an important determinant for epithelial cell invasion. *Infect Immun* *76*, 4431-4438.
- Lu, X., Huang, Q., Miller, W.G., Aston, D.E., Xu, J., Xue, F., Zhang, H., Rasco, B.A., Wang, S., and Konkel, M.E. (2012). Comprehensive detection and discrimination of *Campylobacter* species by use of confocal micro-Raman spectroscopy and multilocus sequence typing. *J Clin Microbiol* *50*, 2932-2946.
- Ma, A.T., McAuley, S., Pukatzki, S., and Mekalanos, J.J. (2009). Translocation of a *Vibrio cholerae* type VI secretion effector requires bacterial endocytosis by host cells. *Cell host & microbe* *5*, 234-243.

- Ma, A.T., and Mekalanos, J.J. (2010). In vivo actin cross-linking induced by *Vibrio cholerae* type VI secretion system is associated with intestinal inflammation. *Proceedings of the National Academy of Sciences of the United States of America* 107, 4365-4370.
- Ma, L.S., Narberhaus, F., and Lai, E.M. (2012). IcmF family protein TssM exhibits ATPase activity and energizes type VI secretion. *The Journal of biological chemistry* 287, 15610-15621.
- MacIntyre, D.L., Miyata, S.T., Kitaoka, M., and Pukatzki, S. (2010). The *Vibrio cholerae* type VI secretion system displays antimicrobial properties. *Proceedings of the National Academy of Sciences of the United States of America* 107, 19520-19524.
- Malik-Kale, P., Raphael, B.H., Parker, C.T., Joens, L.A., Klena, J.D., Quinones, B., Keech, A.M., and Konkel, M.E. (2007). Characterization of genetically matched isolates of *Campylobacter jejuni* reveals that mutations in genes involved in flagellar biosynthesis alter the organism's virulence potential. *Appl Environ Microbiol* 73, 3123-3136.
- Manes, N.P., Gustin, J.K., Rue, J., Mottaz, H.M., Purvine, S.O., Norbeck, A.D., Monroe, M.E., Zimmer, J.S.D., Metz, T.O., Adkins, J.N., *et al.* (2007). Targeted Protein Degradation by *Salmonella* under Phagosome-mimicking Culture Conditions Investigated Using Comparative Peptidomics. *Molecular & Cellular Proteomics* 6, 717-727.
- Mansfield, J., Moger, J., Green, E., Moger, C., and Winlove, C.P. (2013). Chemically specific imaging and in-situ chemical analysis of articular cartilage with stimulated Raman scattering. *J Biophotonics* 6, 803-814.
- Masters, B.R., and So, P.T. (2004). Antecedents of two-photon excitation laser scanning microscopy. *Microsc Res Tech* 63, 3-11.
- Maue, A.C., Mohawk, K.L., Giles, D.K., Poly, F., Ewing, C.P., Jiao, Y., Lee, G., Ma, Z., Monteiro, M.A., Hill, C.L., *et al.* (2013). The polysaccharide capsule of *Campylobacter jejuni* modulates the host immune response. *Infect Immun* 81, 665-672.
- Miller, J.F., Dower, W.J., and Tompkins, L.S. (1988). High-voltage electroporation of bacteria: genetic transformation of *Campylobacter jejuni* with plasmid DNA. *Proceedings of the National Academy of Sciences of the United States of America* 85, 856-860.
- Miller, W.G., Bates, A.H., Horn, S.T., Brandl, M.T., Wachtel, M.R., and Mandrell, R.E. (2000). Detection on surfaces and in Caco-2 cells of *Campylobacter jejuni* cells transformed with new gfp, yfp, and cfp marker plasmids. *Appl Environ Microbiol* 66, 5426-5436.
- Mixter, P.F., Klena, J.D., Flom, G.A., Siegesmund, A.M., and Konkel, M.E. (2003). In vivo tracking of *Campylobacter jejuni* by using a novel recombinant expressing green fluorescent protein. *Appl Environ Microbiol* 69, 2864-2874.
- Moore, J.E., Corcoran, D., Dooley, J.S., Fanning, S., Lucey, B., Matsuda, M., McDowell, D.A., Megraud, F., Millar, B.C., O'Mahony, R., *et al.* (2005). *Campylobacter*. *Vet Res* 36, 351-382.
- Moore, J.E., and Matsuda, M. (2002). The history of *Campylobacter*: Taxonomy and nomenclature. *Irish Vet. J.* 55, 495-501.

- Mougous, J.D., Cuff, M.E., Raunser, S., Shen, A., Zhou, M., Gifford, C.A., Goodman, A.L., Joachimiak, G., Ordonez, C.L., Lory, S., *et al.* (2006). A virulence locus of *Pseudomonas aeruginosa* encodes a protein secretion apparatus. *Science* 312, 1526-1530.
- Mukherjee, K., Altincicek, B., Hain, T., Domann, E., Vilcinskas, A., and Chakraborty, T. (2010). *Galleria mellonella* as a model system for studying *Listeria* pathogenesis. *Appl Environ Microbiol* 76, 310-317.
- Müller, M., and Zumbusch, A. (2007). Coherent anti-Stokes Raman Scattering Microscopy. *Chemphyschem : a European journal of chemical physics and physical chemistry* 8, 2156-2170.
- Mylonakis, E., Moreno, R., El Khoury, J.B., Idnurm, A., Heitman, J., Calderwood, S.B., Ausubel, F.M., and Diener, A. (2005). *Galleria mellonella* as a model system to study *Cryptococcus neoformans* pathogenesis. *Infect Immun* 73, 3842-3850.
- Naikare, H., Palyada, K., Panciera, R., Marlow, D., and Stintzi, A. (2006). Major role for FeoB in *Campylobacter jejuni* ferrous iron acquisition, gut colonization, and intracellular survival. *Infect Immun* 74, 5433-5444.
- Nasevicius, A., and Ekker, S.C. (2000). Effective targeted gene 'knockdown' in zebrafish. *Nature genetics* 26, 216-220.
- Neal-McKinney, J.M., and Konkel, M.E. (2012). The *Campylobacter jejuni* CiaC virulence protein is secreted from the flagellum and delivered to the cytosol of host cells. *Frontiers in cellular and infection microbiology* 2, 31.
- Neugebauer, U., Grosse, C., Bauer, M., Kemper, B., Barroso-Pena, A., Bauwens, A., Glueder, M., Woerdemann, M., Dewenter, L., Denz, C., *et al.* (2012). From Infection to Detection: Imaging *S. aureus* - host interactions. *Biomedizinische Technik. Biomedical engineering*.
- Newell, D.G., McBride, H., Saunders, F., Dehele, Y., and Pearson, A.D. (1985). The virulence of clinical and environmental isolates of *Campylobacter jejuni*. *The Journal of hygiene* 94, 45-54.
- Nichols, G.L. (2005). Fly transmission of *Campylobacter*. *Emerg Infect Dis* 11, 361-364.
- Novik, V., Hofreuter, D., and Galan, J.E. (2010). Identification of *Campylobacter jejuni* genes involved in its interaction with epithelial cells. *Infect Immun* 78, 3540-3553.
- O'Toole, R., Von Hofsten, J., Rosqvist, R., Olsson, P.E., and Wolf-Watz, H. (2004). Visualisation of zebrafish infection by GFP-labelled **Vibrio anguillarum**. *Microb Pathog* 37, 41-46.
- Paisley, J.W., Mirrett, S., Lauer, B.A., Roe, M., and Reller, L.B. (1982). Dark-field microscopy of human feces for presumptive diagnosis of *Campylobacter fetus* subsp. *jejuni* enteritis. *J Clin Microbiol* 15, 61-63.
- Parker, V. (1965). Antony Van Leeuwenhoek. *Bull Med Libr Assoc* 53, 442-447.

Parkhill, J., Wren, B.W., Mungall, K., Ketley, J.M., Churcher, C., Basham, D., Chillingworth, T., Davies, R.M., Feltwell, T., Holroyd, S., *et al.* (2000). The genome sequence of the food-borne pathogen *Campylobacter jejuni* reveals hypervariable sequences. *Nature* 403, 665-668.

Periasamy, A., Skoglund, P., Noakes, C., and Keller, R. (1999). An evaluation of two-photon excitation versus confocal and digital deconvolution fluorescence microscopy imaging in *Xenopus* morphogenesis. *Microsc Res Tech* 47, 172-181.

Peterson, M.C. (1994). Clinical aspects of *Campylobacter jejuni* infections in adults. *West J Med* 161, 148-152.

Petry, R., Schmitt, M., and Popp, J. (2003). Raman spectroscopy--a prospective tool in the life sciences. *Chemphyschem : a European journal of chemical physics and physical chemistry* 4, 14-30.

Phelps, H.A., and Neely, M.N. (2005). Evolution of the zebrafish model: from development to immunity and infectious disease. *Zebrafish* 2, 87-103.

Pozos, T.C., and Ramakrishnan, L. (2004). New models for the study of *Mycobacterium*-host interactions. *Current opinion in immunology* 16, 499-505.

Prajsnar, T.K., Cunliffe, V.T., Foster, S.J., and Renshaw, S.A. (2008). A novel vertebrate model of *Staphylococcus aureus* infection reveals phagocyte-dependent resistance of zebrafish to non-host specialized pathogens. *Cell Microbiol* 10, 2312-2325.

Prescott, J.F., Barker, I.K., Manninen, K.I., and Miniats, O.P. (1981). *Campylobacter jejuni* colitis in gnotobiotic dogs. *Can J Comp Med* 45, 377-383.

Prescott, J.F., and Karmali, M.A. (1978). Attempts to transmit *Campylobacter* enteritis to dogs and cats. *Can Med Assoc J* 119, 1001-1002.

Pukatzki, S., Ma, A.T., Revel, A.T., Sturtevant, D., and Mekalanos, J.J. (2007). Type VI secretion system translocates a phage tail spike-like protein into target cells where it cross-links actin. *Proceedings of the National Academy of Sciences of the United States of America* 104, 15508-15513.

Pukatzki, S., Ma, A.T., Sturtevant, D., Krastins, B., Sarracino, D., Nelson, W.C., Heidelberg, J.F., and Mekalanos, J.J. (2006). Identification of a conserved bacterial protein secretion system in *Vibrio cholerae* using the *Dictyostelium* host model system. *Proceedings of the National Academy of Sciences of the United States of America* 103, 1528-1533.

Pukatzki, S., McAuley, S.B., and Miyata, S.T. (2009). The type VI secretion system: translocation of effectors and effector-domains. *Current opinion in microbiology* 12, 11-17.

Purcell, M., and Shuman, H.A. (1998). The *Legionella pneumophila* icmGCDJBF genes are required for killing of human macrophages. *Infect Immun* 66, 2245-2255.

Raman, C.V., and Krishnan, K.S. (1928). A New Type of Secondary Radiation. *Nature* 121, 501-502

Renz, M. (2013). Fluorescence microscopy-a historical and technical perspective. *Cytometry A* 83, 767-779.

- Rivera-Amill, V., Kim, B.J., Seshu, J., and Konkel, M.E. (2001). Secretion of the virulence-associated *Campylobacter* invasion antigens from *Campylobacter jejuni* requires a stimulatory signal. *J Infect Dis* 183, 1607-1616.
- Robinson, I., Ochsenkuhn, M.A., Campbell, C.J., Giraud, G., Hossack, W.J., Arlt, J., and Crain, J. (2009). Intracellular imaging of host-pathogen interactions using combined CARS and two-photon fluorescence microscopies. *J Biophotonics* 3, 138-146.
- Rodriguez, L.G., Lockett, S.J., and Holtom, G.R. (2006). Coherent anti-stokes Raman scattering microscopy: a biological review. *Cytometry A* 69, 779-791.
- Rosales-Reyes, R., Aubert, D.F., Tolman, J.S., Amer, A.O., and Valvano, M.A. (2012). *Burkholderia cenocepacia* type VI secretion system mediates escape of type II secreted proteins into the cytoplasm of infected macrophages. *PloS one* 7, e41726.
- Rosef, O., and Kapperud, G. (1983). House flies (*Musca domestica*) as possible vectors of *Campylobacter fetus* subsp. *jejuni*. *Appl Environ Microbiol* 45, 381-383.
- Rounioja, S., Saralahti, A., Rantala, L., Parikka, M., Henriques-Normark, B., Silvennoinen, O., and Ramet, M. (2012). Defense of zebrafish embryos against *Streptococcus pneumoniae* infection is dependent on the phagocytic activity of leukocytes. *Developmental and comparative immunology* 36, 342-348.
- Ruiz-Palacios, G.M., Escamilla, E., and Torres, N. (1981). Experimental *Campylobacter* diarrhea in chickens. *Infect Immun* 34, 250-255.
- Russell, A.B., Hood, R.D., Bui, N.K., LeRoux, M., Vollmer, W., and Mougous, J.D. (2011). Type VI secretion delivers bacteriolytic effectors to target cells. *Nature* 475, 343-347.
- Russell, R.G., Blaser, M.J., Sarmiento, J.I., and Fox, J. (1989). Experimental *Campylobacter jejuni* infection in *Macaca nemestrina*. *Infect Immun* 57, 1438-1444.
- Saar, B.G., Freudiger, C.W., Reichman, J., Stanley, C.M., Holtom, G.R., and Xie, X.S. (2010). Video-rate molecular imaging in vivo with stimulated Raman scattering. *Science* 330, 1368-1370.
- Samuelson, D.R., Eucker, T.P., Bell, J.A., Dybas, L., Mansfield, L.S., and Konkel, M.E. (2013). The *Campylobacter jejuni* CiaD effector protein activates MAP kinase signaling pathways and is required for the development of disease. *Cell communication and signaling : CCS* 11, 79.
- Sana, T.G., Hachani, A., Bucior, I., Soscia, C., Garvis, S., Termine, E., Engel, J., Filloux, A., and Bleves, S. (2012). The second type VI secretion system of *Pseudomonas aeruginosa* strain PAO1 is regulated by quorum sensing and Fur and modulates internalization in epithelial cells. *The Journal of biological chemistry* 287, 27095-27105.
- Sanyal, S.C., Islam, K.M., Neogy, P.K., Islam, M., Speelman, P., and Huq, M.I. (1984). *Campylobacter jejuni* diarrhea model in infant chickens. *Infect Immun* 43, 931-936.

- Schell, M.A., Ulrich, R.L., Ribot, W.J., Brueggemann, E.E., Hines, H.B., Chen, D., Lipscomb, L., Kim, H.S., Mrazek, J., Nierman, W.C., and Deshazer, D. (2007). Type VI secretion is a major virulence determinant in *Burkholderia mallei*. *Molecular microbiology* 64, 1466-1485.
- Schlieker, C., Zentgraf, H., Dersch, P., and Mogk, A. (2005). ClpV, a unique Hsp100/Clp member of pathogenic proteobacteria. *Biological chemistry* 386, 1115-1127.
- Schwarz, S., West, T.E., Boyer, F., Chiang, W.C., Carl, M.A., Hood, R.D., Rohmer, L., Tolker-Nielsen, T., Skerrett, S.J., and Mougous, J.D. (2010). *Burkholderia* type VI secretion systems have distinct roles in eukaryotic and bacterial cell interactions. *PLoS Pathog* 6, e1001068.
- Shneider, M.M., Buth, S.A., Ho, B.T., Basler, M., Mekalanos, J.J., and Leiman, P.G. (2013). PAAR-repeat proteins sharpen and diversify the type VI secretion system spike. *Nature* 500, 350-353.
- Silverman, J.M., Brunet, Y.R., Cascales, E., and Mougous, J.D. (2012). Structure and regulation of the type VI secretion system. *Annual review of microbiology* 66, 453-472.
- Sivadon-Tardy, V., Orlikowski, D., Porcher, R., Ronco, E., Caudie, C., Roussi, J., Fauchere, J.L., Megraud, F., Tabor, H., Sharshar, T., *et al.* (2010). Detection of *Campylobacter jejuni* by culture and real-time PCR in a French cohort of patients with Guillain-Barre syndrome. *J Clin Microbiol* 48, 2278-2281.
- Skirrow, M.B. (1977). *Campylobacter* enteritis: a "new" disease. *Br Med J* 2, 9-11.
- Skirrow, M.B. (2006). John McFadyean and the centenary of the first isolation of *Campylobacter* species. *Clin Infect Dis* 43, 1213-1217.
- Squirrell, J.M., Wokosin, D.L., White, J.G., and Bavister, B.D. (1999). Long-term two-photon fluorescence imaging of mammalian embryos without compromising viability. *Nat Biotechnol* 17, 763-767.
- Stahl, M., Friis, L.M., Nothaft, H., Liu, X., Li, J., Szymanski, C.M., and Stintzi, A. (2011). L-fucose utilization provides *Campylobacter jejuni* with a competitive advantage. *Proceedings of the National Academy of Sciences of the United States of America* 108, 7194-7199.
- Strachan, N.J., and Forbes, K.J. (2010). The growing UK epidemic of human campylobacteriosis. *Lancet* 376, 665-667.
- Suarez, G., Sierra, J.C., Erova, T.E., Sha, J., Horneman, A.J., and Chopra, A.K. (2010). A type VI secretion system effector protein, VgrG1, from *Aeromonas hydrophila* that induces host cell toxicity by ADP ribosylation of actin. *Journal of bacteriology* 192, 155-168.
- Sugai, M., Kawamoto, T., Peres, S.Y., Ueno, Y., Komatsuzawa, H., Fujiwara, T., Kurihara, H., Suginaka, H., and Oswald, E. (1998). The cell cycle-specific growth-inhibitory factor produced by *Actinobacillus actinomycetemcomitans* is a cytolethal distending toxin. *Infect Immun* 66, 5008-5019.

- Taylor, D.N., Echeverria, P., Pitarangsi, C., Seriwatana, J., Bodhidatta, L., and Blaser, M.J. (1988). Influence of strain characteristics and immunity on the epidemiology of *Campylobacter* infections in Thailand. *J Clin Microbiol* 26, 863-868.
- Tobin, D.M., May, R.C., and Wheeler, R.T. (2012). Zebrafish: a see-through host and a fluorescent toolbox to probe host-pathogen interaction. *PLoS Pathog* 8, e1002349.
- Trede, N.S., Langenau, D.M., Traver, D., Look, A.T., and Zon, L.I. (2004). The use of zebrafish to understand immunity. *Immunity* 20, 367-379.
- van der Sar, A.M., Musters, R.J., van Eeden, F.J., Appelmelk, B.J., Vandenbroucke-Grauls, C.M., and Bitter, W. (2003). Zebrafish embryos as a model host for the real time analysis of *Salmonella typhimurium* infections. *Cell Microbiol* 5, 601-611.
- van Vliet, A.H., Wooldridge, K.G., and Ketley, J.M. (1998). Iron-responsive gene regulation in a *Campylobacter jejuni* fur mutant. *Journal of bacteriology* 180, 5291-5298.
- Vucic, S., Kiernan, M.C., and Cornblath, D.R. (2009). Guillain-Barre syndrome: an update. *J Clin Neurosci* 16, 733-741.
- Wang, L. (2010). Zebrafishing for tuberculosis infection. *Protein Cell* 1, 309-311.
- Wang, W., Liu, X., Gelinis, D., Ciruna, B., and Sun, Y. (2007). A fully automated robotic system for microinjection of zebrafish embryos. *PloS one* 2, e862.
- Wang, Y., and Taylor, D.E. (1990). Chloramphenicol resistance in *Campylobacter coli*: nucleotide sequence, expression, and cloning vector construction. *Gene* 94, 23-28.
- Wassenaar, T.M., Bleumink-Pluym, N.M., and van der Zeijst, B.A. (1991). Inactivation of *Campylobacter jejuni* flagellin genes by homologous recombination demonstrates that flaA but not flaB is required for invasion. *The EMBO journal* 10, 2055-2061.
- Watson, R.O., and Galan, J.E. (2008). *Campylobacter jejuni* survives within epithelial cells by avoiding delivery to lysosomes. *PLoS Pathog* 4, e14.
- Webb, D.J., and Brown, C.M. (2013). Epi-fluorescence microscopy. *Methods in molecular biology* 931, 29-59.
- Weber, B., Hasic, M., Chen, C., Wai, S.N., and Milton, D.L. (2009). Type VI secretion modulates quorum sensing and stress response in *Vibrio anguillarum*. *Environmental microbiology* 11, 3018-3028.
- Weerakoon, D.R., and Olson, J.W. (2008). The *Campylobacter jejuni* NADH:ubiquinone oxidoreductase (complex I) utilizes flavodoxin rather than NADH. *Journal of bacteriology* 190, 915-925.
- Wiesner, R.S., Hendrixson, D.R., and DiRita, V.J. (2003). Natural transformation of *Campylobacter jejuni* requires components of a type II secretion system. *Journal of bacteriology* 185, 5408-5418.
- Willett, C.E., Cortes, A., Zuasti, A., and Zapata, A.G. (1999). Early hematopoiesis and developing lymphoid organs in the zebrafish. *Dev Dyn* 214, 323-336.

- Williams, S.G., Varcoe, L.T., Attridge, S.R., and Manning, P.A. (1996). *Vibrio cholerae* Hcp, a secreted protein coregulated with HlyA. *Infect Immun* 64, 283-289.
- Wosten, M.M., Boeve, M., Koot, M.G., van Nuenen, A.C., and van der Zeijst, B.A. (1998). Identification of *Campylobacter jejuni* promoter sequences. *Journal of bacteriology* 180, 594-599.
- Wu, H.Y., Chung, P.C., Shih, H.W., Wen, S.R., and Lai, E.M. (2008). Secretome analysis uncovers an Hcp-family protein secreted via a type VI secretion system in *Agrobacterium tumefaciens*. *Journal of bacteriology* 190, 2841-2850.
- Yao, R., Alm, R.A., Trust, T.J., and Guerry, P. (1993). Construction of new *Campylobacter* cloning vectors and a new mutational cat cassette. *Gene* 130, 127-130.
- Young, K.T., Davis, L.M., and Dirita, V.J. (2007). *Campylobacter jejuni*: molecular biology and pathogenesis. *Nat Rev Microbiol* 5, 665-679.
- Young, V.B., Knox, K.A., and Schauer, D.B. (2000). Cytolethal distending toxin sequence and activity in the enterohepatic pathogen *Helicobacter hepaticus*. *Infect Immun* 68, 184-191.
- Yu, Y., Yang, H., Li, J., Zhang, P., Wu, B., Zhu, B., Zhang, Y., and Fang, W. (2012). Putative type VI secretion systems of *Vibrio parahaemolyticus* contribute to adhesion to cultured cell monolayers. *Archives of microbiology* 194, 827-835.
- Zhang, M.J., Xiao, D., Zhao, F., Gu, Y.X., Meng, F.L., He, L.H., Ma, G.Y., and Zhang, J.Z. (2009). Comparative proteomic analysis of *Campylobacter jejuni* cultured at 37C and 42C. *Japanese journal of infectious diseases* 62, 356-361.
- Zheng, J., Ho, B., and Mekalanos, J.J. (2011). Genetic analysis of anti-amoebae and anti-bacterial activities of the type VI secretion system in *Vibrio cholerae*. *PloS one* 6, e23876.
- Zheng, J., and Leung, K.Y. (2007). Dissection of a type VI secretion system in *Edwardsiella tarda*. *Molecular microbiology* 66, 1192-1206.
- Zhou, Y., Tao, J., Yu, H., Ni, J., Zeng, L., Teng, Q., Kim, K.S., Zhao, G.P., Guo, X., and Yao, Y. (2012). Hcp family proteins secreted via the type VI secretion system coordinately regulate *Escherichia coli* K1 interaction with human brain microvascular endothelial cells. *Infect Immun* 80, 1243-1251.
- Zilbauer, M., Dorrell, N., Wren, B.W., and Bajaj-Elliott, M. (2008). *Campylobacter jejuni*-mediated disease pathogenesis: an update. *Trans R Soc Trop Med Hyg* 102, 123-129.
- Zumbusch, A., Holtom, G.R., and Xie, X.S. (1999). Three-Dimensional Vibrational Imaging by Coherent Anti-Stokes Raman Scattering. *Physical Review Letters* 82, 4142-4145.